Association des copolymères à séquences (1->4)-a-L-guluronane en présence d'ions calcium

Anna Wolnik

UNIVERSITÉ DE GRENOBLE

THÈSE

Pour obtenir le grade de

DOCTEUR DE L'UNIVERSITÉ DE GRENOBLE

Spécialité : **Sciences des Polymères**

Arrêté ministériel : 7 août 2006

Présentée par

« Anna WOLNIK »

Thèse dirigée par **Karim MAZEAU**
et co-encadrée par **Frédéric DUBREUIL**

préparée au sein du **Centre de Recherches sur les Macromolécules Végétales (CERMAV), CNRS**
dans **l'École Doctorale Chimie et Sciences du Vivant**

Association des copolymères à séquences (1→4)-α-L-guluronane en présence d'ions calcium

Ca^{2+} - driven association of polymers featuring (1→4)-α-L-guluronan sequences

Thèse soutenue publiquement le **« 5 février 2014 »**,
devant le jury composé de:

Madame Anne MILET
Professeur, Département de Chimie Moléculaire, Grenoble (Président du Jury)
Monsieur Alain BULÉON
Directeur de Recherche, Institut National de la Recherche Agronomique, Nantes (Examinateur)
Monsieur Luc PICTON
Professeur, Université de Rouen, Laboratoire Polymères, Biopolymères, Surfaces, Mont-Saint-Aignan (Rapporteur)
Monsieur Patrick GUENOUN
Chercheur CEA, Laboratoire Interdisciplinaire sur l'Organisation Nanométrique et Supramoléculaire, Paris (Rapporteur)
Monsieur Karim MAZEAU
Directeur de Recherche, CERMAV-CNRS, Grenoble (Directeur de thèse)
Monsieur Frédéric DUBREUIL
Maître de conférences, CERMAV-CNRS, Grenoble (Invité)

Université Joseph Fourier

This thesis is dedicated to my parents,

for their love and unlimited support !

Table of contents

Acknowledgements

First of all, I would like to express my special appreciation to my Ph.D. supervisors: *Dr. Karim Mazeau* and *Dr. Frédéric Dubreuil* for their support and belief in me to complete my doctoral project.

Karim is a direct person but also very honest. After a short scientific discussion with him, you can discover that he is an expert in his field and a scientist not by coincidence but by choice. Thus he has high expectations from his students but it encouraged me to work even harder. I am also very grateful for his availability, he was always present in his office, ready to answer my scientific questions or give me valuable suggestions when I got stuck and could not find any solution. I really appreciate that I had an opportunity to work with you Karim !

Fred, as an expert of Atomic Force Microscopy, familiarized me with the instrument and gave me the freedom to work independently. Despite traversing long distances to work every day and teaching assignments, he always had time for me. Fred was not only my advisor but also a person who was able to understand how it is to be a student in a foreign country. I am very thankful to you for helping me with filling up many administrative documents and for your support, especially towards the finishing line of my Ph.D.

My appreciation goes also to *Dr. Luca Albertin*, who was not my official supervisor but a person who took great care of me. I am sure that without his help my Ph.D. work would not have been as good as it is. Luca is one of the smartest people I know but he never showed it during our discussions, on the contrary explained everything with fatherly patience. Luca has another rare ability, he is not afraid of saying 'I don't know' but even if it happens he will never leave you alone with your problem. I admire him also for his organization skills – I wish to be as organized as he is. Luca was also a person who explained me how the scientific world works and strengthened my belief that no matter what we do in life we should be content with it. I was very lucky to be a part of your project Luca and I am glad that I could meet such a good scientist as you definitely are.

This Ph.D. work would not have been completed without help of *Prof. Marguerite Rinaudo*. I owe to her mainly supervising me in experiments performed by light scattering and rheology. *Dear Madame Rinaudo*: I have never met a person in my life who is as

dedicated to scientific work as you are. Your professionalism, wide knowledge, experience, enthusiasm, passion for work and modesty inspires me to become a scientist like you. Meeting you and working with you was a real pleasure ! I am grateful to you not only for your help in scientific work but also for taking care of me always. Très grand merci Madame Rinaudo !

Furthermore, I thank *Dr. Frédéric Pignon* from Laboratoire de Rhéologie et Procédés (Grenoble) for giving me the opportunity to perform my rheological experiments in his laboratory and both for his technical as well as scientific advices.

I would also like to extend my thanks to *Eric Reynaud* and *Lionel Dumas* who synthesized polymers for me and to *Landry Charlier* and *Pan Chen* for their patience in teaching me how to use the GROMACS software.

Since my doctoral project was multidisciplinary, thus I was working almost on each floor of CERMAV. I would like to give special thanks to all my groups to which I belonged: Structure et propriétés des glycomatériaux and Physicochimie des glycopolymères but also to a group of Glycobiologie moléculaire of which I somehow became a part.

In addition, thank you Agence Nationale de la Recherche (ANR) for funding my doctoral scholarship and to *Redouane Borsali* for giving me financial support for my last five months of stay in CERMAV in order to complete this Ph.D. work.

I also thank my committee members: *Prof. Anne Milet*, *Dr. Alain Buléon*, *Prof. Luc Picton* and *Dr. Patrick Guenoun* not only for their time but also for their insightful comments.

The beginning of my stay in Grenoble was not easy … mainly due to the lack of knowing French. However, since my arrival, I have been meeting wonderful people and I really began to love this place ! Therefore, I would like to mention below the names of My Friends, without whom I would not have been able to survive in Grenoble and finish my doctoral project.

The first people I met in Grenoble were *Josiane and Gaston Zarka* who rented me a room in their house. They were not only owners but soon became my real friends who were waiting for me to return from work every day. Due to their hospitality and kindness I was not

feeling as lonely as I would in a new city. Their home became my second home very fast and I am extremely grateful to fate for taking me there. I will never forget all you did for me.

Zarka's home was a place full of life, mainly due to *Josiane* who is one of the most energetic people I know but also due to international flat-mates. I had a chance to meet there my first Indian friends in Grenoble: *Priyanka* and *Pavani* who were just awesome ! I will never forget the day when Pavani saw snowfall for the first time in her life and did not know how she should dress during the winter time ☺ Then, when I had started to like them very much, the first time (one of many ☹) to say 'Goodbye' in Grenoble had come … But my Indian flat-mates were replaced by *Bilel* from Tunisia and *Dominika Świder* from Poland. We had many common parties and trips and somehow they became like my brother and sister who I used to meet every evening after a hard working day.

Due to this particular ambiance in my new home I was able to go to work with a smile on my face. Admittedly, at work I have also made many friendships. The first friend I met in CERMAV was *Pan Chen* – a person who introduced me not only to a new place and the people working there, but who has been helping and supporting me during my whole stay in France. Pan is a true friend of mine because I know that I can rely on him anytime and he has always been with me in good and bad times. He believed in completing my Ph.D. sometimes more than I did. I am extremely happy to have you as My Friend Pan Pan ☺

Once you have chosen being a Ph.D. student, you firstly integrate with people who are similar to you, that is other Ph.D. students. I thank *Emilie Hachet, Antoine Bailly, Matthieu Fumagalli, Firas Azzam, Géraldine Ganne* and *Agathe Bélime* for their help and company during the first months of my stay in CERMAV. However, each year new Ph.D. students come … I am equally grateful for meeting: *Antoine Duval, Jing Jing, Gaëlle Batot, Félix Cicéron, Remi Chambon, Harisoa Radavidson* and *Clelia Martin* who always had a warm smile for me. However, among them were also people who deserve special mention.

I would like to thank *Ali Ghadban* for introducing me to real Ph.D. life and for being such a nice friend. Since Ali had been working in the same scientific project, he really knew my subject. Thank you Ali for your insightful and professional advices. The time we were sharing an office in CERMAV was for sure one of the best periods of my stay there !

The next person who I want to mention is *Ilham Mkedder*. In the beginning she did not want to speak in English with me, but after realizing that I really did not know any French, she

changed her attitude towards me and began to teach me French and Arabic. Besides common lunches and coffee breaks we used to share together also our spare time and have become close friends. *Dear Ilham*: I am very glad that I could meet such a nice person who you definitely are ☺

My stay in CERMAV would not have been as enjoyable as it was without *Djamila Ouhab*. We were sharing an office together, belonged to the same research groups … thus spending a lot of time together… *Dear Jamimi*: thank you for your help (not only with French administrative paperwork but mainly for your support, belief in me and all common moments we shared together). You are surely make the best pancakes that I have ever eaten !

Writing the thesis was much easier due to the presence of *Dörte Hundling* who used to come to my office and say: 'Anna! Let's have a break' *Dear Dörte*: thank you for taking me for walks, for your herbal teas and for taking care of me, especially during this 'writing period'. It would be very difficult for me to reach the finishing line without you !

I am also glad to know *Soorej Basheer* – a person with a wonderful smile, *Axel Ettori* – who I usually used to meet on the stairs, in rush between running experiments … but he always had a while to chat with me, *Anna Szarpak-Jankowska* – with whom I could not only speak Polish but who was always very helpful, *Aline Thomas* – a very nice person (thank you for dinners chez *Aline*, common lunches and coffee breaks) and *Armelle Roncin* – who I met during the last months of my stay in CERMAV but nevertheless we spent nice time together.

A special thanks goes also to *Bruno Frka-Petešić* – who helped me a lot, especially during the period of my Ph.D. when I was really stuck. His advices, wide knowledge and determination pushed me to move on. *Bruno*: I admire not only your wisdom (both scientific and spiritual) but also your empathy towards others. I am thankful for improving me … I have always learnt something from our conversations either about science or life … you are like my elder brother who I have never had and this is a great feeling !

My stay in CERMAV was very pleasant and memorable due to many international friends ! I would like to thank the Brazilian community with special thanks to: *Eliana Endo, André Ricardo Fajardo, Antônia Sâmia Fernandes, Clayton Fernandes de Souza, Tamiris Figueiredo, Letícia Mazzarino, Carolina Montanheiro Noronha, Tati Popiolski, Luis Silva, Talitha Stefanello, Soraia Zaioncz* and *Karine Zepon*.

I also had a change to meet Japanese people … I would like to thank: *Daisuke Sawada* (for his company in Barcelona), *Noriyuki Isobe* (for his unexpected birthday gift) and of course *Yoko & Issei Otsuka*. *Otsuka* family is a wonderful family, I am extremely happy that I could meet *Yoko* – a person with a BIG and sensitive heart, *Issei* – not only a very good scientist but also a person with many talents ! I admire them as a couple, parents of *Ryosei* (the cutest Japanese boy I have ever seen) and also as human beings. Thank you for your help, dinners chez *Otsuka*, your hospitality and for being such wonderful Friends !!!

One day, when *Marina Osaka* – a Japanese student came to do internship in CERMAV, my life changed completely. I have never met a person who is as energetic as she is. Her optimism and positive energy is like a hypnosis which you follow just spontaneously. I used to come to work with even bigger smile on my face than before because of You *Marina*! Thank you for your messages and little gifts which you used to leave on my desk every morning, for your smile, company and everything you did for me. I have no words to express how thankful I am to God for coming across you in my journey of life ! People like you are very rare and the modern world needs more people like you *Marina*, so please keep smiling to people as long as you can. You are my *Super Hero* and I admire you for just being as you are - an AWESOME FRIEND of mine ☺ In addition, I am also very grateful to you for introducing me to your Friends. I would like to thank *Yoko Sugaya* – a very sweet person, *Nana Arizumi* – who I admire for her wisdom and modesty, *Ehsan Rezaie* – very crazy person but in a very positive way, *Alejandra Sève, Patricia Courbet, Fuad Karim* and many others whose all names I am not able to mention here, unfortunately.

The beauty of science is partially related to hosting international interns who bring 'fresh air' to the institute. I am very glad that I could meet: *Benjamin Briois (Mister B ☺), Francisco Sánchez* (*Fran*: thank you for convincing me to rent a Métrovélo bike, I will never forget this day)*, Chiara Bertolina, Giulio Marti (Aoringo), Camille Cuier, Brendan Galesne, Mohamad Mehdi Seyed Mousavi, Islem Younes, Marie Pascaline Rahelivao, Hana Maalej, Juan Carlos Muñoz Garcia, Philippe Bourassa, Yasmina Hammoui, Andrea Wilches Torres, Jérôme Iseni* and *Shivalika Tanwar*. You made my lunch breaks unforgettable!

My stay in CERMAV gave me one treasure more – a special Friend: *Anita Sarkar* ! *Anita* is a person with many talents and it is a real honor to have a Friend in her ! Her wide knowledge and mature advices helped me to go through many difficulties in life. Thank you for everything you do for me and for being *My Dear Twin* who I can call and talk to whenever

I need ! The wonderful time we spent together in Grenoble will remain in my heart forever ☺ *Dear Ani*: I am also very grateful to you for introducing me to your Indian friends.

Special thanks goes to *Dibyendu Hazra* for finding time in his busy schedule to meet with me from time to time. *Dear Busy Man*: I admire your wide knowledge, excellent writing skills and your honesty ! Thank you for the common discussions and cooking for me, I always appreciate the time we share together !

The next person without whom my life would not be the same is *Akash Chakraborty*. His support, care and experience about life gave me new energy to move on whenever I got stuck. Therefore, this manuscript is partially also your success *Akash*. You are among those rare people who give more than take from the others. *Dear Akash*: you have many talents but what I admire the most is your modesty. I am extremely happy to have a real Friend in You on whom I can always rely on ☺

Thanks to Anita, I have also met *Dilyara Timerkaeva*. Oh *Dear Dila* … what can I say … I just simply love you ! My heart is always smiling whenever I see you because the way in which you say hello to me is just simply awesome ! I am very happy that I met you in my life!

My stay in Grenoble was much easier due to some wonderful Polish people who I met usually either in the bus or in the church ☺

On my way back to Grenoble after Christmas I met *Ania Adamiok*. It was January 2011, we spent 27 hours in the bus and somehow I had the feeling that *Ania* is my kindred spirit. *Dear Ania*: there are not enough words to express my appreciation to you. Meeting you was definitely one of the best surprises which life has given me ! Thank you for the common journeys (wherever I travel with you, I have always a great time), care, support and for hosting me many times in Marseille (my third home in France, after Zarka's one). You are a very courageous person with many talents ! I wish our friendship lasts forever !

Next Polish person, who I met was *Asia Andrecka* – a person with a big heart. *Dear Asia*: I admire your cognitive curiosity of the World and amazing courage ! Sometimes I wonder how do you get so much energy to change places so quickly ? It is incredible ! I am very happy to know You Asia and have a Friend in You !

I would also like to thank *Joanna Górniak* for all the common moments (trips, dinners chez *Joanna*, cooking, baking, *etc.*) we had spent in Grenoble. *Dear Joanna*: I admire your organization skills and determination in achieving the goals that you have set. I wish you all the best for your future life !

Thanks also goes to *Patrycja Siemiginowska*, *Jarek Sar* and *Olga Matusik* who I met in the Polish church. Our coffee meetings made my Sundays brighter ☺ You are very valuable people ! *Dear Pati*: listening to your speeches in very proper Polish was a real pleasure for me ! *Dear Jaro*: your jokes made our meetings very funny ! *Dear Olga*: your keeping abreast about social activities in Grenoble made us more familiar with the Grenobloise community.

Another person, who I met in the bus was Iza Petrykiewicz. We occupied seats far from each other so had only few short conversations at that time … but we exchanged phone numbers … and met in Grenoble again. Oh … in fact we had spent many many common moments ! *Dear Iza*: Thank you for parties chez *Iza*, baking Christmas cookies (I have never seen so many homemade cookies together, as at your place), common: lunches, coffee breaks, trips, *etc*. You are very intelligent, mature, organized and of course You bake awesome cakes! I am very glad to know such a wonderful person like You ☺

Next people whom I would like to thank are *Olesia Danyliv & Oleksandr Nechyporchuk*. I am very glad to have Friends in you. *Dear Olesia*: thank you for your help anytime ! It would be very difficult for me to handle all my problems without you. Your support, care and true friendship confirmed my beliefs that with Friends we are able to go through difficult times in our lives much easily ! I am extremely happy to know You and Sasha and I wish that our friendship lasts forever !

My stay in Grenoble would not have been the same without continued support of *Marta Peukert*. Despite a long distance between us, we kept in touch, whether through phone calls, or email. *Dear Martusia*: thank you for being my Friend and for your belief in completing my Ph.D. from the beginning to the end.

And finally I would like to thank my wonderful FAMILY: my parents, my brother and my grandpa for their unlimited love and immense care. Their belief and support for everything I do, give me courage and energy to achieve the goals I set in my life. There are not enough words to express my gratitude towards you … so I am saying only simple THANK YOU but this comes really from the bottom of my heart !

Ph.D. was not only a scientific exam for myself but mainly a big lesson of life. Today I am a much stronger woman and thus I am grateful to destiny for bringing me to Grenoble. I came here alone … and now I have so many Friends ! I wish to keep in touch with many of you … All the friendships which I made in Grenoble are the biggest treasure from this magnificent city and confirmed my belief that with good people around, we are able to survive anywhere because as Christian Morgenstern wrote: '*Home is not where you live but where they understand you*.'

Abstract

Alginates form transparent hydrogels in aqueous solution upon addition of some divalent cations. This property is mostly due to the formation of junction zones involving (1→4)-α-L-guluronan sequences on adjacent polymer chains. Oligomers of alginates were used as molecular bricks for the synthesis of biohybrid polymers featuring (1→4)-α-L-guluronan sequences as side chains. Rheology and Light Scattering have been applied to investigate their ionotropic gelation. In addition, an atomistic picture of the Ca^{2+}-driven side chain associations was also provided thanks to Molecular Modeling and Atomic Force Spectroscopy.

Biohybrid polymers carrying (1→4)-α-L-guluronan residues formed soft and transparent hydrogels in the presence of Ca^{2+}. The addition of either guluronan, or mannuronan blocks to the pre-formed gel reduced its strength almost with the same efficiency.

A molecular dynamics investigation of fully charged (1→4)-α-L-guluronan sequences in the presence of a neutralizing amount of Ca^{2+} ions suggested that about 8 repeating units may be sufficient to the spontaneous formation of aggregates. Furthermore, conformational analysis of (1→4)-α-L-guluronan chain having 12 repeating units in duplexes revealed a wide variety of accessible conformations, a feature consistent with the general difficulty in obtaining crystals of Ca^{2+}-guluronate with suitable lateral dimensions for crystallographic studies.

The adhesion forces between homo-alginate oligomers in the presence of Ca^{2+} measured by Atomic Force Spectroscopy showed that the strength of interactions increased in the following order:

M-M < M-G or G-M < G-G.

One of the most significant findings to emerge from this study is that mannuronan blocks complexed via calcium ions can be involved in both homotypic and heterotypic associations. This result is consistent with the detection of aggregates observed for mannuronan oligomers by Light Scattering during the addition of $CaCl_2$. Thus, M-blocks also contribute to the gel formation but their strength seemed to be however weaker than G-blocks.

Résumé

Les alginates forment des gels transparents en solution aqueuse en présence de certains ions divalents. Cette propriété est principalement attribuée à la formation de zones de jonction impliquant les séquences (1→4)-α-L-guluronane de chaînes adjacentes. Des oligomères d'alginates ont été utilisés comme briques élémentaires pour la synthèse de polymères biohybrides contenant des chaines pendantes oligo-(1→4)-α-L-guluronane. La rhéologie et la diffusion de la lumière ont permis d'étudier leur gélification ionotropique. De plus, une image atomistique des associations entre chaines latérales a été donnée grâce à la modélisation moléculaire et la microscopie de force atomique.

Les polymères biohybrides portant des résidus pendant (1→4)-α-L-guluronane forment des gels en présence de Ca^{2+}. L'addition de blocs guluronane ou mannuronane au gel préformé fait diminuer sa force avec quasiment la même efficacité.

L'étude par dynamique moléculaire de séquences (1→4)-α-L-guluronan totalement chargées en présence d'ions Ca^{2+} suggère qu'environ 8 unités de répétition sont suffisantes pour former spontanément des agrégats. De plus, l'analyse conformationnelle de duplexes de chaines (1→4)-α-L-guluronane ayant 12 unités de répétition révèle une grande variété de conformations accessibles, ce qui est consistant avec la difficulté d'obtention de cristaux de Ca^{2+}-guluronate de dimension suffisante pour les études cristallographiques.

Les forces d'adhésion entre des homo-oligomères d'alginates en présence de Ca^{2+} mesuré par spectroscopie de force atomique montrent que la force d'interaction croit selon l'ordre suivant:

M-M < M-G or G-M < G-G.

Un résultat important est que les blocs mannuronanes, en complexe avec le calcium, peuvent être impliqués dans des associations homotypiques et hétérotypiques. Ce résultat est consistant avec la détection d'agrégats d'oligomères de mannuronanes observés en diffusion de la lumière pendant l'addition de $CaCl_2$. Les blocs M contribuent donc également à la formation du gel mais la force associée est plus faible que celle des blocs G.

Keys to symbols and constants

$\dot{\gamma}$	shear rate
$N_{Ca^{2+}}$	calcium coordination number
$[\eta]$	intrinsic viscosity
A_2	second virial coefficient
c	concentration
c^*	critical concentration
C_{12}	repulsive term coefficient
C_6	attractive term coefficient
C_∞	characteristic ratio
$Đ$	dispersity index
dn/dc	differential refractive index increment
E	energy or Young's modulus
F	force
f_R	resonance frequency
G'	storage modulus
G''	loss modulus
H	conformational turn angle
k	force constant
k_B	Boltzmann constant
l_K	Kuhn length
l_p	persistence length
M_n	number average molecular weight
M_w	weight average molecular weight
n	refractive index

N_A	Avogadro number
pK_a	dissociation constant
R	end-to-end distance or charge stoichiometric ratio
R_c	critical charge stoichiometric ratio
Re	Reynolds number
R_g	radius of gyration
R_h	hydrodynamic radius
R_θ	Rayleigh ratio
T	temperature
t	time
X	degree of polymerization
z_c	deflection of the cantilever
z_p	displacement of the piezoelectric scanner in the z-direction
η	viscosity
λ	wavelength of light
ρ	density
σ	shear stress

Keys to abbreviations and acronyms

ACPA	4,4'-azobis-(cyanopentanoic acid)
AFM	Atomic Force Miscroscopy
AFS	Atomic Force Spectroscopy
AIBN	2,2'-azobis(2-methylpropionitryle)
APTMS	3-aminopropyl)trimethoxysilane
CECIC	Centre d'Expérimentation et de Calcul Intensif
CVFF	Consistent Valence Force Field
Da	Dalton
DLS	Dynamic Light Scattering
DMF	dimethylformamide
DMSO	dimethyl sulfoxide
DNA	deoxyribonucleic acid
EDAC	1-(3-dimethylaminopropyl)-3-ethylcarbodiimide hydrochloride
EDTA	ethylenediaminetetraacetic acid
EM	Energy Minimization
EXAFS	Extended X-ray Absorption Fine Structure spectroscopy
FF	Force Field
FM	force measurements
G	(1→4)-linked α-L-guluronic acid unit
GDL	D-glucono-δ-lactone
Glc-1-P	α-D-glucose-1-phosphate
GROMACS	GROningen MAchine for Chemical Simulations
$GulA_x$	(1→4)-α-L-guluronan oligomer with *X* repeating units

HA	hyaluronic acid
HBs	hydrogen bonds
HEMA	2-hydroxyethylmethacrylate
HEMAm	2-hydroxyethylmethacrylamide
HIV	human immunodeficiency virus
HPMA	hydroxypropylmethacrylamide
LAXS	Large-Angle X-ray Scattering
LCAO	Linear Combination of Atomic Orbitals
LINCS	LINear Constraint Solver algorithm
LJ	Lennard-Jones
LS	Light Scattering
M	(1→4)-linked β-D-mannuronic acid unit
$ManA_x$	(1→4)-β-D-mannuronan oligomer with *X* repeating units
MD	Molecular Dynamics
MM	Molecular Mechanics
MMA	methyl methacrylate
MOPS	3-[N-morpholino]propanesulfonic acid
NPT	constant number of particles, constant pressure and constant temperature
NVE	constant number of particles, constant volume and constant energy
NVT	constant number of particles, constant volume and constant temperature
PBC	Periodic Boundary Conditions
PCS	Photon Correlation Spectroscopy
PDMS	poly(dimethylsiloxane)
PEG	polyethylene glycol
PEI	poly(ethylene imine)
PES	polyethersulfone

PLL	poly(L-lysine)
PSA	piperidine-N-sulfonic acid
QELS	Quasi-Elastic Light Scattering
QM	Quantum Mechanics
RDF	Radial Distribution Function
RMSD	root mean square positional difference
SAXS	Small-Angle X-ray Scattering
SEC	Size Exclusion Chromatography
SHO	Simple Harmonic Oscillator
SLS	Static Light Scattering
SPC	Simple Point Charge
SPM	Scanning Probe Microscopy
TGA	thermogravimetric analysis
VAA	vinylbenzyl amylose amide
VDW	van der Waals
VMD	Visual Molecular Dynamics

Chapter I:

Introduction to the thesis

Polysaccharides are biopolymers composed of carbohydrate units linked together covalently by glycosidic linkages. Indeed, they are the most abundant natural polymers (more than 150,000 million tons of polysaccharides are produced per year compared to about 140 million tons of synthetic polymers)[1], widely diffused in nature (*e.g.* plants, animals and microorganisms). The majority of natural polysaccharides are located in plants. In the vegetable kingdom, they are the indirect product of the photosynthetic process and represent the major component of the earth's biomass. As a result of their abundance and distinct properties, polysaccharides were among the first polymers exploited by man, forming the basis of several technical and industrial applications.

Natural polysaccharides from plants (*e.g.* alginates) are biocompatible, biodegradable and water soluble, making them suitable for different biomedical applications. However, while using natural polysaccharides it is important to note the intrinsic variability of their physico-chemical properties that is dependent upon several factors such as the source species, conditions of growth, the period of harvest and the extraction process. Thus in recent years, the use of these biopolymers as a source of building blocks of functional materials is rapidly growing. A general synthetic procedure of such biopolymers is as follows:

- depolymerization of a natural polysaccharide into well-defined oligomers
- separation the oligosaccharides on the basis of their size and chemical nature
- functionalization at the chain-end with a group suitable for polymerization
- controlled polymerization of these functionalized oligomers to obtain neo-polysaccharides (biohybrid polymers) with well-defined macromolecular architecture and composition

Alginate as a natural polysaccharide is composed of (1→4)-linked α-L-guluronic acid and β-D-mannuronic acid units. It is a highly interesting subject of research since it combines very interesting properties (*e.g.* complexation of some divalent cations, known as ionotropic gelation), with great structural and compositional variability and the possibility to be depolymerized into chemically homogeneous oligomers of different nature and sizes.

Basic information about gels and the gelation mechanism of the ionotropic gelation phenomenon as well as an introduction to alginates is described in ***Chapter II: The State of the Art***.

Since natural alginates possess the intrinsic variability of physico-chemical properties, mainly due to their chemical and macromolecular heterogeneity, which limits their range of use, the ALGIMAT (Advanced functional **MAT**erials from algal **ALGI**nates) project (financed by the ANR) was constituted to study their chemical modifications. Alginates were used as a primary source of molecular bricks for the synthesis of alginate-derived semi-synthetic polymers (biohybrid polymers or neo-alginates) with a well-defined structure. A brief overview of synthetic polysaccharide graft copolymers, with regard to those, which incorporate grafted (1→4)-α-L-guluronan or (1→4)-β-D-mannuronan chains is provided in ***Chapter II: The State of the Art***.

The main objective of this doctoral thesis was aimed to study biohybrid polymers featuring (1→4)-α-L-guluronan sequences as side chains synthesized by other members of the ALGIMAT project. Since many applications of alginate derivatives are related to their gelation, thus the fundamental issue of this study was a progressive Ca^{2+}-driven association of neo-alginates probed via Light Scattering (first indication of the junction zones), and a formation of their 3D network (mechanism of ionotropic gelation) investigated via rheology (***Chapter V: Probing the association by experimental techniques***).

Guluronan blocks which play a major role in the gelation process are incorporated in the case of neo-alginates in grafted chains, thus the epicentre of Ca^{2+} association is located at this juncture. Subsequently, detailed examination of interactions between (1→4)–α-L-guluronan chains via Ca^{2+} was carried out by molecular modeling (***Chapter IV: Probing the ionotropic association by molecular modeling***).

In order to complete the atomistic picture of side chain associations mediated by Ca^{2+}, force measurements (via Atomic Force Microscopy) were performed. Those studies

considered not only (1→4)-α-L-guluronan sequences but also (1→4)-β-D-mannuronan ones to probe their role in the junction zones of natural alginates at the molecular level, which had never been studied previously (***Chapter V: Probing the association by experimental techniques***).

Chapter III: Investigation techniques contains a brief description of the techniques used during this PhD project, namely molecular modeling, Atomic Force Microscopy, Light Scattering and rheology (written to familiarize the basics concepts as well as the specific terminologies used in the following chapters).

Publications:

1. Albertin, L.; Wolnik, A.; Ghadban, A.; Dubreuil, F., *Aqueous RAFT Polymerization of N -Acryloylmorpholine, Synthesis of an ABA Triblock Glycopolymer and Study of its Self-Association Behavior*, *Macromol. Chem. Phys.* **2012**, *213*, 1768-1782.
2. Wolnik, A.; Albertin, L.; Charlier, L.; Mazeau, K., *Probing the helical forms of Ca^{2+}-guluronan junction zones in alginate gels by molecular dynamics 1: Duplexes*, *Biopolymers*, **2013**, 99(8): p. 562-571.

References:

1. Navard, P., *Editorial: EPNOE: The New European Polysaccharide Network of Excellence.* Cellulose, **2005**. 12(4): p. 337-338.

Chapter II:

The State of the Art

Table of contents

1. Introduction

This chapter gives a brief introduction of the gelation process, commonly occurring in alginates, which undergo ionotropic gelation in the presence of some divalent cations. In addition, a description of chemical structure and important properties of these natural polysaccharides is given. However, since the utilization of natural alginates is limited due to their chemical and macromolecular heterogeneities, thus the attempts of synthesizing new molecular architectures featuring oligoalginate chains available in the literature are also reported.

2. Gels and gelation

A gel is a three-dimensional network composed of molecules, polymers, particles, colloids, *etc.* connected via specific parts (cross-links) such as functional groups and associative groups.[1] Based on the nature of the bonds involved in crosslinking region, gels are classified into chemical gels and physical gels. Chemical gels are formed by covalent bonds while physical ones by physical bonds. In order to prepare chemical gels by the polymerization of small molecule, multifunctional molecules with functionality ≥ 3 are required.[2] By contrast, physical gels can be formed by different types of cross-links and classified into six categories (Figure 2.1).[1]

Polymer chains can be connected by hydrogen bonds, dipole interaction (aggregation of the dipole moments), hydrophobic interaction (micellization of the hydrophobic groups in water) or ionic bonds (complex junction zones typical for alginates). However, some physical gels (gels with microcrystalline junctions) can be also obtained as a result of cooling of crytallizable polymers below their melting point. The last category is known more like 'pseudo-network' created by entanglements of long-chain rigid polymers which may appear in highly concentrated solutions or in the molten state.

According to thermal, optical and mechanical properties, gels can be classified either as thermoreversible (mostly physical gels) or as thermoirreversible (chemical gels).[3] This categorization of gels is closely related to process called gelation (or sol-gel transition) defined as the appearance of a macroscopic object in the product.[1]

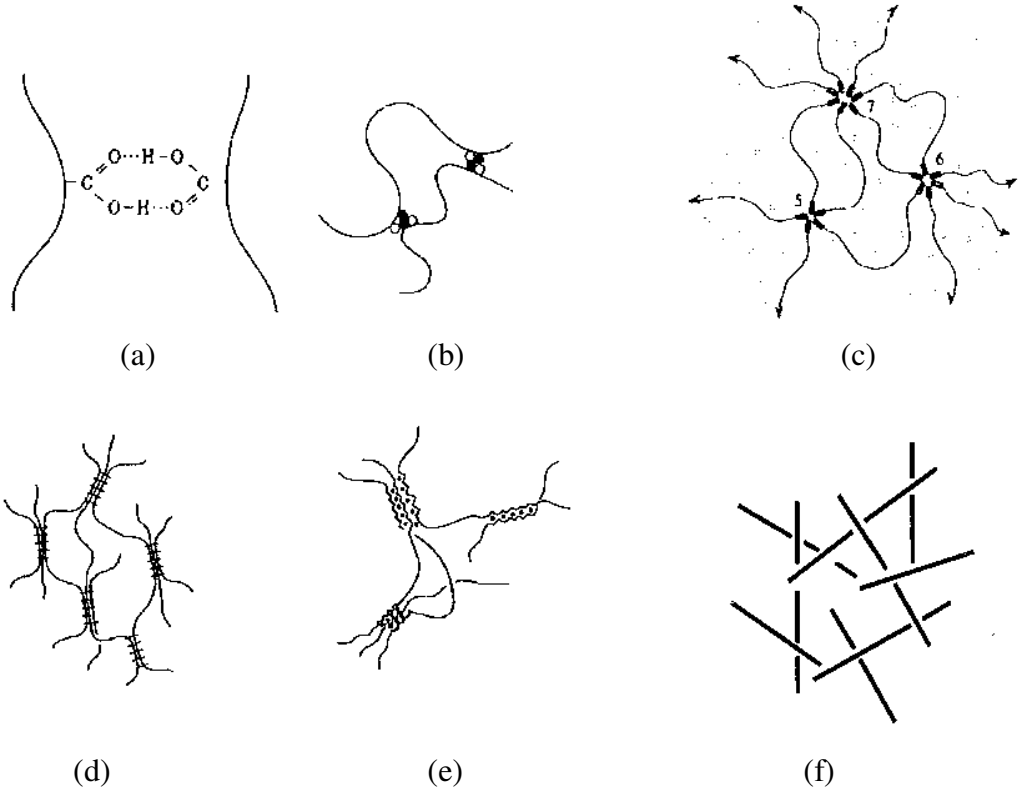

Figure 2.1 *Types of physical cross-links according to Tanaka's classification [1]: (a) hydrogen bonds, (b) dipole association, (c) micellar formation of hydrophobic groups, (d) microcrystalline junction, (e) ion association and complex formation, (f) entanglements of long rigid polymers.*

3. Hydrogels from ionotropic gelation

In recent years, there has been an increasing interest in hydrogels which are three dimensional hydrophilic polymer networks swollen with water or biological fluids. Their high water content and soft rubbery consistence make them suitable for medical and pharmaceutical applications, including the mimicking of biological tissues (biomimetic materials) or development of novel drug carriers.[4]

The ability of polymer chains to crosslink through ionic interactions is called ionotropic gelation.[4,5] The term ionotropy (*ionos* = ion, *trepein* = turn) was created by Heinrich Thiele [6] in 1964 and the phenomenon of ionotropic gelation was first observed for alginates and pectins (biopolymers) which undergo gelation upon addition of multivalent cations such as Ca^{2+}.

At atomistic level it can be interpreted as the formation of complexes, in which the crosslinking cations occupy a central position.[7] This kind of complex is observed for instance in alginate-Ca^{2+} hydrogels and identification of the atoms surrounding each calcium ion

(ligand atoms) is essential for elucidating the structure of the complex, leading to the determination of the calcium coordination number ($N_{Ca^{2+}}$) (Chapter IV).

4. Alginates: natural polymers containing (1→4)-α-L-guluronan sequences

Alginates are well-known natural polysaccharides mainly due to their high ability to form gels in the presence of calcium ions. Therefore, the knowledge of structure-property relationships of alginates plays an essential role in understanding the mechanism of gelation. On the other hand, this knowledge is also an important issue for their various biological functions and industrial applications.

4.1 Origin and chemical structure

Alginates were discovered in 1881 by the British chemist E.C.C. Stanford [8] and are also known as *alginic acid* or *algin*.[9] The main source of these natural polysaccharides is the cell wall of brown seaweeds (such as: *Laminaria hyperborea* or *Ascophyllum nodosum*) but they are also isolated from soil bacteria (*e.g. Azotobacter vinelandii* and *Pseudomonas species*). Additionally, bacterial alginates are usually partially acetylated (*O*-acetyl groups at C2 and/or C3 of M units).[10]

From the chemical point of view, alginates are linear unbranched copolymers composed of (1→4)-linked β-D-mannuronic acid (M) and α-L-guluronic acid (G) units (Scheme 2.1).

Haug *et al.* studies [11-13] on the partial acidic hydrolysis and fractionation of alginates gave the first information about the distribution of the monomers along the polymer chain. It was found that the two repeating units are distributed in long homopolymer blocks (*e.g.* MMMM or GGGG) and in shorter statistical or strictly alternating copolymer blocks (MGMG).

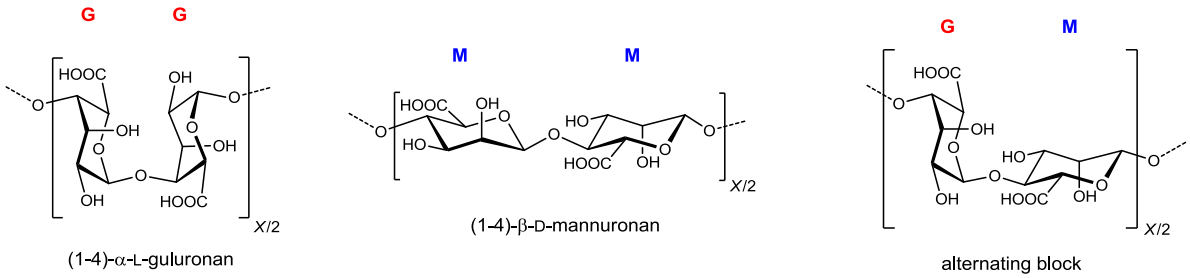

Scheme 2.1 *Structure of the three constituent blocks of natural alginate.*

Several attempts [14-17] have been made to describe in detail the crystalline structure of mannuronan and guluronan. X-ray fiber diffraction photographs of mannuronate-rich (96% of mannuronic acid) and guluronate-rich (73% of guluronic acid) alginates obtained by Atkins *et al.* [14] showed that M-units have $^4C_1$ ring conformation and are linked diequatorially while G-units contain diaxially linked sugar units with $^1C_4$ ring conformation. In the same study, it was also reported that the presence of mannuronic acid units in guluronate-rich samples does not impact on the X-ray diffraction pattern due to their low resolution. Mannuronan is a flat ribbon-like chain with a molecular repeat of 10.35 Å, and two β-D-mannuronic acid residues per unit cell. In contrast, guluronan has a rod-like conformation with a molecular repeat of 8.7 Å composed of two α-L-guluronic acid residues (Figure 2.2).

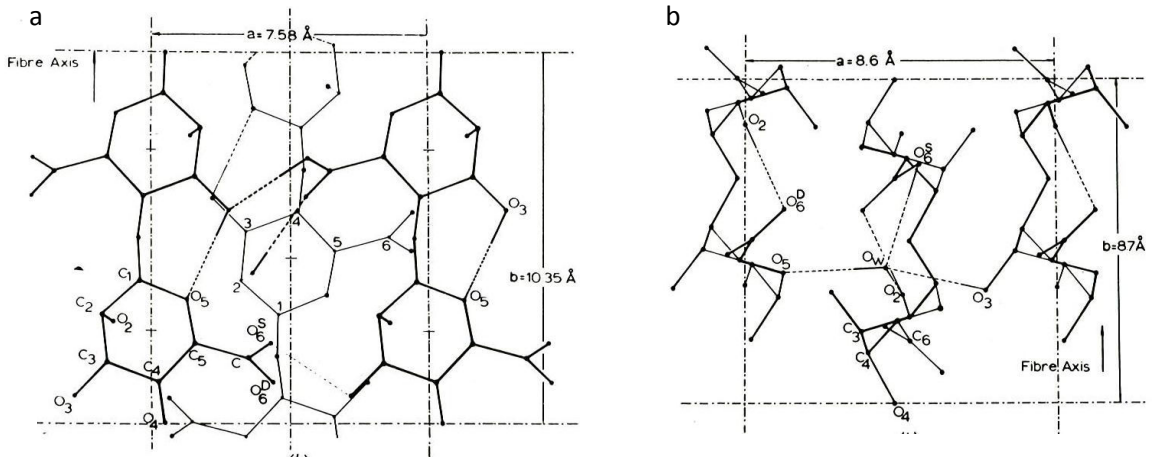

Figure 2.2 *Crystalline structure of polymannuronic acid (a) and polyguluronic acid (b) taken from Ref.* [15].

4.2 Physico-chemical properties of alginates in solution

In the native state, algal alginates occur as insoluble salt form of mixed counterions present in seawater (mostly Na^+, Mg^{2+} and Ca^{2+}).[18] In order to transform them into a water-soluble form, an extraction process followed by purification is required.

The origin of alginate, algae species (type and age), the season of harvest and also the extraction process strongly affect the molecular weight, composition (M/G ratio) and distribution of M and G units along the chain. These parameters play a critical role in the physico-chemical properties of alginates. For instance, the stripe and holdfast of *Laminaria hyperborea* from coastal area have a very high content of G-units resulting in high mechanical rigidity. By contrast, the leaves of the same algae from streaming water contain much less G-units and lead to a more flexible texture.[19,8]

4.2.1 Solubility

The solubility of alginates is strongly related to the pH and the ionic strength of the medium. It was found by potentiometric titration that the dissociation constants (pK_a) for mannuronic and guluronic acid units are 3.38 and 3.65, respectively, and are approximately the same for the alginate polymer.[8] However, at pH lower than pK_a, the precipitation of the polymer occurs due to loss of Columbic repulsion while a slow and controlled addition of protons may lead to acid gel formation. It was also reported that alginates with alternating sequences precipitate at lower pH values than homogeneous blocks (even at a pH = 1.4).[20] This phenomenon is based on the differences in the formation of aggregates by individual blocks: Homogeneous ones facilitate precipitation thanks to their stereoregularity. By contrast, in the case of heterogeneous blocks the level of disorder is higher so it is more difficult to form a regular structure.

The ionic concentration of the solution also plays an important role on solubility of alginates. For instance, at high ionic strengths due to high concentration of inorganic salts (*e.g.* KCl) alginate chains enriched in mannuronate residues tend to precipitate (salting-out effect).[21] Likewise, the 'hardness' of water (*i.e.* Ca^{2+} ions) may also affect the solubility of alginates: In general alginate can be solubilized in aqueous media containing concentrations of Ca^{2+} up to 3mM, whereas above that, the addition of a complexing agent (polyphosphates or citrate) is required.[8]

4.2.2 Stability

The degradation of alginates was investigated at different pH by Haug *et al.*[22] In this study, the change in the intrinsic viscosity of alginate extracted from *Laminaria digitata* was measured at 68°C as a function of pH. It was found that alginate solutions are stable around neutral pH. By contrast, in acidic conditions (pH < 5) the instability occurs due to proton-catalyzed hydrolysis, whereas in basic conditions (pH >10) the degradation of alginates is caused by a β-elimination reaction.

Detailed examination of the alkaline degradation of alginates was performed by the same research group.[23] This study has shown that the rate of degradation of alginate at pH values above 11 mainly depends on the ionic strength, presence of counter-ions such as: Na^+, Ca^{2+} or Mg^{2+} and the concentration of some specific anions. Generally, the higher the ionic strength the faster degradation occurs. Also, the rate of degradation increases when the ions with high tendency for ion pair formation are present. However, it was noticed that addition of sodium chloride to the solution containing Mg^{2+} decreases the rate of degradation due to ion exchange. The β-elimination reaction is a general base catalyzed reaction since it is catalyzed by hydroxyl ions but also by carbonate and phosphate ions. It is interesting to note that the rate of β-elimination is 10^4-10^5 times faster in the case of esterified alginates since the electron-withdrawing effect of the neutral carboxyl group at C6 increases the rate of abstraction of H5.

Furthermore, it has been shown that sterilization of alginate solutions and powders often leads to depolymerization, loss of viscosity and may also reduce the gel strength.[8] On the other hand, heating (autoclaving) of an alginate solution may also contribute to polymer breakdown. Nevertheless, for immobilisation purposes, sterilization has been recommended rather than autoclaving to preserve constant viscosity of the initial alginate solution.[24]

4.2.3 Ionic Selectivity

Alginate salts with monovalent counterions (except Ag^+) are soluble.[9] An important feature of these natural polysaccharides is the selective binding of divalent ions leading to formation of gels or precipitates. It was reported that the affinity of alginates to counterions decreased in the following order: [25]

$$Pb > Cu > Cd > Ba > Sr > Ca > Co, Ni, Zn > Mn >> Mg$$

Furthermore, the selective binding of alkaline earth metal ions (Ba, Sr, Ca, not Mg) is the basis of gel formation. It was found that the binding strength to G-blocks decreases in the order: Ba > Sr > Ca and is related to the ion dimension.[26] The binding of ions to the G-blocks is highly selective in contrast to M-blocks and alternating blocks (MG or GM) which are almost without selectivity.[8] Mørch *et al.* [27] characterized the effect of different alginates and cross-linking ions on forming the alginate microbeads (capsules). It has been shown that barium and strontium cause higher increase in stability and strength of microbeads incorporating G-rich alginate than calcium, which is in agreement with Haug *et al.* observations.[26] Additionally, this study demonstrated that different ions bind to different block structures. Thus, Ca^{2+} bind to G- and MG-blocks, Ba^{2+} to G- and M-blocks and Sr^{2+} to G-blocks only.[27]

4.2.4 Stiffness

Chain stiffness and extension can be defined according to the exponent *a* in the Mark-Houwink equation:

$$[\eta] = KM^{a} \qquad \text{(Eq. 2.1)}$$

where M is the molecular weight of the polymer, $[\eta]$ is the intrinsic viscosity and K and a are the constants depending on the nature of the polymer, solvent and temperature. For most flexible polymers, a is in the range of 0.5 to 0.8 whereas for semi rigid polymers $a > 0.8$ reaching the limiting value of 1.8 for rigid rod like polymers.[28] In addition, a-values were determined experimentally for dilute solutions of alginates by light scattering experiments. Smidsrød *et al.* [29] first examined an alginate sample containing 38.5% of G units in aqueous solution of 0.09 M NaCl and 0.01 M NaF and found the following parameters: $a = 0.98$ and $K = 2.44 \times 10^{-5}$. On the basis of light scattering and viscosity experiments, it was also demonstrated that the relative extension of the three types of sequences in alginate (at ionic strength 0.1 M) increases in the following order:[30]

$$MG < MM < GG$$

This finding was rationalized on the basis of different types of linkages between monosaccharide units (paragraph 4.1) in the alginate chain: Because of the diaxial linkages, guluronate blocks are stiffer than mannuronate and alternating blocks.

Furthermore, Mackie *et al.* [31] analyzed alginate samples with varying composition and observed that constant *a* was increasing for samples with higher content of G units while parameter *K* was decreasing. Thus, *K* and *a* parameters depend on the M/G ratio.

The chain extension of a polymer can be quantified by the characteristic ratio (C_∞) and the persistence length (l_p).[32] The characteristic ratio of the polymer chain is related to the Kuhn length (l_K) which is defined as a ratio of the mean square end-to-end distance $\langle R^2 \rangle$ and its fully extended size R_{max} according to: [33]

$$l_K = \frac{\langle R^2 \rangle}{R_{max}} \quad \text{(Eq. 2.2)}$$

Since the polymer backbone is composed of *N* bonds (N_b) of known bond length (l_b, which in the case of polysaccharides is related to the distance between consecutive glycosidic oxygen atoms), and the rotation around single bonds along the chain backbone is not always free, for instance due to steric repulsions between chemical groups present in consecutive repeating units, thus the mean square end-to-end distance ($\langle R^2 \rangle$) should be expressed as follows:[34]

$$\langle R^2 \rangle = N_b {l_b}^2 \ \frac{1-cos\theta}{1+cos\theta}\sigma^2 \quad \text{(Eq. 2.3)}$$

where θ is a valence angle between two bonds of length l_b, σ is the steric parameter and the term $\frac{1-cos\theta}{1+cos\theta}\sigma^2$ is called the characteristic ratio (C_∞).

Stokke *et al.* [35] predicted by molecular modeling a C_∞ value of about 70 for pure mannuronan, 100 for typical *Laminaria hyperborea* stripe alginate, 175 for pure guluronan and about 50 for a strictly polyalternating alginate.

In addition R_{max} is equal to:[34]

$$R_{max} = N_b l_b \ \sin\left(\frac{\theta}{2}\right) \quad \text{(Eq. 2.4)}$$

Thus, Eq. 2.2 can be written as:

$$l_K = \frac{l_b\, C_\infty}{sin\left(\frac{\theta}{2}\right)} \quad \text{(Eq. 2.5)}$$

However, as it was mentioned before, the chain extension can be also measured by the persistence length (l_p), which for semiflexible chains is equal to one half of the Kuhn length:[36]

$$l_p = \frac{1}{2} l_K \quad \text{(Eq. 2.6)}$$

For instance, Vold *et al.* [37] examined the persistence length for periodate oxidized alginates and found a decrease in persistence length with increasing degree of oxidation (from 15 nm to values below 4 nm at 44% oxidation).

4.2.5 Gelation

Alginates may form either acidic gels, or ionically crosslinked gels. The preparation of alginic acid gels is not trivial because the direct addition of a mineral acid to a Na-alginate solution usually leads to a precipitate, not to a homogeneous gel.[8] Since their applications are not very common, much more attention has been paid to ionic gels, which are formed upon addition of some divalent cations (*e.g.* Ca^{2+}, Ba^{2+}, Sr^{2+} and Zn^{2+}). The strong gelling behavior of alginate in the presence of Ca^{2+} has been mainly attributed to the (1→4)-α-L-guluronan sequences capable of binding Ca^{2+} in a cooperative fashion and to form junction zones. By contrast, it was suggested by Smidsrød that M-blocks and alternating blocks are almost without selectivity but the role of these sequences in the gelling process is not entirely clear.[38,37] Thus, Donati *et al.* [39] have attempted to study in detail the interactions between alternating MG-blocks and calcium ions (Chapter IV). It has been shown that alternating MG-blocks also bind calcium ions and may generate mixed GG/MG junctions as well as extended secondary MG/MG junctions. In these cases, the formed gels are much softer and more elastic due to the higher flexibility of MG-blocks.

The formation of stable junction zones is not only influenced by alginate composition (block structure) but also by its chain length, described by the degree of polymerization (*X*). Kohn *et al.* [40] investigated the effect of *X* of both α-L-guluronan and β-D-mannuronan by monitoring the variation of the activity coefficient of Ca^{2+} ($\gamma_{Ca^{2+}}$). In the case of calcium mannuronans, a steady decrease in $\gamma_{Ca^{2+}}$ up to $X \approx 30$ was observed, whereas calcium guluronnans revealed a sudden drop in $\gamma_{Ca^{2+}}$ in the *X* region 18 ~ 28. The latter result was interpreted as ~18 repeating units being necessary to have cooperative binding of Ca^{2+} ions. A more recent investigation by Stokke *et al.* [41] showed that ~8 repeating may be sufficient to form stable junction zones. Thus, the minimum number of repeating units in a (1→4)-α-L-guluronan block required for the formation of a stable complex with calcium ions is expected to lay in the range 8 to 18.

The mechanism of calcium complexation by alginate chains was first explained on the basis of the "egg-box" model proposed by Grant *et al.*[42], and later revisited by other

authors[43,44] (will be described in depth in Chapter IV together with the atomistic structure of the junction zones of Ca^{2+}-alginate gels). Morris *et al.* [45] suggested that the primary mechanism of interchain association is the dimerization of G-blocks. But, depending on the amount of calcium ions, the subsequent calcium binding to previously formed dimer may also occur, leading to either specific "half egg-box" binding (involving carboxylate groups on the exterior faces of the dimers), or further aggregation of dimeric junction zones (Figure 2.3).

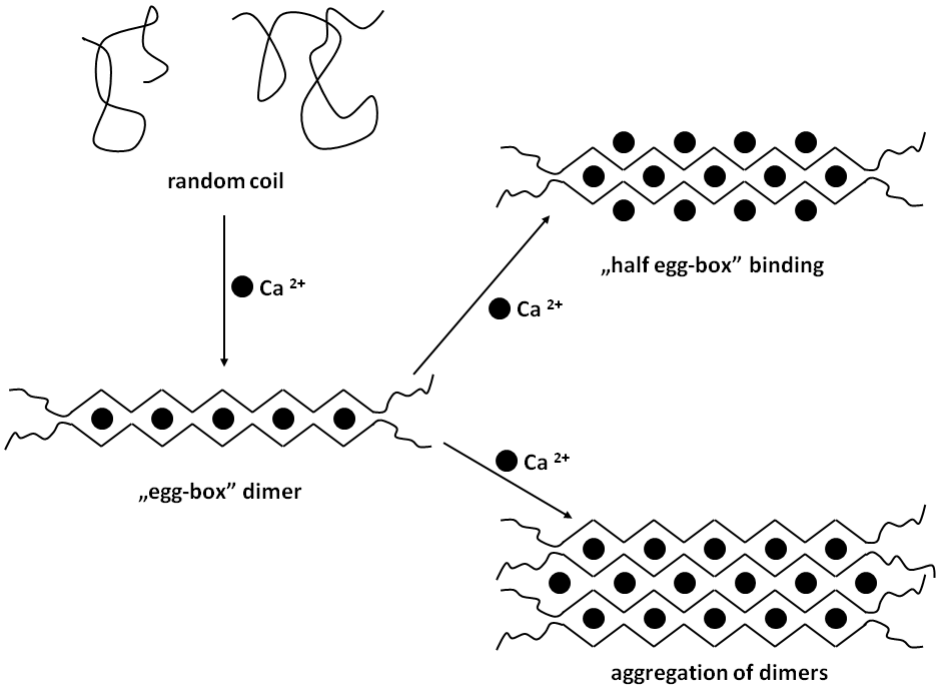

Figure 2.3 *Mechanism of calcium ions binding to G-blocks, proposed by Morris et al.*[45]

However, the regular structures hypothesized in this mechanism of gelation are unlikely to be observed experimentally since they are incompatible with a rapid gelation process. Therefore, gelation is considered rather as chain association (involving mainly G-blocks) in the presence of Ca^{2+} ions. Moreover, even if a germ of the primary gel network is formed fast; it is not tantamount with the end of the gelation process: As far as elastic segments with free G-blocks and free calcium ions are still present, the network will keep enlarging in size. Thus, it is important to highlight that the gelation of alginate solution is a multi-step process of slow association of the chains and should be rather illustrated as it is shown in Figure 2.4.

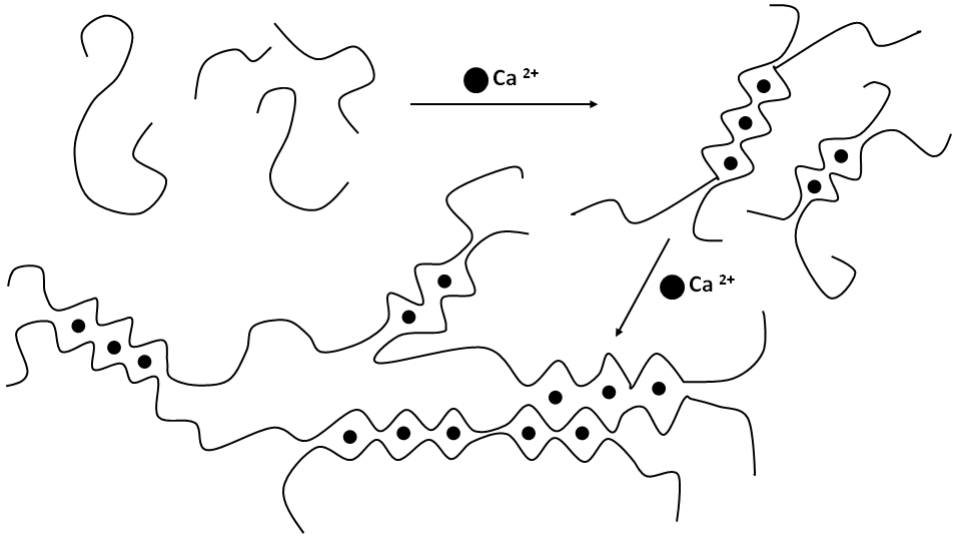

Figure 2.4 *Chain association of alginate solution involving G-blocks and calcium ions leading to gelation.*

Generally, the direct mixing of alginate with divalent cations does not lead to a homogeneous gel due to the rapid and irreversible binding of ions.[38] Indeed, in order to prepare a homogeneous alginate gel, a controlled and slow addition of Ca^{2+} is required. Alginate gels are usually formed by two methods: the diffusion method (called external gelation) and the internal setting method.

- In the *diffusion setting technique*, an alginate solution is either extruded or atomized into a large reservoir containing a cross-linking solution (usually calcium chloride), or it is dialyzed against the same. This method is characterized by rapid gelling kinetics and it is often used for immobilization purposes.[46] However, one drawback of this approach is that the obtained gels exhibit an inhomogeneous distribution of alginate and Ca^{2+}, with the highest concentration at the surface and a much lower one in the center of the gel.

- In the *internal gelation method*, an inactive form of the cross-linking cation is added into an alginate solution and slowly released over time. Thus, in the case of calcium ions, the insoluble ($CaCO_3$) or slightly soluble ($CaSO_4$) salt may be used or Ca^{2+} may be complexed by a chelating agent (*e.g.* EDTA).[8] The release of cross-linking cations is then induced by a change in pH following the addition of organic acids or lactones. In the case of Ca-EDTA, the pH has to be lowered to around 4.0. Normally, internal gelation of alginate gives a homogeneous gel. Although, a slight heterogeneity can be observed in $CaCO_3$-GDL (D-glucono-δ-lactone) gels containing low-viscosity alginate due to large particle size of the $CaCO_3$ in comparison with low viscous alginate.[47,48]

Besides the two common techniques described above, an ionic gel of alginate can be also formed by *cooling*.[49] In general, it is not trivial to obtain homogeneous gels especially at high calcium concentration but this approach seems to be suitable for that purpose. Papageorgiou *et al.* [50] proposed to mix an alginate solution with a sequestrant (*e.g.* trisodium citrate) and then with a calcium salt at 90 °C and to cool the resulting solution to 5 °C for 72 h. At high temperature, alginate chains have high thermal energy and their alignment is prevented. But upon slow and controlled cooling, homogeneous gels are obtained even for high calcium concentration and the formation of aggregates is prevented even at low calcium concentration.

As it was mentioned before, the physical properties of calcium alginate gels depend on the block composition as well as their length, but the content of G-residues also plays an important role, especially in the stiffness (paragraph 4.2.4) of gels. Additionally, the strength of the gel depends on both alginate and calcium concentration but also on the ionic concentration of the solution: Since alginates are anionic polymers, their dissolution in sodium chloride solution facilitates the formation of gels in comparison with aqueous solution. This is due to the fact that NaCl screens the electrostatic repulsion between charged chains resulting in easier intermolecular interactions and bridging by calcium ions.

4.3 Structure-property relationship

The properties of alginates or alginate gels are strongly related to their chemical structure. However, the utilization of natural alginates is limited by their chemical and macromolecular heterogeneity. Scientists have therefore attempted to modify and control the alginate chain composition in order to obtain desired properties.

For instance, it was found that *Azotobacter vinelandii* produces an enzyme called mannuronan C-5 epimerase which catalyses the conversion of M-units into G-units without breaking the glycosidic bond. Thus, it has enabled the tailoring of alginates and the obtainment of strictly alternating blocks (MG or GM) or very long G-blocks ($X > 100$).[19,51] This method provides the synthesis of different alginates of known sequential structure, facilitating better understanding their function and properties. On the other hand, this possibility of modifying the chemical structure of alginates in terms of their composition allows designing gels of desired strength.

The extension of alginate chains in solution can be also modified by periodate oxidation which is a method for providing additional flexibility to polysaccharides. Lee *et al.* [52] studied the chain stiffness of polyguluronate by determining the exponent *a* of the Mark-Houwink equation (Eq. 2.1) and the persistence length (Eq. 2.6) and concluded that oxidation reduced the chain stiffness. Further work by Vold *et al.* [37] also examined periodate oxidized alginates and revealed that oxidation has an influence on the persistence length (l_p), *i.e.* the higher degree of oxidation is, the shorter l_p is.

4.4 Applications

In general, most applications of alginates are based on their gel-forming ability. These natural polymers are commonly used as food additives in jams, jellies, fruit fillings, *etc.* to improve, modify and stabilize the texture of food.[19] Their thickening and gelling character plays also a role in pharmaceutical applications including islet (producing insulin) transplantation for treatment of type 1 diabets.[53] On the other hand, alginate dressings facilitate wound healing.[54] Alginate is also one of the most frequently used dental materials and has been a staple of most dental practices for many years.[55] Furthermore, alginate gels have been used as drug carriers and have found potential in bone regeneration and reparation of damaged cartilage.[54] Honeycomb alginate scaffolds with aligned pores have been fabricated and could be used as a tube like template for blood vessels.[56, 57]

Alginates have been extensively studied for cell transplantation and tissue engineering applications. However, utilization of natural alginates as a tissue engineering matrix in cell encapsulation and transplantation studies is limited due to weak interactions between cells and unmodified alginate.[58] Therefore, alginate blocks are incorporated into polymers as graft chains (paragraph 5) in order to improve their applications.

5. Biohybrid polymers featuring (1→4)-α-L-guluronan and/or (1→4)-β-D-mannuronan sequences

Polysaccharides are important natural polymers acting as structural materials (cell walls of plant cells) and as energy storage (in the form of starch and glycogen in plant cells or in the liver cells of animals, respectively). They are essential components of our food and the earliest known construction materials, in the form of wood.[59] However, wider applications of polysaccharides as materials require their chemical modifications (‘tailor-made’).

An intriguing way of doing that is the incorporation of these biopolymers into synthetic polysaccharide graft copolymers in order to bestow them with new physico-chemical properties according to our needs.

The design and preparation of alginate-derived polymers (biohybrid polymers or neo-alginates) possessing innovative and well-defined molecular architecture is an attractive goal to achieve, since they could combine the best of synthetic polymers (*e.g.* flexible design, determined composition, architecture and functionality) and polysaccharides (*e.g.* biodegradability) together with a capability of ionotropic gelation under mild conditions.

All polymers used for characterization in this PhD thesis have a synthetic polymeric backbone with grafted oligoalginate chains. Therefore, the literature overview on the synthetic-*graft*-polysaccharide is mainly focused on such kind of polysaccharide-based copolymers.

Basically, polysaccharide graft copolymers can have two types of structures: either a polysaccharide backbone with synthetic graft chains, or a synthetic backbone carrying oligo- or poly-saccharide grafted chains. In this study, the second structure was considered. In order to graft a polysaccharide chain onto a polymeric backbone the following strategies can be applied:

- *Grafting from* approach which is defined as growing of polysaccharide grafts directly from polymer backbone. The advantage of this approach is high density of grafting achieved by good access of the reactive groups to the chain ends of the growing polysaccharide grafts [60] (*e.g.* Pfannemüller and co-workers [61-63]).
- *Grafting to* (or *onto*) method which requires pre-modification of an end-functionalized polymer in order to bind them covalently with polysaccharides (*e.g.* reductive amination from polyamine). This technique usually leads to copolymers with low grafting density due to steric hindrance around functional groups.
- *Grafting through* (or *macromonomer*) approach where a polysaccharide macromonomer (or macromer), *e.g.* vinyl macromonomer of cellulose [60], is homo-or co-polymerized with a co-monomer (usually with a low molecular weight). This method is relatively convenient however it requires the synthesis of polysaccharide-derived macromonomers (*e.g.* Kobayashi *et al.* [64]).

Despite different grafting techniques, the synthesis of well-defined synthetic-*graft*-polysaccharide copolymers of controlled molar mass is not trivial: the limited availability of the polysaccharide reducing-end and the poor solubility of many polysaccharides in organic solvents are reflected in the low number of publications containing these copolymers.

Pioneering work on synthetic-*graft*-polysaccharide copolymers was undertaken by Pfannemüller and co-workers.[61-63] In this investigation, maltooligosaccharide-grafted polymers (with maltooligomeric grafts of DP ≤ 4) were synthesized first and their side chains were elongated to amylose chains of variable but uniform length by phosphorylase-catalysed enzymatic polymerization of α-D-glucose-1-phosphate (Glc-1-P) (*grafting from* method). During the whole process, a glucose unit is transferred from Glc-1-P to the nonreducing 4-OH end of a (1→4)-α-glucan chain leading to the direct formation of amylose with release an inorganic phosphate (P) (Eq. 2.7).

$$[(\alpha, 1\rightarrow4)\text{-Glc}]_n + \text{Glc-1-P} \leftrightarrows [(\alpha, 1\rightarrow4)\text{-Glc}]_{n+1} + \text{P} \qquad \text{(Eq. 2.7)}$$

Further studies have applied the same approach to a variety of synthetic polymer backbones. Hence, maltooligosaccharide-grafted poly(dimethysiloxane)s (PDMS)[65], poly(L-glutamic acid)[66], poly(styrene)s[64,67], poly(acetylene)s[68,69] and poly(vinyl alcohol)[70] were prepared by chemical reaction followed by transformation of maltooligosaccharide side chains to amylose by phosphorylase-catalysed enzymatic polymerization.

In a *grafting to* approach, polysaccharide chains can be grafted onto a backbone by reductive amination. For example, dextran was grafted on linear and branched poly(ethylene imine)s (PEI)s and it was found that some of the resulting polymers improve the stability of the DNA-polymer complexes.[71] Moreover, poly(L-lysine)-graft-dextran, obtained in a similar way was used as a carrier for genetic materials to target cells or tissue in antigenic strategy.[72,73] There are more such examples in the literature: poly(D,L-lactic acid) and poly(L-lysine)-graft-polysaccharide copolymers[74] or polyampholyte comb-type copolymers consisting of a poly(L-lysine) (PLL) backbone and hyaluronic acid (HA) side chains (PLL-graft-HA)[75], both well-known as good DNA carriers.

The *grafting through* approach was much less studied. Kobayashi *et al.* [64] examined a synthesis of amylose-carrying styrene macromonomers (vinylbenzyl amylose amide, VAA; degree of polymerization of amylose: X = 24, 40 or 150) by applying phosphorylase-catalysed enzymatic polymerization of α-D-glucose-1-phosphate (Glc-1-P) The prepared

macromonomers were either homopolymerized, or copolymerized with acrylamide by conventional radical polymerization in water/DMSO mixture to obtain polystyrene-*graft*-amylose and poly(VAA-*co*-acrylamide), respectively with $M_n \cong 2.0 \times 10^5$ Da. In this publication, it is also reported that polystyrene-*graft*-amylose can be synthesized by the radical homopolymerization of maltopentaose-substituted styrene (VM5A) followed by enzymatic elongation of amylose but no experimental details are given ($M_n = 1.2 \times 10^5$ Da and M_w / M_n ($Đ$) = 3.4).

In 2001 Narumi *et al.* [76] demonstrated the synthesis of styrene monomers with three types of saccharides (glucose, maltose and maltohexaose) which were then copolymerized with styrene by conventional radical copolymerization in dry *N,N*-dimethylformamide (DMF) at 60 °C with 2,2'-azobis(2-methylpropionitryle) (AIBN) as the initiator. The incorporation of saccharides led to amphiphilic materials.

Schultze *et al.* [77] claim in their patent the synthesis of many types of synthetic-*graft*-copolymers having polymeric backbone but the examples are given only for dextran-grafted polymethacrylates and polymethacrylamides prepared by oxime ligation in a grafting *to* or grafting *through* approach.

Yoshida *et al.* [78] homopolymerized acetylated 1-O-methacryloyl maltoheptaoside (MA-AcM7), by conventional radical polymerization in benzene solution with AIBN at 60 °C, to obtain polymethacrylates with pendant acetylated maltoheptaose in every repeating unit (poly(MA-AcM7)s) with $M_n = 1.1 \times 10^4$ Da – 15.4×10^4 Da after 24 – 120 hours. The same macromonomer was also copolymerized with methyl methacrylate (MMA) and the resulting poly(MA-AcM7-co-MMA)s had higher molar masses between $M_n = 11.4 \times 10^4$ Da and $M_n = 43.6 \times 10^4$ Da. The main aim of this work was to synthesize polymers having sulphated oligosaccharide side chains with specific biological activity (such as anti-HIV and blood anticoagulant activities). Thus, in order to have sulphated maltoheptaose side chains (poly-MA-SM7), the polymers were first deacetylated and then successfully sulphated with piperidine-*N*-sulfonic acid (PSA) or SO_3-DMF complex.

Coming to alginates, a patent by Mooney *et al.* [58] claims the grafting of (1→4)-α-L-guluronan onto: poly(vinyl alcohol), poly(2-aminoethyl acrylamide-*co*-acrylamide), poly(allylamine), poly(L-lysine), poly(4-aminomethylstyrene) and also hydrazido-modified poly (allylamine) by reductive amination (in the last example the (1→4)-α-L-guluronan with 25 repeating units, $X = 25$ was used). Additionally, hydrazido acrylate monomers were

coupled to G-block polyguluronate to form degradable hydrazone linkages which were reduced to more stable hydrazide linkages by sodium cyanoborohydride. The obtained monomers (alginate-derived monomers: AlgiMERs) were copolymerized by conventional radical polymerization either with: acrylic acid, acrylamide, methyl methacrylate (MMA), 2-hydroxyethylmethacrylate (HEMA), 2-hydroxypropylmethacrylamide (HPMA), allyl amine, dimethylallyl amine (by photoinduced free-radical polymerization), or with diallyldimethyl ammonium chloride and allyldimethyl ammonium chloride in aqueous solution with ammonium persulfate as an initiator. However, no characterization details and experimental procedures about the obtained materials were provided.

Recently, Ghadban *et al.* [79] demonstrated the synthesis of new synthetic-*graft*-alginate copolymers and described the gelation properties of two of them (a part of the ALGIMAT project). In this study, methacrylamide-functionalized (1→4)-β-D-mannuronan (X = 5, 10, 16) and (1→4)-α-L-guluronan (X = 20) macromonomers (AlgiMERs) were prepared via the reductive amination. The obtained macromonomers were then copolymerized by conventional radical copolymerization with 2-hydroxyethylmethacrylamide (HEMAm) in water at 60 °C with 4,4'-azobis-(cyanopentanoic acid) (ACPA) as the initiator. HEMAm was chosen as comonomer because it forms water soluble homopolymers which can be cross-linked to give highly hydrophilic copolymers.[80,81] Polymers carrying (1→4)-α-L-guluronan (X = 20) or (1→4)-β-D-mannuronan (X = 16) residues were dialyzed against $CaCl_2$ and afforded soft hydrogels, thus demonstrating the possibility for biohybrid glycopolymers to undergo ionotropic gelation.

6. Conclusion

Alginate-Ca^{2+} hydrogels are typical example of ionic gels, formed by the exchange between Na^+ and Ca^{2+} counterions. This simple and environmentally friendly method of gelation (incorporating natural polymers without using toxic organic solvents, under mild conditions) together with their original applications has warrant the importance of studying the physico-chemical properties of native alginates and alginate-derived polymers in solution (solubility, stability, ionic selectivity, stiffness and of course gelation).

Although, alginates are composed of only two types of repeating units: (1→4)-linked β-D-mannuronic acid (M) and α-L-guluronic acid (G), their properties vary with the origin of the biopolymer (algae species: type and age, the season of harvest and also the extraction

process) which strongly impacts on their: molecular weight, length, composition (M/G ratio) and the distribution of M and G units along the chain. Alginate solutions are stable at around neutral pH but their solubility is strongly related to the pH and the ionic strength of the medium. However, the most important feature of these natural polysaccharides is the selective binding of divalent ions usually leading to formation of gels. In general, alginates containing many (1→4)-α-L-guluronan sequences form rigid hydrogels in the presence of calcium ions. However, it is worth noting that the strength of alginate gels also depends on the block length, both alginate and cross-linking ion concentration but also on the composition of the aqueous solvent.

Furthermore, in this chapter an overview of synthetic-*graft*-polysaccharide copolymers, especially with regard to those copolymers which incorporate grafting of (1→4)-α-L-guluronan and/or (1→4)-β-D-mannuronan, is reported. Additionally, these polymers may be also suitable for hydrogel preparation with properties similar to natural alginates.

7. References

(1) Tanaka, F. Polymer Physics : Applications to Molecular Association and Thermoreversible Gelation Cambridge University Press: Cambridge, New York, 2011.

(2) De, G. P. G. Scaling Concepts in Polymer Physics; Cornell Univ. Press, 1979.

(3) Tokita, M.; Nishinari, K.; Editors Gels: Structures, properties, and functions: Fundamentals And Applications. [In: Prog. Colloid Polym. Sci., 2009; 136]; Springer GmbH, 2009.

(4) Patil, J. S.; Kamalapur, M. V.; Marapur, S. C.; Kadam, D. V. Digest Journal of Nanomaterials and Biostructures 2010, 5, 241.

(5) Patil, P.; Chavanke, D.; Wagh, M. Int. J. Pharm. Pharm. Sci. 2012, 4, 27.

(6) Thiele, H. Protoplasma 1964, 58, 318.

(7) Davis, T. A.; Volesky, B.; Mucci, A. Water Res. 2003, 37, 4311.

(8) Draget, K. I. Alginates in Handbook of Hydrocolloids; Woodhead Publishing Ltd.: Cambridge, 2000.

(9) Rinaudo, M. In Comprehensive Glycoscience; Johannis, P. K., Ed.; Elsevier: Oxford, 2007.

(10) Skjåk-Bræk, G.; Grasdalen, H.; Larsen, B. Carbohydrate Research 1986, 154, 239.

(11) Haug, A.; Larsen, B.; Smidsroed, O. Acta Chem. Scand. 1966, 20, 183.

(12) Haug, A.; Larsen, B.; Smidsroed, O. Acta Chem. Scand. 1967, 21, 691.

(13) Haug, A.; Smidsroed, O. Acta Chem. Scand. 1965, 19, 1221.

(14) Atkins, E. D. T.; Mackie, W.; Smolko, E. E. Nature (London) 1970, 225, 626.

(15) Atkins, E. D. T.; Mackie, W.; Parker, K. D.; Smolko, E. E. J. Polym. Sci., Part B 1971, 9, 311.

(16) Atkins, E. D. T.; Nieduszynski, I. A.; Mackie, W.; Parker, K. D.; Smolko, E. E. Biopolymers 1973, 12, 1865.

(17) Atkins, E. D. T.; Nieduszynski, I. A.; Mackie, W.; Parker, K. D.; Smolko, E. E. Biopolymers 1973, 12, 1879.

(18) Andriamanantoanina, H.; Rinaudo, M. Carbohydr. Polym. 2010, 82, 555.

(19) Draget, K. I.; Smidsrod, O.; Skjak-Braek, G., 2002; p 215.

(20) Haug, A.; Larsen, B. Acta Chem. Scand. 1963, 17, 1653.

(21) Haug, A. Acta Chem. Scand. 1959, 13, 1250.

(22) Haug, A.; Larsen, B.; Smidsroed, O. Acta Chem. Scand. 1963, 17, 1466.

(23) Haug, A.; Larsen, B.; Smidsroed, O. Acta Chem. Scand. 1967, 21, 2859.

(24) Leo, W. J.; McLoughlin, A. J.; Malone, D. M. Biotechnol. Prog. 1990, 6, 51.

(25) Haug, A. Acta Chem. Scand. 1961, 15, 1794.

(26) Haug, A.; Smidsroed, O. Acta Chem. Scand. 1970, 24, 843.

(27) Mørch, Y. A.; Donati, I.; Strand, B. L.; Skjaak-Braek, G. Biomacromolecules 2006, 7, 1471.

(28) Ghadban, A. PhD thesis, Université de Grenoble, 2012.

(29) Smidsrød, O.; Haug, A. Acta Chem. Scand. 1968, 22, 797.

(30) Smidsrød, O.; Glover, R. M.; Whittington, S. G. Carbohyd. Res. 1973, 27, 107.

(31) Mackie, W.; Noy, R.; Sellen, D. B. Biopolymers 1980, 19, 1839.

(32) Kristiansen, K. A.; Potthast, A.; Christensen, B. E. Carbohydr. Res. 2010, 345, 1264.

(33) Mark, J. E. Physical Properties of Polymers Handbook; Second Edition ed.; Springer, 2007.

(34) Elias, H.-G. An introduction to polymer science; VCH: New York, 1997.

(35) Stokke, B. T.; Smidsroed, O.; Brant, D. A. Carbohydr. Polym. 1993, 22, 57.

(36) Hsu, H.-P.; Paul, W.; Binder, K. Macromolecules (Washington, DC, U. S.) 2010, 43, 3094.

(37) Vold, I. M. N.; Kristiansen, K. A.; Christensen, B. E. Biomacromolecules 2006, 7, 2136.

(38) Draget, K. I.; Taylor, C. Food Hydrocolloids 2011, 25, 251.

(39) Donati, I.; Holtan, S.; Mørch, Y. A.; Borgogna, M.; Dentini, M. Biomacromolecules 2005, 6, 1031.

(40) *Kohn, R.; Larsen, B. Acta Chem Scand 1972, 26, 2455.*

(41) *Stokke, B. T.; Smidsroed, O.; Bruheim, P.; Skjaak-Braek, G. Macromolecules 1991, 24, 4637.*

(42) *Grant, G. T.; Morris, E. R.; Rees, D. A.; Smith, P. J. C.; Thom, D. FEBS Letters 1973, 32, 195.*

(43) *Braccini, I.; Perez, S. Biomacromolecules 2001, 2, 1089.*

(44) *Plazinski, W. J. Comput. Chem. 2011, 32, 2988.*

(45) *Morris, E. R.; Rees, D. A.; Thom, D.; Boyd, J. Carbohydr. Res. 1978, 66, 145.*

(46) *Smidsrød, O.; Skjaak-Braek, G. Trends Biotechnol. 1990, 8, 71.*

(47) *Draget, K. I.; Oestgaard, K.; Smidsroed, O. Carbohydr. Polym. 1991, 14, 159.*

(48) *Draget, K. I.; Moe, S. T.; Skjaak-Braek, G.; Smidsroed, O. Food Sci. Technol. (Boca Raton, FL, U. S.) 2006, 160, 289.*

(49) *Goh, C. H.; Heng, P. W. S.; Chan, L. W. Carbohydr. Polym. 2012, 88, 1.*

(50) *Papageorgiou, M.; Kasapis, S.; Gothard, M. G. Carbohydr. Polym. 1994, 24, 199.*

(51) *Aarstad, O. A.; Tøndervik, A.; Sletta, H.; Skjåk-Bræk, G. Biomacromolecules 2011, 13, 106.*

(52) *Lee, K. Y.; Bouhadir, K. H.; Mooney, D. J. Biomacromolecules 2002, 3, 1129.*

(53) *Soon-Shiong, P.; Heintz, R. E.; Merideth, N.; Yao, Q. X.; Yao, Z.; Zheng, T.; Murphy, M.; Moloney, M. K.; Schmehl, M.; Harris, M.; et, a. Lancet 1994, 343, 950.*

(54) *Lee, K. Y.; Mooney, D. J. Prog. Polym. Sci. 2012, 37, 106.*

(55) *Nandini, V. V.; Venkatesh, K. V.; Nair, K. C. J Conserv Dent 2008, 11, 37.*

(56) *Despang, F.; Dittrich, R.; Gelinsky, M., 2011; p 349.*

(57) *Yamamoto, M.; James, D.; Li, H.; Butler, J.; Rafii, S.; Rabbany, S. Tissue Eng., Part A 2010, 16, 299.*

(58) *Mooney, D. J.; Bouhadir, K. H.; Wong, W. H.; Rowley, J. A. In PCT; The regents of the University of Michigan: WO, 1998.*

(59) *Sen, G.; Sharon, A.; Pal, S., 2011; p 99.*

(60) *Roy, D.; Semsarilar, M.; Guthrie, J. T.; Perrier, S. Chem. Soc. Rev. 2009, 38, 2046.*

(61) *Andresz, H.; Richter, G. C.; Pfannemueller, B. Makromol. Chem. 1978, 179, 301.*

(62) *Emmerling, W. N.; Pfannemueller, B. Makromol. Chem. 1978, 179, 1627.*

(63) *Ziegast, G.; Pfannemueller, B. Carbohydr. Res. 1987, 160, 185.*

(64) *Kobayashi, K.; Kamiya, S.; Enomoto, N. Macromolecules 1996, 29, 8670.*

(65) *von, B. V.; Jonas, G.; Stadler, R. Macromolecules 1995, 28, 17.*

(66) *Kamiya, S.; Kobayashi, K. Macromol. Chem. Phys. 1998, 199, 1589.*

(67) *Narumi, A.; Kawasaki, K.; Kaga, H.; Satoh, T.; Sugimoto, N.; Kakuchi, T. Polym. Bull. (Berlin, Ger.) 2003, 49, 405.*

(68) *Sasaki, Y.; Kaneko, Y.; Kadokawa, J.-i. Polym. Bull. (Heidelberg, Ger.) 2009, 62, 291.*

(69) *Kadokawa, J.-i.; Nakamura, Y.; Sasaki, Y.; Kaneko, Y.; Nishikawa, T. Polym. Bull. (Heidelberg, Ger.) 2008, 60, 57.*

(70) *Kaneko, Y.; Matsuda, S.-i.; Kadokawa, J.-i. Polym. Chem. 2010, 1, 193.*

(71) *Tseng, W.-C.; Jong, C.-M. Biomacromolecules 2003, 4, 1277.*

(72) *Maruyama, A.; Watanabe, H.; Ferdous, A.; Katoh, M.; Ishihara, T.; Akaike, T. Bioconjugate Chem. 1998, 9, 292.*

(73) *Ferdous, A.; Watanabe, H.; Akaike, T.; Maruyama, A. J. Pharm. Sci. 1998, 87, 1400.*

(74) *Maruyama, A.; Ishihara, T.; Kim, J.-S.; Kim, S. W.; Akaike, T. Bioconjugate Chem. 1997, 8, 735.*

(75) *Asayama, S.; Nogawa, M.; Takei, Y.; Akaike, T.; Maruyama, A. Bioconjugate Chem. 1998, 9, 476.*

(76) *Narumi, A.; Kaga, H.; Kawasaki, K.; Taniguchi, Y.; Satoh, T.; Kakuchi, T. J. Polym. Sci., Part A: Polym. Chem. 2001, 39, 4061.*

(77) *Schultze, X.; Dublanchet, A.-C.; Hernandez, F.; L'Oreal, Fr. . 2010.*

(78) Yoshida, T.; Akasaka, T.; Choi, Y.; Hattori, K.; Yu, B.; Mimura, T.; Kaneko, Y.; Nakashima, H.; Aragaki, E.; Premanathan, M.; Yamamoto, N.; Uryu, T. J. Polym. Sci., Part A: Polym. Chem. 1999, 37, 789.

(79) Ghadban, A.; Albertin, L.; Rinaudo, M.; Heyraud, A. Biomacromolecules 2012, 13, 3108.

(80) Rijcken, C. J. F.; Veldhuis, T. F. J.; Ramzi, A.; Meeldijk, J. D.; van, N. C. F.; Hennink, W. E. Biomacromolecules 2005, 6, 2343.

(81) Rijcken, C. J.; Snel, C. J.; Schiffelers, R. M.; van, N. C. F.; Hennink, W. E. Biomaterials 2007, 28, 5581.

Chapter III:

Investigation techniques

Table of contents

1. Introduction

This chapter gives a brief description of the investigation techniques (such as Molecular Modeling, Atomic Force Microscopy (AFM), Light Scattering (LS) and Rheology) applied in this PhD project.

2. Molecular modeling

Pensak [1] defined modern molecular modeling as *"anything which is done to depict, describe or evaluate any aspect of the properties or structure of a molecule that requires the use of a computer"*. Thus, the main goal of computer simulations of molecular system is to compute macroscopic properties from microscopic interactions.[2] In order to achieve this goal we must go through a multi-step process (Scheme 3.1), in fact not so different from doing experimental chemistry.

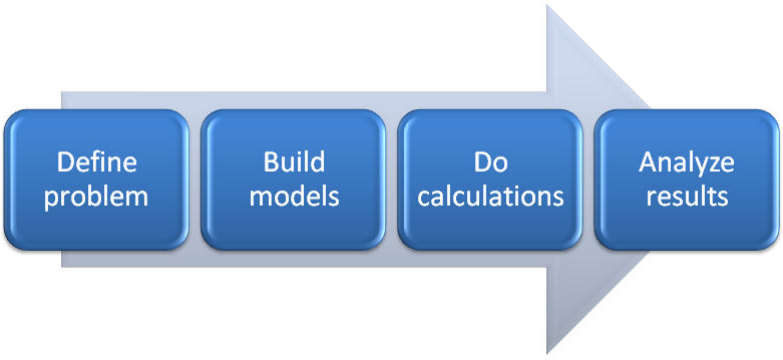

Scheme 3.1 *Molecular modeling as a multi-step process.*

Molecular modeling is a tool which enables calculating the energy of a given molecular structure. In general, three main approaches have been developed to compute the energy of a molecule: Quantum Mechanics (QM), semi-empirical and empirical (also called Molecular Mechanics - MM) methods.

Although molecular modeling may never replace experimental chemistry, it is a tool which helps to interpret, understand and predict experimental results. Therefore, it plays an essential role in establishing of the structure-property relationships.

2.1. Ab-initio Quantum Mechanics (QM)

In Quantum Mechanics approach, which is usually applied for small molecular systems, molecules are composed of nuclei and electrons and the energy is computed in terms of motions of electrons by solving the Schrödinger equation:

$$\left(\underbrace{\frac{-h^2}{8^2 m}\nabla^2}_{\text{kinetic energy}} + \overbrace{V(x,y,z)}^{\text{potential energy}}\right)\underbrace{\psi\,(x,y,z)}_{\text{wavefunction}} = \overbrace{\mathrm{E}}^{\text{total energy}}\,\psi\,(x,y,z) \qquad \text{(Eq. 3.1)}$$

However, this equation can be only solved for a one-electron system (*e.g.* the hydrogen atom) which is not really useful. Therefore, for a multinuclear and multielectron system, it has been generalized to the following equation:

$$\hat{\mathrm{H}}\,\Psi = \mathrm{E}\,\Psi \qquad \text{(Eq. 3.2)}$$

where $\hat{\mathrm{H}}$ is the Hamiltonian operator and Ψ is the many-electron wavefunction. Nevertheless, it is not possible to solve the Schrödinger equation for multielectron systems, thus some approximations are needed. Firstly, the Born-Oppenheimer approximation assumes that nuclei do not move (their movement is very slow in comparison with electrons so it can be neglected). Then, the Hartree-Fock approximation separates electron motions and considers that every electron is moving within an average field of all the other electrons.[3] But, since molecules are composed of many atoms, the description of electronic motion in the whole molecule is needed, not only electronic motion in atoms. Therefore, the Linear Combination of Atomic Orbitals (LCAO) approximation was developed in order to calculate molecular orbitals which give information about the molecular structure as well as bonding. Here, it is worth noting that different approximations lead to different results. Thus, the set of used approximations should be specified according to analyze molecular properties.

2.2. Molecular Mechanics (MM)

2.2.1 Potential energy function

Molecular Mechanics considers a molecule as a system composed of rigid balls (corresponding to the atoms) connected via springs (the bonds)[4] (Figure 3.1). In this concept, the energy of the molecule depends on bond stretching, angle bending, dihedral twisting (called bond terms) as well as non-bonded van der Waals and Coulombic interactions (Figure 3.2).

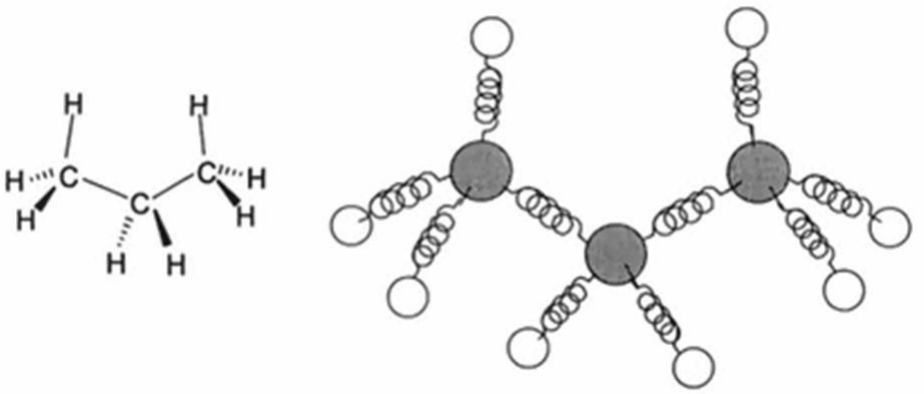

Figure 3.1 *Molecular Mechanics (MM) description of propane as a collection of balls (the atoms) held together by springs (the bonds) taken from Ref.* [4].

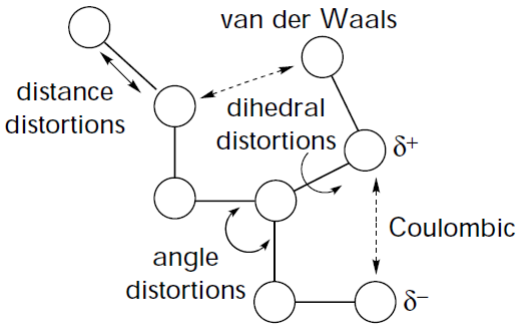

Figure 3.2 *Different types of distortions and interactions determining the geometry of a molecule and its energy taken from Ref* [5].

The energy of the molecule is often called "strain energy" because it reflects the "strain" inherent to a "real" molecule relative to some idealized form [3] and can be written as following (Eq. 3.3):

$$E^{strain} = \sum_{A}^{bonds} E_A^{stretch} + \sum_{A}^{\substack{bond\\angles}} E_A^{bend} + \sum_{A}^{\substack{torsion\\angles}} E_A^{torsion} + \sum_{A}\sum_{B} E_{AB}^{non-bonded} \qquad \text{(Eq. 3.3)}$$

Stretch and bend terms are given on the basis of Hook's law (Eq. 3.4 and Eq. 3.5).

$$E_{stretch}(r) = \frac{1}{2}\, k_{stretch}\, (r - r_0)^2 \qquad \text{(Eq. 3.4)}$$

$$E_{bend}(\alpha) = \frac{1}{2}\, k_{bend} (\alpha - \alpha_0)^2 \qquad \text{(Eq. 3.5)}$$

r and α correspond to actual bond length and bond angle, respectively, while r_0 and α_0 values are defined for the hypothetical (unstrained) model with an ideal geometry, taken either from

experimental data or from QM calculations. Additionally, $k_{stretch}$ and k_{bend} are the bond-stretching and angle-bending force constants, respectively.

$E_{torsion}$ term corresponds to torsional motion related to the rotation around single bonds and is shown in Eq. 3.6

$$E_{torsion}(\omega) = k_{\omega}\left(1 + cos(n\omega - \omega_0)\right) \quad \text{(Eq. 3.6)}$$

where k_ω is the torsional barrier, ω is the actual torsional angle, ω_0 is the reference torsional angle and n is the periodicity (number of energy minima during a full cycle).

Besides bonded terms, the non-bonded interactions are composed of van der Waals (VDW) and Coulombic interactions. The van der Waals interactions are usually represented by a Lennard-Jones potential as a sum of repulsive and attractive terms (Eq. 3.7),

$$E_{VDW}(r) = \sum_{A,B}\left(\frac{C_{12}}{r^{12}} - \frac{C_6}{r^6}\right) \quad \text{(Eq. 3.7)}$$

where C_{12} is the repulsive term coefficient, C_6 is the attractive term coefficient and r is the distance between the atoms A and B.

On the other hand, the Coulombic term describes the electrostatic interactions of charges (Q) (Eq. 3.8).

$$E_{Coulombic}(r) = \frac{1}{\varepsilon}\frac{Q_A Q_B}{r} \quad \text{(Eq. 3.8)}$$

The atomic charges (Q) can be either treated as parameters, or be taken from QM calculations. In addition, r is the non-bonded distance and ε is the dielectric constant.

The Molecular Mechanics model ignores electrons and considers bonding as "part of input" in contrast to QM, where bonding is "part of output".[3] In general MM may be performed easily on molecules composed of several thousands of atoms. Additionally, it gives a chemically reasonable picture of molecular structure, including conformational analysis which is perhaps the most important application of this method.

2.2.2 *Force Fields (FFs) – empirical approximations*

Simulation methods rely on a set of parameters, determined experimentally or by quantum mechanical calculations, called Force Fields (FFs). Each force field defines a set of atom types (called Force Field Atom Types) with the whole characteristic such as name, mass, parameters of bonding as well as VDW and Coulombic interactions and charges. It is

worth noting that a force field is usually designed for a specific group of molecules such as proteins, carbohydrates, *etc.* Thus, in order to perform any simulations, chosen force field must represent each atom in the system and contain the set of equations and parameters (such as force constants) required to calculate the potential energy and forces of analyzed molecular system. A great variety of force fields exists but the choice of the most appropriate force field strongly depends on the molecular property which is computed, the required accuracy and the availability of computing power.[2]

2.2.3 Energy minimization (EM)

In general, a potential energy surface contains many local minima and a global minimum. So far, no practical minimization method exists that guarantees the determination of the global minimum. Therefore, the energy minimization is defined as optimization of the system to the nearest local minimum (Figure 3.3).

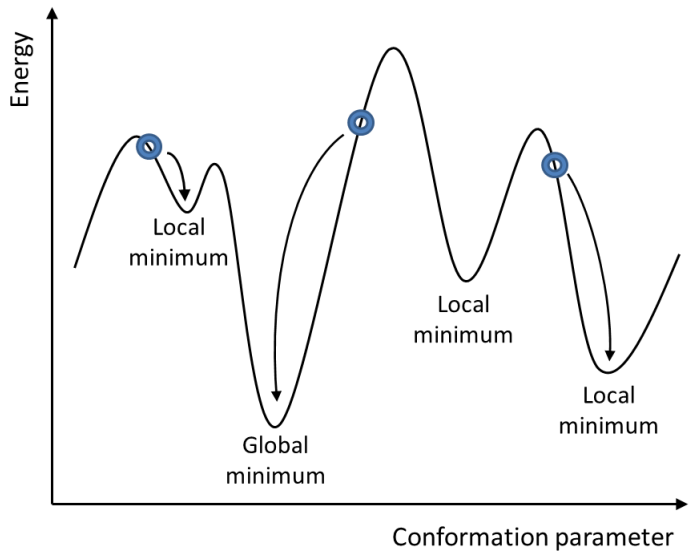

Figure 3.3 *Potential energy vs. displacement of conformation parameter illustrating many local minima and one global minimum.*

Most energy minimizations are achieved by applying the steepest descent method and/or the conjugate gradient method. The steepest descent algorithm first calculates the initial forces F_i (Eq. 3.10) of all atoms in the system and the potential energy for initial geometry. Then, the atoms are moved in a small increment in the direction of decreasing energy and new positions of atoms are calculated. The process stops when a predetermined threshold condition is fulfilled (*i.e.* number of force evaluations defined by user). This method is preferable especially for structures which are far from a minimum. On the other hand, the

conjugate gradient method applies the same parameters and stop criterion which are used for steepest descent. On one side, the conjugate gradient method is slower in the early stages of the minimization but on the other one more efficient close to the energy minimum. In practice (in order to complete the minimization process), both algorithms are used: the steepest descent algorithm being followed by the conjugate gradient method. The choice of the minimization method depends on two factors: the size of the system and the current state of the optimization.

2.2.4 Molecular Dynamics (MD)

The first molecular dynamics simulation was performed in 1957 by Berni Alder and Tom Wainwright [6] who studied the phase transition for molecules represented as "hard spheres". Molecular Dynamics is any molecular simulation method which computes the motions of individual molecules.[7] The goal of energy minimization (EM) is to optimize structure (as it was mentioned before), while the aim of Molecular Dynamics (MD) is to simulate the actual changes in the (macro)molecular system as a function of time. Basically, the task of MD is to explore the conformational space, in contrast to EM which optimizes the system to the nearest local minimum.

From a mathematical point of view, MD simulations solve Newton's equations of motions for a system composed of *N* interacting atoms (Eq. 3.9):

$$m_i \frac{\partial^2 r_i}{\partial t^2} = F_i \,, \; i = 1, \ldots, N \qquad \text{(Eq. 3.9)}$$

where the forces (F_i) are the negative derivatives of a potential function $V(r_1, r_2, \ldots, r_N)$:

$$F_i = -\frac{\partial V(r_1, r_2, \ldots, r_N)}{\partial r_i} \qquad \text{(Eq. 3.10)}$$

In practice, the equations are solved in small time step under required conditions (paragraph 2.2.4.1) and the coordinates are saved as a function of time in a trajectory file, from which a variety of properties can be calculated.

2.2.4.1. Molecular Dynamics Ensembles

The "natural" ensemble for MD is the microcanonical ensemble: NVE (constant number of particles, constant volume and constant energy). However, typical simulations are performed under constant temperature and/or constant pressure. Therefore canonical ensembles such as NVT (constant number of particles, constant volume and constant

temperature) and NPT (constant number of particles, constant pressure and constant temperature) exist. In order to maintain constant temperature and/or constant pressure near a desired setpoint, the thermostat and/or barostat approaches available in the softwares are applied. For instance in GROMACS [8], temperature coupling is usually achieved by applying either the Berendsen algorithm, which slowly corrects the deviation of the system temperature from desired value, or the velocity rescaling thermostat which additionally generates a correct distribution of the kinetic energy. Furthermore, the correct average pressure may be ensured by the Berendsen algorithm which scales the coordinates and box vectors every step until the desired value. In fact, controlling the temperature and/or the pressure of the system allows avoiding drifts in the desired values which may affect the obtained results.

2.2.4.2. *Benefits and limitations of MD*

One major advantage of MD calculations is the continuous motion provided during the whole simulation time. However, care should be taken about the accuracy of the applied force field as well as the adequacy of the time and size scales, explored especially for biological processes. For instance, the nitric oxide (NO) rebinding to myoglobin takes tens of picoseconds whereas protein folding may take minutes.[9]

2.2.4.3. *Water models*

Most chemical experiments are not performed in the gas phase but rather in solution. Basically, solvation can be treated either explicitly or implicitly:

- In the *explicit approach* a molecule (the solute) is immersed in a box containing a large but finite number of solvent molecules. This allows estimating the specific solvent-solute and solvent-solvent interactions but also the effect of bulk solvent. One major disadvantage of this approach is computational cost and the great variety of existing models.

- On the other hand, in the *implicit approach* the specific solvent-solute interactions are replaced by an average field. In this way, the electrostatic effects of solvent molecules are more easily represented and the equilibration of water molecules around the solute is not required, thus reducing computational time.

Selecting the proper approach mainly depends on the type of interactions deemed to be of importance. For carbohydrates, the explicit solvation is preferable, due to possibility of interactions between numerous hydroxyl groups (present in carbohydrates) and water

molecules. MD simulations performed in aqueous solution usually incorporate the Simple Point Charge (SPC) water molecules. This model is often applied because the SPC water molecules are able to move fast due to the missing two lone electron pairs.

2.2.4.4. *Periodic Boundary Conditions (PBC)*

As it was mentioned in paragraph 2.2.4.3, explicit solvation requires an additional computational effort. In order to reduce the computational workload and to minimize edge effects in a finite system, the (macro)molecular system is generated in a small volume *V* (the primary cell) and the periodic boundary conditions (PBC) (Figure 3.4) are applied during MD simulations. This approach involves the generation of (macro)molecules in a small volume *V* (the primary cell) and in the replication of the primary cell in all directions, thus giving the picture of an infinitely large system. It is worth noting that the image cells do not have only the same size and shape but also contain particles that are images of the particles in the primary cell. In addition, the cells are separated by open boundaries, so the particles can easily move between all cells facilitating the natural motion of the system.[10]

In order to reduce the instabilities in energy, some cut-off schemes are quite often applied. In these schemes, particles in the system can only interact either with the closest periodic image of other particles (called minimum image), or with particles present in a sphere of radius $R_{cut\text{-}off}$ (Figure 3.4).

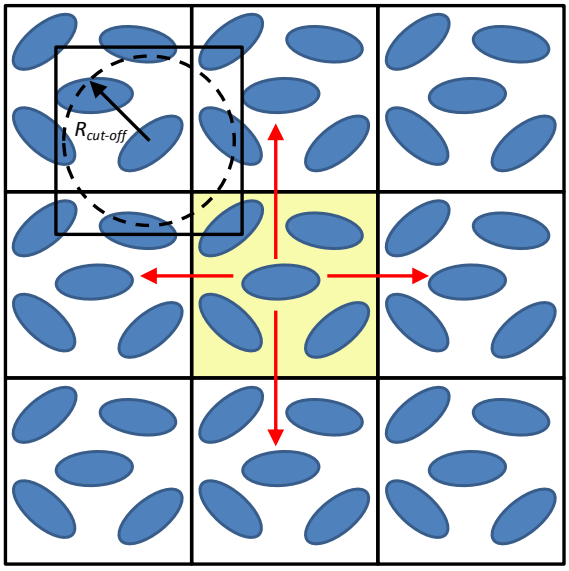

Figure 3.4 *Periodic Boundary Conditions (PBC) in two dimensions with the primary cell (yellow one) surrounded by its images. The minimum image and spherical cut-off are also shown.*

3. Atomic Force Microscopy (AFM)

Atomic Force Microscopy (AFM), also called Scanning Force Microscopy (SFM), was invented by Binnig *et al.*[11] in 1986 and covers a wide range of Scanning Probe Microscopy (SPM) techniques. Gerd Binnig and Heinrich Rohrer have received the Nobel Prizes in Physics for this invention.

In the beginning, AFM was mainly known as a nanoscale imaging technique useful for describing the topography of solid surfaces at high resolution.[12] However, this method has evolved into more sophisticated measurements like force interactions in liquid environment at the nanonewton and piconewton scale.[13] For instance, it has been extensively used to characterize a wide range of biomolecules, even biological cells or tissues [14] and in recent years, there has been an increasing interest in force measurements (FM) providing information about intermolecular interactions.

In a typical AFM measurement, the sample is scanned by a sharp tip (probe) which is mounted to the cantilever spring (Figure 3.5). In order to obtain the topographic image of the sample, one of the following scanning mechanisms is applied: [15]

- '*Constant-force mode*', *i.e.* constant cantilever deflection which is maintained by adjustment of the height of the sample by varying the voltage applied to the *z* position of the 3D piezoelectric scanner onto which it is mounted. Thus, the topography signal is obtained by the vertical movement of the scanner in the *z*-direction.
- In the '*variable-deflection mode*' or '*constant-height mode*' the signal is registered by measuring the cantilever deflection which is proportional to the change in the tip-sample interaction.

In practice, the deflection of the cantilever *vs.* its position on the sample is monitored by an optical detector, in which a laser beam is focused directly over the tip and then reflected off to give a spot onto a photodiode detector. The photodiode (Figure 3.5) is split into four segments (A, B, C and D). The difference in laser intensity between segments (A+B)-(C+D) corresponds to the motion of the tip perpendicularly to the long cantilever axis which gives topographical data [15], whereas the (A+C)-(B+D) signal is observed following a lateral or twisting motion of the tip, which provides frictional information related to lateral forces.[14]

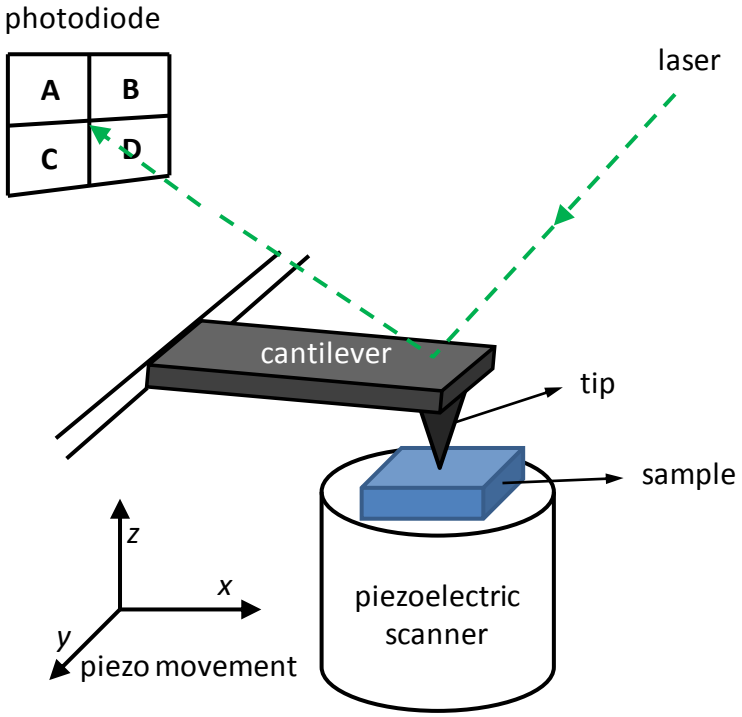

Figure 3.5 *Typical AFM setup. The photodiode is split into four segments. (A+B)-(C+D) corresponds to the motion of the tip perpendicularly to the long cantilever axis which gives topographical data [15], whereas the (A+C)-(B+D) signal is observed due to lateral or twisting motion of the tip, providing frictional information which is related to lateral force.*[14]

3.1 Tips and cantilevers

The tip is sometimes considered as the heart of AFM because it interacts with the sample. The cantilever-tip assembly (Figure 3.6) is generally made of silicon or silicon nitride due to their hardness and wear resistance.[14] On the other hand, tips and cantilevers are often coated with another material, which can be a conductor or an insulator. For instance, in order to monitor cantilever deflection, they are coated with a thin aluminium layer to improve their reflectivity.[14] Manufactured cantilevers can have two basic geometries:

- *triangular*, known as '*V-shape*' which was designed to minimize twisting of the cantilever during scanning process
- *rectangular* with a greater degree of rotational freedom which is used to measure the frictional properties of a sample and lateral forces.

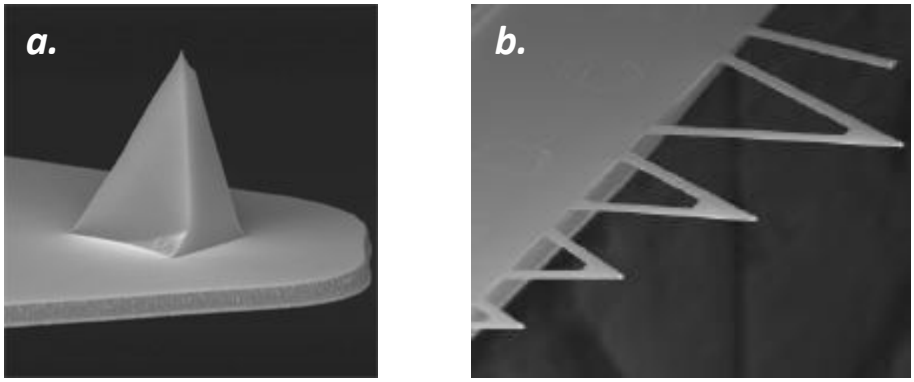

Figure 3.6 *AFM cantilever-tip assembly (a), model: MSNL-10 produced by Brucker made of silicon nitride, back side coated with reflective gold and top layer back with 45 ± 5 nm of Ti/Au. Both triangular and rectangular geometries of cantilevers are shown (b).*

Irrespective of geometry, the force contribution (F) can be estimated from the bending of the cantilever by multiplying the deflection of the cantilever (z_c) with its force (or spring) constant k:

$$F = k \cdot z_c \qquad \text{(Eq. 3.11)}$$

The spring constant can be calculated either from Eq. 3.11 or from equations defined according to the geometry of the cantilever. For instance, for a cantilever with a rectangular shape of width w, length L and thickness t, k is expressed as follows: [12]

$$k = \frac{F}{z_c} = \frac{Ewt^3}{4L^3} \qquad \text{(Eq. 3.12)}$$

where E is the Young's modulus of the cantilever material.

It is worth noting that the thickness of cantilevers (typically 1-2 μm) may vary a lot (10-20%), especially for modified tips (paragraph 3.4.1), so it is difficult to measure it precisely. However, numerous techniques to measure the spring constant of cantilever independently of its material or coating have been developed [16] in order to overcome this problem.

In general, k increases with cantilever thickness but decreases with its length. Therefore, longer cantilevers are more sensitive, so shorter ones are more applicable for imaging rough samples. Furthermore, cantilevers have also defined resonance frequency which should be at least ten times higher than the fastest scan speed to provide good quality of images.

Interestingly, recent developments have shown that the AFM tips can be also modified (functionalized) in order to investigate particular types of tip-sample interactions (Chapter V).

3.2 Sample preparation

In general, samples for AFM imaging in the air are prepared by the deposition of the solution to analyze on atomically flat substrates such as silicon wafer or mica. In the case of silicon wafer, the substrate is first cleaned by a piranha solution (*i.e.* mixture of strong acid such as sulfuric acid (H_2SO_4) with hydrogen peroxide (H_2O_2) in a 3:1 proportion) at 80°C for 2 hours in order to remove organic contaminants and create a high hydroxyl group density, followed by extensive rinsing with deionized water. On the other hand, mica is mounted on a small metal disc by double sided adhesive tape in order to prevent movement during imaging. It is then cleaved by normal tape and the solution can be directly deposited on the newly formed mica surface. AFM imaging in the air requires dried samples, which are usually obtained by leaving them in a desiccator (over silica gel) at least for one night (depending on the sample).

AFM in liquid solution can be also performed. But, in that case, a liquid cell is needed to provide a stable optical path for the laser beam which is reflected off the back of the cantilever.[14]

3.3 Surface forces and imaging modes

As it's name suggests, Atomic **Force** Microscopy is based on the forces arising between the tip and the surface of the sample. In general, the intermolecular surface forces can be interpreted in terms of basic interactions such as: van der Waals, electron donor-acceptor (hydrogen bonding) as well as electrostatic interactions.[17] As it was mentioned before (paragraph 2.2.1), van der Waals interactions are defined by a Lennard-Jones function (Eq. 3.7), whereas the electrostatic or Coulombic forces which appear in ionic bonds can be determined from Eq. 3.8. It is worth noting that at relatively large separations (few hundred of nm) the force between the tip and the sample is almost equal zero, while as the separation is reduced the force rises rapidly [14] (Figure 3.7).

In general, at short distances, the very short range (≈ 0.1 nm) Born repulsive forces and the longer-range (up to 10 nm) van der Waals forces are occurring.[15] In that case, the repulsive forces are predominant because the tip and the sample are close to each other (they are 'in contact'). Thus, in order to examine such kind of surface interactions the contact mode is applied. In principal, *contact or DC mode* records the static deflection of the cantilever so it is also called static or *constant force mode*. This mode is the easiest one to use and is

especially recommended for inexperienced users: the tip is brought into direct contact with the surface of the sample and the cantilever deflection is kept constant during scanning. Image contrast depends on the applied force which is related to the cantilever spring constant *k* (paragraph 3.1). The value of the initial force should be adjusted manually in order to avoid damage to the sample. Another solution to overcome the damage is to use softer cantilevers for softer samples or to perform this mode under liquid in order to get rid of capillary forces.

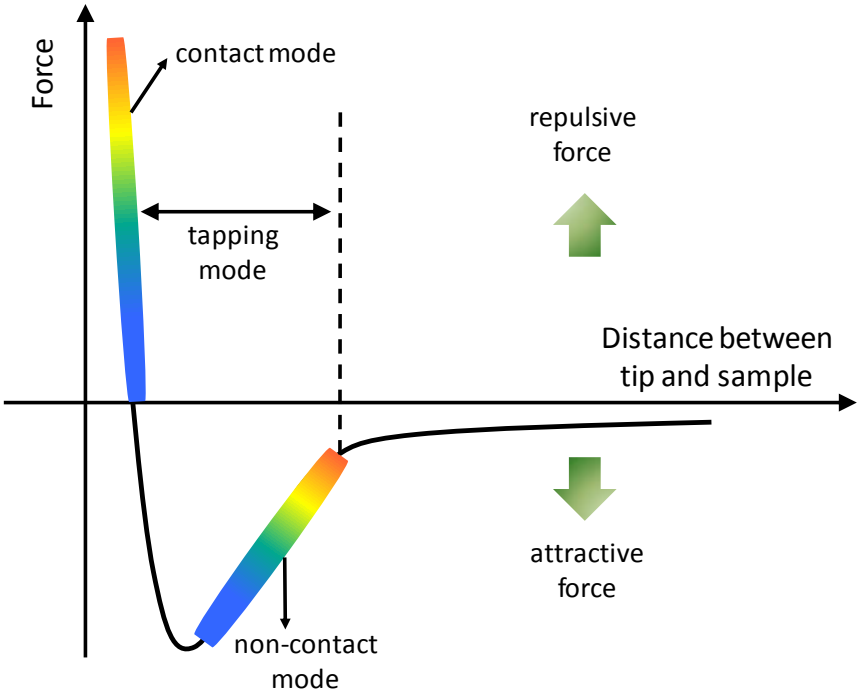

Figure 3.7 *Idealized plot of the forces between tip and sample according to Braga et al.*[18] *The occurrence of different AFM operation modes is shown.*

On the other hand, the tip-sample interaction can be monitored by longer range attractive forces, which are weaker than the repulsive forces observed in contact mode. In that case, *AC or resonant modes* are used which keep constant amplitude of the oscillation of the cantilever while scanning the surface. Two types of *AC modes* can be used:

- In *noncontact mode*, a vibrating tip is brought close to the surface of the sample in order to sense attractive forces, but does not touch the surface. The image is obtained by monitoring the amplitude of the cantilever oscillation at a fixed frequency. Since the tip-sample interactions are small, achieving good vertical resolution is easier in comparison with other modes. In general this mode is used in the air but in principle it could be also used in liquid environment. However, in the latter case, the quality factor of cantilever

oscillations (Q) is low due to fluid dampening which may cause some artifacts in the obtained images.

- In *intermittent contact (tapping) mode* the oscillation amplitude of the cantilever is larger than in non-contact. This mode is the most common one because good vertical as well as lateral resolution is achieved. Furthermore, since weaker interactions with the sample are observed (in comparison with contact mode), lateral forces are reduced and the technique is applicable to delicate samples. Additionally, it is appropriate for experiments performed both in the air and in liquid environment.

3.4 Force measurements (FM)

Force measurements (also called Atomic Force Spectroscopy; AFS) enable the direct investigation of molecular interactions between molecules attached to the AFM probe and to the surface of interest. Thus, it seems to be particularly attractive for understanding the specific molecular forces between individual receptors and ligands in molecular recognition measurements.[13]

3.4.1. Functionalization strategies

In order to attach (or graft) a molecule on a tip or a surface, the latter is usually pre-functionalized with a suitable chemical group, such as: carboxyl (–COOH), hydroxyl (–OH) or amino.[12]

Before attaching a molecule to desired surface, several issues should be taken into account:

- Firstly, an appropriate AFM probe must be chosen, *i.e.* soft cantilevers with $k < 0.1$ N/m are preferable

- Then, the functionalization method must be applied according to examined chemical molecules. One must mention that the molecule must be attached to the tip or surface strongly enough, in order to study the specific interactions without breaking the formed bonds.

The choice of functionalization method depends strongly on the material from which the tip and the surface are made. The strategy of modification is almost the same for the tip and the surface, but tip functionalization is more delicate and will be described below.

In order to attach a molecule to silicon or silicon nitride (Si_3N_4) tips, one of following approaches is generally applied:

- *silanization reaction* where silanes (SiX_3R) react with silanol groups (SiOH) on silicon tips according to: [12]

$$SiOH + SiX_3R \rightarrow SiOSiX_2R + XH \qquad \text{(Eq. 3.13)}$$

Silicon (or silicon nitride) materials are spontaneously oxidized by the air at ambient temperature, resulting in a thin layer of silicon dioxide. This oxide layer contains also silanol groups which can be used for further chemical functionalization. In the case of silicon wafers, the cleaning by a piranha solution (paragraph 3.2) is applied in order to ensure complete oxidation of silicon material. It is worth noting that silanes are consist of a silicon atom, reactive groups (X_i) such as hydroxyl (–OH), chlorine (–Cl), methoxy ($–OCH_3$) or ethoxy ($–OC_2H_5$) in a number up to three and one organic rest group R. Therefore, the reaction described above can occur with more than one reactive group. However, in biomedical research, grafting of biomolecules is mainly achieved via amino group $–NH_2$. The amino group can be introduced:

- by *amination* of the tip rich in silanol groups with APTES (3-aminopropyltriethoxysilane)[19] via a *silanization reaction* (sometimes called *aminosilanization*)

- or by *esterification* with ethanolamine [$HO–(CH_2)_2–NH_2$].[19]

Once, the AFM tip is activated with NH_2 groups, the next step of tip functionalization is to attach the desired molecule by applying appropriate chemical method.

Gold tips and surfaces are also of great interest because the gold-thiol self-assembly method can be applied. Thiols contain a sulfhydryl group (–SH) and bind easily to gold surfaces in closed vessels. In practice, thiols are first dissolved in a suitable solvent like ethanol or dichloromethane at a concentration of typically 1 mM, then the tip or surface of interest is immersed in this solution for 1-12h and finally rinsed several times to get rid of excess thiols.[12] This strategy is particularly attractive because it is very simple and provides a formation of strong chemical bonds between the tip and grafted molecule. However, gold-coated tips and surfaces are not universally available and are much more expensive in comparison with silicon ones.

3.4.2. *Force curves*

Once the tip and the surface of interest are functionalized (paragraph 3.4.1), a force measurement can be performed. To this end, the cantilever deflection (z_c) *vs.* displacement of the piezoelectric scanner in the z-direction (z_p) is measured. In practice, the tip is first slowly brought to contact the surface resulting in blue trace showed in Figure 3.8a, and then the tip is retracted and moves back to its original position (red trace in Figure 3.8a).

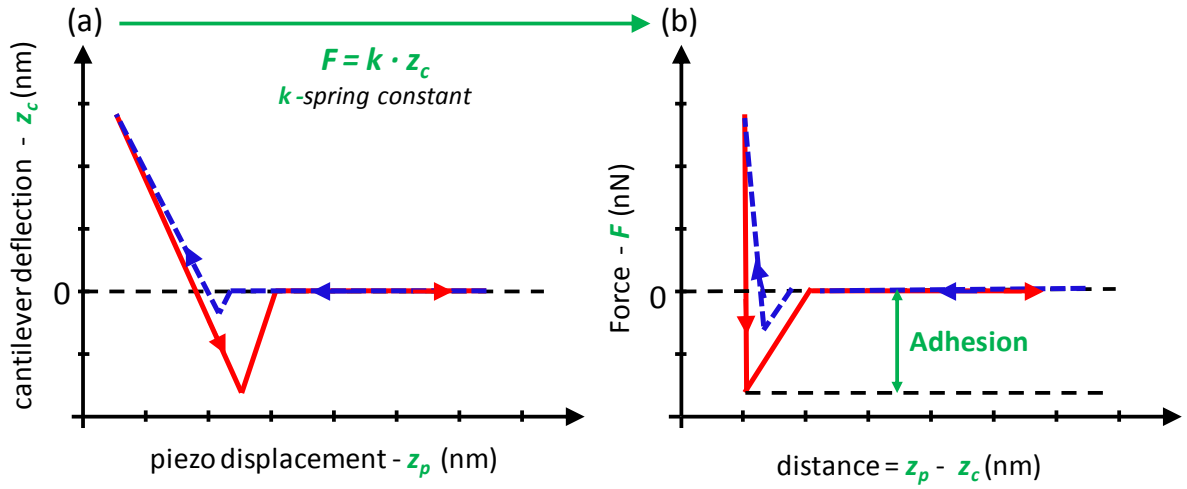

Figure 3.8 *Idealized force curve obtained during a force measurement sometimes called approach/retract cycle.*[13] *The deflection of cantilever is monitored vs. vertical position of the tip provided by the vertical movement of the piezoelectric scanner in the z-direction (a). Curve (a) is then converted to force vs. distance curve (b). Both approach (blue trace) and retraction (red trace) curves are shown.*

In order to obtain a force *vs.* distance curve (Figure 3.8b), the z_c and z_p have to be converted into force (F) and distance (D).[12] The force is calculated according to Eq. 3.11, whereas the tip-sample separation (D) is equal to:

$$D = z_p - z_c \qquad \text{(Eq. 3.14)}$$

Finally, from the curve showed in Figure 3.8b, the maximum tip-sample adhesion can be calculated which gives information about the interaction between molecules attached to the tip and sample surfaces.

One difficulty often occurring during force measurements is that the tip-sample adhesion is observed also for non-functionalized tips, which corresponds to non-specific interactions. Since it is important to distinguish between specific and non-specific

interactions, some spacers (*e.g.* PEG) are used with various ratio between reactive/non-reactive groups to get a control of the grafting density.

3.5 Advantages and limitations

Atomic Force Microscopy is a characterization technique which provides significant information about surface features with high resolution and three-dimensional projection. Furthermore, sample preparation is quite easy and rapid (especially for AFM imaging). Another advantage is that most of AFM modes can operate either in the air or in liquid environment, which is suitable for studying biological macromolecules and even living organisms.

However, as for all scanning techniques, AFM only gives information about a very small area that is not necessarily representative of the whole examined sample. Also, the scanning speed is a limitation and it takes several minutes to obtain a single image.

Beside the possibility of performing high-resolution imaging, AFM has become of great interest for studying specific interactions between molecules (Atomic Force Spectroscopy; AFS). This method enables to evaluate the maximum tip-sample adhesion providing information about intermolecular interactions at the nano- or sometimes even pico-meter scale. For instance, Christendat *et al.* [20] performed force measurements between carboxylate- and amine-functionalized polymer microspheres glued onto the cantilever and a hydrophilic silica wafer. The obtained results have shown that measured adhesion forces depend on surface functional groups, pH, salt concentration as well as the valency of cationic species. Furthermore, it has been found that the strong adhesion interactions observed between the carboxylate-functionalized probe and silica surface are mainly the result of hydrogen-bonding interactions between the surfaces. Additionally, it was noticed that in the presence of calcium ions, the adhesion interactions between surfaces of interest decreased due to the specific absorption of positively charged calcium ions on silica which reduced the potential for hydrogen bonding within the contact region.

Recently, AFS experiments have been extensively used for studying single interactions.[21] This can be achieved via incorporation of intermediate molecules called spacers or linkers to control the grafting density. However, this method is quite new and is still under development.

4. Light Scattering (LS)

Light scattering is one of the most common and significant method for characterizing macromolecules.[22] The replacement of conventional light sources by lasers has provided intense and monochromatic light, which, together with efficient spectrum analyzers and autocorrelators, has enabled to study macromolecular motion in solution.

A typical set-up for light scattering experiments is shown in Figure 3.9 and is basically comprised of a laser light which illuminates the sample particles within a cell and a detector. Most of the light passes straight through the sample but some of it is scattered by particles within the sample and recorded at scattering angle θ.[23]

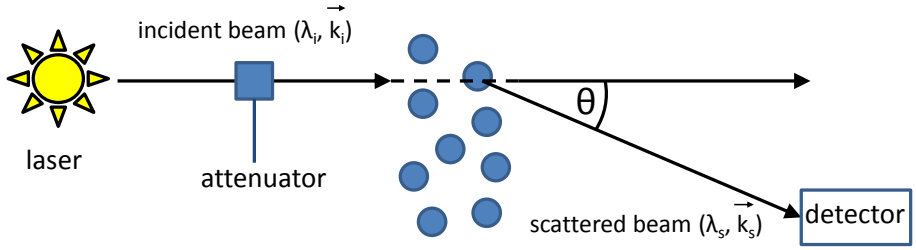

Figure 3.9 *Typical light scattering apparatus, λ is a wavelength of light and $\vec{k}$ is the propagation vector of the incident light (index i) or the scattered light (index s).*

In general, large particles scatter light more efficiently than small ones. However, large particles can scatter too much light for the detector to function properly and modern LS systems are also equipped with an attenuator which is used to reduce the intensity of the laser source, thus resulting in lower scattering intensity.

The propagation vectors of the incident and scattered beams have magnitudes $|\overrightarrow{k_i}| = \frac{2\pi}{\lambda_i}$ and $|\overrightarrow{k_s}| = \frac{2\pi}{\lambda_s}$, respectively, where λ is the wavelength of the beams. Since the wavelength of the incident beam (λ_i) is not changing too much in the scattering process, it can be assumed that $|\overrightarrow{k_i}| \cong |\overrightarrow{k_s}|$. The difference between vectors $\overrightarrow{k_s}$ and $\overrightarrow{k_i}$ is called the scattering wave vector $\vec{q}$ (Eq. 3. 15).

$$\vec{q} = \overrightarrow{k_s} - \overrightarrow{k_i} \qquad \text{(Eq. 3.15)}$$

In addition,

$$|\overrightarrow{k_s} - \overrightarrow{k_i}| = 2\sin\theta/2 \qquad \text{(Eq. 3.16)}$$

Thus the magnitude of the scattering vector q is:[24]

$$|\vec{q}| = \frac{2\pi}{\lambda_i}\left|\overrightarrow{k_s} - \overrightarrow{k_i}\right| = \frac{4\pi}{\lambda_i} sin\frac{\theta}{2} \quad \text{(Eq. 3.17)}$$

Since the wavelength of the medium (λ) is equal to λ_0/n, so Eq. 3.17 can be written as follows:

$$|\vec{q}| = \frac{4\pi n}{\lambda_0} sin\frac{\theta}{2} \quad \text{(Eq. 3.18)}$$

where n is the refractive index of the solution and λ_0 is the wavelength of light in vacuum.

If the scattered light is analyzed in terms of its average intensity $I(\theta, t)$, we talk of Static Light Scattering – SLS (paragraph 4.1). However, due to Brownian motion of molecules in solution, the fluctuations of the scattering intensity with time can also be examined and this approach is known as Dynamic Light Scattering – DLS (paragraph 4.2).

4.1. Static Light Scattering (SLS)

Static Light Scattering gives the time-average intensity of scattered light. Performing measurements at different concentrations enables to determine the weight-average molecular weight (M_w) of analyzed sample as well as the second virial coefficient (A_2), which describes the interaction strength between the particles and the solvent ($A_2 > 0$ for a good solvent, $A_2 = 0$ for a theta solvent), according to the Rayleigh equation (Eq. 3.19)

$$\frac{Kc}{\Delta R_\theta} = \frac{1}{\overline{M_w} P(\theta)} + 2A_2 c \quad \text{(Eq. 3.19)}$$

K is the scattering constant defined in Eq. 3.20, c is the polymer concentration expressed in g mL^{-1}, ΔR_θ is the difference between the Rayleigh ratios R_θ of solution and solvent and $P(\theta)$ is the particle scattering factor.

$$K = \frac{4\pi^2 {n_0}^2}{N_A {\lambda_0}^4}\left(\frac{dn}{dc}\right)^2 \quad \text{(Eq. 3.20)}$$

Here, n_0 is the refractive index of solvent, (dn/dc) is the refractive index increment of the solution, N_A is the Avogadro number and λ_0 is the wavelength of light in vacuum.

The Rayleigh ratio is defined as: [25]

$$R_\theta = \frac{I_\theta}{I_0} r^2 \frac{1}{1+cos^2\theta} \quad \text{(Eq. 3.21)}$$

where I_0 and I_θ are the intensities of incident and scattered light, respectively and r is the distance between the sample and detector.

Experimentally, the R_θ is determined by using toluene as the reference standard, from following equation:

$$R_\theta = \frac{(I_{sample} - I_{solvent})}{I_{toluene}} \left(\frac{n_{solvent}}{n_{toluene}}\right)^2 R_{(\theta)\ toluene} \quad \text{(Eq. 3.22)}$$

SLS provides information about the overall size of the (macro)molecule described by its radius of gyration (R_g), which is defined as the root mean square distance of any point (R_i) in the object (polymer coil) from its center of mass (R_c) according to:

$$R_g = \sqrt{\sum_i \frac{(R_i - R_c)^2}{N}} \quad \text{(Eq. 3.23)}$$

Thus, the radius of gyration can be determined via the Static Light Scattering method either from Guinier plot, or Zimm plot.

- André Guinier, a French physicist found that R_g can be calculated from the measured scattered intensity $I_s(q)$ by using a logarithmic plot [$\ln(I_s(q))$ *vs* q^2] of the Eq. 3.24 known as *Guinier equation*:

$$\ln I_s(q) = \ln I_i - \frac{q^2 {R_g}^2}{3} \quad \text{(Eq. 3.24)}$$

However, this equation is only true for small scattering angles ($qR_g \ll 1$). Thus, R_g obtained from the slope of a linear plot [24] is equal $\frac{{R_g}^2}{3}$.

- *Zimm plot*

For a dilute polymer solution at a relatively small scattering angle θ, the particle scattering factor $P(\theta)$ is related to the average extension of the polymer chain described by R_g according to the following relation:

$$P(\theta) \approx 1 - \frac{q^2}{3} {R_g}^2 \quad \text{(Eq. 3.25)}$$

Combining the Eq. 3.19 and Eq. 3.25 gives:

$$\frac{Kc}{\Delta R_\theta} \approx \frac{1}{M_w}\left(1 + \frac{1}{3} {R_g}^2 q^2\right) + 2A_2 c \quad \text{(Eq. 3.26)}$$

Bruno H. Zimm [26] plotted $Kc/\Delta R_\theta$ as a function of $q^2+k_c\,c$ (k_c is a constant which gives a convenient spacing of the data points on the graph). Then, the points at a given concentration were extrapolated to zero angle, whereas the points corresponding to a given angle were extrapolated to zero concentration. The extrapolation $(Kc/\Delta R_\theta)_{c\to 0,q\to 0}$ gives the $\frac{1}{M_w}$ value. On the other hand, the slopes of $(Kc/\Delta R_\theta)_{c\to 0}$ versus q^2 and $(Kc/\Delta R_\theta)_{q\to 0}$ versus c lead to obtain R_g and A_2 values, respectively.[27] This graphical method is called Zimm plot from the name of its inventor. It has enabled to obtain information about the particle weight-average molecular weight, the shape characterized by the radius of gyration and the interaction strength between the molecule and the solvent described by the second virial coefficient. The negative values of A_2 correspond to bad solvent, positive for good solvent and if this parameter is equal zero, it means that a theta (θ) solvent has been used. Recently, SLS detectors are also incorporated into the Size Exclusion Chromatography (SEC) systems, allowing measuring the molecular weight distribution.

4.2. *Dynamic Light Scattering (DLS)*

Dynamic Light Scattering (DLS) is also known as Photon Correlation Spectroscopy (PCS) or Quasi-Elastic Light Scattering (QELS). However, DLS seems to be the most descriptive term because this method basically relies on the motion (or the dynamics) of the scattering objects in liquids.[28] In solution, particles are constantly moving due to the bombardment by fast solvent molecules. This phenomenon is known as Brownian motion. DLS monitors this movement by recording the fluctuations in the intensity of light scattered with time at a given scattering angle.[29] In practice, the statistics of the scattering signal are computed by an autocorrelator (a computer) as the normalized time autocorrelation function $g^{(2)}(q,t)$ of the scattered intensity defined as:

$$g^{(2)}(q,t) = \frac{\langle I(q,t_0)I(q,t_0+\mathrm{t})\rangle}{\langle I(q,t_0)\rangle^2} \qquad \text{(Eq. 3.27)}$$

where $I(q, t_0)$ and $I(q, t_0+t)$ are the scattering intensities at time 0 (t_0) and at certain delay time t later. It is worth noting that $g^{(2)}(q,t)$ can be written in terms of scattered electric field as the normalized first order time autocorrelation function $g^{(1)}(q,t)$ through the Siegert relation:[22,30]

$$g^{(2)}(q,t) = A + \beta\left|g^{(1)}(q,t)\right|^2 \qquad \text{(Eq. 3.28)}$$

where A is the baseline and β is the coherence factor determined by the geometry of the detection (specific experimental setup). In an ideal apparatus, the constant β is equal to 1 but

in practice $\beta < 1$.[29] Additionally, at long delay times the baseline value should be close to 1, so Eq. 3.27 can be written as:

$$g^{(2)}(q,t) = 1 + \beta\left|g^{(1)}(q,t)\right|^2 \quad \text{(Eq. 3.29)}$$

Experimentally, $[g^{(2)}(q,t)-1]$ is measured. In order to obtain information about the size of particles, different mathematical approaches have to be applied (depending on the type of dispersion of the particles in dilute solution).

4.2.1. Monodisperse systems

In the case of *monodisperse objects*, $g^{(1)}(q,t)$ is denoted as a single exponential function of decay time:

$$g^{(1)}(q,t) = exp(-\Gamma t) \quad \text{(Eq. 3.30)}$$

Γ is the decay rate related to the diffusion coefficient D by:

$$\Gamma = Dq^2 \quad \text{(Eq. 3.31)}$$

where q is the scattering vector.

So, the approximated diffusion coefficient (D) can be computed according to:[22]

$$D = \frac{\Gamma}{q^2} \quad \text{(Eq. 3.32)}$$

from which the hydrodynamic radius (R_h) of spherical particles can be estimated according to the Stokes-Einstein equation:

$$R_h = \frac{k_B T}{6\pi\eta D} \quad \text{(Eq. 3.33)}$$

where k_B is the Boltzmann constant, T is temperature and η is the viscosity of the solvent.

In principle, a measurement at only one scattering angle is required to obtain an apparent D value. However, in order to determine the true diffusion coefficient (hence R_h), the decay rate (Γ) of $g^{(1)}(q,t)$ measured at different scattering angles is plotted versus q^2 and the diffusion coefficient is taken as the slope of $(\Gamma/q^2)_{q\to 0}$.[29]

4.2.2. Non-uniform systems

In most cases, analyzed samples are non-uniform in size. So far, two methods have been extensively used for the analysis of such samples.

- *The CONTIN method* developed by Steven Provencher [31,32]

In order to obtain the distribution function of decay time *A(t)* and the size dispersity, the first order time autocorrelation function $g^{(1)}(q,t)$ can be treated either as a sum of decay rates:

$$g^{(1)}(q,t) = \sum_i A_i exp(-\Gamma_i t) \quad \text{(Eq. 3.34)}$$

or as an integral over a distribution function of decay rates obtained by applying an inverse Laplace transform:

$$g^{(1)}(q,t) = \int_0^\infty A\,(\Gamma)\; exp(-\Gamma t)\; d\Gamma \quad \text{(Eq. 3.35)}$$

resulting in $g^{(1)}(q,t)$ expressed as a distribution function of decay time *A(t)*. The local maxima of *A(t)* correspond to the decay time (*t*), from which Γ can be calculated according to:

$$\Gamma = \frac{1}{t} \quad \text{(Eq. 3.36)}$$

In addition, $A(\Gamma)$ can be written as the distribution function of R_h by applying the equations 3.32 and 3.33 from which the hydrodynamic radii can be calculated.

- *Method of CUMULANTS* introduced by Koppel in 1972 [33,34]

On the other hand, the analysis of DLS data for non-uniform samples can be carried out by the *method of CUMULANTS*. In this approach, the logarithm of the $g^{(1)}(q,t)$ is expanded as a power series in time *t*:

$$ln\left(g^{(1)}(q,t)\right) = \Gamma_0 - \Gamma_1 \cdot t + \frac{\Gamma_2}{2!} \cdot t^2 + \cdots \quad \text{(Eq. 3.37)}$$

where Γ_0, Γ_1, Γ_2 and Γ_3 are the cumulants. The first cumulant Γ_1 and the second cumulant Γ_2 can be related to the diffusion coefficient *D* (Eq. 3.38) and the dispersity index – $Đ_M$ (Eq. 3.39), respectively.[35]

$$D = \Gamma_1 q^2 \quad \text{(Eq. 3.38)}$$

$$\Gamma_2/\Gamma_1^{\,2} = Đ_M = M_w/M_n \quad \text{(Eq. 3.39)}$$

where M_w is the weight-average molar mass and M_n is the number-average molar mass of a polymer.

However, the cumulant method is valid for small decay times and sufficiently narrow size distributions, thus it is widely used for narrow monomodal distributions.[36] On the other hand, the CONTIN method gives good estimates for the widths and peaks of unimodal and bimodal (when the separation of the $A(\Gamma)$ peaks is about a factor of two or more and the areas under the peaks are not very different) distributions,[29] so is applied more often.

4.3. *Advantages and limitations*

Static Light Scattering of dilute solutions is a powerful technique for use in biochemistry. Measurements of the scattered intensity at different angles enable to determine the molecular weight, the radius of gyration and the thermodynamic interactions between solvent and solute. Additionally, DLS investigations give information about the size expressed in terms of hydrodynamic radii. Furthermore, the results obtained from SLS and DLS can be combined in order to estimate the shape factor (ρ) defined as ratio of the radius of gyration to hydrodynamic radius (R_g/R_h). This ρ-parameter allows to distinguish whether a particle is a loosely coiled linear chain or more compact structure.[24] For instance, the ρ-parameter for homogeneous (hard) spheres is equal to 0.78, whereas for random coil linear chains (non-uniform) it is much higher: 1.73 or 2.03 in θ-solvent or good solvent, respectively.[24] Despite many advantages, Laser Light Scattering has also some limitations. It is only applicable for transparent samples and cannot be used for highly concentrated solutions.

DLS is a relatively fast method for characterizing the size of (macro)molecules in solution. In general, the measurement takes only few minutes and gives the approximated size of particles. It may also detect the presence of aggregates. For instance, a progressive formation of aggregation can be determined by this technique (Chapter V).

5. Rheology

The term rheology derives from the Greek word *rheos* which means flow and was first used in physics and chemistry by E.C. Bingham and M. Reiner in 1929 when the American Society of Rheology was founded in Columbus, Ohio.[37] Thus, rheology is the science of flow but also deformation because during the flow materials undergo continuous deformations due to external forces. Accordingly, rheometry describes the measuring methods and devices used to determine the rhelogical properties of materials, whereas rheology includes everything dealing with mechanical behavior [38] such as: fluid dynamics, viscosity measurements, molecular conformations and interactions but also solid mechanics.

5.1. Viscosity

The viscosity of a liquid is usually described on the basis of the parallel plate model shown in Figure 3.10.

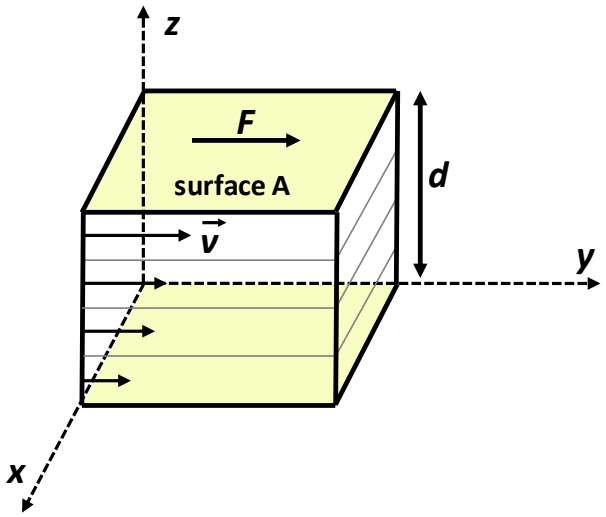

Figure 3.10 *Parallel plate model.*

In this model a liquid is placed between two parallel plates separated by distance *d*. The bottom plate is in a fixed position, whereas the top one moves in the *y* direction, perpendicular to the *z*-axis. In a laminar flow, the liquid flows with a stationary velocity field $\vec{v}$ having a constant velocity gradient or shear rate ($\dot{\gamma}$), due to the applied force *F* on a surface *A*, results in a shear stress (σ).

$$\frac{F}{A} = \sigma \qquad \text{(Eq. 3.40)}$$

According to the laminar model described above, the layers are moving due to molecular interactions at a decreasing rate from the top to the bottom expressed as:

$$\frac{dv}{dz} = \dot{\gamma} \quad \text{(Eq. 3.41)}$$

and named the shear rate ($\dot{\gamma}$).

By definition, the coefficient relating σ and $\dot{\gamma}$ is the viscosity η.

$$\sigma = \eta\,\dot{\gamma} \quad \text{(Eq. 3.42)}$$

In addition, the rate of shear change can be also defined as the strain change $d\gamma$ during a period of time dt:[39]

$$\dot{\gamma} = \frac{d\gamma}{dt} \quad \text{(Eq. 3.43)}$$

where γ is equal to:

$$\gamma = \frac{dy}{dz} \quad \text{(Eq. 3.44)}$$

Thus, Eq. 3.43 can be written as follows:

$$\dot{\gamma} = \frac{d\gamma}{dt} = \frac{d}{dt}\frac{dy}{dz} = \frac{d}{dz}\frac{dy}{dt} = \frac{dv}{dz}\left[\frac{1}{s}\right] \quad \text{(Eq. 3.45)}$$

which is equivalent to the equation 3.41.

5.2. *Newtonian and non-Newtonian fluids*

Viscosity depends on many factors such as: temperature, shear rate, time, pressure, pH, *etc.* However, the most important factor is the examined material, or actually its physical and chemical properties. Fluids are generally classified into two categories: Newtonian fluids (*e.g.* water, syrup, honey, mineral oils) and non-Newtonian fluids (*e.g.* mayonnaise, paint, molten plastics, foams).[37] In the case of Newtonian fluid the proportionality between σ and $\dot{\gamma}$ in laminar flow is maintained according to Eq. 3.42. Thus, the viscosity is equal to the slope of the straight line in a plot shear stress (σ) *vs.* shear rate ($\dot{\gamma}$) called *flow curve* (Figure 3.11). In other words, in a Newtonian fluid η is independent of shear rate.

If the viscosity is dependent on the rate of shear and/or time (Eq. 3.46), a fluid is called non-Newtonian.

$$\sigma = \eta(\dot{\gamma}, t)\,\dot{\gamma} \quad \text{(Eq. 3.46)}$$

Non-Newtonian materials whose viscosity is time independent can be classified as (Figure 3.11):

- *shear thinning* (*pseudoplastic* fluids): the viscosity decreases with increasing shear rate, *e.g.* polymer solutions exhibit pseudoplastic flow but also melts, paints and many cosmetics

- *shear thickening* (*dilating*) materials which increase their viscosity upon stirring or shearing,[40] *e.g.* wet sand

- *plastic* fluids: sometimes before the material starts to flow like a liquid, an additional force must be applied. Eugene Bingham showed that some fluids must achieve a critical level of shear stress (called yield stress) in order to initiate Newtonian flow, thus these materials are known as *Bingham plastic liquids e.g.* ketchup (we need to shake a bottle to make the ketchup flow).[40] However most materials do not exhibit Newtonian flow after the yield stress but rather a shear thinning flow. Such materials are called *viscoplastic* fluids, *e.g* lipsticks, toothpaste.

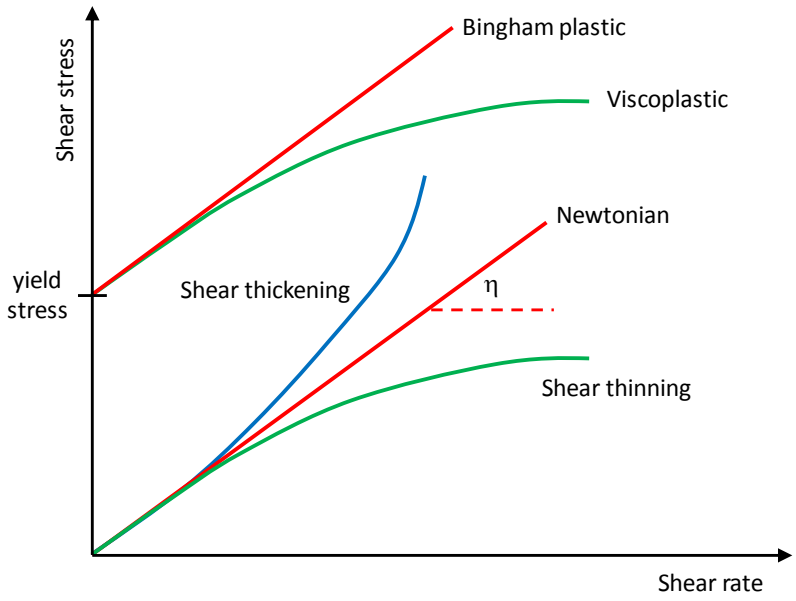

Figure 3.11 *Flow curves for Newtonian and non-Newtonian fluids.*

Often, during flow, the viscosity changes with time. Two types of such fluids are distinguished:

- *thixotropic* fluids: their viscosity first decreases over time and then after a period of rest it increases again. Modern latex paints are a perfect example here because when the box is opened, the paint has a very high viscosity but after stirring for a while, it gets thinner and finally the viscosity increases again when the paint stays on the wall.[39] In order to confirm a thixotropic flow behavior, a loop test is usually performed. So the shear rate is first increasing and then decreasing in the same order. In most cases, the hysteresis loop is observed, proving a thixotropic properties of analyzed material.

- *rheopectic* fluids: their viscosity first increases with time of stirring and then after a period of rest decreases. This phenomenon is also studied by a loop test, however in contrast to thixotropy, rheopexy is very rare.

5.3. Elasticity

In the case of an elastic material, deformation occurs due to an external force but, once the force removed, the deformation disappears (*e.g.* rubber ball). For fully elastic materials the ratio between the stress σ (Eq. 3.42) and the strain γ (Eq. 3.44) is constant and is called shear modulus *G* (for shear) or Young's modulus *E* (for tension) according to:

$$\frac{\sigma}{\gamma} = G \text{ or } E \ [Pa] \qquad \text{(Eq. 3.47)}$$

5.4. Viscoelasticity and oscillatory rheology

Viscoelastic materials feature both viscous (liquid) and elastic (solid) properties. For instance a grocery plastic bag shows typical viscoelastic behavior. This is true for all polymeric materials and their viscous-like and elastic-like properties can be studied by oscillatory measurements (*oscillatory rheology* or *mechanical spectroscopy*). This is one of the most common methods used to characterize them in terms of their dynamic properties. Gels are also considered as viscoelastic materials under various conditions of time, temperature or other factors.[41]

In small-strain oscillatory experiments, *i.e.* with strain in the range of 0.01 % - 25 %[41] according to the nature of the tested system, the sample is deformed sinusoidally. This sinusoidal strain is induced with angular frequency ω given by:[38]

$$\gamma = \gamma_0 \, sin(\omega t) \quad \text{(Eq. 3.48)}$$

where γ_0 is the amplitude of the applied deformation.

At the same frequency, strain oscillations lead to stress oscillations which are shifted by a phase angle δ: [38]

$$\sigma = \sigma_0 \, sin(\omega t + \delta) \quad \text{(Eq. 3.49)}$$

Therefore, the stress wave can be decomposed into two waves of frequency ω, one in phase with the strain wave (sin ωt) and one 90° out of phase (cos ωt). It follows that:

$$\sigma = \sigma' + \sigma'' = \sigma_0' \sin \omega t + \sigma_0'' \cos \omega t \quad \text{(Eq. 3.50)}$$

The applied decomposition leads to two dynamic moduli:

$$G' = \frac{\sigma_0'}{\gamma_0} \quad \text{(Eq. 3.51)}$$

named the in-phase or storage modulus and

$$G'' = \frac{\sigma_0''}{\gamma_0} \quad \text{(Eq. 3.52)}$$

i.e. the out-of-phase or loss modulus.

Thus, the viscoelastic behavior of a system at the oscillatory frequency ω is characterized by a storage modulus G', a loss modulus G'' and the resulting stress response for a viscoelastic material, described according to the following equation:[38]

$$\sigma = G'\gamma_0 sin(\omega t) + G''\gamma_0 cos(\omega t) \quad \text{(Eq. 3.53)}$$

Additionally, G' and G'' can be used to define the amplitude of the complex modulus G^* expressed as: [41]

$$|G^*| = \sqrt{(G')^2 + (G'')^2} \quad \text{(Eq. 3.54)}$$

which allows to define the complex viscosity η^*:

$$|\eta^*| = \frac{|G^*|}{\omega} \quad \text{(Eq. 3.55)}$$

It is worth noting that the logarithmic dependence of G' and G'' versus log ω, called mechanical spectrum [41], is often measured in order to establish if the analyzed sample is a solid-like material or a very viscous fluid. From the example in Figure 3.12 it appears that at

low frequencies, G'' is greater than G' (solution-like behavior), whereas at a higher frequency there is a cross-over point, after which the G' becomes higher than G'' (gel-like behavior due to entanglements). Also, at higher frequencies G' and G'' can be less frequency dependent, what is called the "rubbery plateau" region.[41]

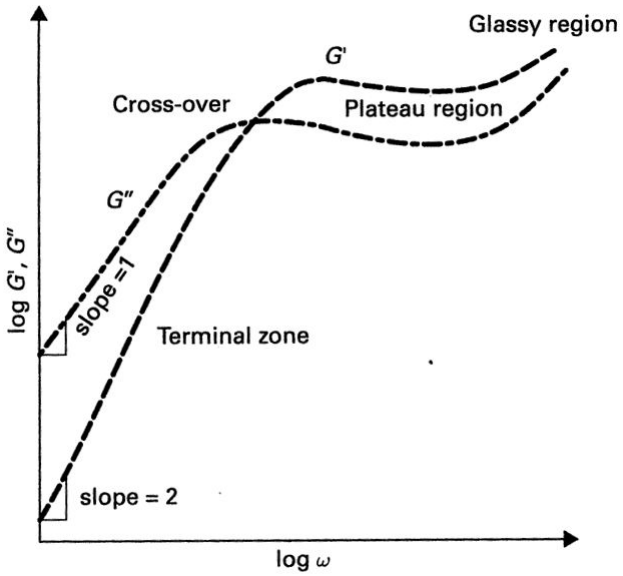

Figure 3.12 *Mechanical spectrum of a polymer solution – viscoelastic liquid (Figure 2.16 taken from Djabourov et al. [41]).*

The relation between the storage and loss moduli (G', G'') gives information about the molecular structure in gels and polymer structures [39] (Table 3.1).

Oscillatory measurements can be also performed in tension/compression mode, thus leading to the storage (E') and loss (E'') Young's moduli.

Table 3.1 *Relations between G', G'' and viscoelastic behavior.*[39]

G′, G″ (ω)	Behavior zone
$G' < G''$	Viscoelastic liquid
$G' = G''$	Transition
$G' > G''$	Viscoelastic solid

5.5. Gel formation, gel point and percolation

In the case of polymers which undergo gelation under specific conditions, studying the sol (a liquid state) - gel (a solid-like state) transition is of great importance. In order to determine the sol-gel transition, different parameters can be examined such as temperature (in thermodynamics) or microscopic parameters (interchain interactions) which enable the network formation in the case of gelation. Different mechanisms are proposed to interpret gelation either in terms of tree-like model or percolation. Both phenomena are based on bond formation, but percolation is considered as a critical phenomenon. The analogy between chemical gelation and percolation is given in Table 3.2. Since gelation is described in Chapter II, the central attention of this paragraph will be paid to the percolation.

The percolation theory has been developed by Paul John Flory (1941) and Walter Hugo Stockmayer (1943) but the term percolation was introduced by mathematician John Michael Hammersley in 1957.[42] It can be explained on the basis of either statistical geometric model, in which a liquid can flow through a porous medium along the specific path called the percolation path (analogy to coffee preparation in traditional Italian espresso pot),[41] or a lattice model,[43] in which neighboring units may react (*i.e.* form bonds) and create a "molecule" of specific size. The fraction of reacted bonds is usually called p and allows determining the size of the system: [43]

- at small p → small formed clusters
- at large p, $p = p_c$, *i.e.* percolation threshold → infinite clusters

De Gennes [43] showed that the properties of large clusters near the gelation threshold, *i.e.* for which p is slightly smaller than p_c ($p_c - p = \Delta p$), can be estimated by determining some exponents strongly depending on space dimensionality d. For instance, mean cluster size can be determined according to:[41]

$$s_{av} \propto (p_c - p)^{-\gamma} \text{ with } (p_c - p) \to 0 \text{ , for } p < p_c \qquad \text{(Eq. 3.56)}$$

which is directly related to the weight average degree of polymerization (N_w) and where γ is equal to 1.7 for $d = 3$.[41]

Analogously, the viscosity of the system is predicted to scale as:[44]

$$\eta \propto (p_c - p)^{-s} \qquad \text{(Eq. 3.57)}$$

with s = 0.7 for $d = 3$.

Another exponent can be found from the probability $P(p)$ of a bond to connect to the infinite cluster, which is related to the gel fraction (Table 3.2):[41]

$$P \approx (p - p_c)^{\beta} \text{ with } (p - p_c) \to 0, \text{ for } p > p_c \qquad \text{(Eq. 3.58)}$$

where $\beta = 0.40$ for $d = 3$.[41]

Table 3.2 *Analogy between percolation and gelation (on the basis of Table 3.3 from Ref. [41]).*

Percolation	Chemical gelation
Percolation threshold p_c	Gel point
Connected bond	Reacted functional group
Lattice for $p < p_c$	Sol state
Lattice for $p > p_c$	Gel state
Infinite cluster	Gel network
Mean cluster size $s_{av}(p)$, $p < p_c$	Average molecular mass
Percolation probability $P(p)$, $p > p_c$	Gel fraction

5.6. *Advantages and limitations*

Rheology is an interdisciplinary science that can be used to study the relationship between the mechanical properties of a material and its molecular structure. For instance, studying polymer solutions under different shear profiles can provide some insight into the molecular weight, shape and flexibility of a polymer. Furthermore, the possibility to examine the processes occurring during deformation plays an essential role in the technological applications of various polymeric materials.

The main limitations are related to the measuring methods and devices (rheometry). For instance, the examined sample should be homogeneous and adhere to the two plates of rheometer, which can be a problem in the case of slippery samples such as hydrogels. For liquid samples, the cone-plate measuring geometry is one of the most effective ones because it provides constant shear rates during measurements and requires small quantities of sample.

6. Conclusion

This chapter describes the investigation techniques that will be used for studying the Ca^{2+}- driven association of polymers. Molecular modeling was chosen because it provides a three-dimensional picture of the molecules and their assemblies but also because it predicts both experimental results and the appropriate properties of oligosaccharides in terms of segment length, chemical nature of the sugars, ionization state, *etc.* Nonetheless, results from molecular modeling need to be complemented and compared to those obtained with experimental techniques. Atomic Force Microscopy (AFM), Light Scattering (LS), and rheology were identified as the most suitable methods for studying physico-chemical properties relevant to Ca^{2+}- driven association. AFM provides not only high-resolution imaging but also the study of the interactions between molecules (Atomic Force Spectroscopy; AFS). Laser Light Scattering enables the determination of macromolecular dimensions, whereas rheology describes mechanical behavior of materials during the flow. Nevertheless, in order to get accurate results from measurements, it is of major importance to plan and perform the experiments carefully. This is more easily achieved when the results obtained by molecular modeling are already available.

7. References

(1) Pensak, D. A. Pure Appl. Chem. 1989, 61, 601.

(2) van Gunsteren, W. F.; Berendsen, H. J. C. Angewandte Chemie International Edition in English 1990, 29, 992.

(3) Hehre, W. J. A Guide to Molecular Mechanics and Quantum Chemical Calculations; Wavefunction, Incorporated, 2003.

(4) Lewars, E. Computational Chemistry: Introduction to the Theory and Applications of Molecular and Quantum Mechanics; Kluwer Academic Publishers, 2004.

(5) Hehre, W. J.; Shusterman, A. J.; Molecular Modeling in Undergraduate Chemistry Education http://www.wavefun.com/support/MMUndEd.pdf Irvine, Portland.

(6) Alder, B. J.; Wainwright, T. E. J. Chem. Phys. 1957, 27, 1208.

(7) Allen, M. P.; Tildesley, D. J. Computer Simulation of Liquids; Oxford Univ. Press, 1987.

(8) Hess, B.; Kutzner, C.; van der Spoel, D.; Lindahl, E. Journal of Chemical Theory and Computation 2008, 4, 435.

(9) Meller, J. Encyclopedia of Life Sciences 2001, 1.

(10) Le, T. C. Computational simulation of hyperbranched polymer melts under shear Ph.D. Thesis, Swinburne University of Technology, 2010.

(11) Binnig, G.; Quate, C. F.; Gerber, C. Physical Review Letters 1986, 56, 930.

(12) Butt, H.-J.; Cappella, B.; Kappl, M. Surf. Sci. Rep. 2005, 59, 1.

(13) Berquand, A.; Ohler, B. In Application Notes; Bruker Corporation Santa Barbara, CA USA, 2010; Vol. AN130, Rev. A0.

(14) Morris, V. J.; Kirby, A. R.; Gunning, A. P. Atomic Force Microscopy for Biologists; Imperial College Press London: Norwich, UK, 1999.

(15) Leite, F. L.; Herrmann, P. S. P. Journal of Adhesion Science and Technology 2005, 19, 365.

(16) Cook, S. M.; Schaeffer, T. E.; Chynoweth, K. M.; Wigton, M.; Simmonds, R. W.; Lang, K. M. Nanotechnology 2006, 17, 2135.

(17) Vezenov, D. V.; Zhuk, A. V.; Whitesides, G. M.; Lieber, C. M. J Am Chem Soc 2002, 124, 10578.

(18) Braga, P. C.; Ricci, D. Atomic Force Microscopy: Biomedical Methods and Applications. [In: Methods Mol. Biol. (Totowa, NJ, U. S.), 2004; 242]; Humana Press Inc., 2004.

(19) Riener, C. K.; Stroh, C. M.; Ebner, A.; Klampfl, C.; Gall, A. A.; Romanin, C.; Lyubchenko, Y. L.; Hinterdorfer, P.; Gruber, H. J. Anal. Chim. Acta 2004, 506, 115.

(20) Christendat, D.; Abraham, T.; Xu, Z.; Masliyah, J. J. Adhes. Sci. Technol. 2005, 19, 149.

(21) Hegner, M.; Grange, W.; Bertoncini, P. Methods Mol. Biol. (Totowa, NJ, U. S.) 2004, 242, 369.

(22) Johnson, C. S.; Gabriel, D. A. Laser Light Scattering; DOVER Publications: New York, 1994.

(23) Zetasizer; Zetasizer Nano User Manual http://www.malvern.com/, August 2009.

(24) Burchard, W. Light Scattering from Polysaccharides; Marcel Dekker, Inc.: New York, 2005.

(25) Huglin, M. B.; Editor Light Scattering from Polymer Solutions. Vol. 20; Academic, 1972.

(26) Zimm, B. H. J. Chem. Phys. 1948, 16, 1099.

(27) Korchagina, E. V.; Philippova, O. E. Biomacromolecules 2010, 11, 3457.

(28) Dalgleish, D. G.; Hallett, F. R. Food Research International 1995, 28, 181.

(29) Pecora, R. J. Nanopart. Res. 2000, 2, 123.

(30) Patty, P. J.; Frisken, B. J. Appl Opt 2006, 45, 2209.

(31) Provencher, S. W. Computer Physics Communications 1982, 27, 213.

(32) Provencher, S. W. Computer Physics Communications 1982, 27, 229.

(33) Koppel, D. E. J. Chem. Phys. 1972, 57, 4814.

(34) Frisken, B. J. Appl Opt 2001, 40, 4087.

(35) Schweins, R.; Hollmann, J.; Huber, K. Polymer 2003, 44, 7131.

(36) Hassan, P. A.; Kulshreshtha, S. K. J. Colloid Interface Sci. 2006, 300, 744.

(37) Morrison, F. A. Ind. Phys. 2004, 10, 29.

(38) Macosko, C. W. Rheology: Principles, Measurements, and Applications; VCH: New York, 1994.

(39) Smidsrød, O.; Moe, S. T. Biopolymer chemistry; Tapir Academic Press: Trondheim, 2008.

(40) Franck, A. In Understanding Rheology of Structured Fluids; TA Instruments; Vol. AAN016.

(41) Djabourov, M.; Nishinari, K.; Ross-Murphy, S. B. Physical Gels from Biological and Synthetic Polymers; Cambridge University Press, 2013.

(42) Hammersley, J. M. Proc. Cambridge Philos. Soc. 1957, 53, 642.

(43) De Gennes, P. G. Scaling Concepts in Polymer Physics; Cornell University Press: Ithaca and London, 1979.

(44) Mercier, C.; Rinaudo, M. International Workshop on Plant Polysaccharides, Structure and Function: July 9-11, 1984, Nantes; I.N.R.A, 1984.

Chapter IV:

Probing the ionotropic association by molecular modeling

Table of contents

1. Introduction: Atomistic picture of the junction zones

The atomistic structure of the junction zone of alginate gels is commonly described in the light of the "egg-box" model initially proposed by Grant *et al.* [1] in 1973. However, it was revisited many times by both numerical and experimental studies, thus a brief state of this issue is described below.

1.1. "Egg-box" structure

1.1.1. The calcium coordination number and Ca–O distance

The calcium coordination number ($N_{Ca^{2+}}$) corresponds to the number of oxygen atoms which participate in the chelation.

- *in carbohydrate complexes*

In order to estimate the $N_{Ca^{2+}}$ in carbohydrate complexes, a survey of crystallographic data was conducted by M. L. Dheu-Andries *et al.* [2] It was found that the calcium coordination number varies from 7 to 9 (but 8 was the most common) including from one to four oxygen atoms which belong to water molecules. Moreover, the distance between calcium and oxygen atoms was in the range 2.30 Å - 2.85 Å.

- *in aqueous solution*

Recently, F. Jalilehvand *et al.* [3] have examined the local structure around the hydrated Ca^{2+} in aqueous solution by Extended X-ray Absorption Fine Structure spectroscopy (EXAFS), Large-Angle X-ray Scattering (LAXS) and molecular dynamics (MD). They found a mean Ca–O bond distance of 2.46 Å with rms variation of about ± 0.09 Å. It is worth noting that the LAXS studies showed also a second coordination sphere around the calcium ion with a mean $Ca\cdots O_{II}$ distance of 4.58(5) Å ± 0.20(3) Å. In addition, MD simulation at 300 K revealed mainly an eight-coordinated tendency for calcium ions. These results are consistent with those obtained by M. L. Dheu-Andries *et al.* [2]

- *in solid form of calcium oligo(α-L-guluronate)*

*G*eometrical features of the binding sites of calcium ions in the junction zones have been already examined by EXAFS experiments which enable to determine the first coordination shell (paragraph 3.1.1). Alagna *et al.* [4] have found that for calcium oligo(α-L-guluronate) in solid form the Ca–O distance is in the range of 2.33 Å to 2.76 Å.

1.1.2. Grant's idea

It has been suggested by Grant *et al.* [1], on the basis of circular dichroism and X-ray fibre diffraction of polyguluronic acid, that polyguluronate chains (two or more) associate in either two- or three-fold helical conformation via calcium ions (called eggs). Furthermore, it has been suggested that the specific sites for the chelation of calcium ions are provided via interactions with four oxygen atoms from each polyguluronate chain: O6 from carboxylate group, O5, and O2 with O3 on the next residue in the non-reducing direction (Figure 4.1).

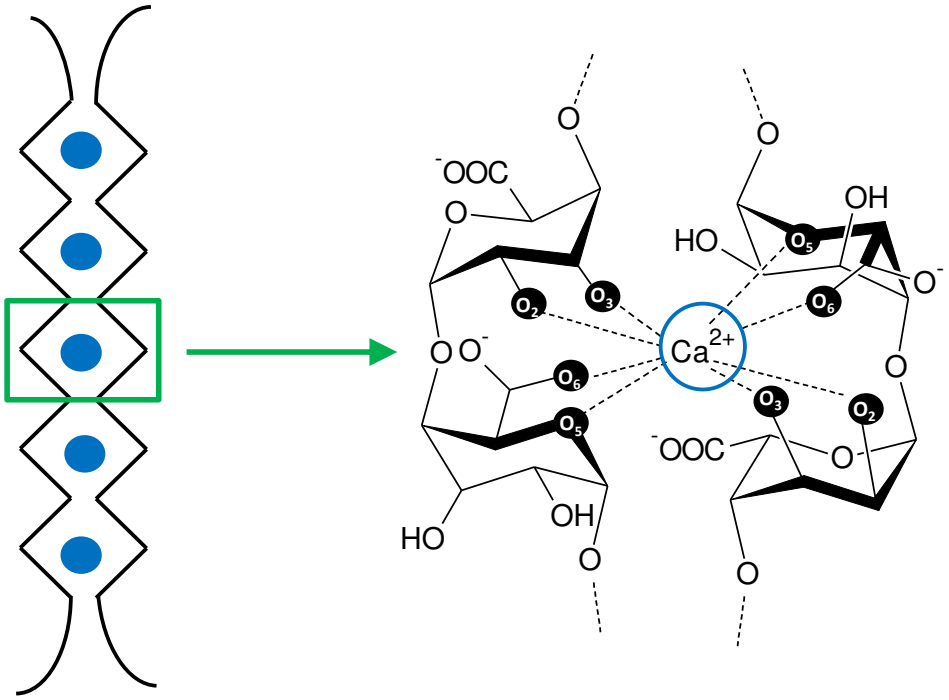

Figure 4.1 *Calcium binding pattern with the oxygen atoms of two G blocks proposed by Grant et al.* [1]

In fact, this conceptual model proposed by Grant *et al.* [1] is attractive because it correctly accounts for the observed cooperativity of association and is consistent with the experimental stoichiometry of one calcium ion for four guluronic acid residues.[5] Nevertheless, precise experimental measurements supporting its correctness are lacking (paragraph 1.2)

1.1.3. *Revisited "egg-box" model*

Several attempts have been made to describe and explain in detail the association of alginate chains in the presence of Ca^{2+} via molecular modeling, which are summarized below.

- *duplexes of G-blocks*

Braccini *et al.* [6] studied calcium-uronate chain. This work did not take into account water molecules because they were not supposed to be involved in the formation of junction zones according to the "egg-box" model suggested by Grant *et al.*[1] In detail, pairs of 2_1 helical, rigid guluronan chains (X = 6) either in a parallel or antiparallel arrangement were modeled. In the case of the parallel arrangement, calcium ions were coordinated by five uronate oxygen atoms: O3 from one chain and O6, O5, O4 and O3 from the other one ($N_{Ca^{2+}} = 5$), Figure 4.2a, Table 4.1. By contrast, the antiparallel chains were interacting with calcium ions via O6 from one chain and O6, O2 and O3 from the second chain ($N_{Ca^{2+}} = 4$), Figure 4.2b, Table 4.1. Additionally, the structure with antiparallel oriented chains was also stabilized by two complementary interchain hydrogen bonds (O2···O6 and O3···O5), Figure 4.2b.

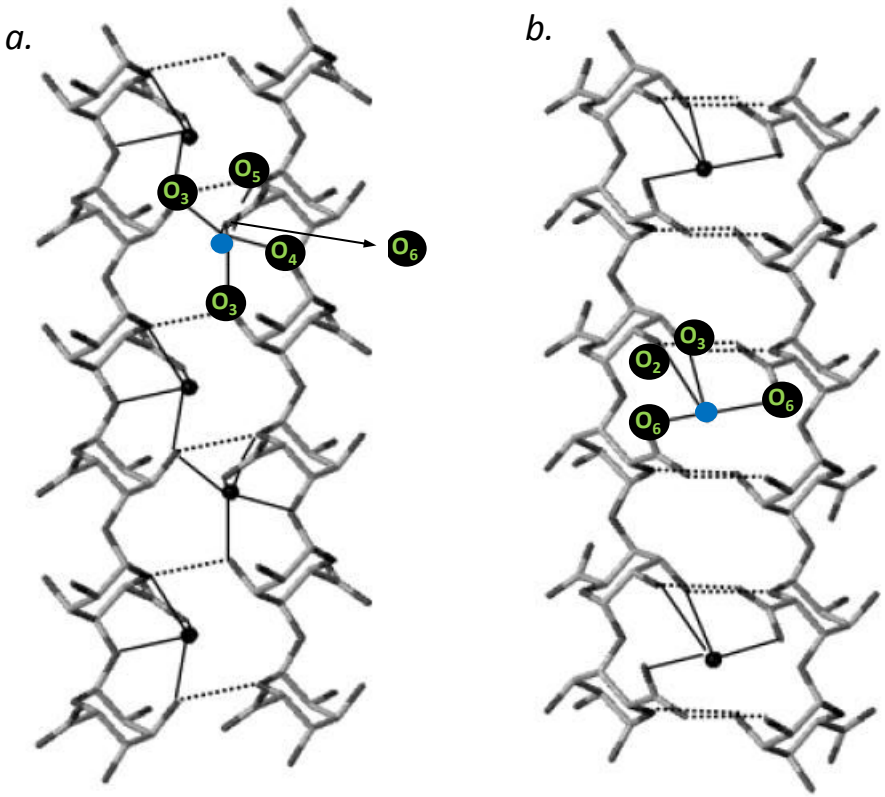

Figure 4.2 *Calcium binding pattern with the oxygen atoms of two G blocks (X = 6) either in a parallel (a) or antiparallel (b) arrangement proposed by Braccini et al.* [6]

It is worth noting that since the hydrogen bonds is one of the factors which impacts on the gel strength, thus the antiparallel arrangement of chains seems to be favorable in the gel state. Furthermore, it was found that the best association of antiparallel chains occurs when the chains are slightly shifted to each other (1.1 Å). Therefore, the new model proposed by Braccini *et al.* [6] has been named: "*shifted-egg-box model*". Nevertheless, the calcium coordination number differed from 8, thus it suggests that water molecules should participate in the calcium binding process. In addition, an investigation of the crystalline structure of guluronic acid by Atkins and co-workers [7,8] revealed that the presence of water molecules increases the number of intermolecular hydrogen bonds between chains resulting in better association of guluronan chains.

Therefore, further studies performed by Plazinski [9] took into account water molecules. The aim of this work was studying the complexation of Ca^{2+} ions by two finite guluronan chains (X = 10) in an initial 2_1 helical conformation (oriented parallel or antiparallel) using MD. It has been found that the association of polyguluronate chains is maintained via strong interaction between calcium ions and oxygen atoms of the carboxylate groups from two guluronate residues belonging to two different chains and four oxygen atoms of water molecules ($N_{Ca^{2+}} = 8$, Figure 4.3). Nevertheless, besides this calcium complexation pattern, the presence of intensive network of both intra- and inter-chain hydrogen bonds has also stabilized the formation of junction zones for both parallel and antiparallel oriented chains. The summary of the evolution of the calcium coordination number, estimated for calcium ions complexed by two guluronan chains is provided in Table 4.1.

Table 4.1 *The calcium coordination number ($\boldsymbol{N_{Ca^{2+}}}$) estimated by different authors for Ca^{2+} complexation by two guluronan chains.*

Model	$\boldsymbol{N_{Ca^{2+}}}$	**Atoms involved in $\boldsymbol{N_{Ca^{2+}}}$**
Grant *et al.* [1] (2- or 3-fold)	8	chain 1: O6, O5, O2, O3 chain 2: O6, O5, O2, O3
Braccini *et al.* [6] (2_1 parallel)	5	chain 1: O3 chain 2: O6, O5, O4, O3
Braccini *et al.* [6] (2_1 antiparallel)	4	chain 1: O6 chain 2: O6, O2, O3
Plazinski [9] (2_1 parallel & 2_1 antiparallel)	8	chain 1: 2 × O6 chain 2: 2 × O6 and: 4 × O_W

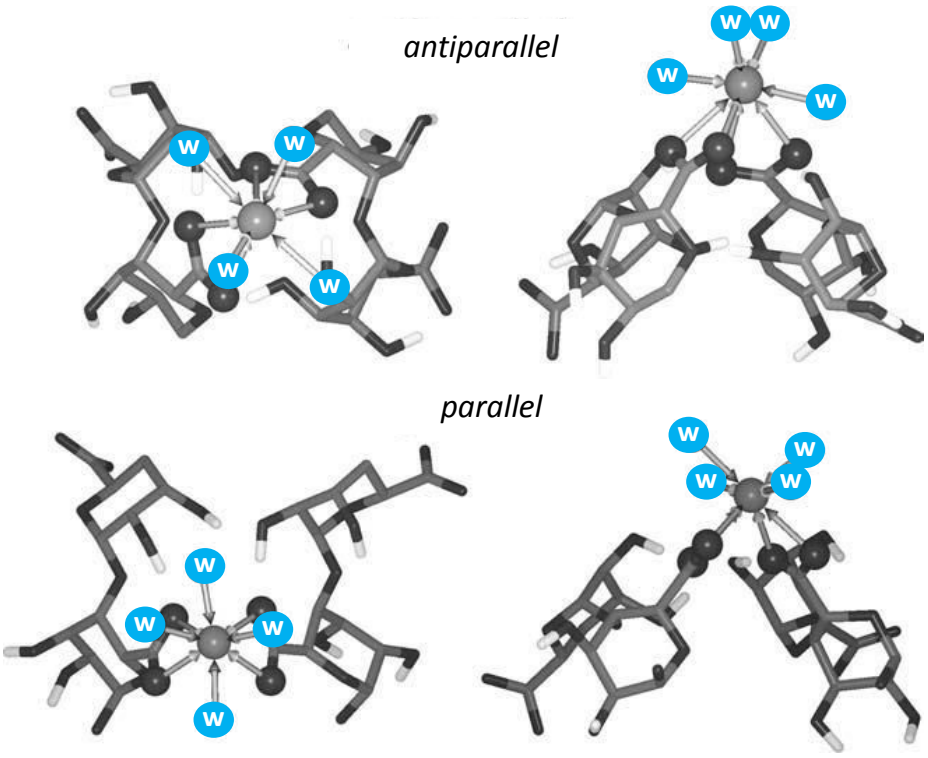

Figure 4.3 *Calcium binding pattern with the oxygen atoms of two G blocks (X = 10) and water oxygens (w) either in an antiparallel or parallel arrangement proposed by Plazinski* [9].

- *single G-blocks and M-blocks*

Some studies incorporating water molecules have been also carried out for single infinite guluronan or mannuronan chains in the presence of Ca^{2+}.

Plazinski and Drach [10] have investigated chains in 2_1 helical conformation (X = 8). Their analysis was mainly focused on the examination of calcium binding mechanism. It was found that the number of water molecules involved in the calcium coordination number ($N_{Ca^{2+}}$) varies from 8 (for free, *i.e.* unbounded Ca^{2+}) to 6 (for fully, *i.e.* bidentately bound Ca^{2+}). In addition, it was noticed that the partially, *i.e.* monodentately bound calcium ion (interacting directly with only one oxygen atom of the carboxylate group) phenomenon occurs rarely and is unstable. This results together with another work (considering single and antiparallel oriented infinite guluronan chains in 2_1 helical conformation, X = 8) performed by the same authors [11] highlighted the involvement of water molecules in the calcium binding process. It has been shown that water molecules may also play a bridging role in linking carboxyl group with the calcium ion, which may facilitate the formation of the junction zones.

On the other hand, Peric *et al.* [12] performed MD simulations of guluronan and mannuronan chains but in both 2_1 ($X = 8$) and 3_2 ($X = 9$) helical conformations. It was found that the binding of Ca^{2+} is non-specific and does not depend on the type of blocks (G or M) as well as the initial helical conformation. Another aim of this study was conformational analysis of the guluronan and mannuronan chains which revealed that the chain conformation is varying both in time and along the chain. Later, Peric *et al.* [13] studied the interactions of guluronan chains in 2_1 helical conformation ($X = 12$) in the presence of monovalent (Na^+, K^+) and divalent (Mg^{2+}, Ca^{2+}) cations. It has been concluded that the affinity of guluronan chains to examined ions decreases in the following order: $Ca^{2+} > Mg^{2+} > K^+ \sim Na^+$ but the chain conformation and flexibility is not related to the type of counter ions.

- *4 chains composed of G-blocks*

Recently, Plazinski *et al.* [14] have attempted to examine the association of two dimers of guluronan chains ($X = 8$, oriented antiparallel to each other) in aqueous environment. It was found that the chain association occurs mainly due to interactions between calcium ions and oxygen atoms of the carboxylate groups because the hydrogen bonding-type interactions were too weak to ensure the junction network. Furthermore, the stability of formed complex was better in the case of the parallel arrangement of two dimers.

- *alternating blocks*

The seminal Grant's paper has already mentioned that polymannuronate chains with both two- and three-fold symmetry are able to complex calcium ions at some higher ion concentrations. Further, it has been shown experimentally by Donati *et al.* [15] that alternating MG-blocks undergo gelation in the presence of calcium ions, thus it has encouraged scientists to probe interactions of alternating blocks (present in natural alginate chains) with Ca^{2+} by molecular modeling.

For instance, Dentini *et al.* [16] have attempted to explain how calcium ions are complexed via alternating blocks, *i.e.* MG, $X = 7$. In detail, short (9.5 ns) MD simulations in aqueous environment were performed for poly(MG) as well as for poly(G) duplexes. The Poly(G)-Ca^{2+} gel model was constructed as a comparative model, in which guluronan chains ($X = 7$) had 2_1 initial conformation and were oriented antiparallel to each other, according to structural parameters indicated by Braccini *et al.* [6] The poly(MG) chain was modeled on the basis of poly(G) chain by flipping the chirality of C-5 carbons of alternating G residues. Figure 4.4 shows the structures observed for poly(G)-Ca^{2+} and poly(MG)-Ca^{2+}. In both cases

the helical twist was equal to 19°, but the fluctuations were higher for alternating blocks what suggests higher flexibility of MG blocks. From this study, it was also noticed that in the case of poly(MG)-Ca^{2+} gel model, the electrostatic interactions between Ca^{2+} ions and carboxylate oxygens (*i.e.* O6) of both M and G units seem to play the main driving force in the gel formation.

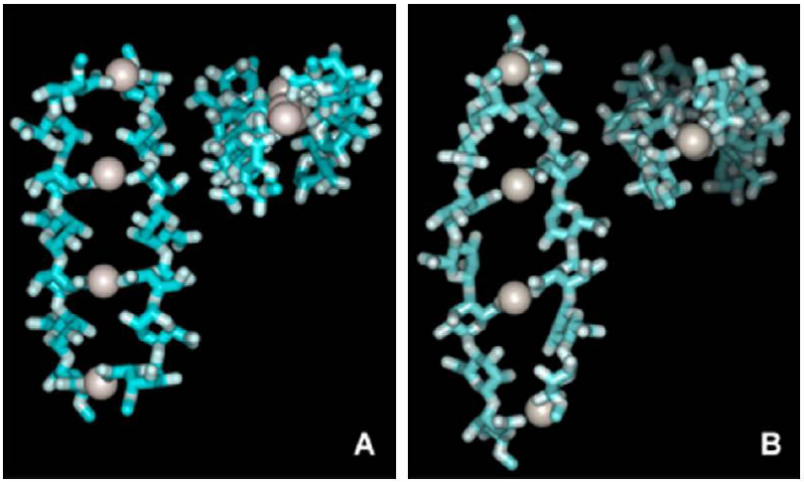

Figure 4.4 *Representation of the "egg-box" models for poly(G)-Ca^{2+} gel (a) and poly(MG)-Ca^{2+} gel (b) proposed by Dentini et al.* [16]

This observation was confirmed by Plazinski [17] who performed MD simulations for different disaccharides, including also the alternating ones: GG, GM, MG and MM. The detailed analysis of calcium binding by G and/or M units has shown that calcium ions interact with alginate chains via oxygen atoms from carboxylate groups (O6). He claimed that "*the calcium binding mode is very similar, independently of the disaccharide composition and ionic strength of the solution*".

From the literature overview presented above, the following conclusions can be drawn. First of all, the interactions between Ca^{2+} and O6 are predominant in the formation of the junction zones and can be considered as specific type of binding. Secondly, the calcium binding pattern is strictly related to applied simulation environment (vacuum or water). But since alginate-Ca^{2+} hydrogels contain water, thus involving water molecules in computer simulations should be considered in order to reflect natural conditions and realistic structure of the junction zones. Therefore, the model proposed by Plazinski seems to be the most appropriate so far.

1.2. Probing the conformations of guluronan chains involved in the junction zones of alginate hydrogels

Grant *et al.* [1] suggested that polyguluronate chains can associate either in two- or three-fold helical conformation via calcium ions, but at that time no experimental evidences were provided. Later, scientists have started to claim that chains adopt a perfect helical conformation with two residues per turn (2_1 helices) what was inspired by a similarity to X-ray fibre diffraction data obtained with (1→4)–α-L-guluronan in the acid form and as Li^+, NH_4^+ or K^+ salt.[18,19] In fact, Mackie *et al.*[19], Sikorski *et al.*[20] and Li *et al.*[21] have attempted to prepare crystalline samples of Ca^{2+}-alginate but good crystallographic data of Ca^{2+}-gel fibres have not been reported (Figure 4.5). Although published X-ray fibre diffraction patterns contain at most three signals and the authors suggested 2_1 or 3_2 conformation, their unambiguous interpretation is impossible (Figure 4.5).[20,21]

Since, X-ray crystallography is based on stereoregularity along the chain and lateral directions and involves the orderly packing of regular helices within a crystal, thus the crystalline state cannot reflect the weaker packing and dominant hydration forces in the junction zones of an alginate-Ca^{2+} hydrogel. It is worth noting that the interactions between guluronan chains and Ca^{2+} in natural environment are based on the movement of chains leading to their conformational disorder, which cannot be described by X-ray techniques.

Therefore in that case, atomistic modeling, as another method, can be applied to probe the structure of the junction zones in Ca^{2+}-alginate gels. This technique allows examining many aspects of the gel network including calcium complexation mechanism which is the driving force in the formation of this specific network, the structure of chains (length, *i.e.* degree of polymerization – *X*, conformation and/or orientation in the case of duplexes or aggregates) as well as number of chains involved into it.

Since the question of the chain length of (1→4)–α-L-guluronan chains incorporated into the junction zones has never been addressed by molecular modeling, thus it has become one of the objects of this PhD thesis (paragraph 3.1). In detail, both single systems and duplexes have been examined in order to highlight the importance of the chain pairing required in the formation of the junction zones.

Besides necessity of studying the chain length effect, one other issue was lacking. From the literature overview given in paragraph 1.1.3 it could be noticed that new "egg-box"

model proposed by Plazinski [9] was mainly described in terms of the calcium binding pattern. This description is satisfactory, but the conformational analysis of guluronan chains involved in the junction zones of alginate hydrogels was omitted. Some attempts concerning chain conformation analysis were made by Peric *et al.* [12,13] However, by imposing an artificial periodicity along the chain axis in order to have formally infinite chains, the accessible conformations were strongly restricted, what finally precluded a proper analysis of chain flexibility in those studies. Therefore, a molecular dynamics investigation of the helical forms adopted by (1→4)–α-L-guluronan chains in explicit water environment has been a topic of paragraph 3.2.

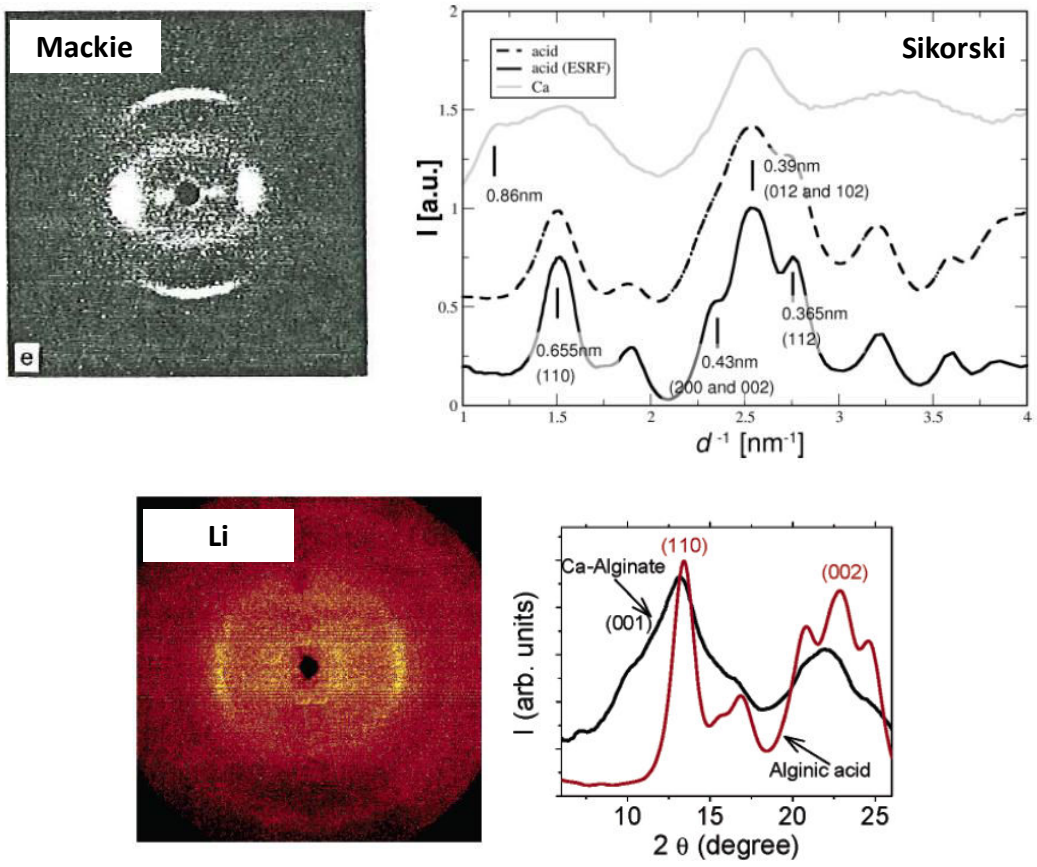

Figure 4.5 *X-ray diffraction data obtained for Ca^{2+}-alginate gels by Mackie et al.[19], Li et al.[21] and Sikorski et al.[20]*

2. Methods

2.1. Modeled systems

The initial twofold (2_1) and/or threefold (3_2) helical conformations of guluronan chains were generated according to Braccini *et al.* [22] and used as starting point for Molecular Dynamics simulations. Each system was neutralized by adding the appropriate number of calcium ions and hydrated using Simple Point Charge (SPC) water molecules. Periodic Boundary Conditions (PBC) were applied throughout the calculations.

2.1.1. Chain length effect

Single chains systems and duplexes having both parallel (para) and antiparallel (anti) chains were modeled, starting from 2_1 helical conformation. In order to study the chain length effect, models of varying degree of polymerization (X) in the range from 2 to 20 were prepared.

2.1.2. Conformational analysis of oligomer of (1→4)-α-L-guluronan

The object of this study was an oligomer of (1→4)-α-L-guluronan having 12 fully charged repeating units (X = 12). Both single chains and paired (parallel and antiparallel) chains in 2_1 and 3_2 initial helical conformations were modeled.

2.2. Modeling strategy

The initial complexes were prepared in the gas phase using Cerius 2 (Accelrys Inc., San Diego, CA, USA). The energy of a system comprising one or two (1→4)-α-L-guluronan chains and a neutralizing amount of calcium ions was minimized using rigid body displacements to ensure that the helical conformation was preserved. Each system was then placed in a rectangular parallelepiped periodic box whose edges were 1.0 nm from the chains; the sole exception was the 3_2 para model for which the box was 5 nm × 5 nm × 9 nm in size. The empty space of the box was then filled with SPC water molecules using GROMACS.[23] Structures were optimized by the *steepest descent* method followed by the *conjugate gradient* approach with a convergence criterion of 1000 kJ mol^{-1} nm^{-1}. The system was then heated from 0 K to 300 K in 50 K steps (each step was followed by an annealing period of 2.5 ps and the whole process lasted 50 ps) and equilibrated at 1 atm for 100 ps. A slightly different procedure was applied for 3_2 duplexes: 12 steps of 25 K increments followed by equilibration

over a 400 ps period. MD simulations were performed during 50 ns and 100 ns for single chain and duplex systems, respectively. Both equilibration and MD simulations were carried out in canonical NPT ensemble (with constant number of particles, pressure and temperature). All systems were allowed full conformational freedom.

2.3. *Computed values*

All the computed values were analyzed either during the whole trajectory of MD or during its end. As can be seen from Figure 4.6, the root mean square positional difference (RMSD) of the coordinates of selected models between the structure at a given time and the initial one remained at a constant value for production step. Therefore, the analyzed systems can be considered as properly equilibrated.

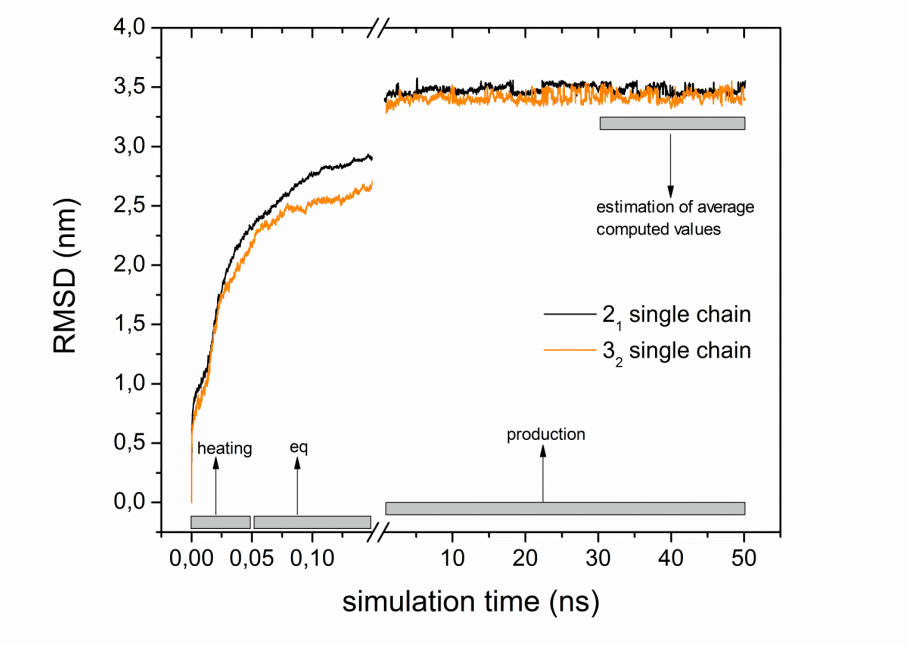

Figure 4.6 *The root-mean-square deviation (RMSD) of the coordinates of the system during simulation time for the single chain helical models (degree of polymerization, X = 12) with initial 2_1 and 3_2 conformation. RMSD during last 20 ns is equal to 3.48 ± 0.03 nm for 2_1 single chain and 3.43 ± 0.04 nm for 3_2 single chain, respectively.*

2.3.1. *The calcium coordination number*

Since, it was found that the Ca–O bond distance is in the range from 2.30 Å to 2.85 Å in carbohydrate complexes (paragraph 1.1.1), thus in order to determine the $N_{Ca^{2+}}$, only the oxygen atoms located in the distance lower than 3 Å from each calcium ion were taken into account.

2.3.2. *Hydrogen bonds (HBs)*

Hydrogen bonds (HBs) are the bonds between donors (D) and acceptors (A). However, in order to determine if an H-bond exists, specific geometrical criteria (Figure 4.7) should be met.

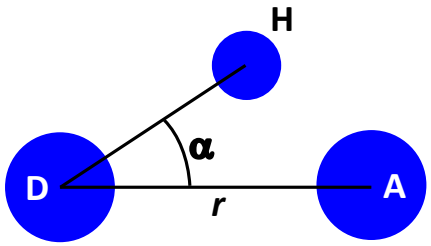

Figure 4.7 *Geometrical hydrogen bond criterion.*

In GROMACS [23] the H-bond exists if:

$$r \leq r_{HB} = 0.35\ nm \quad \text{(Eq. 4.1)}$$

$$\alpha \leq \alpha_{HB} = 30° \quad \text{(Eq. 4.2)}$$

2.3.3. *The end-to-end distance (R) and the conformational pitch*

The *end-to-end distance* (*R*) corresponds to the distance between the O4 atom of the non-reducing residue (residue 1) and O1 atom of the reducing residue (the last residue) of the chain. In addition, by dividing the maximum of the distribution of *R* by number of repeating units in the chain, the *conformational pitch* can be estimated.

2.3.4. *The glycosidic dihedral angles* (Φ, Ψ)

The glycosidic dihedral angles Φ and Ψ are defined as O_5–C_1–O_1–C_4' and C_1–O_1–C_4'–C_5', respectively (Figure 4.8)

2.3.5. *The conformational turn angle* (H)

The conformational turn angle (H) is estimated by the dihedral angle defined by the C_6'–C_5'–C_5–C_6 atoms of two consecutive α-L-guluronic acid residues (Figure 4.8).

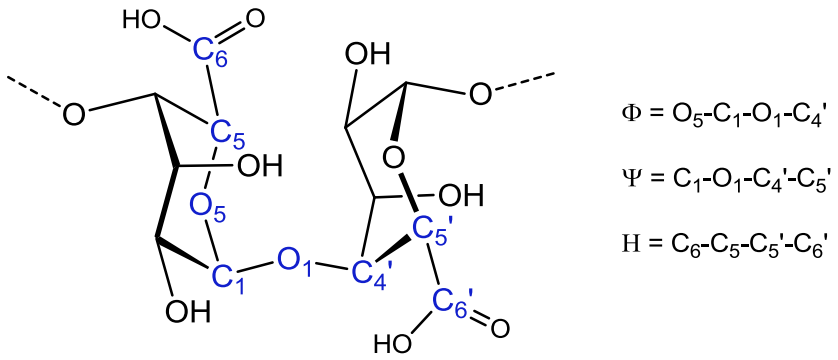

Figure 4.8 *Schematic representation of a (1→4)-α-L-guluronan chain showing the torsion angles used for conformation analysis.*

2.4. Computational Details

In Cerius2 software, the Dreiding 2.21 force field [24] was used. All molecular dynamics simulations were performed in GROMACS software (version 4.5.4.) [23] using Gromos53a6 force field.[25] Both programs were run on workstations connected to the local *Centre d'Expérimentation et de Calcul Intensif* (CECIC). Specific parameters described by Peric *et al.* [12] for L-guluronate residues were applied. In addition, Plazinski [9] modified the Lennard-Jones (LJ) parameters describing the interaction between a calcium ion (Ca^{2+}) and the oxygen of the carboxylate group to $C_6 = 2.0 \times 10^{-3}$ kJ nm^6 mol^{-1} and $C_{12} = 1.67 \times 10^{-6}$ kJ nm^{12} mol^{-1} according to the suggestion of Project *et al.* [26], thus the same LJ parameters were used. Equations of motion were solved using the leapfrog algorithm [27] with time steps of 2 fs. In order to constrain bond lengths, the LINear Constraint Solver (LINCS) algorithm [28] was applied. A cut-off distance of 0.9 nm was applied for both Coulomb and van der Waals interactions. The electrostatic energies and forces were evaluated using the particle-mesh Ewald method proposed by Tom Darden [29,30] with a cut-off at 0.9 nm. The temperature was controlled with velocity rescaling thermostat [31] and the pressure was regulated by Berendsen algorithm (1 atm, isotropic coordinate scaling).[27] All trajectories were visualized in VMD software (*version* 1.9.1).[32]

3. Results: from (1→4)-α-L-guluronan single chains to duplexes

The applied modeling strategy was focused on two aspects: the chain length effect of (1→4)–α-L-guluronan chains incorporated into junction zones and their conformation.

3.1. Chain length effect

The aim of this study was to examine how the length of guluronan chains impacts the formation of the junction zones.

3.1.1. The calcium coordination number

The calcium coordination number ($N_{Ca^{2+}}$) was calculated for both types of duplexes: parallel and antiparallel. In all systems, calcium ions complexed via two guluronan chains were bound mainly bidentate. Furthermore, the average total coordination number of calcium was 8 and involved four oxygen atoms of the carboxylate groups and four oxygen atoms of water molecules (Figure 4.9a). These results are consistent with those found by Plazinski [9] (paragraph 1.1.3).

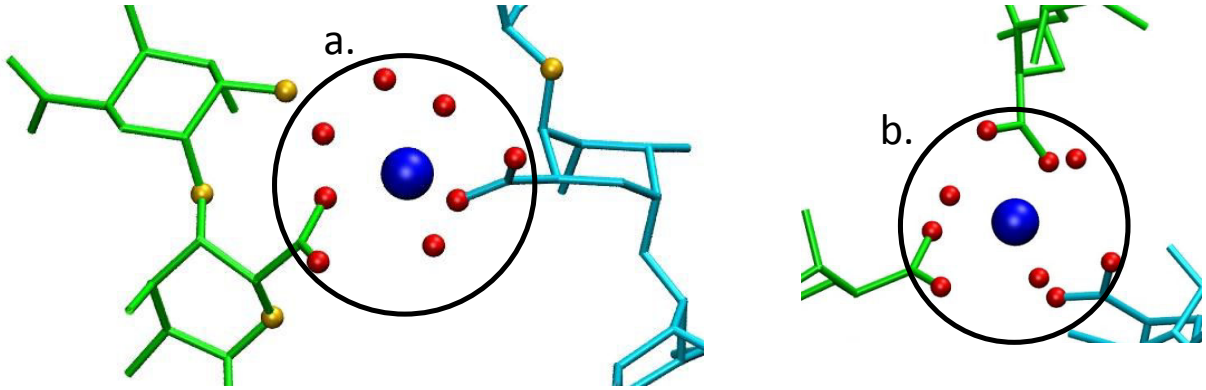

Figure 4.9 *Selected examples of the calcium coordination pattern in 2_1 parallel guluronan duplexes: (a) degree of polymerization, X = 10, (b) X = 6. The red oxygen atoms are involved into the first coordination shell of Ca^{2+}, whereas the yellow ones into the second coordination shell of Ca^{2+}.*

Interestingly, in some models (*e.g.* duplex parallel, $X = 6$) some Ca^{2+} ions were coordinated by six carboxyl oxygens belonging to three different chains and three water oxygens, $N_{Ca^{2+}} = 9$ (Figure 4.9b). This phenomenon could be observed due to applied Periodic Boundary Conditions (PBC) throughout the calculations. The calcium complexation pattern described above involves the oxygen atoms located in the nearest neighborhood of

Ca^{2+} (in a distance lower than 3 Å), which is often called *the first coordination shell of* Ca^{2+} (Figure 4.9, red oxygen atoms). But, the guluronan chains have also other oxygen atoms, *i.e.* O1, O2, O3, and O5 which may be considered as potential ligands that bind Ca^{2+}. However, Ca–O bond distances are in these cases usually longer than 3 Å, thus those ligands belong to *the second coordination shell of* Ca^{2+} (Figure 4.9a, yellow oxygen atoms).

The interactions between guluronan chains and calcium ions can be described by the Radial Distribution Function (RDF) plots computed for the distance between Ca^{2+} and oxygen atoms in the system. As can be seen from Figure 4.10, plotted for 2_1 parallel guluronan duplex (degree of polymerization, X = 10), the first peak (around 2.5 Å) is intense and sharp and corresponds to the first coordination shell of Ca^{2+}, whereas the second one (around 4.6 Å – 5.3 Å) is broad and corresponds to the second coordination shell of Ca^{2+}. The Ca–O distance of 2.5 Å is in good agreement with distance of 2.46 Å determined by F. Jalilehvand *et al.* [3] (paragraph 1.1.1). In addition, Plazinski [17] plotted similar curves for distance between the carboxyl groups and calcium ions and obtained two peaks at 2.5 Å and 4.6 Å, respectively, which lie in the same range as those determined in these studies.

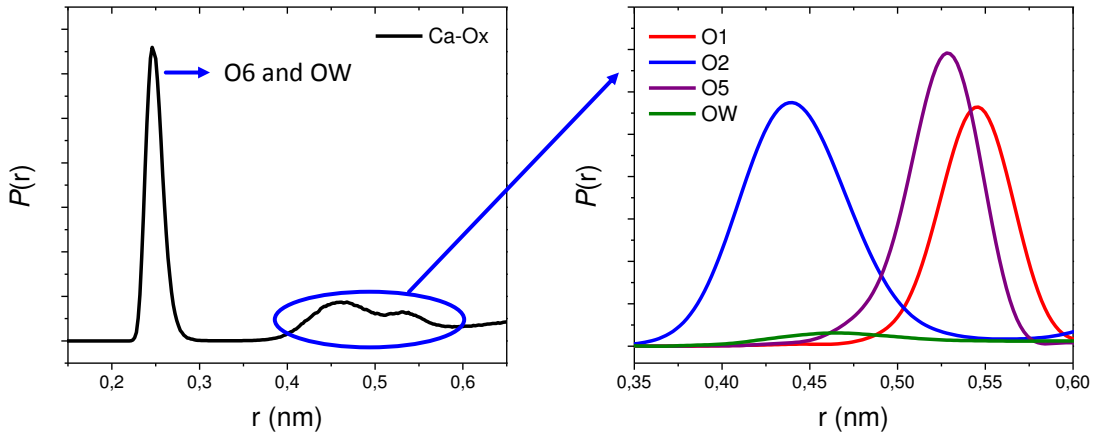

Figure 4.10 *The radial distribution function, P(r) plotted for* 2_1 *parallel guluronan duplex (degree of polymerization, X = 10) for the distance between calcium ions and all oxygen atoms in the model.*

The number of calcium ions interacting simultaneously with two carboxylate groups were determined and plotted as a function of degree of polymerization (X) (Figure 4.11). Since the modeled duplex systems contained the neutralized amount of calcium ions, thus the number of Ca^{2+} in each system is equal to X. It can be seen from Figure 4.11 that for parallel oriented chains, for $X > 8$ more than 50% of calcium ions present in the system were complexed by two carboxylate groups of guluronan chains. On the other hand, in all

antiparallel models 50% of Ca^{2+} were complexed, however in some models (X = 8, 10, 14, 16) the complexation by two chains was even higher.

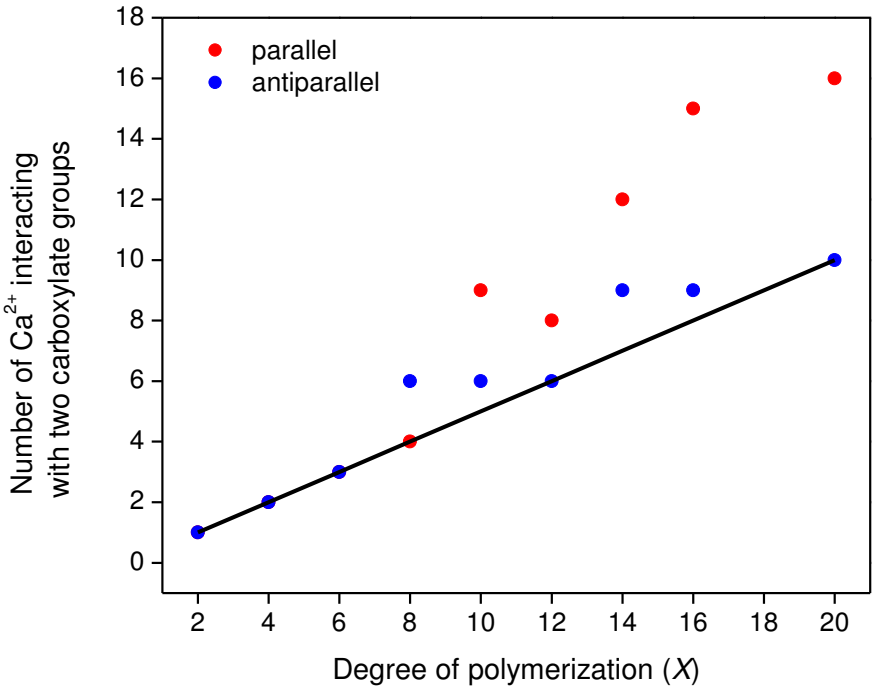

Figure 4.11 *Number of Ca^{2+} complexed by two carboxylate groups of guluronan chains, having 2_1 initial conformations, of varying degree of polymerization (X) plotted as a function of X. The black line corresponds to a half of the amount of calcium ions present in each system.*

The higher amount of calcium ions interacting with guluronan chains can be explained by the formation of aggregates of chains via calcium ions. This is observed as a result of applied PBC. For instance, the network formed by inter-chain Ca^{2+} complexation involving more than two chains was observed in parallel oriented duplex (X = 14), shown in Figure 4.12.

In addition, Small-Angle X-ray Scattering (SAXS) measurements of alginic acid gels[33] and Ca-alginate gels [34,35] have already suggested that the junction zones are formed by lateral association of guluronic acid residues. Furthermore, it was observed that the size of formed aggregates is increasing with time up to bundles composed of even 16 chains.[35] Nevertheless, besides an interest in studying aggregates of chains, this aspect is not covered in this manuscript.

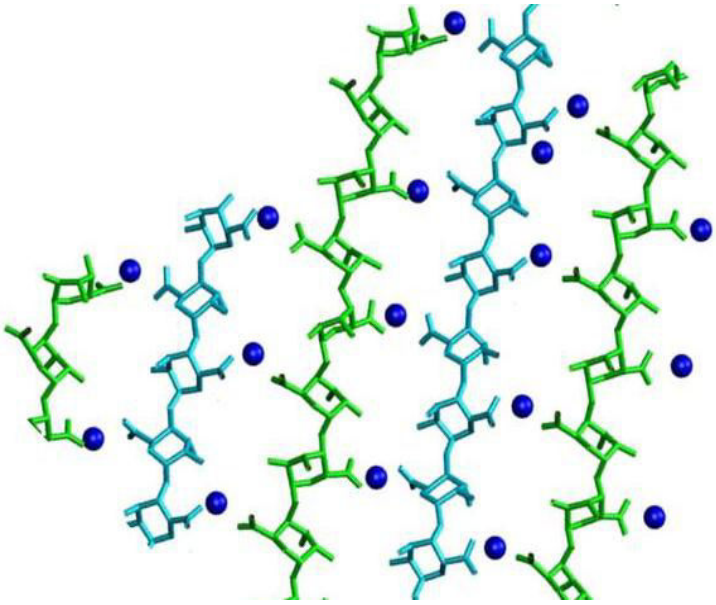

Figure 4.12 *The network formed by inter-chain interactions via calcium ions (navy blue atoms). Initial 2_1 parallel oriented duplex (X = 14) composed of two guluronan chains evolved to the specific network involving more chains as a result of applied Periodic Boundary Conditions (PBC) throughout the calculations.*

3.1.2. Hydrogen bond (HB) pattern

Duplexes of varying *X* were also analyzed in terms of both intra- and inter-chain HBs. As can be seen from Figure 4.13, the O2···O6 type of intrachain hydrogen bonding was observed in every model what is in agreement with the findings from Plazinski studies.[9]

On the other hand, detailed analysis of interchain HBs (Figure 4.14) revealed that parallel oriented chains may interact with each other also via some HBs such as O2···O6 and O3···O3, occasionally present in some examined models. By contrast, in antiparallel systems, the number of HBs is much higher and involves mainly following interchain HBs: O2···O6, O3···O6 and O3···O5 as it was found by Plazinski [9] for *X* = 10. The present study on antiparallel systems confirms the previous result obtained by Braccini *et al.* [6] and Plazinski [9], thus contributes additional evidence that the structure of the junction zones involving guluronan chains in antiparallel arrangement is also stabilized by strong interchain hydrogen bonds (mainly between O2···O6, Figure 4.15)

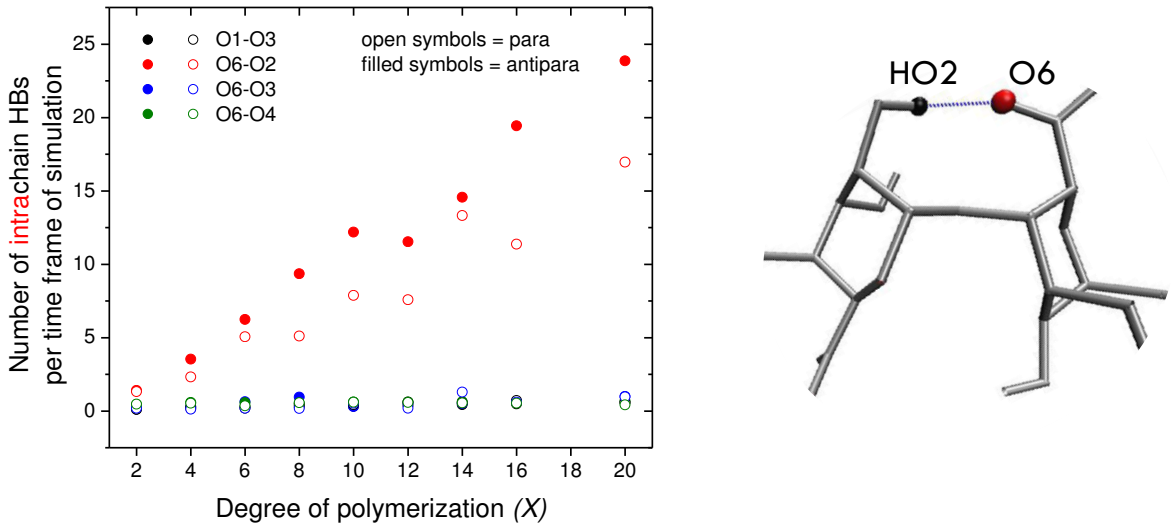

Figure 4.13 *Number of intrachain hydrogen bonds (HBs) for duplexes (parallel and antiparallel) composed of guluronan chains in 2_1 helical initial conformation at 300 K.*

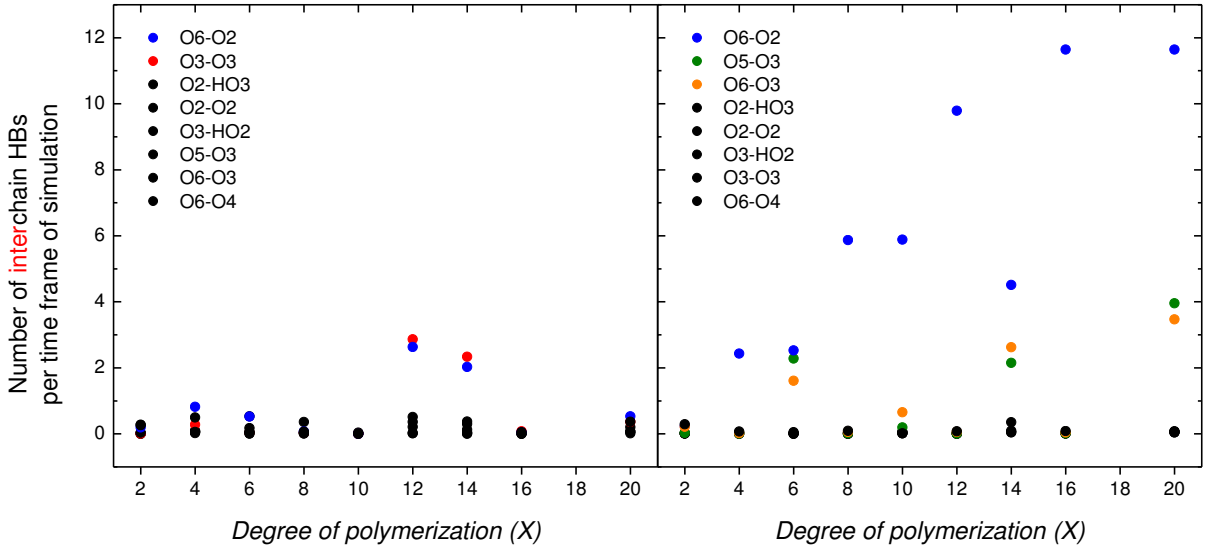

Figure 4.14 *Number of interchain hydrogen bonds (HBs) for duplexes: parallel (on the left side) and antiparallel (on the right side) composed of guluronan chains in 2_1 helical initial conformation at 300 K.*

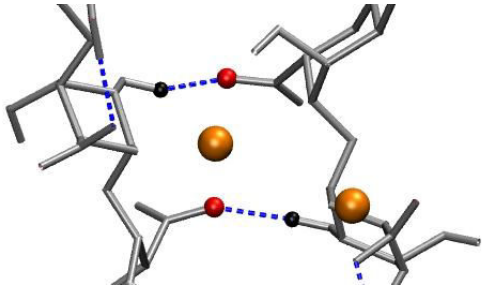

Figure 4.15 *The interchain HBs involving O6 (red atom) and HO2 (black atom).*

3.1.3. *Normalized end-to-end distance (R)*

Figure 4.16 shows the average end-to-end distance (R) calculated during simulation time normalized by the number of degree of polymerization (X) for different systems: single or duplex chains (parallel and antiparallel). It can be seen from this graph that the values obtained for single chains are lower than for individual chains in duplexes. This result indicates that the single chains are more coiled than the duplexes due to higher rotational freedom. By contrast, the flexibility of chains in paired systems is more limited, thus leading to more extended structures. Furthermore, the comparison of individual chains in duplexes reveals no significant differences between both chains in parallel duplexes, whereas in the case of antiparallel oriented duplexes, above X = 12, the chains has begun to behave slightly differently.

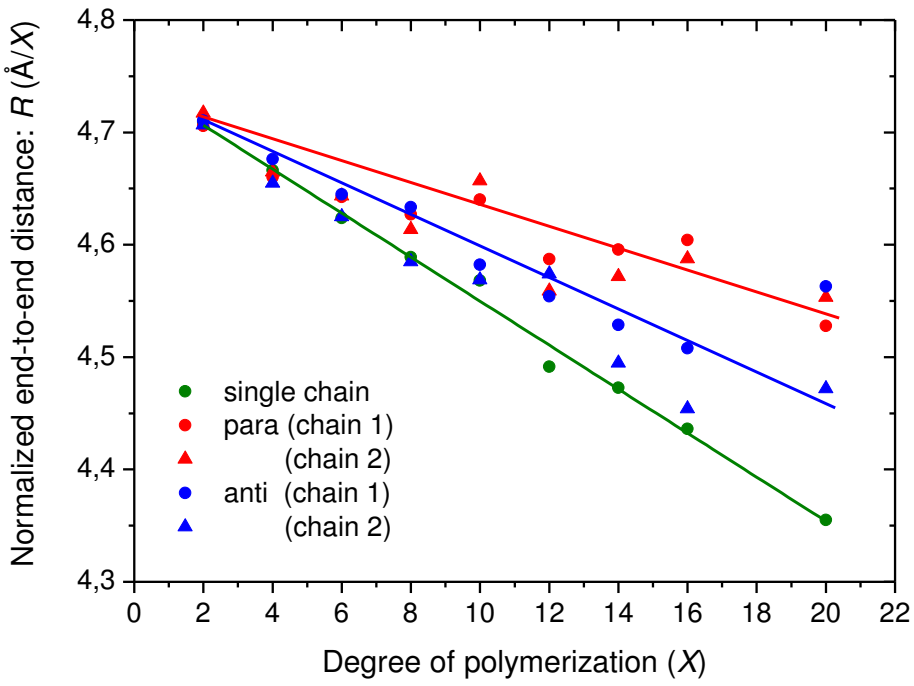

Figure 4.16 *Average end-to-end distance (R) computed during simulation time, normalized by the degree of polymerization (X) in the simulated systems composed of guluronan chains in 2_1 helical initial conformation at 300 K.*

3.1.4. *The conformational turn angle* (H)

H should take the value of 180° for perfect 2_1 helix. Despite all simulated systems had an initial 2_1 helical conformation (H_0 = 180°), the average value of H, analyzed for both single and paired systems having $4 \leq X \leq 20$ during MD simulations, differs from 180° (Table 4.2). In the case of single systems, all values are almost independent of the degree of

polymerization, in contrast to duplexes (Figure 4.17). However, a calculation of the average turn angle for each type of modeled system, *i.e.* single, parallel and antiparallel has shown twisted 2_1 helices with a twist around 10° (Table 4.2).

Table 4.2 *Statistics about the turn angle (H) for single chains and duplexes initiated with 2_1 helical conformation (average value and standard deviation).*

System	single		para		anti	
X	<H> [°]	σ [°]	<H> [°]	σ [°]	<H> [°]	σ [°]
4	186	30	193	30	199	23
6	189	30	189	28	175	22
8	189	30	189	26	187	29
10	189	29	186	18	196	31
12	189	30	197	25	199	17
14	191	31	195	23	181	37
16	190	30	186	24	197	21
20	191	30	190	23	187	29
All	**189**	**30**	**191**	**24**	**190**	**29**

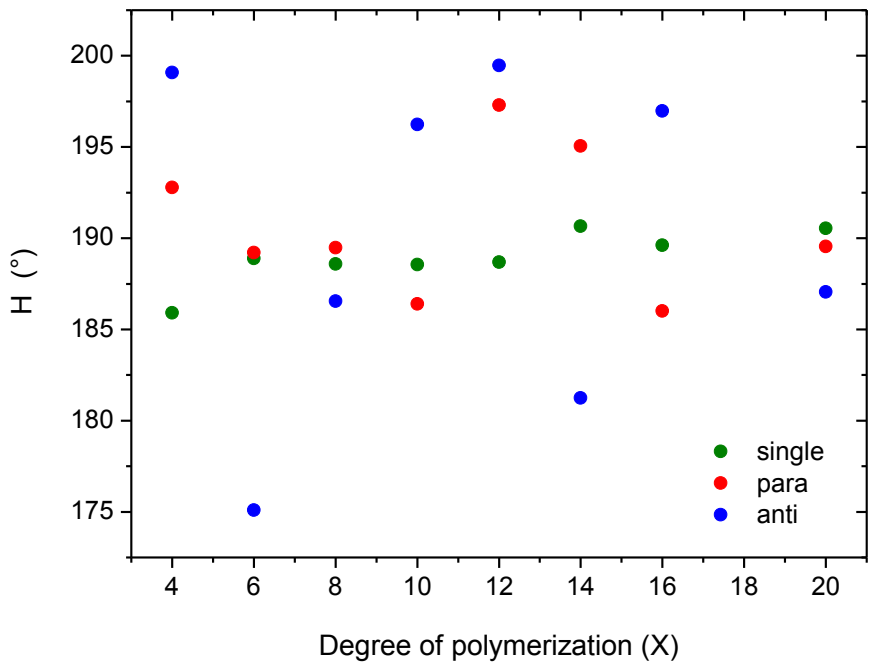

Figure 4.17 *Averages of the turn angle (H) in the simulated systems with an initial 2_1 conformation at 300 K.*

3.2. Conformation analysis of oligomer (X = 12) in single chain systems and duplexes

Since the previous studies suggested that the guluronan chains involved in the junction zones of alginate hydrogels are twisted, thus the necessity of detailed analysis of (1→4)-α-L-guluronan blocks in terms of the chain conformation has appeared.

The main goal of this work was probing the helical forms of Ca^{2+}-guluronan junction zones in alginate gels. Thus, a molecular dynamics investigation of the conformation adopted by (1→4)–α-L-guluronan chains (X = 12), both single and paired (parallel and antiparallel) having 2_1 and 3_2 initial helical conformation, in the presence of calcium ions and in explicit water environment were studied. The obtained results have been already published as a paper: *Probing the helical forms of Ca^{2+}-guluronan junction zones in alginate gels by molecular dynamics 1: Duplexes*.[36]

3.2.1. The calcium coordination number and HBs

In this study both for 2_1 and 3_2 duplexes, the same calcium coordination shell and hydrogen-bonding pattern reported by Plazinski [9] for 2_1 duplex systems (paragraph 1.1.3) was observed so it will not be described again.

3.2.2. O1-O4 distances between successive glycosidic oxygen atoms

In all models, the pyran ring of guluronic acid explored the expected $^1C_4$ chair conformation exclusively and the O1-O4 distances between successive glycosidic oxygen atoms remained constant throughout calculations (Table 4.3). Nevertheless, the predicted average distance of 4.82 ± 0.12 Å was larger than the value estimated from *ab initio* calculations in vacuum (4.56 Å), [37] and that of the monomer length used by Atkins *et al.* [8] to build the crystal structure of the acid form of (1→4)–α-L-guluronan (4.35 Å).

Table 4.3 *Statistics about the O1-O4 distance (average value and standard deviation).*

System	Helix 2_1		Helix 3_2	
	Distance O1-O4 (Å)	σ [Å]	Distance O1-O4 (Å)	σ [Å]
Single	4.80	0.12	4.80	0.12
Para (chain 1)	4.82	0.12	4.82	0.12
(chain 2)	4.81	0.12	4.81	0.12
Anti (chain 1)	4.83	0.12	4.81	0.12
(chain 2)	4.82	0.12	4.82	0.12

3.2.3. The end-to-end distance (R) and the conformational pitch

Figure 4.18 shows the probability distribution of the end-to-end distance of the individual chains for different systems: single or duplex chains, parallel or antiparallel with a 2_1 or 3_2 initial helical conformation. Average values and standard deviations are also indicated in Figure 4.18. The mean conformational pitches were estimated by simply dividing the most populated end-to-end distance by the number of residues in the chain (X = 12). The results are summarized in Table 4.4.

Table 4.4 *Average conformational pitches for (1→4)-α-L-guluronan chains.*

	Pitch (Å)	
System	**Helix 2_1**	**Helix 3_2**
this study		
Single	4.57	4.61
Para (chain 1)	4.62	4.63
(chain 2)	4.59	4.50
Anti (chain 1)	4.61	4.21/4.63
(chain 2)	4.61	3.78/4.41
previous modeling		
Single (Braccini *et al.*) [22]	4.27	4.42
Single infinite (Peric *et al.*) [12]	4.59	4.73
X-ray fibre diffraction		
Acid gel (Sikorski *et al.*) [20]	4.36	-
Ca^{2+} gel (Li *et al.*) [21]	-	3.90

In the two single chain systems and in the duplexes with an initial 2_1 helical conformation the distribution of the end-to-end distance was unimodal and centered around 54 Å-56 Å, with typical standard deviations (σ) of less than 2 Å. This indicates extended and stable conformations with average helical pitches of 4.57 Å and 4.59 Å-4.62 Å for single and duplex chains, respectively.

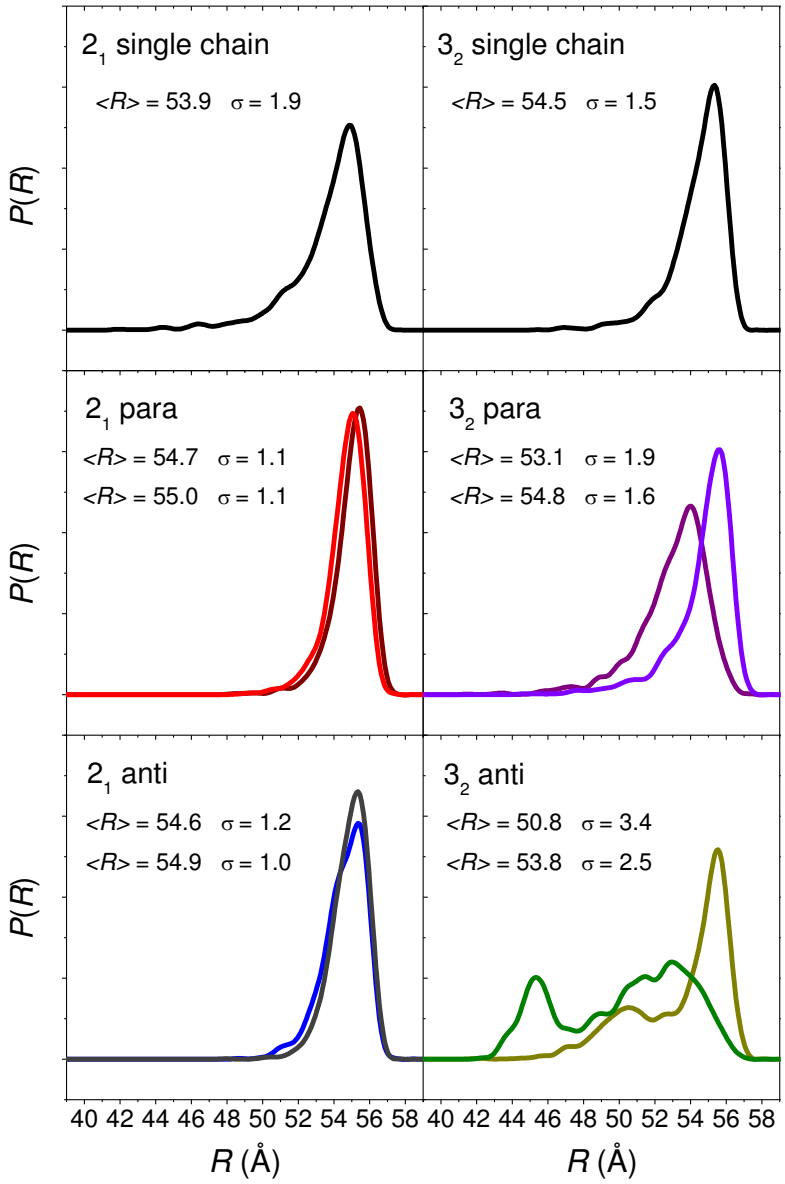

Figure 4.18 *Distribution of the end-to-end distances R in the simulated systems at 300 K. P(R) is the probability of having a value R during simulation time. Left, systems with a 2_1 initial conformation; right, systems with a 3_2 initial conformation; from top to bottom, single chains, duplexes parallel, duplexes antiparallel. Average values (<R>) and the standard deviations (σ) are also reported.*

Also, nearly identical distributions were observed for the two chains in duplex systems. By contrast, starting from a 3_2 helical conformation led to markedly different end-to-end distances for the two chains in the duplex and to broader distributions (σ = 1.6-1.9 Å for the parallel model and σ = 2.5-3.4 Å for the antiparallel model). In particular, multimodal distributions were observed for the antiparallel model. This result indicates a significant conformational disorder and a strong nonequivalence of the chains for 3_2 models.

Table 4.4 summarizes the predicted pitches and compares them with literature values obtained either from the modeling of single chains or by X-ray fibre diffraction. Globally, the new values are higher than those predicted by Braccini *et al.* [22] for perfectly regular helices built from the repetition of the lowest energy conformation of a neutral GG disaccharide. These differences are unsurprising since Braccini's model corresponds to a static view of the chain conformation whereas molecular dynamics takes into account the conformational fluctuations and disorder induced by thermal energy. A better agreement was observed with the values reported by Peric *et al.* for single chains systems in explicit water environment.[12,13] Since the molecular dynamics procedure was similar (the only difference in the force field parameters being the non-bonded parameters for the interaction between carboxylate groups and Ca^{2+}), the small differences observed must be a consequence of the infinite chain approach used by Peric compared to the finite-chain strategy used in this study.

Computed values are systematically higher than the experimental ones from the literature.[21,20] Part of the difference may be ascribed to an overestimation of the O1-O4 distance due to force field parameters incapable to correctly describe the puckering amplitude of the pyran ring; but the fundamental reason is that experimental data were either obtained for an acid gel of guluronan (2_1 helical conformation)[20], or were based on poor crystallographic data (Ca^{2+}-gel, 3_2 helical conformation).[21] Moreover, whereas experimental pitches are extracted from a solid crystalline state, the predicted ones correspond to solvated chains with ample conformational freedom.

Visual inspection of the systems in their most probable conformations (Figure 4.19) shows that individual chains are extended but slightly curved and that duplexes are made of intertwined chains.

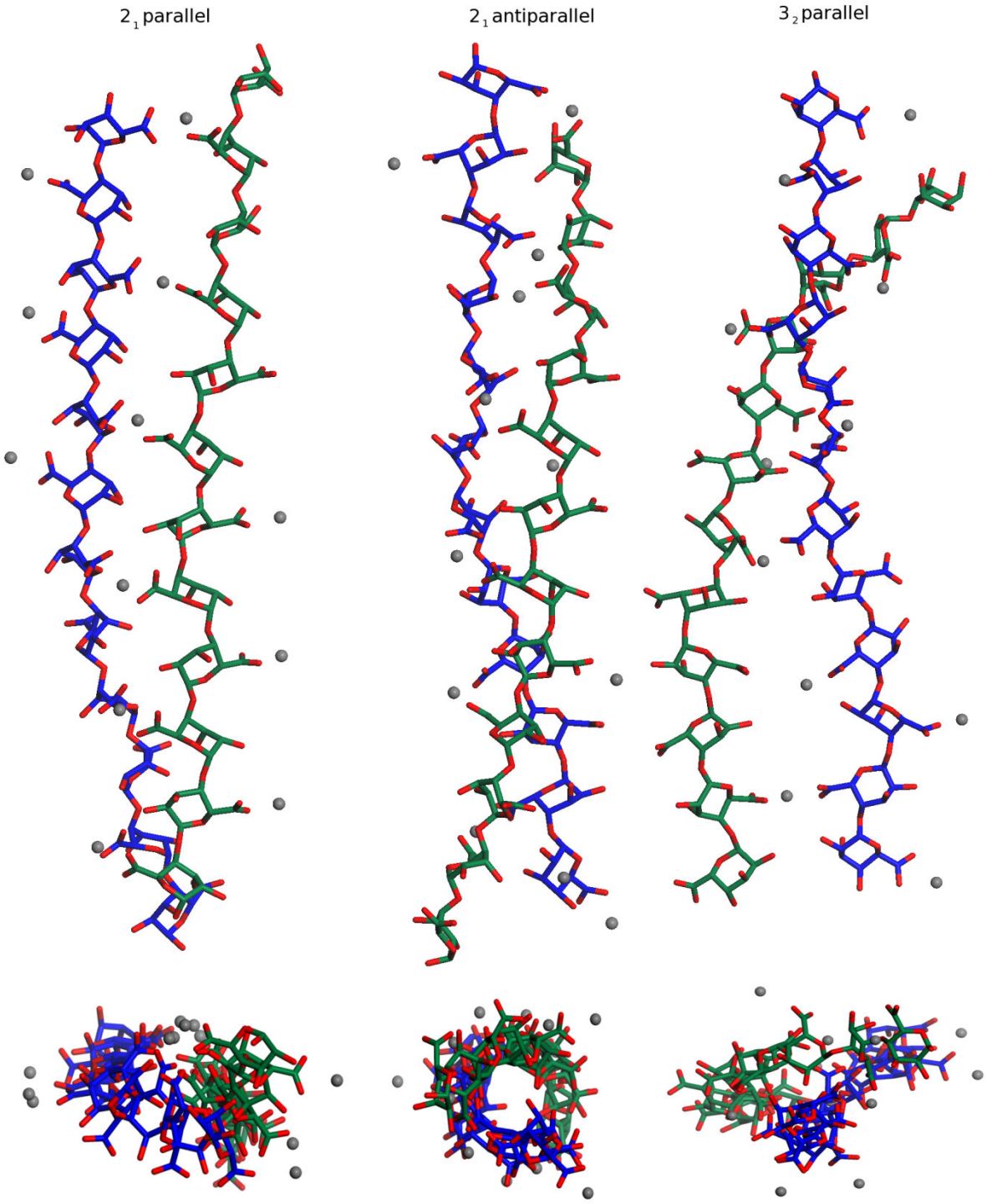

Figure 4.19 *Conformation adopted by duplex systems towards the end of the simulation. View along the chain axis (bottom) and perpendicularly to it (top).*

3.2.4. *The conformational space explored by chains*

Figure 4.20 and Figure 4.21 show the conformational space (Φ, Ψ, H) explored by single chains system and duplex chains during simulation, respectively. The local helical conformation is indicated by a color code and is given by the turn angle H, which corresponds to the relative orientation of two contiguous residues (Figure 4.8).

Interestingly, the explored area of the graphs corresponds to the lowest energy well previously identified by Perry *et al.* [38] by a systematic variation of the torsion angles (Φ, Ψ) of a dimer using the CVFF force field. In that study, a grid searching procedure revealed several additional higher energy conformations accessible at 300 K which were not explored in our MD simulations.

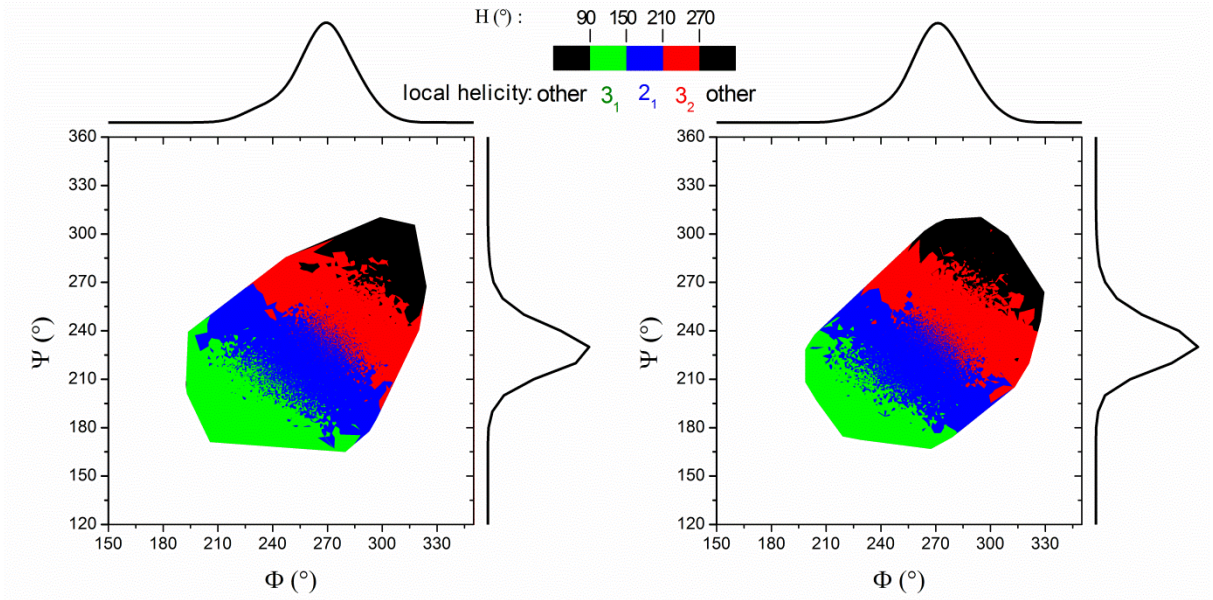

Figure 4.20 *Conformational space explored by single chains with initial 2_1 and 3_2 conformation, respectively. The (Φ, Ψ, H) values taken by all disaccharide residues are reported. The two curves located outside each graph correspond to the probability distribution of the two torsion angles* Φ *(upper curve) and* Ψ *(at the right).*

All systems behaved similarly and led to mostly extended chains with no kinks. For instance, starting from the 2_1 model, average values of 268° and 229° were obtained for the Φ and Ψ torsion angles, respectively, with $\sigma < 21$ ° (see Appendix, Tables: 4A.1 - 4A.4). As described by Peric *et al.* [12,13], H should take the values of 180° ± 30° for the 2_1 helical conformation and 240° ± 30° or 120° ± 30° for the 3_2 and 3_1 conformations, respectively. Hence, all values outside these ranges are quoted as 'other' in Figure 4.20 and Figure 4.21. In

the present study all canonical helical conformations were significantly explored: The 2_1 and 3_2 helical forms run diagonally across the center of the map, whereas the 3_1 is located in the southwest corner and 'other' conformations mostly occupy the northeast one. The last two conformations were totally unexpected: Since the 3_1 form had been described as not particularly stable in a previous study, [22] it was not considered as a starting model for our calculations. Here it is worth noting that the diffuse borders delimiting the different forms in Figure 4.20 and Figure 4.21 are a consequence of the full conformational freedom allowed for MD simulations.

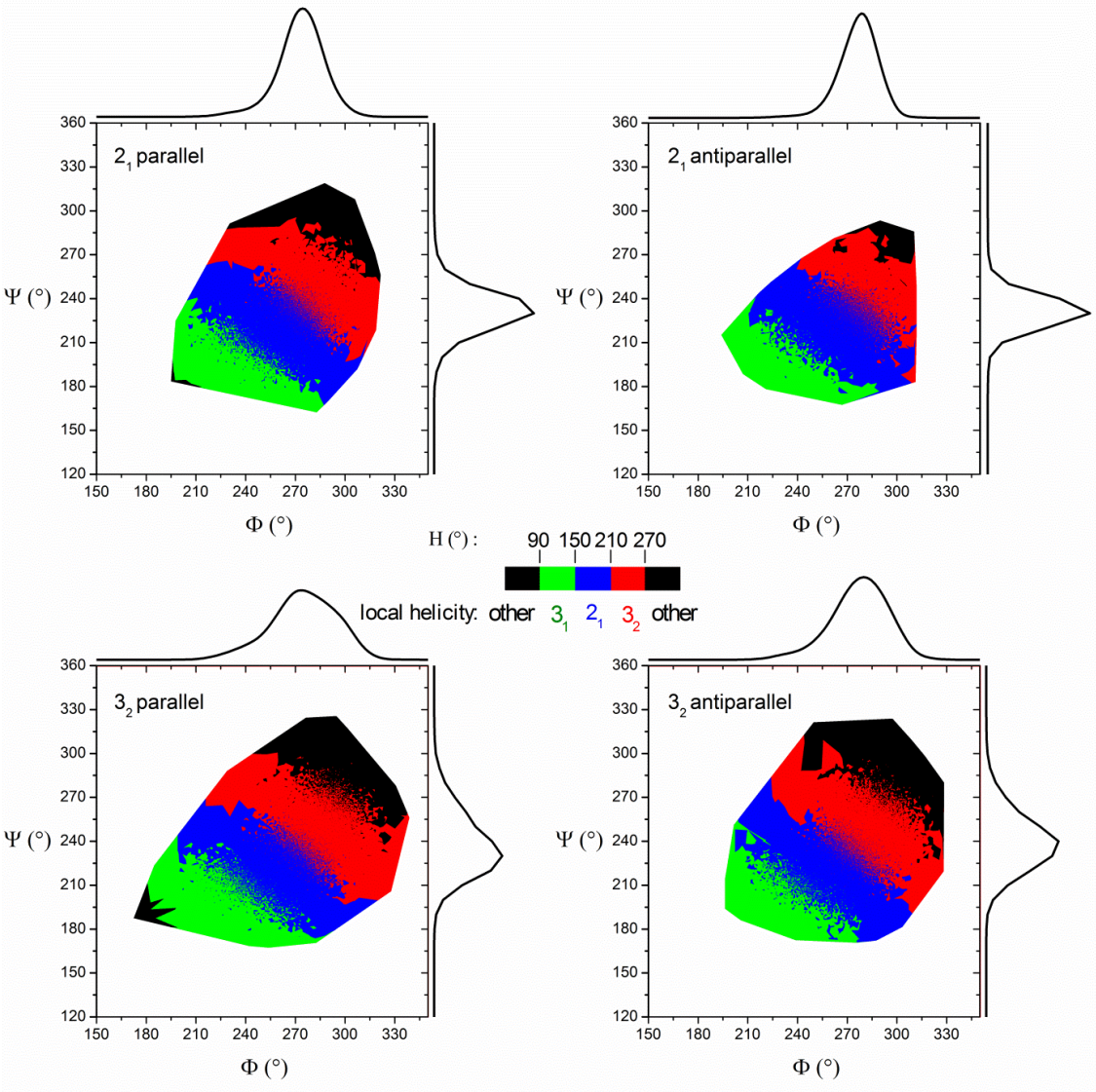

Figure 4.21 *Conformational space explored by chains in duplex models. The* (Φ, Ψ, H) *values taken by all disaccharide residues are reported. The two curves located outside each graph correspond to the probability distribution of the two torsion angles* Φ *(upper curve) and* Ψ *(at the right).*

3.2.5. *The conformational turn angle* (H)

The probability distribution of the turn angle H for the different systems is shown in Figure 4.22 and its mean values and standard deviations are reported in Table 4.5.

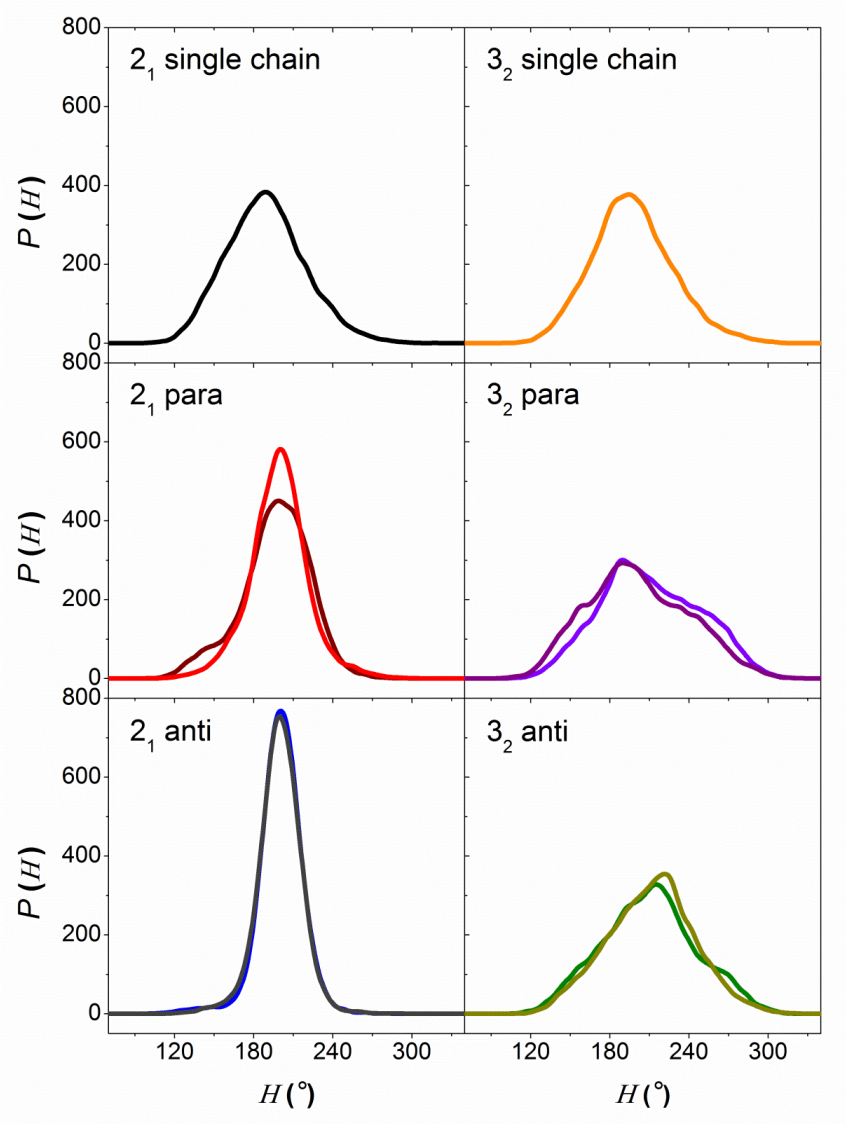

Figure 4.22 *Probability distribution of the turn angle (H) in the simulated systems. Left, systems with an initial 2_1 conformation; right, systems with an initial 3_2 conformation; from top to bottom, single chains, parallel duplexes, antiparallel duplexes.*

Detailed turn angles of each glycosidic bond in each system are given in Appendix, Table 4A.5 – Table 4A.8. All predicted values fall in the range 190° - 210° and deviate from those of canonical helical conformations; accordingly, the helices observed by molecular dynamics simulations could be qualified as irregular. Similar results are common in conformational analysis of carbohydrates: Although adiabatic Φ and Ψ mapping of the dimer

coupled with additional unconstrained minimizations locates the exact (Φ, Ψ) coordinates of the most stable geometries, they rarely coincide with those of integer helices. [39] For instance, from the lowest energy minima of the (1→4)–α-L-guluronan dimer, the prediction of the perfect 2_1 helix by Braccini *et al.* required shifting of Φ and Ψ by 15° and 14°, respectively.[22] This discrepancy is due to the fact that packing forces dominate in the crystalline state and favor perfect integer helices, whereas hydration forces dominate in solution and lead to noninteger helices.

Table 4.5 *Statistics about the turn angle (average value and standard deviation).*

System	Helix 2_1		Helix 3_2	
	<H> [°]	σ [°]	<H> [°]	σ [°]
Single	189	30	197	31
Para (chain 1)	196	26	210	38
(chain 2)	199	23	201	39
Anti (chain 1)	200	17	209	36
(chain 2)	199	17	211	33

For single chain systems, the average value of H was 189°-197°, which indicates a slightly twisted 2_1 helix. Also, when an initial 2_1 helical conformation was used for simulation, a broader distribution of the turn angles was observed for single chains than for duplexes, thus implying a larger conformational freedom for the former. Interestingly, during the MD simulation of duplexes, chains with an initial 2_1 helical conformation (H_0 = 180°) saw their turn angle increase to 196°-200°, whereas those with an initial 3_2 conformation (H_0 = 240°) saw it decrease to 201°-211°. The two models hence appear to converge towards the same twisted helical conformation, although the 3_2 duplex systems clearly lead to a greater conformational disorder, as indicated by the broader distribution of turn angles (Figure 4.22).

3.2.6. Types of helical forms occurring during MD

In order to analyze the local helical forms occurring during MD simulations, the graphs of time evolution of the conformation of each glycosidic bond during simulation for 2_1 and 3_2 helical single chain systems and duplexes (parallel and antiparallel) were plotted (Figure 4.23, Figure 4.24 and Figure 4.25). It is clear that the perfect initial helices with integral screw symmetries were lost at the very beginning of simulation (t < 1 ns). Also, the local dynamical behavior of the chains was characterized by rapid, asynchronous and non-cooperative inter-conversions between the different conformations. The corresponding statistics are reported in Table 4.6. In all studied systems, glycosidic bonds adopted the 2_1 and

3_2 helical conformations for over 80% of the time, whereas the 3_1 and "other" conformations were of limited occurrence and mostly concerned the ends of chain. Interestingly, 3_1 conformation was mostly explored by parallel duplex models.

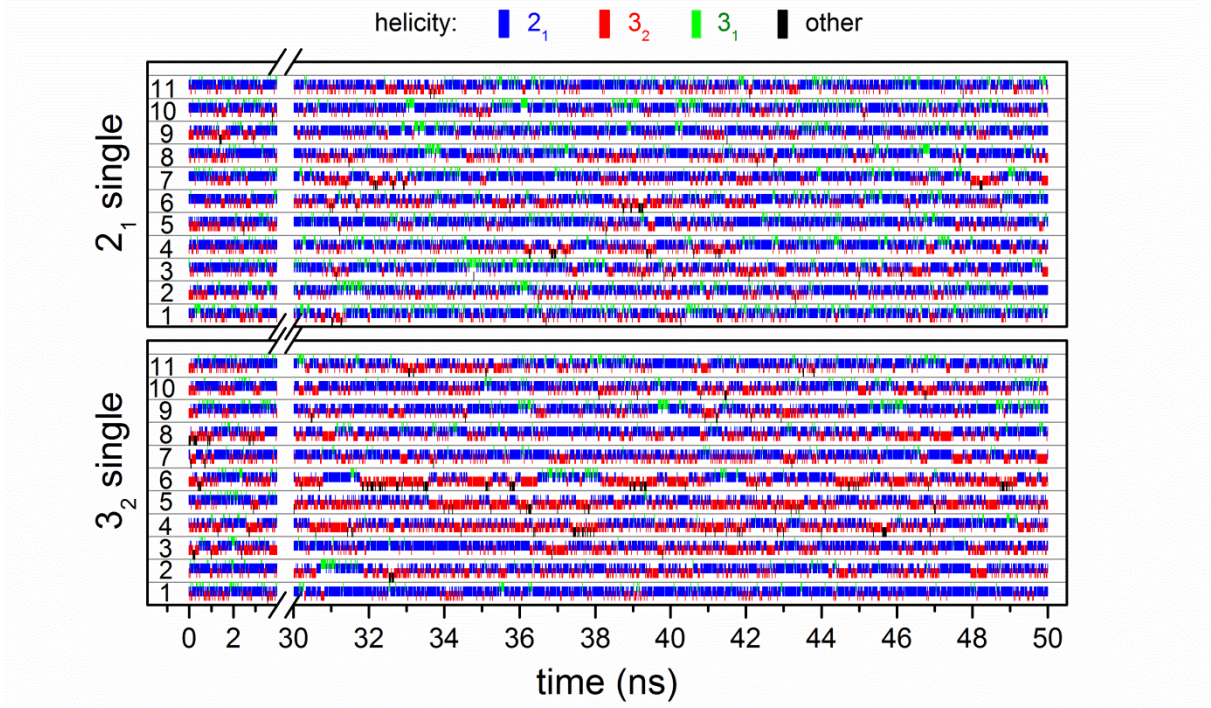

Figure 4.23 *Conformations explored by each glycosidic bond during simulation time for the 2_1 and 3_2 helical single chain systems. The numbers on the left vertical axis indicate the position of the glycosidic bond within the dodecamer (1→4)-α-L-guluronan chain. Note that horizontal axis is discontinuous.*

Table 4.6 *Occurrence of the different helical forms during the last 40 ns and 20 ns of simulation for duplexes and single chains, respectively.*

	This study				Peric *et al.*			
Model	**3_1**	**2_1**	**3_2**	**other**	**3_1**	**2_1**	**3_2**	**other**
2_1 single	10.7	69.1	19.4	0.7	12.9	75.2	11.9	0.0
2_1 para (chain 1)	6.4	62.6	30.7	0.2	-	-	-	-
(chain 2)	2.3	66.3	30.6	0.8	-	-	-	-
2_1 anti (chain 1)	1.3	72.7	26.0	0.1	-	-	-	-
(chain 2)	0.9	75.1	24.0	0.1	-	-	-	-
3_2 single	4.2	61.4	32.9	1.5	0.0	11.9	79.0	9.1
3_2 para (chain 1)	4.3	48.1	42.6	4.9	-	-	-	-
(chain 2)	11.7	53.8	32.5	2.0	-	-	-	-
3_2 anti (chain 1)	4.4	45.6	46.8	3.2	-	-	-	-
(chain 2)	4.5	42.9	50.4	2.1	-	-	-	-

Note: Data are given as time fraction. Peric et al. values for the 2_1 and 3_2 single chain models were taken from Table 2 in Ref. [13] (X = 12) and Table 6 in Ref. [12] (X = 9) and were obtained for formally infinite chains.

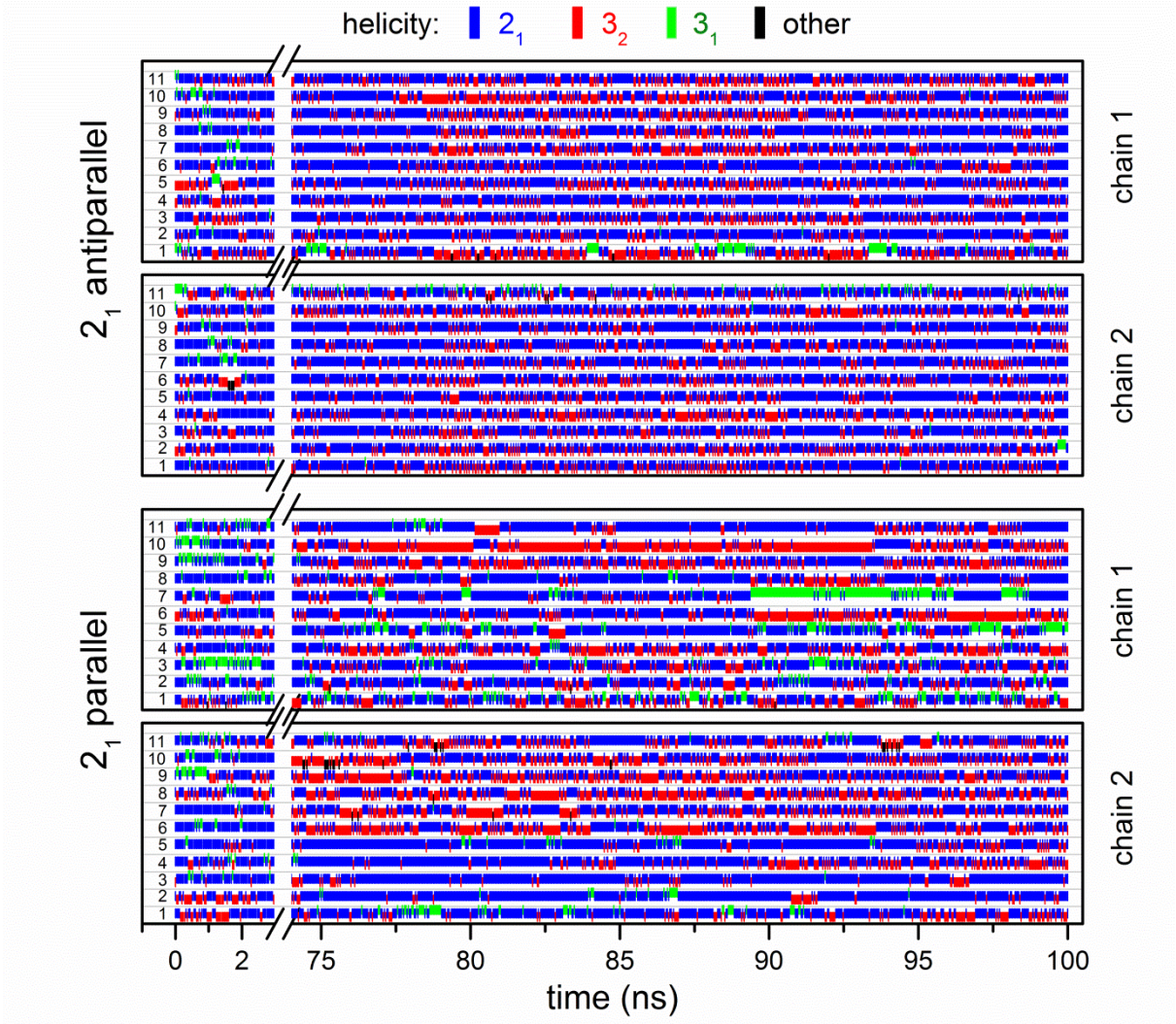

Figure 4.24 *Conformations explored by each glycosidic bond during simulation time for the 2_1 helical duplexes (parallel and antiparallel). The numbers on the left vertical axis indicate the position of the glycosidic bond within the dodecamer (1→4)-α-L-guluronan chain. Note that horizontal axis is discontinuous.*

For single chain simulations, the 2_1 helical conformation predominated (60% - 70% of time) and 3_2 one accounted for most the remaining time. An interesting comparison can be drawn between these results and those obtained by Peric.[12,13] Starting from a 2_1 helix, Peric's system equilibrated at 2_1 local helical conformations for 75% of the time. When the initial model was a 3_2 helix though, the chain equilibrated to 3_2 local helical conformations for 79% of time, which contrasts with the findings of the present study. This difference most likely originates from Peric's use of formally infinite chains. The latter are obtained by adding a covalent bond between one end of the mother chain and the other end of the image chain across the periodic cell. Commonly used to model crystals of polysaccharides, [40] this strategy has the disadvantage of imposing *a priori* conformational constraints in order to ensure

continuity between periodic cells. By contrast, the finite length of the models used in the present study resulted in a greater conformational freedom of chains, as it is clearly visible in Figure 4.24 and Figure 4.25.

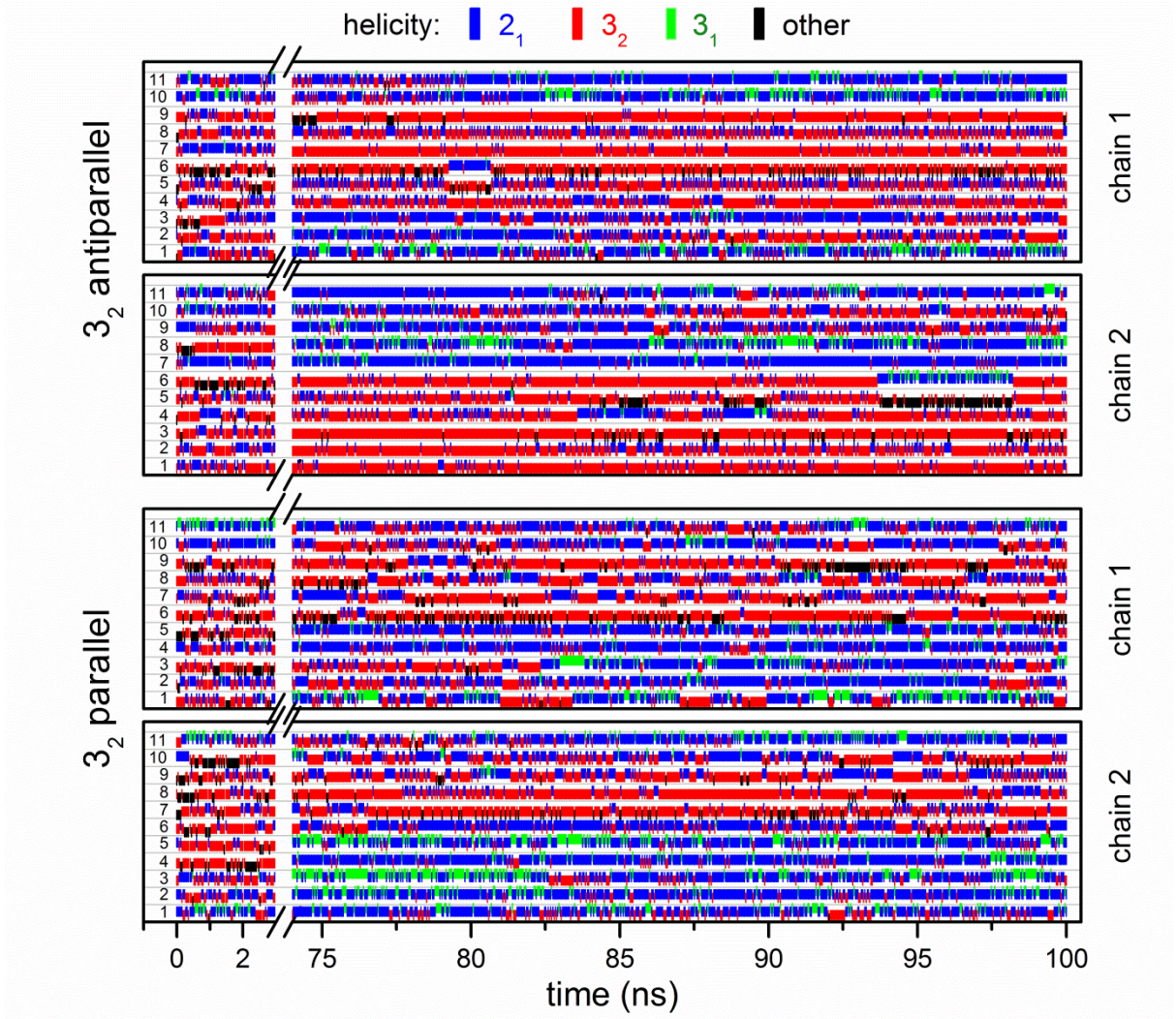

Figure 4.25 *Conformations explored by each glycosidic bond during simulation time for the 3_2 helical duplexes (parallel and antiparallel). The numbers on the left vertical axis indicate the position of the glycosidic bond within the dodecamer (1→4)-α-L-guluronan chain. Note that horizontal axis is discontinuous.*

Concerning duplex systems, a completely different behavior was observed for 2_1 and 3_2 helical models. When the simulation was initiated with a 2_1 helical conformation, the two chains behaved similarly (Figure 4.18 and Figure 4.22) and, even after extensive equilibration, possessed a 2_1 local conformation for 63% - 75% of the time. By contrast, an initial 3_2 conformation led to different chains at equilibrium (Figure 4.18) which explored a

much broader conformational space (Figure 4.22) in which 2_1 and 3_2 local helical conformations were almost equally represented (Table 4.6).

4. Conclusion

The bibliographic studies of the atomistic structure of the junction zone of Ca^{2+}-alginate have thrown up many questions in need of further investigation. Despite the calcium complexation pattern described by Plazinski [9] is satisfactory and was confirmed in this study, the description of structural properties of guluronan chains involved in junction zones provided in the literature is not clear. Therefore, this question has become the main object of this chapter. In the present study, guluronan chains were analyzed in terms of two aspects: chain length and helical conformation.

The ionotropic association between guluronan chains via calcium ions (neutralized amount) was probed by using MD simulations in explicit water environment at 300 K. In addition, all systems were allowed full conformational freedom.

The chain length effect, *i.e.* influence of degree of polymerization ($2 \leq X \leq 20$) of guluronan chains in single chain systems and duplexes (parallel and antiparallel) starting from 2_1 helical conformation, was examined during MD simulation. These studies revealed that in duplexes with $X \geq 8$, more than 50% of calcium ions present in examined systems were complexed by two carboxylate groups of guluronan chains. Thus, chains having ~8 (1→4)-α-L-guluronic acid residues units form aggregates. This result is correlated with previous investigations by Stokke *et al.* [41,42] which showed that ~8 repeating units are required to form stable junction zones. However, the most interesting finding was a helical twist (around 10°) observed in simulated systems (both: single and paired, *i.e.* parallel and antiparallel, systems: $4 \leq X \leq 20$), which encouraged us to analyze in depth the chain conformation of (1→4)-α-L-guluronan blocks involved in the junction zones.

In order to address this question, a molecular dynamics investigation of the helical forms adopted by (1→4)-α-L-guluronan was carried out. Single chains and duplexes were modeled starting both from 2_1 or 3_2 helical conformation. It has been noticed that the initial perfect helices with integral screw symmetries were lost at the very beginning of simulations. In fact, two distinct behaviors were observed:

- At equilibrium 2_1 models mostly retained 2_1 local helical conformations while exploring 3_2 ones the rest of the time. In duplexes the two chains behaved similarly, were well extended and slightly twisted.

- By contrast, the chains in 3_2 duplex models were dissimilar and explored a much broader conformational space in which 2_1 and 3_2 local helical conformations were dominant and equally represented, but 3_1 and other conformations were also present.

It is worth noting that the wide variety of conformations revealed in this study is consistent with the general difficulty in obtaining crystals of Ca^{2+}-guluronate with suitable lateral dimensions for crystallographic studies.[19-21] Thus, it can be postulated that the substantial conformational disorder of the chains in the junction zone precludes their lateral association. Additionally, the association of chains was also observed in present studies, *e.g.* in parallel 2_1 duplex model, $X = 14$ (Figure 4.12). Furthermore, a recent molecular dynamics study performed by Plazinski and Rudzinski [14] has revealed several stable modes of association of two dimers of guluronan chains. Thus, studying the association of (1→4)-α-L-guluronan duplexes in the presence of Ca^{2+} ions could be an important issue for future research.

5. Appendix

Table 4A.1 *Statistics of Φ and Ψ angles for single chain initiated with 2_1 helical conformation (average values with standard deviation).*

Glycosidic linkage	Φ [°]	σ [°]	Ψ [°]	σ [°]
1	255.3	20.6	223.0	15.5
2	260.6	17.2	223.5	15.8
3	261.3	17.0	223.4	15.7
4	260.2	17.0	224.6	16.2
5	261.4	16.3	222.5	15.0
6	266.8	16.4	226.3	16.9
7	265.7	17.4	225.7	16.7
8	265.8	17.2	227.5	16.0
9	261.7	17.7	224.7	15.4
10	264.7	16.8	225.4	16.9
11	259.8	17.6	223.2	15.9
ALL	262.1	17.7	224.5	16.1

Table 4A.2 *Statistics of Φ and Ψ angles for single chain initiated with 3_2 helical conformation (average values with standard deviation).*

Glycosidic linkage	Φ [°]	σ [°]	Ψ [°]	σ [°]
1	258.5	16.7	224.1	13.2
2	265.8	15.9	229.7	15.7
3	269.7	16.0	227.5	15.7
4	270.9	16.8	235.3	18.1
5	274.8	16.2	231.9	15.9
6	271.5	17.2	233.7	20.7
7	262.5	16.2	227.3	13.5
8	267.9	15.8	226.4	16.5
9	259.5	17.1	225.3	15.2
10	262.8	17.0	225.7	15.0
11	261.7	16.5	224.3	15.3
ALL	265.9	17.3	228.3	16.4

Table 4A.3 *Statistics of Φ and Ψ angles for duplexes initiated with 2_1 helical conformation (average values with standard deviation).*

	Model: 2_1 parallel								*Model: 2_1 antiparallel*							
	chain 1				chain 2				chain 1				chain 2			
Glycosidic linkage	Φ [°]	σ [°]	Ψ [°]	σ [°]	Φ [°]	σ [°]	Ψ [°]	σ [°]	Φ [°]	σ [°]	Ψ [°]	σ [°]	Φ [°]	σ [°]	Ψ [°]	σ [°]
1	258.9	19.0	220.0	15.3	261.6	16.3	224.2	12.1	266.5	18.4	222.7	16.1	263.0	12.7	225;6	10.0
2	266.8	15.5	230.0	14.3	267.2	12.6	229.5	14.2	267.8	11.4	227.4	9.7	276.4	8.9	226.3	11.3
3	263.0	16.3	217.0	15.8	267.3	11.0	228.0	10.8	275.9	8.7	225.8	10;7	269.2	10.8	227.4	9.4
4	271.6	13.3	231.7	12.0	269.8	11.5	230.3	13.4	269.1	11.0	226.6	9.3	276.0	8.4	225.8	10.4
5	265.0	14.3	218.3	14.2	270.1	11.0	228.0	11.7	275.9	8.9	225.6	10,5	268.5	11.1	226.6	9.2
6	275.1	12.2	231.4	11.1	268.3	11.9	229.8	11.7	270.1	10.6	226.4	9.4	275.7	8.8	226.4	10.7
7	264.2	13.2	219.1	13.7	270.6	14.1	230.0	12.1	275.8	8.7	225.2	10.5	269.9	10.9	226.1	9.6
8	270.4	14.1	226.8	11.7	267.8	11.1	229.7	12.2	267.5	10.7	227.2	9,6	275.1	8.9	225.1	10.4
9	269.7	11.4	225.6	12.9	269.9	13.7	231.2	11.5	275.6	8.8	225.9	10.4	270.6	11.8	227.5	9.7
10	275.9	13.8	232.4	13.0	268.9	13.4	228.8	14.8	268.7	3.1	228.9	10.2	275.2	9.4	225.7	11.0
11	270.3	12.8	224.6	14.3	265.9	15.1	223.3	17.1	275.5	9.0	225.6	11.5	263.1	17.0	225.3	15.2
ALL	268.2	15.2	225.2	14.7	267.9	13.2	228.4	13.2	271.7	11.8	226.1	10.9	271.2	12.0	226.2	10.8

Table 4A.4 *Statistics of Φ and Ψ angles for duplexes initiated with 3_2 helical conformation (average values with standard deviation).*

	Model: 3_2 parallel								*Model: 3_2 antiparallel*							
	chain 1				chain 2				chain 1				chain 2			
Glycosidic linkage	Φ [°]	σ [°]	Ψ [°]	σ [°]	Φ [°]	σ [°]	Ψ [°]	σ [°]	Φ [°]	σ [°]	Ψ [°]	σ [°]	Φ [°]	σ [°]	Ψ [°]	σ [°]
1	257.8	21,9	228.8	17.1	255.5	19.5	221.5	14.5	255.1	19.0	223.6	16.5	272.0	10.6	237.1	13.0
2	267.4	15.2	225.1	14.8	260.6	15.5	220.5	15.3	269.0	17.5	229.5	15.4	283.1	11.4	235.7	11.7
3	265.1	19.1	229.3	17.2	258.4	19.1	222.0	16.2	272.8	14.1	231.5	20.3	285.9	10.9	259.2	12.6
4	267.9	15.6	229.1	17.6	260.5	17.9	219.6	18.4	276.7	11.6	237.9	14.4	279.5	11.9	235.8	14.2
5	266.3	16.6	230.6	16.1	259.2	21.9	225.2	19.5	277.2	14.2	237.0	16.0	272.8	14.6	242.6	16.4
6	290.1	14.3	254.9	18.1	270.2	16.4	232.2	16.1	288.7	11.5	262.1	15.5	285.9	13.6	248.7	19.3
7	281.3	15.9	246.6	18.0	279.7	15.1	246.8	19.2	275.0	11.8	229.7	17.2	261.6	14.7	219.9	14.1
8	278.0	15.5	237.5	18.3	286.5	11.9	247.9	15.1	273.9	12.8	241.8	12.9	260.1	18.0	227.4	17.0
9	287.0	13.9	257.3	19.4	273.6	17.1	234.4	18.4	283.9	10.9	245.1	16.8	270.4	15.0	224.8	15.2
10	272.9	13.7	227.9	15.3	278.0	16.8	247.7	24.0	256.1	17.9	223.4	13.7	265.7	16.7	229.1	16.3
11	260.8	18.1	220.6	16.4	260.4	17.2	223.7	16.7	260.0	15.3	220.6	14.3	264.2	16.5	221.9	15.2
ALL	272.3	19.3	235.3	20.8	267.5	20.0	231.1	20.9	271.7	17.8	234.8	19.5	272.8	16.9	234.7	19.0

Table 4A.5 *Statistics of the turn angle (H) for single chain initiated with 2_1 helical conformation (average values with standard deviation and maxima).*

Glycosidic linkage	<H> [°]	σ [°]	Maxima [°]	
1	183	32	194	-
2	185	28	183	-
3	187	30	182	-
4	187	30	184	-
5	185	27	177	-
6	196	30	190	-
7	193	31	191	-
8	195	30	185	203
9	188	29	191	-
10	192	31	188	-
11	185	30	186	-
ALL	189	30	188	

Table 4A.6 *Statistics of the turn angle (H) for single chain initiated with 3_2 helical conformation (average values with standard deviation and maxima).*

Glycosidic linkage	<H> [°]	σ [°]	Maxima [°]			
1	189	26	184	195	-	-
2	198	29	191	-	-	-
3	198	28	193	-	-	-
4	210	33	193	206	223	-
5	208	30	189	205	-	-
6	209	37	195	209	229	-
7	191	26	185	198	-	-
8	197	30	199	224	-	-
9	187	29	182	194	226	-
10	191	29	155	182	197	234
11	188	29	189	-	-	-
ALL	197	31	195			

Table 4A.7 *Statistics of the turn angle (H) for duplexes initiated with 2_1 helical conformation (average values with standard deviation and maxima).*

	Model: 2_1 parallel								*Model: 2_1 antiparallel*							
	chain 1				chain 2				chain 1				chain 2			
Glycosidic linkage	<H> [°]	σ [°]	Maxima [°]		<H> [°]	σ [°]	Maxima [°]		<H> [°]	σ [°]	Maxima [°]		<H> [°]	σ [°]	Maxima [°]	
1	183	32	189	-	192	24	197	-	193	32	137	204	197	17	197	-
2	200	27	206	-	200	24	202	-	198	15	200	-	202	15	202	-
3	180	29	187	-	195	17	193	-	202	14	203	-	200	14	198	-
4	207	21	212	-	206	21	202	-	198	14	199	-	201	14	203	-
5	184	25	191	-	196	19	198	-	202	14	201	-	198	14	199	-
6	211	18	217	-	204	20	199	-	199	13	199	-	203	14	202	-
7	183	23	189	-	199	23	205	-	200	14	202	-	198	14	196	-
8	200	21	208	-	202	19	200	-	197	14	198	-	200	14	198	-
9	198	21	196	-	200	21	200	-	202	14	204	-	199	15	200	-
10	210	22	217	-	202	25	203	-	200	17	198	-	204	15	201	-
11	198	24	198	-	189	28	180	-	204	16	204	-	190	29	182	196
ALL	196	26	199		199	23	200		200	17	201		199	17	199	

Table 4A.8 *Statistics of the turn angle (H) for duplexes initiated with 3_2 helical conformation (average values with standard deviation and maxima).*

	Model: 3_2 parallel										*Model: 3_2 antiparallel*							
	chain 1					chain 2					chain 1				chain 2			
Glycosidic linkage	<H> [°]	σ [°]	Maxima [°]			<H> [°]	σ [°]	Maxima [°]			<H> [°]	σ [°]	Maxima [°]		<H> [°]	σ [°]	Maxima [°]	
1	196	38	157	191	213	183	31	184	-	-	184	33	175	195	220	21	224	-
2	194	27	194	-	-	183	27	179	191	-	201	30	198	216	221	18	225	-
3	198	34	189	207	-	182	32	160	186	-	206	34	193	-	251	19	255	-
4	199	31	190	276	-	182	31	164	183	-	220	22	216	-	216	22	219	-
5	198	30	187	-	-	183	41	141	154	187	216	27	207	-	221	27	216	273
6	248	29	262	-	-	209	28	199	-	-	259	22	268	-	235	31	157	231
7	230	31	193	209	237	231	33	205	254	-	204	31	156	225	181	23	182	-
8	218	33	205	247	-	232	23	230	-	-	218	23	213	-	188	33	157	193
9	248	29	205	247	-	213	32	194	232	-	235	25	234	-	199	27	200	-
10	199	26	236	270	-	232	40	209	234	247	178	27	186	-	196	29	188	198
11	182	32	188	-	-	182	31	178	-	-	182	26	181	-	187	26	189	-
ALL	210	38	190			201	39	190			209	36	215		211	33	222	

6. References

(1) Grant, G. T.; Morris, E. R.; Rees, D. A.; Smith, P. J. C.; Thom, D. FEBS Letters 1973, 32, 195.

(2) Dheu-Andries, M. L.; Pérez, S. Carbohydrate Research 1983, 124, 324.

(3) Jalilehvand, F.; Spaangberg, D.; Lindqvist-Reis, P.; Hermansson, K.; Persson, I.; Sandstroem, M. J. Am. Chem. Soc. 2001, 123, 431.

(4) Alagna, L.; Prosperi, T.; Tomlinson, A. A. G.; Rizzo, R. J. Phys. Chem. 1986, 90, 6853.

(5) Smidsrød, O. Faraday Discussions of the Chemical Society 1974, 57, 263.

(6) Braccini, I.; Perez, S. Biomacromolecules 2001, 2, 1089.

(7) Atkins, E. D. T.; Mackie, W.; Parker, K. D.; Smolko, E. E. J. Polym. Sci., Part B 1971, 9, 311.

(8) Atkins, E. D. T.; Nieduszynski, I. A.; Mackie, W.; Parker, K. D.; Smolko, E. E. Biopolymers 1973, 12, 1879.

(9) Plazinski, W. J. Comput. Chem. 2011, 32, 2988.

(10) Plazinski, W.; Drach, M. Applied Surface Science 2012, 262, 153.

(11) Plazinski, W.; Drach, M. J. Comput. Chem. 2012, 33, 1709.

(12) Peric, L.; Pereira, C. S.; Perez, S.; Hunenberger, P. H. Mol. Simul. 2008, 34, 421.

(13) Peric-Hassler, L.; Hunenberger, P. H. Mol. Simul. 2010, 36, 778.

(14) Plazinski, W.; Rudzinski, W. Struct. Chem. 2012, 23, 1409.

(15) Donati, I.; Holtan, S.; Mørch, Y. A.; Borgogna, M.; Dentini, M. Biomacromolecules 2005, 6, 1031.

(16) Dentini, M.; Rinaldi, G.; Barbetta, A.; Risica, D.; Anselmi, C.; Skjåk-Bræk, G. Carbohydrate Polymers 2007, 67, 465.

(17) Plazinski, W. Carbohydr. Res. 2012, 357, 111.

(18) Mackie, W. Biochem. J. 1971, 125, 89p.

(19) Mackie, W.; Perez, S.; Rizzo, R.; Taravel, F.; Vignon, M. Int. J. Biol. Macromol. 1983, 5, 329.

(20) Sikorski, P.; Mo, F.; Skjk-Brk, G.; Stokke, B. T. Biomacromolecules 2007, 8, 2098.

(21) Li, L.; Fang, Y.; Vreeker, R.; Appelqvist, I.; Mendes, E. Biomacromolecules 2007, 8, 464.

(22) Braccini, I.; Grasso, R. P.; Perez, S. Carbohydr. Res. 1999, 317, 119.

(23) Hess, B.; Kutzner, C.; van der Spoel, D.; Lindahl, E. Journal of Chemical Theory and Computation 2008, 4, 435.

(24) Mayo, S. L.; Olafson, B. D.; Goddard, W. A., III J. Phys. Chem. 1990, 94, 8897.

(25) Oostenbrink, C.; Villa, A.; Mark, A. E.; van, G. W. F. J. Comput. Chem. 2004, 25, 1656.

(26) Project, E.; Nachliel, E.; Gutman, M. Journal of Computational Chemistry 2008, 29, 1163.

(27) Berendsen, H. J. C.; Postma, J. P. M.; Van, G. W. F.; DiNola, A.; Haak, J. R. J. Chem. Phys. 1984, 81, 3684.

(28) Hess, B.; Bekker, H.; Berendsen, H. J. C.; Fraaije, J. G. E. M. J. Comput. Chem. 1997, 18, 1463.

(29) Darden, T.; York, D.; Pedersen, L. J. Chem. Phys. 1993, 98, 10089.

(30) Essmann, U.; Perera, L.; Berkowitz, M. L.; Darden, T.; Lee, H.; Pedersen, L. G. J. Chem. Phys. 1995, 103, 8577.

(31) Bussi, G.; Donadio, D.; Parrinello, M., 2007; p COMP.

(32) Humphrey, W.; Dalke, A.; Schulten, K. J. Mol. Graphics 1996, 14, 33.

(33) Draget, K. I.; Stokke, B. T.; Yuguchi, Y.; Urakawa, H.; Kajiwara, K. Biomacromolecules 2003, 4, 1661.

(34) Stokke, B. T.; Draget, K. I.; Smidsrod, O.; Yuguchi, Y.; Urakawa, H.; Kajiwara, K. Macromolecules 2000, 33, 1853.

(35) Yuguchi, Y.; Urakawa, H.; Kajiwara, K.; Draget, K. I.; Stokke, B. T. J. Mol. Struct. 2000, 554, 21.

(36) Wolnik, A.; Albertin, L.; Charlier, L.; Mazeau, K. Biopolymers 2013, 99, 562.

(37) Avaltroni, F.; Seijo, M.; Ulrich, S.; Stoll, S.; Wilkinson, K. J. Biomacromolecules 2007, 8, 106.

(38) Perry, T. D. I. V.; Cygan, R. T.; Mitchell, R. Geochim. Cosmochim. Acta 2006, 70, 3508.

(39) Pérez, S.; Kouwijzer, M.; Mazeau, K.; Engelsen, S. B. Journal of Molecular Graphics 1996, 14, 307.

(40) Mazeau, K. Cellulose (Dordrecht, Neth.) 2005, 12, 339.

(41) Stokke, B. T.; Smidsroed, O.; Bruheim, P.; Skjaak-Braek, G. Macromolecules 1991, 24, 4637.

(42) Stokke, B. T.; Smidsroed, O.; Zanetti, F.; Strand, W.; Skjaak-Braek, G. Carbohydr. Polym. 1993, 21, 39.

Chapter V:

Probing the association by experimental techniques

Table of contents

1. Introduction

The first part of this chapter is dedicated to probing the association between either the same type of homo-alginate oligomers (*i.e.* (1→4)-α-L-guluronan or (1→4)-β-D-mannuronan) called homotypic interactions, or different ones (*i.e.* heterotypic interactions) in the presence of calcium ions by Atomic Force Spectroscopy (AFS).

The second part is also related to the association of selected materials (commercial alginate chosen as the reference, different homo-alginate oligomers and biohybrid polymers featuring (1→4)-α-L-guluronan sequences as side chains) in the presence of Ca^{2+}. However, the main attention of this paragraph will be paid to determining a sol-gel transition during progressive addition of $CaCl_2$ in both dilute solutions (via LS) and semi-dilute solutions (via rheology). Furthermore, rheological characterization of some hydrogels prepared by dialysis against $CaCl_2$ will be also reported.

2. Force measurements

2.1. Introduction

In recent years, Atomic Force Spectroscopy (AFS) has become a method of choice to get an insight into intra- and/or inter-molecular forces at the atomistic level. Thus, on the one hand, this technique provides studying specific interactions between molecules but on the other hand enables examining single interactions as well. For instance, Rief *et al.*[1] has applied AFS to investigate the chain elasticity of dextran. In detail, carboxymethylated dextran chains labelled with streptavidin were chemically bound to a gold surface, and then individual dextran filaments were pulled on by biotin (bound to the AFM tip), as a result of formed biotin-streptavidin bond. Thus, the dextran chains were stretched up to 250 pN which is equivalent to the maximum force (250 ± 25 pN) estimated for the biotin-streptavidin bond. This study probed elastic properties of single polymer strands but also showed that single molecule spectroscopy enables determining mechanical properties of polymers at the molecular level that could not be obtained so easily. In addition, Marszalek and co-workers [2,3] performed similar AFM stretching experiments for dextran and other polysaccharides such as: amylose, pullulan, pectin or cellulose. Interestingly, it has been suggested that obtained force curves, determined via single molecule force spectroscopy, can be used as molecular fingerprints for identifying the individual polysaccharide molecules in complex mixtures.

However, in reviewing the literature, no significant data was found on the investigation of alginates via AFS. So far, only one attempt has been made by Sletmoen *et al.*[4] to study interactions between mannuronan and C-5 mannuronan epimerase enzyme AlgE4. The epimerase AlgE4 generates exclusively alternating MG blocks [5] which in contrast to homopolymeric G blocks do not ensure so easily alginate-gel formation in the presence of Ca^{2+}. In order to examine the interactions of interest, mannuronan was attached covalently to the AFM tip, using EDAC (1-(3-dimethylaminopropyl)-3-ethylcarbodiimide hydrochloride) as a coupling agent; whereas the AlgE4 was immobilized to mica surface via a cross-linking agent (0.5 mg mL^{-1} AlgE4 in 2 mmol $CaCl_2$, 20 mmol MOPS buffer (3-[N-morpholino]propanesulfonic acid), pH = 6.8, 14h).[4] Then, AFS experiments were performed at room temperature in a liquid cell containing aqueous solution, *i.e.* 2 mmol $CaCl_2$, 20 mmol MOPS buffer (pH = 6.8). It has been found that the tip-surface adhesive interactions depend on the mannuronan tip grafting density, which could be modified by varying the concentration of the EDAC coupling agent, the grafting time as well as the loading rate applied during the measurement. Furthermore, this study revealed that single-molecular pair unbinding forces between AlgE4 and mannuronan are in the range from 52 to 126 pN which is in agreement with physical interactions determined for biological macromolecules.[4]

Since no detailed interactions between oligoglycuronans in solutions at the molecular level have been studied so far, thus it has become one of the issues considered in this chapter. In addition, as it was mentioned in *Chapter II - The State of the Art*, mannuronan blocks of alginate chain have lower affinity to complex Ca^{2+} than guluronan blocks. Therefore, the investigation of differences between M-blocks and G-blocks in interacting with Ca^{2+} will be also discussed.

2.2. Materials

(1→4)-α-L-guluronan oligomer with 20 repeating units (X = 20, $GulA_{20}$) and (1→4)-β-D-mannuronan oligomer of 18 residues (X = 18, $ManA_{18}$) were obtained from Elicityl OligoTech®. Commercial silicon nitride probes (model MSNL-10) and gold tips (model NPG-10) as well as silicon and gold wafers were purchased from Brucker. (3-Aminopropyl)trimethoxysilane (97 %, Aldrich), chloroform (>99.9 %, SdS), sodium cyanoborohydride (95 %, Aldrich), calcium chloride dihydrate (≥99 %, Acros), ethanol (96 %, Carlo Erba), acetone (≥99.8 %, Carlo Erba), NaOH (≥ 97%, Aldrich), NaOH (0.05 N, pure Acros) were used as received. 3-sulfanylpropanehydrazide hydrochloride was a kind gift

of Mark Nitz (Department of Chemistry, University of Toronto, ON, Canada) and the phosphate buffer solution was prepared by Lionel Dumas. All aqueous solutions were prepared with deionized water from MilliQ apparatus (Millipore).

2.3. Methods

2.3.1. Aminofunctionalization of silicon surfaces and oligoalginate grafting

Aminofunctionalization of silicon surfaces was achieved by deposition a solution of (3-Aminopropyl)trimethoxysilane (APTMS) in chloroform at 1 mmol L^{-1} (Scheme 5.1) followed by rinsing the surfaces after one hour with chloroform at least three times. Then, in order to attach the oligomer of interest to previously aminofunctionalized surfaces, solution of $NaBH_3CN$ (10 mg, 1.6×10^{-2} mol) in acetate buffer solution (0.108 mol L^{-1}, pH = 6) was used as a coupling agent. Thus, solutions of oligomers were prepared by dissolving $GulA_{20}$ (48 mg, 1.2×10^{-2} mol) or $ManA_{18}$ (40 mg, 1.2×10^{-2} mol) in 2 mL of acetate buffer solution (0.108 mol L^{-1}, pH = 6) and then two different procedures were applied for tips and wafers, respectively. In the case of silicon nitride probes, a tip was immersed in 1.5 mL previously prepared solution of oligomer ($GulA_{20}$ or $ManA_{18}$) and left for more than 2 hours. Later, 150 μL of $NaBH_3CN$ solution (previously prepared) was added, and the tip was left inside a vial for at least 6 days at room temperature and rinsed with deionized water (Scheme 5.1). The residual solution of oligomer, *i.e.* 0.5 mL was mixed with 50 μL of $NaBH_3CN$ and a drop of it was spread on a silicon wafer and left for 2 days at room temperature. After, the wafer was rinsed with deionized water and a new drop of previously used mixture was deposited on the surface. This procedure was repeated three times. In addition, solutions of oligomers with $NaBH_3CN$ were kept in the freezer between each new deposition.

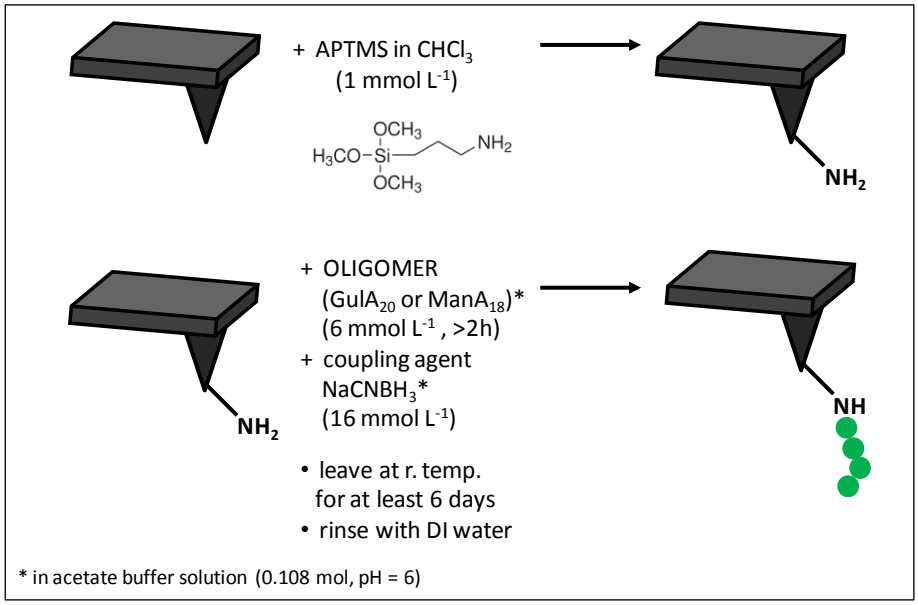

Scheme 5.1 *Grafting an oligomer ($GulA_{20}$ or $ManA_{18}$) to NH_2 activated silicon nitride tip.*

2.3.2. *Thiol-gold chemistry and sample preparation*

An attachment of a carbohydrate to a gold surface can be easily achieved by applying thiol-gold chemistry. The first step is to prepare a well-established thiol, which then may be covalently bound to a gold surface. The desired thiols (structures 2 and 3 in Scheme 5.2) were synthesized by Lionel Dumas - a member of the ALGIMAT project, via condensation of $ManA_{18}$ or $GulA_{20}$ with 3-sulfanylpropanehydrazide hydrochloride (structure 1 in Scheme 5.2) according to the procedure described by Nitz *et al.* [6,7,8]

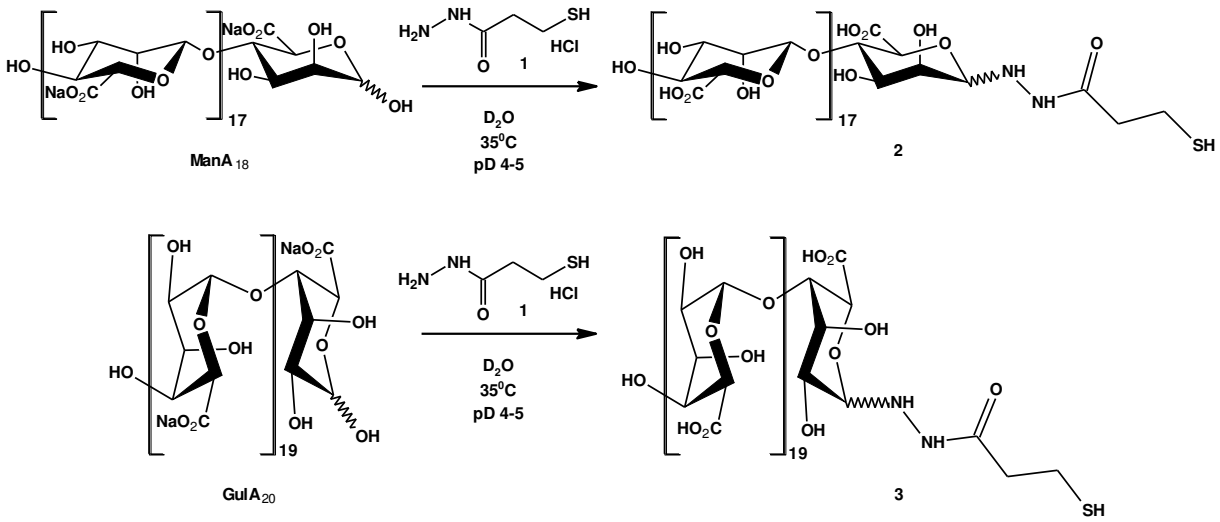

Scheme 5.2 *Schematic representation of the condensation of $ManA_{18}$ or $GulA_{20}$ with 3-sulfanylpropanehydrazide hydrochloride (1).*

However, before grafting the oligomers, gold surfaces were cleaned with ethanol, acetone, again ethanol, rinsed with plenty of DI water and dried with nitrogen gas stream. Later, the solutions of previously prepared thiols at 1.5 mmol L^{-1} in phosphate buffer (1 mmol L^{-1}, pH = 7.0, filtered through 0.22 μm PES filter) were deposited on a clean gold wafer or tip (Scheme 5.3), which were then kept in close vials for 2 days at room temperature and rinsed with plenty of water.

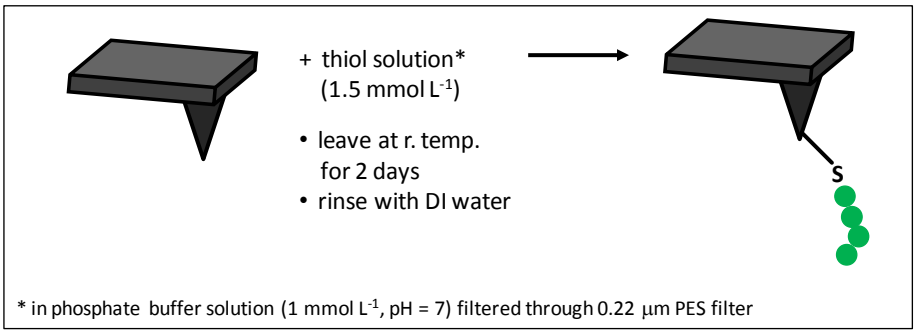

Scheme 5.3 *Attachement of an oligomer ($GulA_{20}$ or $ManA_{18}$) to a gold tip via thiol-gold chemistry.*

2.3.3. AFM measurements

Force measurements were performed on an Agilent Pico Plus AFM/Molecular Imaging apparatus operating in contact mode in the air (to obtain the thermal spectrum, required for calculating correctly the cantilever spring constant) and in a liquid (to perform experiments). The main aim was to study interactions between grafted probes and wafers either with the same type of oligomer (*i.e.* homotypic interactions, Scheme 5.4) or different (*i.e.* heterotypic interactions). In the case of homotypic interactions, force measurements for silicon surfaces were performed in DI water and $CaCl_2$ aqueous solution at 0.01 mol L^{-1}, whereas experiments with gold surfaces were carried out in NaOH solution at 10^{-6} mol L^{-1} (pH ≅ 8.4) and aqueous solution of $CaCl_2$ at 0.10 mol L^{-1} (pH was adjust to 9.0 by the addition of NaOH at 0.05 mol L^{-1}). On the other hand, heterotypic

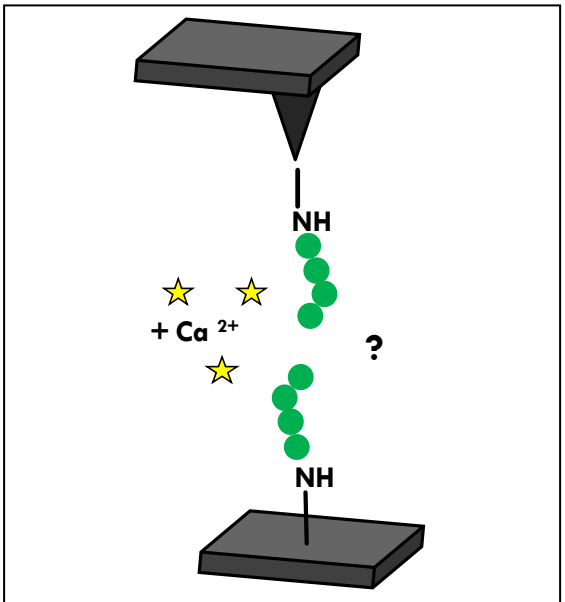

Scheme 5.4 *Schematic representation of AFS measurement between oligomers ($GulA_{20}$ or $ManA_{18}$) attached to silicon surfaces in $CaCl_2$ aqueous solution.*

interactions were examined only for silicon surfaces in DI water (pH was adjust to 7.0 with NaOH at 0.05 mol L^{-1}) and $CaCl_2$ aqueous solution at 0.01 mol L^{-1} (pH = 7.0). Experiments were performed in DI water in order to observe electrostatic repulsions between grafted chains (evidence of successful grafting), thus only measurements performed in $CaCl_2$ are representative. In order to determine oligomer interactions defined in terms of the average adhesion force, 100 curves (cantilever deflection - z_c *vs.* displacement of the piezoelectric scanner in the *z*-direction - z_p) for 5 different positions of the cantilever were registered for each individual experiment. In addition, the sweep duration, corresponding to the time required to perform a single force curve (equivalent with the contact time between the tip and the sample), was set to 1 s, 6 s or 100 s.

2.3.4. Data analysis

The cantilever spring constants of functionalized tips were calculated on the basis of experiments performed in the air by using thermal noise method.[9] This method allows determining the fundamental resonance peak of thermal vibrations of the desired cantilever, which is then fitted to the simple harmonic oscillator (SHO) model according to:[10]

$$P(f) = y_0 + \frac{A_0 {f_R}^4}{\left(f^2 - {f_R}^2\right)^2 + \left(\frac{f f_R}{Q}\right)^2} \quad \text{(Eq. 5 1)}$$

where y_0 is the background term, A_0 is the zero frequency amplitude of the SHO response, f_R is the resonance frequency and Q is the quality factor.

Then, the cantilever spring constant can be calculated from the following equation:[10]

$$k = \frac{2Ck_BT}{\pi A_0 f_R Q} \quad \text{(Eq. 5 2)}$$

where C is the correction parameter and is equal to 0.817 or 0.764 for rectangular or V-shaped cantilevers, respectively, k_B is the Boltzmann constant, T is temperature and the other parameters are obtained from the fit of Eq. 5.1 to the fundamental resonance peak.

In practice, in order to get a correct k value, the sensitivity calibration factor s should be included in the Eq. 5.2 as follows:

$$k = \frac{2Ck_BT}{\pi A_0 f_R Q s^2} \quad \text{(Eq. 5 3)}$$

On the other hand, the cantilever spring constant can be also estimated from the thermal spectrum on the basis of Sader method, including fitting of thermal spectrum to SHO

model (Eq. 5.1) and computation the k value. For instance, Sader *et al.* [11] calculated k for V-shaped cantilevers (type C and D) according to the Reynolds number (Re) which is equal to:[10]

$$Re = \frac{\pi \rho b^2 f_R}{2\eta} \quad \text{(Eq. 5 4)}$$

where ρ is the density of the medium (ρ_{air} = 1.18 kg m^{-3}),[12] b is the width of the cantilever and η is the viscosity of the medium (η_{air} = 1.86 × 10^{-5} kg m^{-1} s^{-1}).[12]

Later, Riet *et al.* [10] modified the equations determined by Sader *et al.* [11] according to the type of chips (MSCT/MLCT). Since, the silicon nitride tips used in these studies (MSNL type) have the same geometry and composition as those used by Riet *et al.* [10], thus the cantilever spring constant for V-shaped cantilevers (type C and D) can be calculated from the following equations:[10]

$$k = 140.94 \rho {b_C}^2 L_C Re^{-0.728+0.00915 ln Re} {f_R}^2 Q \quad \text{(Eq. 5.5)}$$

$$k = 117.25 \rho {b_D}^2 L_D Re^{-0.700+0.0215 ln Re} {f_R}^2 Q \quad \text{(Eq. 5.6)}$$

where b_C or b_D is the width of cantilever and L_C or L_D is the length of the cantilever.

In order to calculate semi-automatically the adhesion force (F) for each measurement, a script written by Frédéric Dubreuil in MATLAB software was applied. This script performs automatically a baseline level correction together with the adjustment of cantilever deflection (z_c) and piezo displacement (z_p) to zero position, followed by calculation the difference in cantilever deflection (Δz_c). Finally, the adhesion force (F) was determined by multiplying Δz_c with its spring constant k according to:

$$F = \Delta z_c \cdot k \quad \text{(Eq. 5.7)}$$

2.3.5. Example of tip calibration

Figure 5.1 presents the thermal spectrum registered for cantilever grafted with (1→4)-β-D-mannuronan oligomer (X = 18, $ManA_{18}$) together with a fit to the simple harmonic oscillator (SHO) model. Such fitting enables to determine the resonance frequency *(f_R)* and the quality factor *(Q)* required for estimating cantilever spring constants k of the grafted probes according to Eq. 5.5 or 5.6. In the case of grafted silicon nitride tips used in this study, important cantilever parameters together with computed k values are reported in Table 5.1.

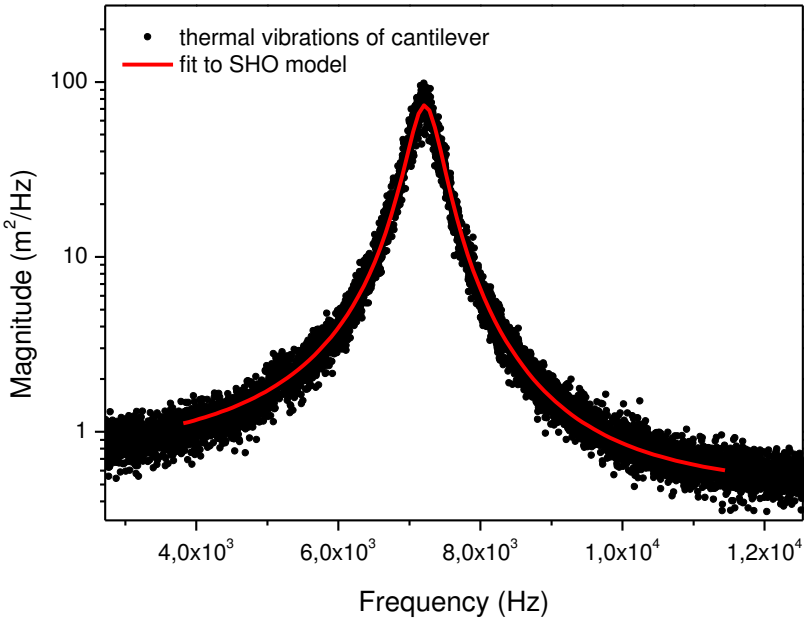

Figure 5.1 *Thermal spectrum registered in the air for probe MSNL (more precisely: V-shaped cantilever C) grafted with (1→4)-β-D-mannuronan oligomer (X = 18, $ManA_{18}$) together with a fit to the simple harmonic oscillator (SHO) model.*

Table 5.1 *Cantilever spring constants (k) calculated for MSNL probes grafted with (1→4)-β-D-mannuronan (X = 18, $ManA_{18}$) or (1→4)-α-L-guluronan (X = 20, $GulA_{20}$) oligomer. The resonance frequency (f_R) and the quality factor (Q) were obtained from a fit to the simple harmonic oscillator (SHO), whereas the values of the width (b) and the length (L) of the cantilever were taken as suggested by Brucker producer.*

Value	***$ManA_{18}$ cantilever C***	***$GulA_{20}$ cantilever D***
f_R (Hz)	7224	14700
Q	14.5	24.7
b (μm)	20	20
L (μm)	310	225
***k* (N/m)**	**0.04**	**0.10**

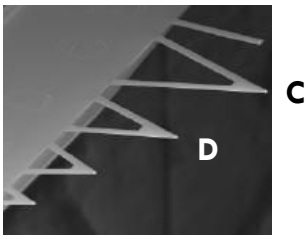

In fact, the obtained *k* values differ from those suggested by Brucker producer, *i.e.* are about three times higher. However, the ratio of three is the same in both cases (tip grafted with $ManA_{18}$ as well as with $GulA_{20}$). This difference can be attributed to the method applied by the manufacturer for determination of the cantilever spring constant, and variations in cantilever thickness due to differences between nominal and real values as well as performed grafting.

2.4. Results

2.4.1. Homotypic interactions: $ManA_{18}$-$ManA_{18}$ and $GulA_{20}$-$GulA_{20}$

2.4.1.1. Silicon surfaces

The difference in interactions between M-blocks and G-blocks with calcium ions was determined on the basis of the difference in the average adhesion force ($\Delta\langle F\rangle$) computed as the difference between values obtained for experiments performed in the presence of $CaCl_2$ aqueous solution and DI water. Typical force curves for both $ManA_{18}$ and $GulA_{20}$ are shown in Figure 5.2. Interestingly, the shape of registered force curves is similar for $ManA_{18}$ and $GulA_{20}$. For each force curve obtained in DI water, a long range electrostatic repulsion (on the approach curve) and some non-specific adhesion (on the retraction curve) were observed. Furthermore, curves determined for the same tip and sample assembly upon addition of $CaCl_2$ show an increase of the adhesion, induced by the presence of salt.

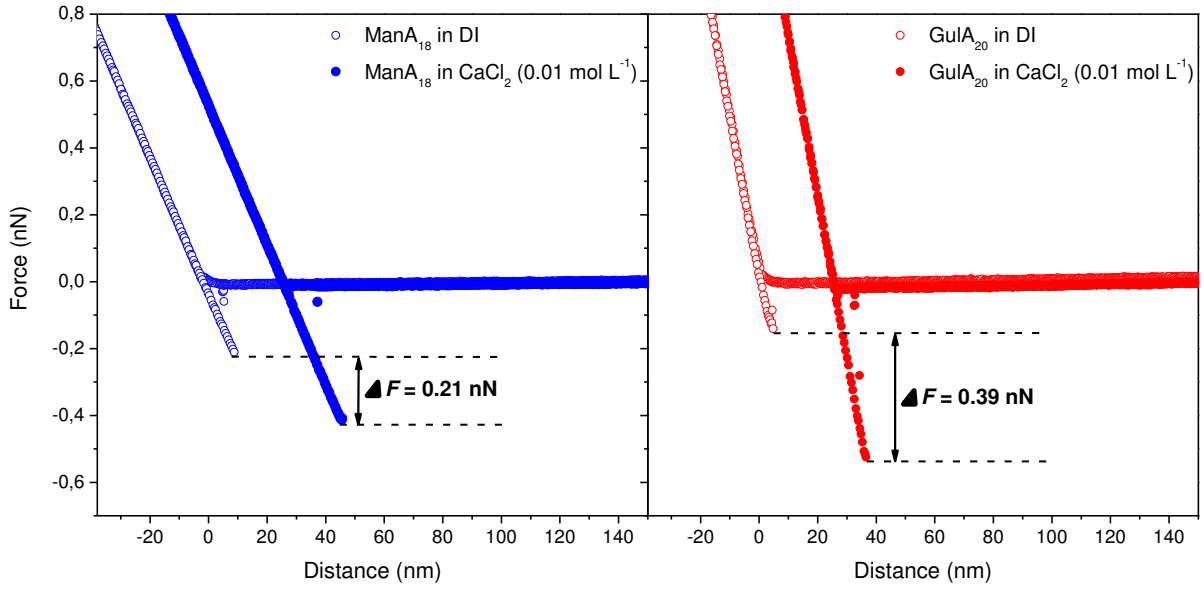

Figure 5.2 *Typical force curves obtained for (1→4)-β-D-mannuronan (X = 18, $ManA_{18}$) and (1→4)-α-L-guluronan (X = 20, $GulA_{20}$) oligomers grafted on silicon surfaces (tips and wafers), performed with sweep duration time = 6 s. In order to show observed differences, the curves obtained in the presence of $CaCl_2$ were shifted in distance around 25 nm.*

A comparison between M-blocks and G-blocks (Table 5.2) reveals that G-blocks associate stronger in the presence of calcium ions. Probably, it is mainly attributed to different chemical structure. However, obtained results suggest that M-blocks also interact via Ca^{2+}, but the strength of their interactions is two times lower. In addition, the experiments for

$GulA_{20}$ were performed with different sweep duration time, *i.e.* 6 or 100 s, respectively (Table 5.2), and no significant differences were found. This result may be explained by the fact that calcium ions occupy the available sites between (1→4)-α-L-guluronan chains immediately (after direct contact with them), thus no changes in complexation appear with time.

Table 5.2 *Average computed values for all registered curves, obtained from force measurements performed for (1→4)-β-D-mannuronan (X = 18, $ManA_{18}$) and (1→4)-α-L-guluronan (X = 20, $GulA_{20}$) oligomers grafted on silicon surfaces (silicon nitride MSNL probes and silicon wafers), in both DI water and $CaCl_2$ aqueous solution.*

Experiment code	*Solution*	*Sweep duration (s)*	$\langle \Delta z_c \rangle$ *(nm)*	*k (N/m)*	$\langle F \rangle$ *(nN)*	$\Delta\langle F \rangle$ *(nN)*
AW-12-01-**$ManA_{18}$**	water (DI)	6	5.2	0.04	0.21	**0.18**
	$CaCl_2$ in DI (0.01 mol L^{-1})	6	9.8	0.04	0.39	
AW-12-01-**$GulA_{20}$**	water (DI)	6	1.4	0.10	0.14	**0.39**
	$CaCl_2$ in DI (0.01 mol L^{-1})	6	5.3	0.10	0.53	
AW-12-01-**$GulA_{20}$**	water (DI)	100	2.5	0.10	0.25	**0.35**
	$CaCl_2$ in DI (0.01 mol L^{-1})	100	6.0	0.10	0.60	

Note: $\langle \Delta z_c \rangle$ is the average difference in cantilever deflection, k is the cantilever spring constant, $\langle F \rangle$ is the average adhesion force and $\Delta\langle F \rangle$ is the difference in the average adhesion force determined from experiments performed in $CaCl_2$ aqueous solution and DI water

In addition, one comment on the statistic values (see Appendix: Table 5A.1) is needed. In each single measurement, the average adhesion force ($\langle F \rangle$) was calculated on the basis of about 100 curves registered at 5 different positions. This procedure minimizes the experimental error linked to grafting heterogeneity of the surface. As can be seen from Table 5A.1 attached in the Appendix, standard deviations computed for the average cantilever deflections are quite high (≈ 30%). Thus, further studies are recommended in order to reduce the experimental errors.

One major drawback of those experiments was the time needed to achieve a good coupling of the oligoalginate to the surface of interest (although it was not optimized). However, instead of optimizing the time, another grafting method, based on the thiol-gold chemistry was applied (paragraphs 2.3.2 and 2.4.1.2).

2.4.1.2. Gold surfaces

It has been found that compounds can be grafted via applying thiol-gold chemistry quite rapidly. Therefore, this method was chosen in order to probe interactions of interest, i.e. between homogeneous oligomers ($ManA_{18}$ or $GulA_{20}$). In those experiments, the cantilever spring constants were calculated according to Eq. 5.3 because the geometry of gold tips differed from silicon nitride ones. The results are given in Table 5.3.

Table 5.3 *Cantilever spring constants (k) calculated for NPG probes grafted with (1→4)-β-D-mannuronan (X = 18, $ManA_{18}$) or (1→4)-α-L-guluronan (X = 20, $GulA_{20}$) oligomer using thermal noise method. The resonance frequency (f_R), the quality factor (Q) and the zero frequency amplitude (A_0) were obtained from a fit to the simple harmonic oscillator (SHO).*

Value	***$ManA_{18}$ cantilever A***	***$GulA_{20}$ cantilever D***
f_R (Hz)	60948	17640
Q	94.03	40.51
A_0 (V^2/Hz)	0.00101	0.00345
s (nm/V)	58	54
k (N/m)	**1.03**	**0.28**

Since the alginate-hydrazide-SH are only stable above pH = 7.0, so the experiments were performed in the presence of NaOH solution at 10^{-6} mol L^{-1} (pH ≅ 8.4) and $CaCl_2$ (pH = 9.0). As can be seen from Table 5.4 and Figure 5.3, the difference in the average adhesion force is much higher for G-G interactions than for M-M ones. This finding confirms the higher affinity of G-blocks to Ca^{2+}. Interestingly, the ratio in $\Delta\langle F\rangle$ between G-G and M-M interactions is equal to four.

Table 5.4 *Average computed values for all registered curves, obtained from force measurements performed for (1→4)-β-D-mannuronan (X = 18, $ManA_{18}$) and (1→4)-α-L-guluronan (X = 20, $GulA_{20}$) oligomers grafted on gold surfaces (gold NPG probes and gold wafers), in both NaOH solution at 10^{-6} mol L^{-1} (pH ≅ 8.4) and aqueous solution of $CaCl_2$ (pH was adjust to 9.0 by the addition of NaOH at 0.05 mol L^{-1}).*

Experiment code	***Solution***	***Sweep duration (s)***	***$\langle\Delta z_c\rangle$ (nm)***	***k (N/m)***	***$\langle F\rangle$ (nN)***	***$\Delta\langle F\rangle$ (nN)***
AW-12-06-**$ManA_{18}$**	NaOH at 10^{-6} mol L^{-1}	1	3.1	1.03	3.19	**0.31**
	$CaCl_2$ in DI (0.10 mol L^{-1})	1	3.4	1.03	3.50	
AW-12-06-**$GulA_{20}$**	NaOH at 10^{-6} mol L^{-1}	1	3.5	0.28	0.98	**1.26**
	$CaCl_2$ in DI (0.10 mol L^{-1})	1	8.0	0.28	2.24	

Note: $\langle\Delta z_c\rangle$ is the average difference in cantilever deflection, k is the cantilever spring constant, $\langle F\rangle$ is the average adhesion force and $\Delta\langle F\rangle$ is the difference in the average adhesion force determined from experiments performed in $CaCl_2$ and NaOH.

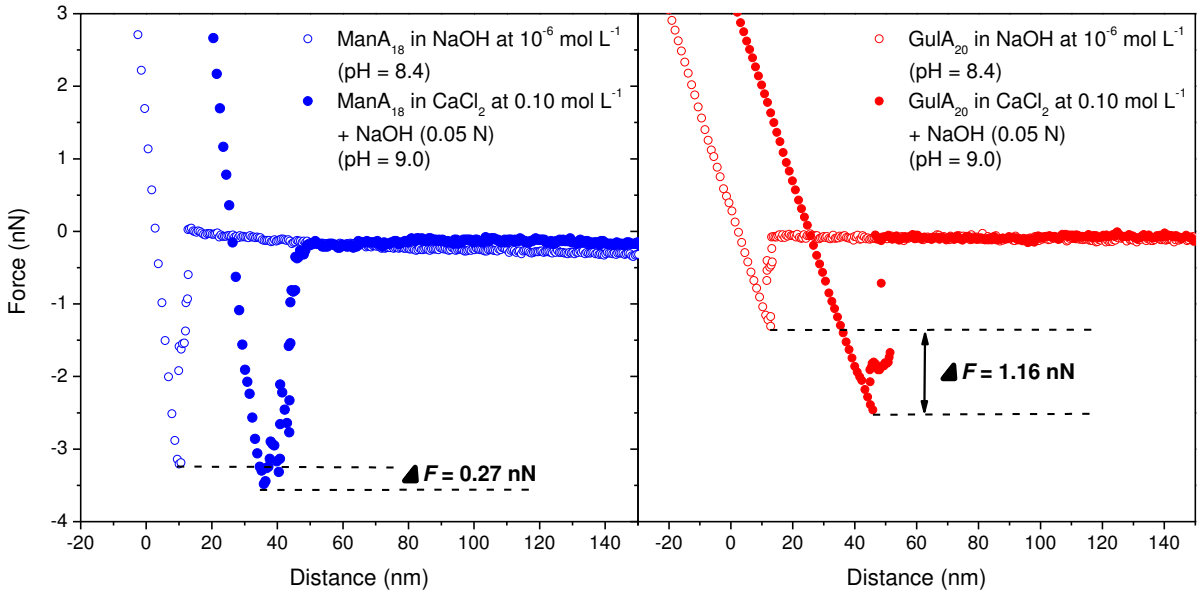

Figure 5.3 *Typical force curves obtained for (1→4)-β-D-mannuronan (X = 18, $ManA_{18}$) and (1→4)-α-L-guluronan (X = 20, $GulA_{20}$) oligomers grafted on gold surfaces (tips and wafers), performed with sweep duration time = 1 s. In order to show observed differences, the curves obtained in the presence of $CaCl_2$ were shifted in distance around 25 nm.*

2.4.2. *Heterotypic interactions*

A natural alginate is composed of heterogeneous types of blocks, hence it has been found interesting to study not only homotypic interactions (*i.e.* $ManA_{18}$-$ManA_{18}$ or $GulA_{20}$-$GulA_{20}$) but also heterotypic ones. On that purpose, new silicon surfaces were grafted with desired oligomers according to the procedure described in paragraph 2.3.1. The cantilever spring constants were calculated on the basis of Eq. 5.6 and are given in Table 5.5.

Table 5.5 *Cantilever spring constants (k) calculated for MSNL probes grafted with (1→4)-β-D-mannuronan (X = 18, $ManA_{18}$) or (1→4)-α-L-guluronan (X = 20, $GulA_{20}$) oligomer. The resonance frequency (f_R) and the quality factor (Q) were obtained from a fit to the simple harmonic oscillator (SHO), whereas the values of the width (b) and the length (L) of the cantilever were taken as suggested by Brucker.*

Value	***$ManA_{18}$ cantilever D***	***$GulA_{20}$ cantilever D***
f_R (Hz)	14751	14934
Q	22.68	24.83
b (μm)	20	20
L (μm)	225	225
k (N/m)	**0.09**	**0.10**

The obtained values are about three times higher than estimated by Brucker producer, what is in agreement with findings from another, similar experiment (see Table 5.1). Probing of homo- and hetero-typic interactions between oligomers have been performed in aqueous solutions of calcium chloride and sodium chloride. The computed average cantilever deflections together with standard deviations are given in the Appendix (Table 5A.3).

Table 5.6 illustrates the main characteristics of the mixed interactions. The results from this study show an increase in the difference in the average adhesion force ($\Delta\langle F\rangle$) in the following order:

$$\text{M-M} < \text{M-G or G-M} < \text{G-G}$$

which confirms generally accepted phenomenon, *i.e.* the higher content of G-units is, the more stable complex is formed. The value of $\Delta\langle F\rangle$ for M-blocks was not that small what suggests that M-blocks also interact via calcium ions that has been also proofed by Ghadban *et al.* [13] and suggested by MD simulations [14-16].

Table 5.6 *Average computed values for all registered curves, obtained from force measurements performed with sweep duration time = 1s for (1→4)-β-D-mannuronan (X = 18, $ManA_{18}$) and (1→4)-α-L-guluronan (X = 20, $GulA_{20}$) oligomers grafted on silicon surfaces (silicon nitride MSNL probes and silicon wafers) in both DI water (pH = 7.0) and $CaCl_2$ aqueous solution (pH = 7.0).*

Experiment code	*Solution*	$\langle\Delta z_c\rangle$ *(nm)*	*k (N/m)*	$\langle F\rangle$ *(nN)*	$\Delta\langle F\rangle$ *(nN)*
AW-12-09-$ManA_{18}$(tip)-$ManA_{18}$(wafer)	DI water	19.5	0.09	1.76	**0.36**
	$CaCl_2$ in DI (0.01 mol L^{-1})	23.5	0.09	2.12	
AW-12-09-$ManA_{18}$(tip)-$GulA_{20}$(wafer)	DI water	17.7	0.09	1.59	**0.53**
	$CaCl_2$ in DI (0.01 mol L^{-1})	23.5	0.09	2.12	
AW-12-09-$GulA_{20}$(tip)- $ManA_{18}$(wafer)	DI water	60.3	0.10	6.03	**0.51**
	$CaCl_2$ in DI (0.01 mol L^{-1})	65.4	0.10	6.54	
AW-12-09-$GulA_{20}$(tip)-$GulA_{20}$(wafer)	DI water	9.9	0.10	0.99	**0.63**
	$CaCl_2$ in DI (0.01 mol L^{-1})	16.2	0.10	1.62	

Note: $\langle\Delta z_c\rangle$ is the average difference in cantilever deflection, k is the cantilever spring constant, $\langle F\rangle$ is the average adhesion force and $\Delta\langle F\rangle$ is the difference in the average adhesion force determined from experiments performed in $CaCl_2$ aqueous solution and DI water.

Surprisingly, the values of the average difference in cantilever deflection ($\langle\Delta z_c\rangle$) were much higher for G-M interactions (see Table 5A.3 in the Appendix) than in other cases, thus the experiment was repeated. Nevertheless, the obtained results were the same. It may be attributed to the grafting density of both tip and wafer which unfortunately so far is not under control. But it is worth noting that $\Delta\langle F\rangle$ calculated for either G-M or M-G interactions was

almost the same (≅ 0.5 nN), see Table 5.6. In addition, on the basis of applied sweep duration time (1s), it can be concluded that the binding process occurred quite fast in all examined types of interactions.

On the other hand, the results obtained in the presence of NaCl (0.02 mol L^{-1}) are difficult for interpretation (see Appendix Table 5A.3). In general, values of the average difference in cantilever deflection ($\langle \Delta z_c \rangle$) were lower in NaCl solution than in $CaCl_2$, except for $GulA_{20}$(tip)-$ManA_{18}$(wafer) interactions. In addition, $\langle \Delta z_c \rangle$ values recorded in NaCl solution were also lower than in DI water what is very surprising. Thus, further work is required.

2.5. *Conclusion*

Atomic Force Spectroscopy (AFS) was a method of choice in order to insight into the formation of the junction zones (the gelation process) at the molecular level.

Firstly, the interactions between homogeneous oligomers ($ManA_{18}$ or $GulA_{20}$) attached to silicon or gold surfaces in the absence and presence of Ca^{2+} were examined. This study showed that guluronan blocks associate via calcium ions stronger than mannuronan blocks.

On the other hand, the heterotypic interactions, *i.e.* between heterogeneous oligomers attached to silicon surfaces were also investigated and revealed that their strength increased in the following order:

M-M < M-G or G-M < G-G.

In addition, observed difference in the average adhesion force ($\Delta\langle F \rangle$) for M-M interactions has proofed that M-blocks complexed via Ca^{2+} can be involved in both homotypic and heterotypic associations. Certainly, their contribution is lower than G-blocks but nevertheless may also impact on the formation of junction zones.

It is worth noting that in this study, interactions between oligomers grafted on two different surfaces (tip and wafer) in the presence of calcium ions were of major importance. In that specific case, oligomers had to be oriented antiparallel to each other. Nevertheless, since on the desired surface more than one oligomer chain was grafted, thus those "antiparallel interactions" could be perturbed by "parallel interactions" (between chains grafted on the same surface).

3. Light Scattering and rheology

3.1. Introduction

It has been already mentioned many times in this PhD manuscript that alginates undergo gelation in the presence of Ca^{2+}. In the previous paragraph of this chapter, it has been found that G-blocks interact via calcium ions stronger than M-blocks. Nevertheless, beside a significant interest in describing the gelation, this paragraph will be mainly dedicated to the sol-gel transition phenomenon in alginate, homo-oligo-(or poly-)alginate and neo-alginate solutions, which is at the heart of understanding the gelation process.

A sol-gel transition in alginate solutions, in the presence of divalent cations such as: Ca, Cu, Mn and Co, has been already studied on several occasions by viscosity measurements[17], rheological experiments[18], ^{13}C-NMR spectroscopic study[19] or SAXS technique[20].

For instance, in order to determine a sol-gel transition, variations of relative viscosity (η^*), defined as a ratio between viscosities of solution with and without divalent cations addition [20], were measured as a function of molar cross-link fraction *(f)* expressed as follows:[17]

$$f = [Ca^{2+}]/[alginate\ residues] \quad \text{(Eq. 5.8)}$$

Furthermore, it was assumed that the value of *f* at the gelation threshold, called f_c can be determined on the basis of critical phenomenon with a power-law relation according to:[17]

$$\eta^* \propto (f_c - f)^{-k} \quad \text{(Eq. 5.9)}$$

where *k* is the critical exponent for the relative viscosity.

It has been found that for Ca-alginate systems, the gel point defined in terms of f_c strongly depends on the alginate concentration, *i.e.* the lower the alginate concentration, the greater f_c.[18]

Interestingly, the transition from liquid to gel state has been also investigated for pectins, which also form gels upon addition of Ca^{2+}. In that case, the sol-gel transition was determined for pectins via LS and rheology [21,22] on the basis of observed changes in the charge stoichiometric ratio (*R*) (Eq. 5.10) during slow and progressive addition of calcium chloride.

$$R = 2[Ca^{2+}]/[COO^{-}] \quad \text{(Eq. 5.10)}$$

Since the formation of Ca^{2+}-alginate junction zone involves both calcium ions and carboxylic groups of the uronic acid residues, so the studies of the sol-gel transition described in this paragraph will be based on the changes in the charge stoichiometric ratio (*R*) (Eq. 5.10).

Two concentration domains were studied: low-concentrated to evidence formation of aggregates (first indication of junction zones) and semi-concentrated to investigate formation of the 3D network (mechanism of gelation).

3.2. Materials

A commercial alginate Satialgine SG150 (~80% of guluronic acid) was purified in agreement with a protocol described in Methods section (paragraph 3.3.1). NaCl (≥99 %, ACS), $NaHCO_3$ (≥99 %, Aldrich), ethylenediaminetetraacetic acid disodium salt dihydrate EDTA-Na_2·$2H_2O$ (≥98.5 %, Aldrich), sodium hydroxide solution (1N, pure Acros), ethanol (96 %, Carlo Erba), calcium chloride dihydrate (≥99 %, Acros) were used as received. (1→4)-α-L-guluronan oligomers with 10 and 20 repeating units (*X* = 10 and 20) and (1→4)-β-D-mannuronan oligomers (*X* = 10 and 18) were obtained from Elicityl OligoTech®. Sample of mannuronan (*X* = 300) was delivered from Norway by G. Skjåk-Braek. Neo-alginates, *i.e.* poly(HEMAm-g-$GulA_X$) (*X* = 10 or 20) were synthesized by Eric Reynaud – a member of the ALGIMAT project. NMR analyses of examined materials were conducted by Luca Albertin (see the Appendix). All aqueous solutions were prepared with deionized water from MilliQ apparatus (Millipore).

3.3. Methods

3.3.1. Alginate purification

A solution of alginate at 5.0 g L^{-1} was prepared in deionized water and left under stirring overnight. Next day the pH of the solution was adjusted to 7.0-7.5 with solid sodium bicarbonate ($NaHCO_3$). Then, the solution was firstly filtered on a sintered glass filter with porosity 3 (a pore diameter of 16-40 μm) followed by filtration through 1.2 μm nylon filter. Separately, the solution of sodium chloride at 0.8 mol L^{-1} and ethylenediaminetetraacetic acid disodium salt dihydrate at 16 mmol L^{-1} were prepared in deionized water (their pH was adjusted to 7.0 by adding sodium hydroxide at 1.0 mol L^{-1}) and mixed with filtered solution

of alginate. After stirring overnight, the mixture was transferred to larger flask and the alginate was precipitated by the addition of ethanol up to 80% v/v (under vigorous stirring). The whole suspension was filtered on a sintered glass filter with porosity 3 and the obtained precipitate was re-solubilized in 100 mL of deionized water and precipitated again with ethanol (80% v/v). Finally, the precipitate was rinsed twice with water : EtOH mixture (20 : 80 v/v), followed by rinsing with pure ethanol two times and dried overnight at room temperature and then in desiccator for 24 hours. This alginate purification was performed twice. However, ^{1}H NMR spectral analysis of purified alginate showed presence of residual EDTA; so, in order to remove it, the dialysis purification against water was performed. Firstly, alginate powder was re-dissolved in 40 mL of water and then transferred to dialysis cassette (Slide-A-Lyzer 20K G2; 20000 Da molecular weight cut-off). Dialysis purification was performed at room temperature over 4 days against deionized water which was changed after 2, 17, 26, 42 and 49 hours. Then, the solution from dialysis cassette was placed in a round bottom flask, frozen in liquid nitrogen and freeze dried over 72 hours (^{1}H NMR spectral analysis confirmed that EDTA was completely removed, see Figure 5A.2 in the Appendix). Residual solvent content was determined by thermogravimetric analysis (TGA) by Eric Bayma.

3.3.2. *Poly(HEMAm-g-GulAx) synthesis*

Poly(HEMAm-g-GulA$_X$) neo-alginates were synthesized in the intended manner, *i.e.* to contain almost the same number of grafted guluronan units (either GulA$_{20}$ or GulA$_{10}$) by Eric Reynaud via conventional radical copolymerization (Scheme 5.5) according to the procedure used by Ghadban *et al.* [13]

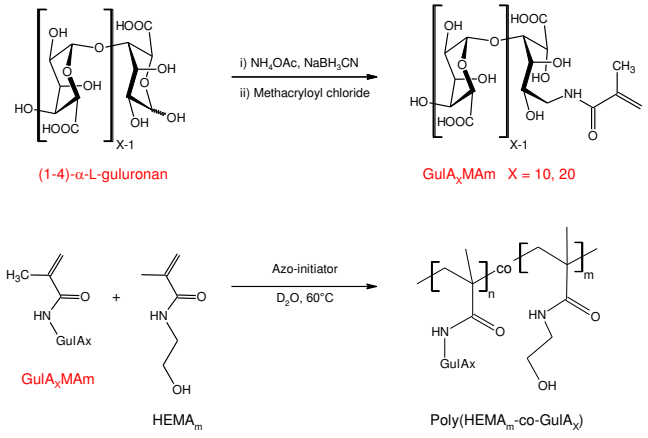

Scheme 5.5 *Schematic representation of synthesis of Poly(HEMAm-g-GulA$_x$) via conventional radical copolymerization.*

3.3.3. LS measurements and sample preparation

Light Scattering measurements were performed with a commercial Zetasizer (Zetasizer NanoZS, Malvern, Worcestershire, UK) equipped with the standard 633 nm laser. In all cases, measurements were carried out at 23°C at the scattering angle of 90°. Solutions of known volume were prepared in Erlenmeyer flasks in deionized water (DI) or NaCl (0.05 mol L^{-1}; filtered through 0.2 μm nylon filter) and then filtered again through a filter specified in Table 5.7 before measurements. Additionally, solutions were prepared in the intended manner, *i.e.* to contain almost the same uronic acid concentration, in order to make a comparison.

Table 5.7 *Summary of sample preparations for LS measurements.*

Sample	***Experimental code***	***solvent***	***c*** ***(g L^{-1})***	***c_{Gul}*** ***(g L^{-1})***	***filter***	***Time EQ*** ***(min)***
Alginate SG150	*AW-12-10-SG150*	NaCl	0.20	0.16	0.2 μm nylon	8
Alginate SG150	*AW-12-10-SG150*	NaCl	0.60	0.48	0.2 μm nylon	4
$OligoGulA_{20}$	*AW-12-10- $GulA_{20}$*	NaCl	0.12	0.12	0.2 μm nylon	10
$OligoGulA_{20}$	*AW-12-10- $GulA_{20}$*	DI	0.12	0.12	0.45 μm nylon	4
$OligoGulA_{10}$	*AW-12-10- $GulA_{10}$*	NaCl	0.12	0.12	0.2 μm nylon	5
$OligoManA_{18}$	*AW-13-02- $ManA_{18}$* *AW-13-17- $ManA_{18}$*	NaCl	0.12	-	0.2 μm nylon	4
$OligoManA_{10}$	*AW-13-18- $ManA_{10}$*	NaCl	0.12	-	0.2 μm nylon	10
*$ManA_{300}$**	*AW-13-13*	NaCl	0.12	-	0.2 μm nylon	7
*$ManA_{300}$**	*AW-13-13*	DI	0.12	-	0.2 μm nylon	7
Poly(HEMAm-g-$GulA_{20}$)	*AW-13-11*	NaCl	0.43	0.12	1.2 μm GF	5
Poly(HEMAm-g-$GulA_{20}$)	*AW-13-11*	DI	0.43	0.12	1.2 μm GF	5
Poly(HEMAm-g-$GulA_{10}$)	*AW-13-12*	NaCl	0.28	0.12	1.2 μm GF	5
Poly(HEMAm-g-$GulA_{10}$)	*AW-13-12*	DI	0.28	0.12	1.2 μm GF	5

** Mannuronan (X = 300) isolated from C5 epimerase negative mutant of Pseudomonas fluorescens*
Note: Solution of NaCl at 0.05 mol L^{-1} was filtered through 0.2 μm nylon filter.

Next step was slow addition of dilute solution of calcium chloride solution prepared at 0.005 mol L^{-1} (filtered through 0.22 μm filter) under vigorous stirring till observing a huge increase in the registered intensity. It is noteworthy to mention that after each increment of calcium chloride concentration, the solution was left under stirring for few minutes (according to the time EQ given in Table 5.7, needed to obtain stable values of registered intensity) in order to provide proper homogeneous calcium complexation. Each time measured solution was placed inside the quartz cuvette and equilibrated for 120 s before intensity measurement.

Then it was recovered and transferred back to the flask. Calculated intensity was equal to average intensity taken from 18 runs.

3.3.4. Gel preparation and rheological analysis

3.3.4.1. Alginate gel preparation

Firstly, solution of alginate was prepared in NaCl (0.05 mol L^{-1}; filtered through 0.2 μm nylon filter) at 14 g L^{-1}. Then, this solution was divided into few vials in order to prepare samples of varying concentration of calcium chloride (different *R*). In all cases, the final alginate concentration (≈5 g L^{-1}) and the total volume of all samples (4.2 mL) were unchanged due to compensation of extra volume of $CaCl_2$ by addition of NaCl solution (0.05 mol L^{-1}). It is worth nothing that due to rapid calcium binding by alginate, direct mixing of alginate with calcium chloride very rarely lead to obtain homogeneous gel.[23] Thus, calcium chloride at 0.05 mol L^{-1} (filtered through 0.2 μm nylon filter) was slowly dripping into solution of alginate in NaCl placed in oil bath at 85°C under vigorous stirring (according to the procedure used by Cardenas *et al.* [22]) in order to enable formation of homogeneous gel. Before rheological analysis (paragraph 3.3.4.5) all samples were left overnight at room temperature to reach equilibrium.

3.3.4.2. Poly(HEMAm-g-GulA$_{20}$) gel preparation

In the beginning, the idea was to prepare samples according to the protocol used in the case of alginate gel (paragraph 3.3.4.1). However, it has been found that the final polymer concentration about 5 g L^{-1} is not sufficient to form a gel. Therefore, before preparing a new series of experiments, a gelation test has been performed. As can be seen from Figure 5.4, a self-standing gel was obtained as a result of dissolution of neo-alginate in NaCl at 0.05 mol L^{-1} (filtered through 0.2 μm nylon filter) followed by dripping a calcium chloride solution at 0.05 mol L^{-1} (filtered through 0.2 μm nylon filter) until the final polymer concentration was equal to 20 g L^{-1} and $R = 0.8$.

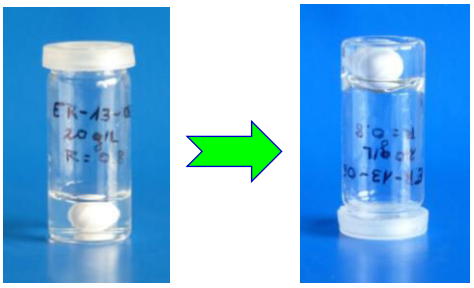

Figure 5.4 *Gelation test performed for poly(HEMAm-g-GulA$_{20}$) neo-alginate, $c_{polymer}$ = 20 g L^{-1} and R = 0.8.*

Since the gelation test was positive, thus new samples with final polymer concentration = 20.38 g L^{-1}, R = 0.0, 0.2, 0.3, 0.4, 0.6, 0.8 and total volume = 2.3 mL were prepared according to the protocol described in paragraph 3.3.4.1.

3.3.4.3. *Poly(HEMAm-g-GulA$_{10}$) gel preparation*

Samples with final polymer concentration equal to 20.48 g L^{-1} (or 19.6 g L^{-1} for samples at R = 0.7 and 0.9) and total volume = 2.63 mL (or about 2 mL for samples at R = 0.7 and 0.9) were prepared either in NaCl (0.05 mol L^{-1} filtered through 0.2 µm nylon filter) with R = 0.0, 0.2, 0.3, 0.4, 0.6, 0.7, 0.8 and 0.9, or in DI water (R = 0.0, 0.6, 0.7, 0.8 and 0.9) according to the protocol described in paragraph 3.3.4.1.

3.3.4.4. *Alginate and poly(HEMAm-g-GulA$_{20}$) hydrogels prepared by dialysis*

Solutions of alginate and poly(HEMAm-g-GulA$_{20}$) were prepared in NaCl (0.05 mol L^{-1} filtered through 0.2 µm nylon filter) at ~4 times the critical overlapping concentration (c*) as estimated from their intrinsic viscosity reported in Table 5.8 ($c^* \approx 1/[\eta]$). Then, each solution was injected into separate dialysis cassette (Slide-A-Lyzer, 2000 MWCO Da, 0.5-3.0 mL capacity, Pierce) and dialyzed against $CaCl_2$ (0.5 mol L^{-1}) for 24 hours. In order to recover obtained gels from dialysis cassettes, membranes were cut off with a scalpel. The resulting materials were punched into disks (diameter = 2 cm) and their rheological properties were measured in oscillatory and compression mode at 25°C with a cone-plate geometry (diameter = 60 mm, angle = 1° and truncation gap = 14 µm).

3.3.4.5. *Rheological analysis*

All samples were characterized with an AR-G2 rheometer (TA Instruments) at 25 °C with a cone-plate geometry either (60 mm, 2°, 54 µm) in the case of alginate gels (paragraph 3.3.4.1) or (60 mm, 1°, 29 µm) in the case of neo-alginate gels (paragraph 3.3.4.2 and

3.3.4.3). Strain sweep step was performed previously to determine a domain of strain value (γ) for which the storage modulus (G') and the loss modulus (G'') are strain independent (linear viscoelastic region). Then estimated value of strain was applied to performing frequency sweep step (between 0.5 to 10 Hz) followed by steady state flow step (from 0.5 to 10 or 20 s^{-1}).

3.4. Results

3.4.1. Sample characteristics

Detailed characteristics of purified alginate and synthesized polymers needed for experimental studies are given in Table 5.8. In addition, their NMR spectra are attached in the Appendix placed in the end of this chapter (Figure 5A.4 and Figure 5A.5).

Table 5.8 *Characteristics of purified commercial alginate and synthesized neo-alginates.*

	Alginate SG150	***poly(HEMAm-g-GulA$_{20}$)***	***poly(HEMAm-g-GulA$_{10}$)***
Experimental code	SG150_ppt_DIA	ER-13-06	ER-13-15_DF2
M_n (Da)	37250	276000	257100
M_w (Da)	97560	616000	683700
$F_{m,\ GulA}$ (%)	81	28	42.6
X of GulA graft chains	-	20	10
Average number of GulA side chains per polymeric chain	-	20	56
Đ	2.62	2.23	2.66
[η] (mL g^{-1})	320	200	190
*c** (g L^{-1})	3.1	5.0	5.3
dn/dc	0.165	0.196	0.190
% H_2O	17.7 (F1) or 11.9 (F2)	11.4	11.2

Note: F_m is the weight fraction of guluronan in polymer, X is the degree of polymerization, Đ is the molar mass dispersity, [η] is the intrinsic viscosity measured in 0.1 mol L^{-1} $NaNO_3$, c is the critical concentration and dn/dc is the refractive index increment.*

3.4.2. Determination of the critical point of percolation by LS

Light Scattering is a technique which enables revealing the formation of aggregates by monitoring scattered intensity. In terms of percolation approach, the number of aggregation (N) could be estimated from the following ratio proposed by Thibault *et al.* [21]:

$$\frac{(I_{meas}-I_{solvent})}{(I_0-I_{solvent})} \sim \frac{\bar{M}_{app}}{\bar{M}_0} \cong N \qquad and \qquad N \propto (R_c - R)^{-n} \qquad \text{(Eq. 5.11)}$$

where $\bar{M}_0$ is the initial average molecular weight, $\bar{M}_{app}$ is the apparent average molecular weight. The critical characteristics of the percolation process are expressed by the critical

percolation threshold R_c and the critical percolation exponent n. The critical value R_c corresponds in the case of anionic polymers cross-linked via Ca^{2+} to the critical charge stoichiometric ratio. Thus, R_c and exponent n are obtained from the best linear fitting of the log/log plot for low values of $(R_c - R)$ *vs.* $\frac{(I_{meas}-I_{solvent})}{(I_0-I_{solvent})}$, where n is equal to the determined slope (as an example see Figure 5A.6 in the Appendix).

Since alginates as well as any alginate derivatives are negatively charged, thus all experiments were performed in the presence of NaCl to screen electrostatic repulsions between the charged chains. However for a comparison, some single measurements were carried out also in aqueous solution.

3.4.2.1. Alginate

Alginate samples were examined in the presence of sodium chloride at two different concentrations: 0.2 g L^{-1} and 0.6 g L^{-1}. As can be seen from Figure 5.5, the formation of aggregates is slightly shifted to lower R_c values at higher alginate concentration.

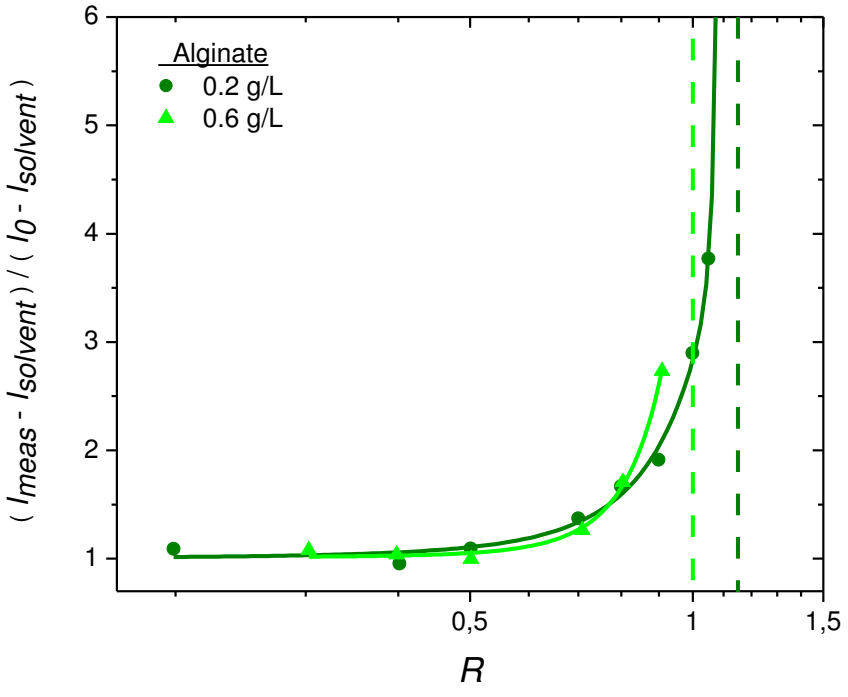

Figure 5.5 *Changes in scattered intensity of alginate solution in NaCl (0.05 mol L^{-1}) during the addition of calcium chloride (0.005 mol L^{-1}). The dashed lines correspond to determined critical charge stoichiometric ratio (R_c).*

Then, in order to determine the starting point of aggregate formation, defined in terms of the critical ratio (R_c) and exponent n according to equation Eq. 5.11, linear fitting method

proposed by Thibault *et al.* [21] was applied (see Figure 5A.6 in the Appendix). It has been found that the threshold of aggregate formation appears about R_c = 1.15 or 1.0 at alginate concentration = 0.2 g L^{-1} or 0.6 g L^{-1}, respectively, which correspond to exponents n = 0.74 or 0.66. Interestingly, the value of n calculated for alginate at 0.2 g L^{-1} is in the same range as in the previous studies performed for pectins [21] where at the same polymer concentration n was equal to 0.71.

3.4.2.2. *GulA10, GulA20, ManA10, ManA18 and ManA300*

Separately, changes in scattered intensity were investigated for solutions of (1→4)-α-L-guluronan ($GulA_{10}$ and $GulA_{20}$) and (1→4)-β-D-mannuronan ($ManA_{10}$, $ManA_{18}$ and $ManA_{300}$) at 0.12 g L^{-1} during the addition of calcium chloride (0.005 mol L^{-1}). As shown in Figure 5.6, there is no significant difference between experiment performed in DI water or NaCl ($GulA_{20}$ and $ManA_{300}$). But, it can be seen that the R_c is slightly shifted to lower values in the case of $GulA_{20}$ in the presence of NaCl, what confirms that NaCl favors the association of $GulA_{20}$ as it was suggested before.

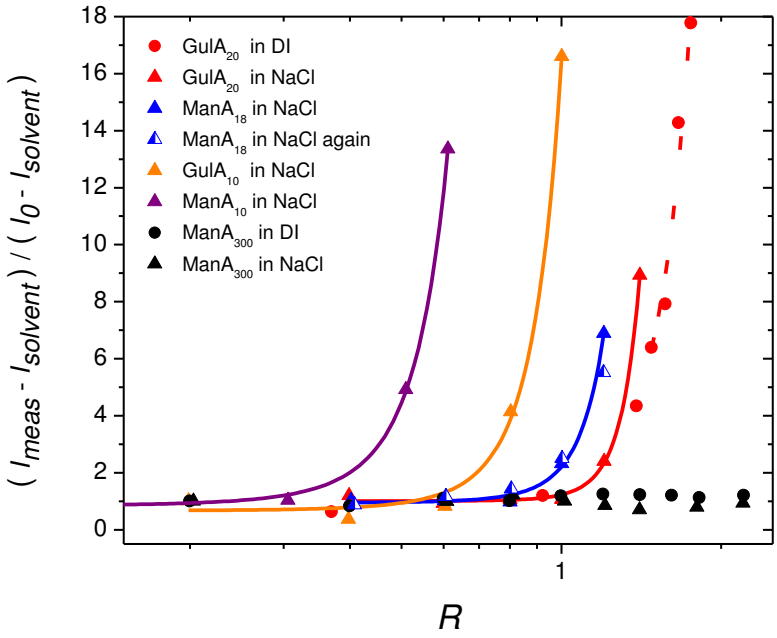

Figure 5.6 *Changes in scattered intensity of homo-oligo-(or poly-)alginates at 0.12 g L^{-1} in DI water or NaCl solution (0.05 mol L^{-1}) during the addition of calcium chloride (0.005 mol L^{-1}).*

In these conditions, formation of aggregates was observed in all cases except $ManA_{300}$. In addition, a huge increase in the scattered intensity was also noticed in oligomannuronan samples ($ManA_{10}$ and $ManA_{18}$) what was surprising because it is

reported [24-26] that mannuronan blocks (M-blocks) have much lower ability to complexation with calcium ions than guluronan blocks (G-blocks). Thus, the experiment was repeated for $ManA_{18}$ and the same results were obtained. Furthermore, the effect of degree of polymerization (X) was also examined and it has been found that for samples having lower X, the threshold of aggregate formation appeared faster, *i.e.* at lower R_c values.

Since the concentration of examined homo-oligoalginates was the same in each measurement (0.12 g L^{-1}), the results can be compared on the basis of R/R_c, called the normalized parameter. Thus, first the R_c value was estimated for each experiment, according to the method proposed by Thibault *et al.* [21], and then the changes in scattered intensity were plotted as a function of the normalized parameter calculated according to found R_c values. As can be seen from Figure 5.7, aggregates are formed faster when the degree of polymerization (X) of homo-oligoalginate is lower.

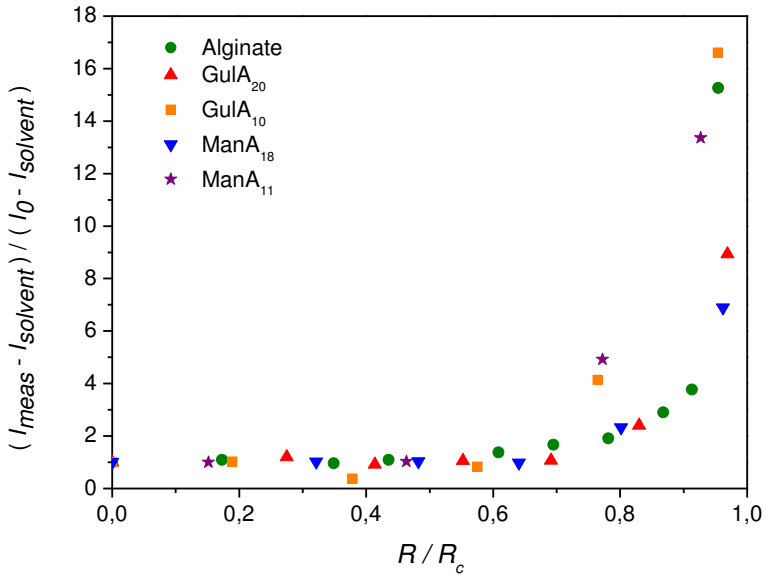

Figure 5.7 *Aggregate formation shown on the basis of the normalized parameter R/R_c computed for alginate and homo-oligoalginates in NaCl solution (0.05 mol L^{-1}) during the addition of calcium chloride (0.005 mol L^{-1}).*

It is worth noting that the same concentration of homo-oligoalginate expressed in g L^{-1} is not equivalent with the same number of chains. Thus, the number of chains is higher for shorter homo-oligoalginates, which perhaps favors aggregation. However, high affinity of oligomannuronan chains to the complex formation with Ca^{2+} is still surprising. It can be explained in part by the probability of association of single oligomannuronan chains leading to aggregate formation detected via LS. In the case of $ManA_{300}$, no aggregates were observed,

probably due to the presence of long chains (X = 300) with lower probability to meet. These findings suggest that the mechanism of aggregate formation depends on the structure, *i.e.* degree of polymerization (X) and configuration (Man or Gul). Furthermore, the results obtained for alginate with almost comparable concentration of guluronan (c_{Gul} = 0.16 g L^{-1}) were also plotted in Figure 5.7. Interestingly, all registered points indicate the same increasing tendency as it was determined for homo-oligoalginate with higher X ($GulA_{20}$ and $ManA_{18}$). In addition, this study gives a direct information about the probability to form multimers at given concentration.

3.4.2.3. *Poly(HEMAm-g-GulA$_{20}$) and poly(HEMAm-g-GulA$_{10}$)*

In the case of synthesized neo-alginates, the experiments were first performed in NaCl but small changes in scattered intensity, compared with alginate (Figure 5.5) and homo-oligoalginates (Figure 5.6) as well as DI water environment (Figure 5.8), were registered. It was observed that the thresholds of aggregate formation determined in DI water for both neo-alginates were almost the same. This result is satisfactory because in fact those polymers have been synthesized in the intended manner, *i.e.* to contain almost the same number of grafted guluronan units (either $GulA_{20}$ or $GulA_{10}$).

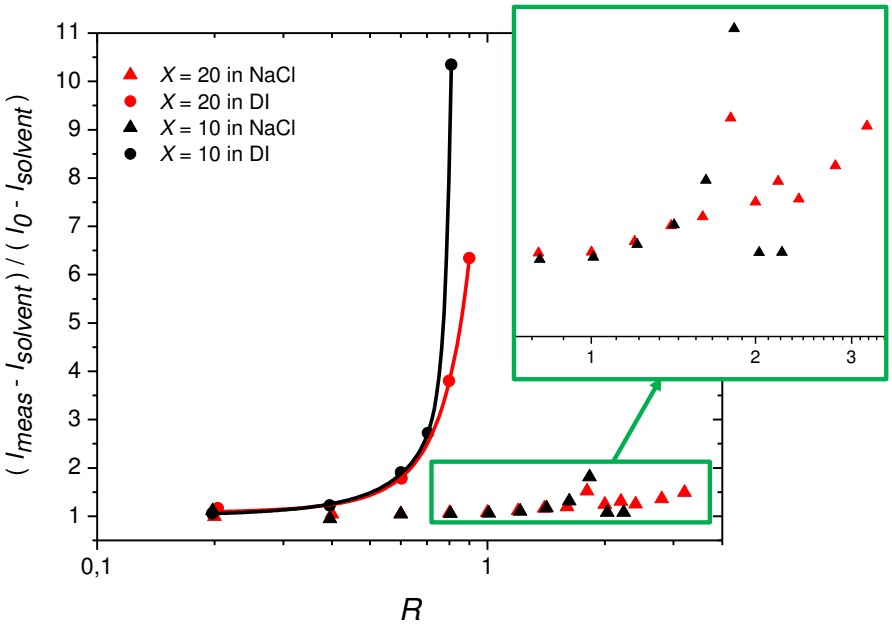

Figure 5.8 *Changes in scattered intensity of synthesized neo-alginates: poly(HEMAm-g-GulA$_X$), at 0.43 g L^{-1} (for X = 20) or at 0.28 g L^{-1} (for X = 10) in DI water and NaCl solution (0.05 mol L^{-1}) during the addition of calcium chloride (0.005 mol L^{-1}).*

By contrast, in the presence of NaCl, which screens the electrostatic repulsions between charged chains, the result indicates loose polymer chain-chain interactions, which may involve intra- or inter-chain interactions between few grafted G-blocks with low cooperativity, due to large distance between grafted chains (min. 20 nm). Thus, probably the observed increase in scattered intensity is a result of polymer chain-chain "antiparallel interactions". In addition, in excess of NaCl, an ion exchange between Ca^{2+} and Na^{+} in excess may dissociate the aggregates formed in distilled water.

3.4.3. Sol-gel transition by rheology and some gel properties

3.4.3.1. Alginate

- *Sol-gel transition*

Gelation behavior was investigated for alginate-gel of fixed polysaccharide concentration (5.3 g L^{-1}) and varying amounts of added calcium chloride solution (R = 0.0, 0.1, 0.2, 0.3 and 0.4).

Figure 5.9 presents the dependence of storage modulus (G') and the loss modulus (G'') on frequency (ω) of the gels obtained for R = 0.2, 0.3 and 0.4. Sample at R = 0.2 reveals a transition from a solution to a gel-like behavior in contrast to samples at higher R (0.3 and 0.4) which give clearly soft gels (G' over G'').

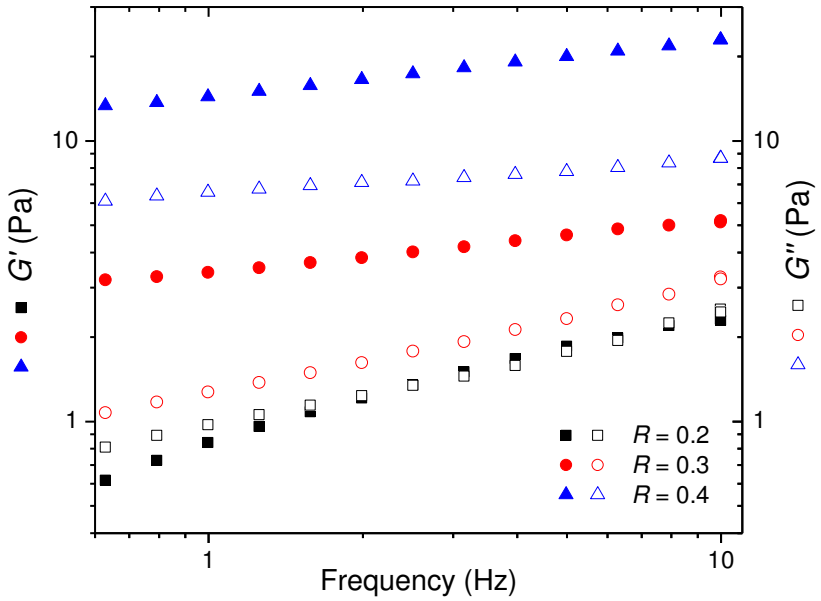

Figure 5.9 *Variation of G' and G'' with frequency for alginate solutions ($c_{alginate}$ = 5.3 g L^{-1}) in NaCl (0.05 M L^{-1}) at varying R = 2[Ca^{2+}]/[COO^{-}] at 25°C.*

In order to estimate the maximal R ratio (R_{max}), first the viscosity (η) was taken from the curve $\eta(\dot{\gamma})$ (at shear rate $(\dot{\gamma})$ = 5 s^{-1}) and the storage modulus (G') from the curve G' (ω) (at ω = 0.63 Hz) and then their normalized values were plotted as a function of R (Figure 5.10).

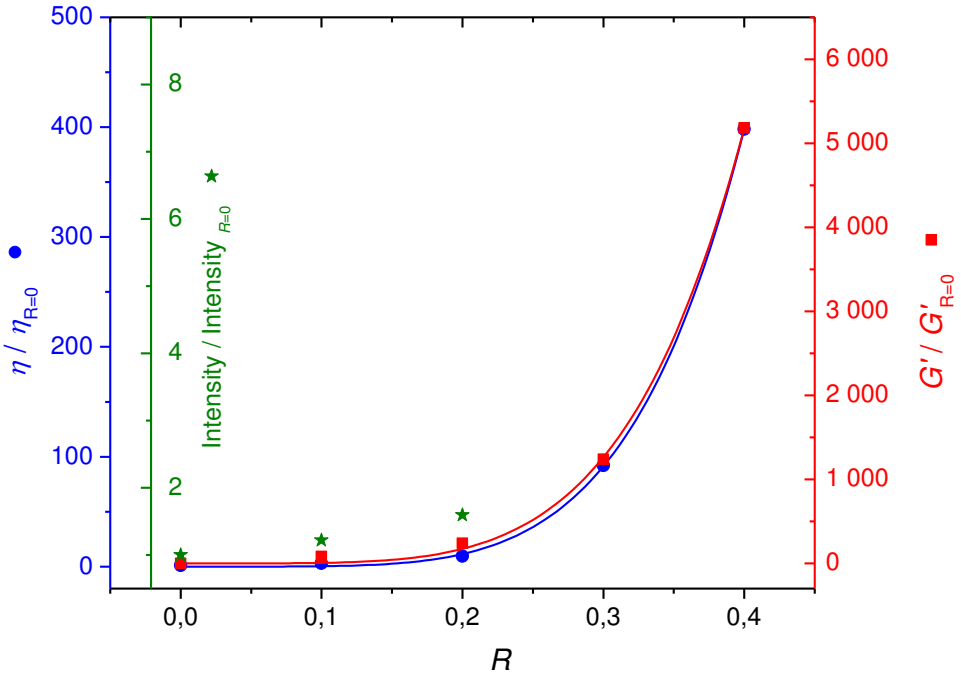

Figure 5.10 *Dependence of normalized viscosity and storage modulus (G') on varying $R = 2[Ca^{2+}]/[COO^{-}]$ for alginate solutions ($c_{alginate}$ = 5.3 g L^{-1}) in NaCl (0.05 mol L^{-1}) at 25°C. In addition, normalized scattered intensities for samples at R = 0.0, 0.2 and 0.3 registered by LS at 23°C are also shown.*

It is apparent from the observed gradual increase in viscosity and G' that the maximal ratio is approximately 0.4. Furthermore, the strong relationship between R and viscosity indicates progressive gel formation. After rheological measurements, samples at $0.0 < R < 0.2$ were examined by LS at 23°C in order to verify if the gradual aggregation found by rheology could be also observed by LS. As can be seen from Figure 5.10 (green points) the results obtained by both techniques: rheology and LS are in good agreement. This study has also shown that the critical charge stoichiometric ratio is lower at higher concentration of alginate (5.3 g L^{-1}), what was already noticed in dilute solutions studied by LS (paragraph 3.4.2.1).

- *Gel properties*

Interestingly, it has been demonstrated by Morris *et al.* [27] that addition of short chain segments (oligosaccharide blocks in our case) to a gelling polymer can either increase the aggregate network, or disconnect previously formed junction zones. Therefore, in order to examine this phenomenon, first the free G-block with 20 repeating units (X = 20) was added at a [$GulA_{20}$(free)]/[$GulA_{20}$(grafts)] ratio of 1 to the formed gel (R = 0.3 and 0.4). It can be seen from Figure 5.11 that the addition of the free G-block resulted in transition from a gel-like to a sol-like state ($G''>G'$) in both cases (R = 0.3 and 0.4). It is obvious that difference between G' and G'' for the sample at R = 0.4 with G-block is smaller than for sample at R = 0.3 with G-block because at higher R the gel is stronger what makes it more difficult to break. Results from this investigation confirm that addition of free G-blocks dissociates the initial junction zones.

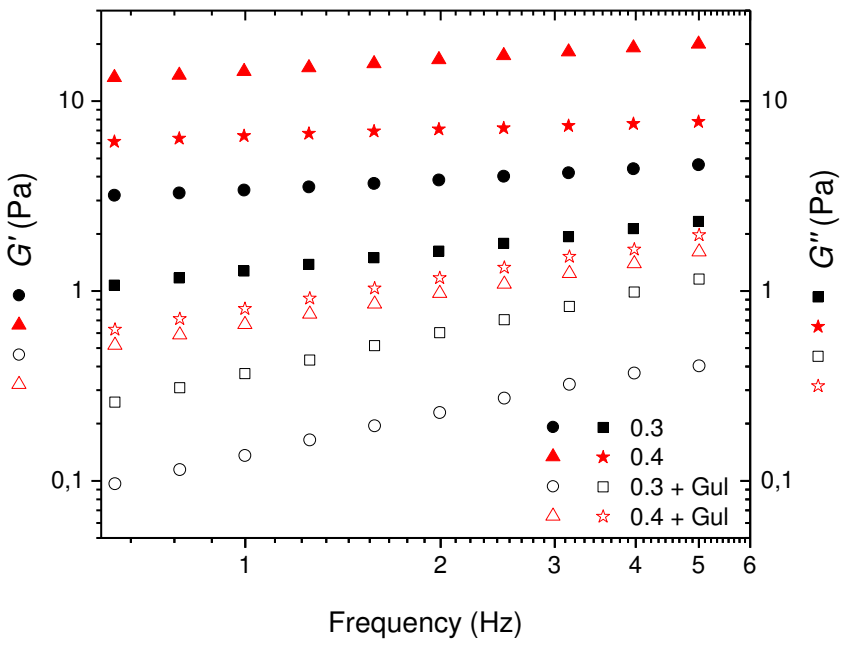

Figure 5.11 *Variation of G' and G'' with frequency for alginate gels ($c_{alginate}$ = 5.3 g L^{-1}) in NaCl (0.05 mol L^{-1}) at R = 0.3 and 0.4 with or without the addition of free G-block (with 20 repeating units), where R = 2[Ca^{2+}]/[COO^-] at 25°C.*

Later, since the high affinity of M-block to calcium chloride was observed via LS (Figure 5.6) and AFM (Table 5.2, Table 5.6), the role of free M-block (X = 18) was also examined. In that case, a new alginate-gel at R = 0.3 was prepared. Then, the obtained gel was divided into 3 vials. One of them was measured directly under rheometer and for two others, free homo-oligoalginate blocks were added (ratio [$GulA_{20}$ or $ManA_{18}$(free)]/[$GulA_{20}$(grafts)]

= 1) under stirring. Figure 5.12 shows that in the presence of free homo-oligoalginate blocks the gel disappeared ($G''>G'$) in both cases. The influence of M-block is higher than G-block (lower values of G' and G'' for alginate-gel with $ManA_{18}$ than with $GulA_{20}$; Figure 5.12), what corresponds to LS data (Figure 5.6). However, observed difference is not very significant.

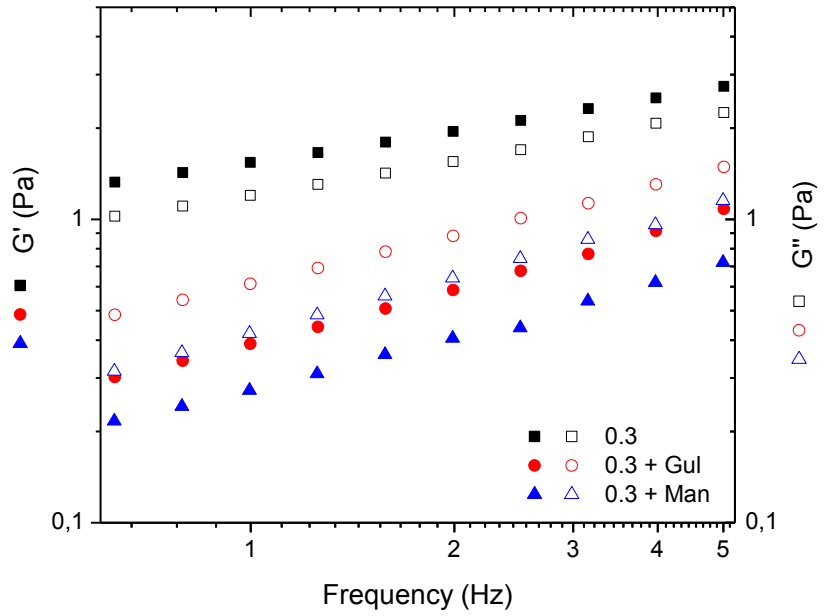

Figure 5.12 *Variation of G' and G'' with frequency for alginate gels ($c_{alginate}$ = 5.3 g L^{-1}) in NaCl (0.05 mol L^{-1}) at R = 0.3 and with the addition of free G-block (with 20 repeating units, X = 20) and free M-block (X = 18) where R = 2[Ca^{2+}]/[COO^-] at 25°C.*

In order to check thixotropic behavior of the gel, the shear stress *vs.* shear rate was measured, first by increasing the shear rate ($\dot{\gamma}$) from 0.0 to 5.0 s^{-1}, and then by immediate decreasing $\dot{\gamma}$ back from 5.0 to 0.0 s^{-1} (Figure 5.13). In the case of alginate-gel at R = 0.3, during measurement performed directly after frequency sweep step, the two curves did not superimpose and defined a small rheological hysteresis loop. However, repeating the experiment resulted in disappearing the loop what indicates that loose interactions do not reform during the delay between two experiments (5 min). G-blocks are known to dissociate the junction zones [27] in contrast to M-blocks, never studied before for this gel control. For this reason, the influence of free M-blocks was investigated under the same conditions as alginate at R = 0.3. In the presence of free M-blocks, the viscosity was lower and no hysteresis was observed. This study confirms that the addition of free M-blocks also dissociates the loose interactions between alginate chains and Ca^{2+} at R = 0.3 and the effect is stable over time at room temperature.

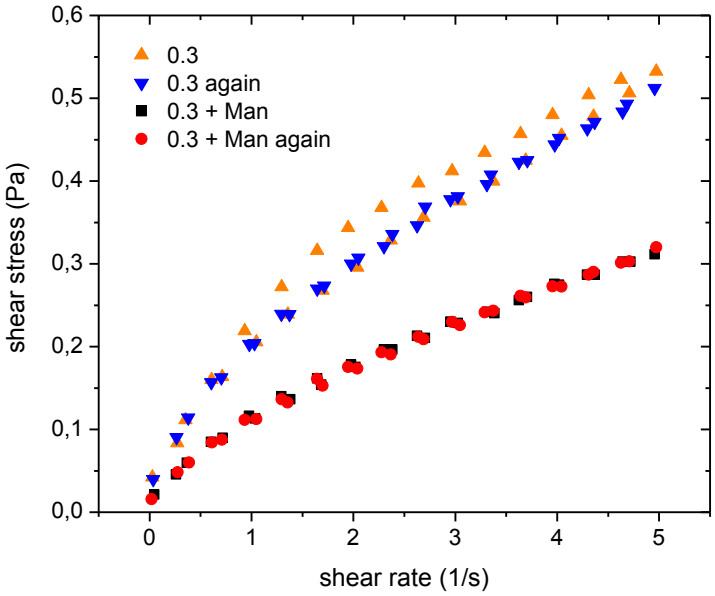

Figure 5.13 *Variation of shear stress with shear rate (increase and decrease) for alginate gels ($c_{alginate}$ = 5.3 g L^{-1}) in NaCl (0.05 mol L^{-1}) at R = 0.3 and with the addition of free M-block (with 18 repeating units, X = 18) measured directly and again (after a first $\dot{\gamma}$ cycle) at 25°C, where R = 2[Ca^{2+}]/[COO^-].*

3.4.3.2. Poly(HEMAm-g-GulA$_{20}$)

- *Sol-gel transition*

Figure 5.14 illustrates changes in the dynamic moduli (G', G'') with frequency (ω) for poly(HEMAm-g-GulA$_{20}$) solutions in NaCl 0.05 mol L^{-1} at varying R values.

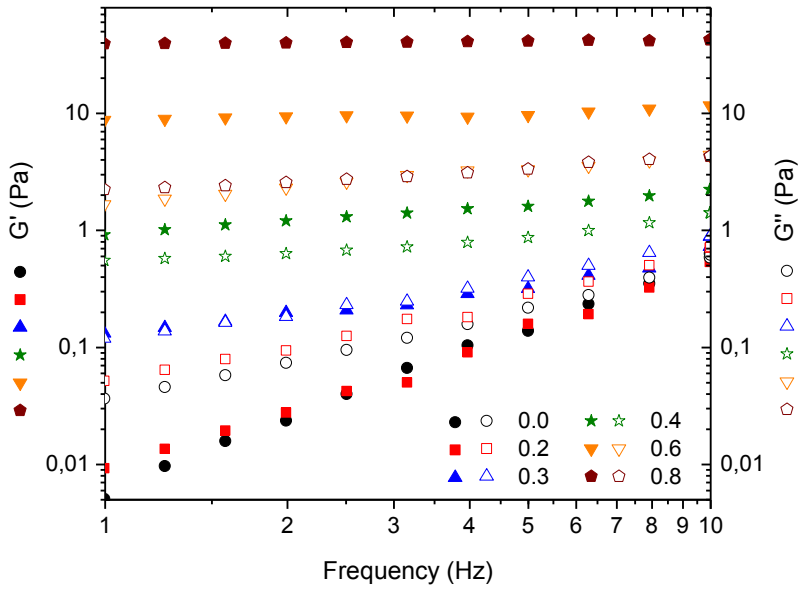

Figure 5.14 *Variation of G' and G'' with frequency for poly(HEMAm-g-GulA$_{20}$) solutions ($c_{polymer}$ = 20.4 g L^{-1}) in NaCl (0.05 mol L^{-1}) at varying R = 2[Ca^{2+}]/[COO^-] at 25°C.*

It can be seen from this graph that the transition from a sol-like to a gel-like state appeared at nearly $R = 0.3$ because at higher R, a gel-like behavior (G' over G'') was observed.

The maximal charge stoichiometric ratio (R_{max}) about 0.8 was estimated from the plot of normalized viscosity and storage modulus G' *vs.* R (Figure 5.15), as in the case of examined alginate (Figure 5.10).

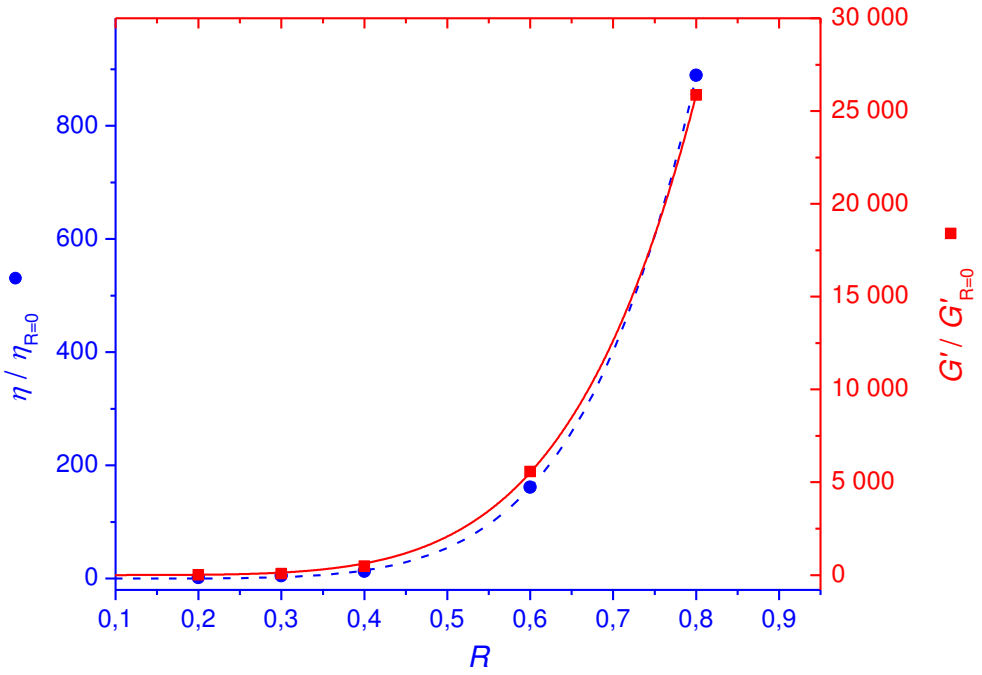

Figure 5.15 *Dependence of normalized viscosity and storage modulus (G') on varying* $R = 2[Ca^{2+}]/[COO^-]$ *for poly(HEMAm-g-GulA$_{20}$) solutions* ($c_{polymer}$ = 20.4 g L^{-1}) *in NaCl (0.05 mol L^{-1}) at 25°C.*

- *Gel properties*

New samples with final polymer concentration = 20.48 g L^{-1} and R = 0.8 were prepared according to the protocol described in paragraph 3.3.4 in order to study the influence of the addition of free chains (*i.e.* $GulA_{20}$, $ManA_{18}$ and $ManA_{300}$ at a ratio [free chains]/[graft chains] of 1). As can be seen from Figure 5.16, the addition of any free chain resulted in decreasing values of the dynamic moduli (G', G''). The effect of free $GulA_{20}$ chains is stronger what is reflected by obtaining lower values. Nevertheless, free mannuronan chains, either $ManA_{18}$ or $ManA_{300}$, also play a significant role in reducing the strength of the gel network. No differences were found between $ManA_{18}$ and $ManA_{300}$ in contrast to the probability of aggregate formation determined via LS measurements performed in dilute solutions (Figure 5.6). It can be related to polymer concentration. In addition, in all samples,

the transition from a gel-like to a sol-like state was not observed (in comparison with alginate studied near the limit of gelation, at R = 0.3, Figure 5.12). Most probably the amount of added homo-oligoalginate was not sufficient to break a strong, self-standing gel at R = 0.8, which was examined in this study.

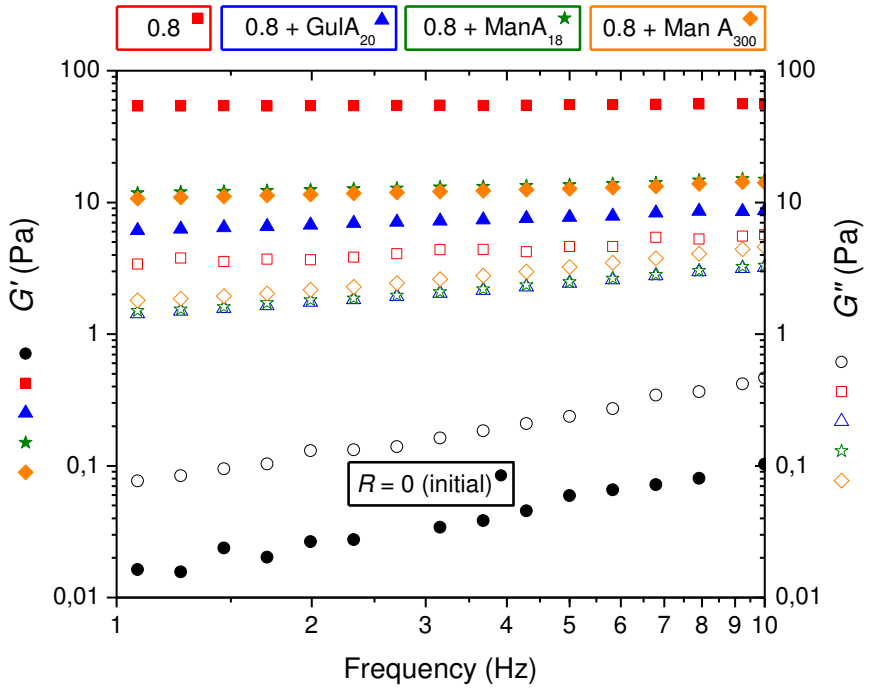

Figure 5.16 *Variation of G' and G'' with frequency for poly(HEMAm-g-GulA$_{20}$) initial solution and gel at R = 0.8 ($c_{polymer}$ = 20.5 g L^{-1}) in NaCl (0.05 mol L^{-1}), where R = 2[Ca^{2+}]/[COO$^-$] at 25°C. Influence of the addition of free G-block (with 20 repeating units, X = 20) and free M-blocks (X = 18, 300), is also shown.*

Furthermore, the thixotropic behavior was examined for samples at R = 0.0, 0.2 (solutions) and R = 0.3 (Figure 5.14, $G' = G''$ (ω), transition from a sol-like to a gel-like state) according to the procedure used for alginate solutions (paragraph 3.4.3.1). At the initial state (R = 0.0), up and down curves are almost superimposed (Figure 5.17), thus no thixotropic structures existed. By contrast, at R = 0.2 a very small hysteresis loop was observed, whereas at R = 0.3, the shape of the up curve has changed significantly. The appearance of the hysteresis is attributed to the loose interchain interactions in the presence of Ca^{2+}, corresponding to starting point of gelation (compare with Figure 5.14).

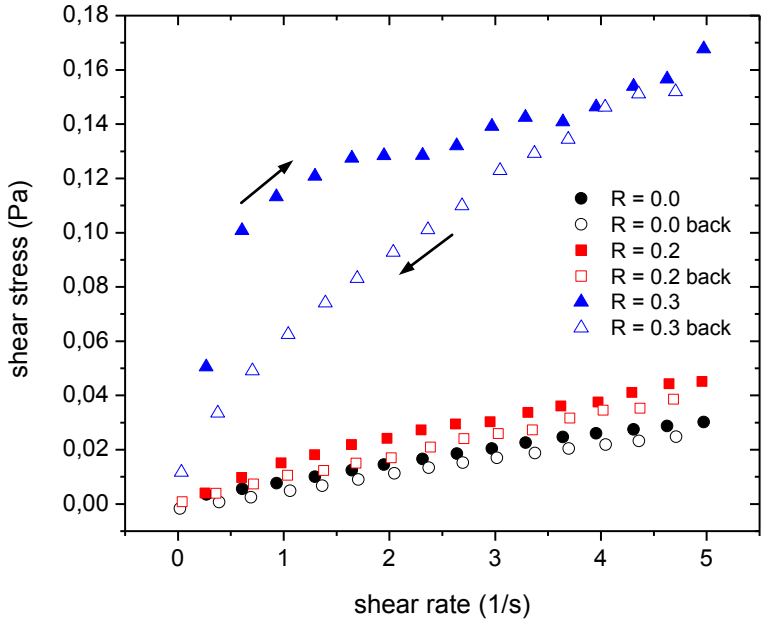

Figure 5.17 *Variation of shear stress with shear rate for poly(HEMAm-g-GulA$_{20}$) solutions ($c_{polymer}$ = 20.4 g L^{-1}) in NaCl (0.05 mol L^{-1}) at R = 0.0, 0.2 and 0.3 measured at 25°C, where R = 2[Ca^{2+}]/[COO$^-$].*

3.4.3.3. Poly(HEMAm-g-GulA$_{10}$)

- *Sol-gel transition*

A progressive formation of association has been already studied for this polymer by LS in dilute solutions either in NaCl solution or DI water (Figure 5.8). Those studies revealed loose association in the presence of NaCl in contrast to DI water, where larger aggregates were formed. The rheological analysis was performed both in NaCl and in DI water. As can be seen from Figure 5.18, the transition from a sol-like to a gel-like state in the presence of NaCl appears at nearly R = 0.8. In the case of water environment (Figure 5.19), sample at R = 0.8 reveals still a sol-like behavior (G'' over G'), whereas sample at R = 0.9 features definitely a gel-like behavior (G' over G''), thus starting point for cross-linked domains must be at 0.8 < R < 0.9.

In addition, the maximal charge stoichiometric ratio (R_{max}) equals to about 0.9 for both NaCl and water environment was estimated from the plot of normalized viscosity and storage modulus (G') *vs.* R (Figure 5.20). This result is correlated with R_{max} = 0.8 found for poly(HEMAm-g-GulA$_{20}$).

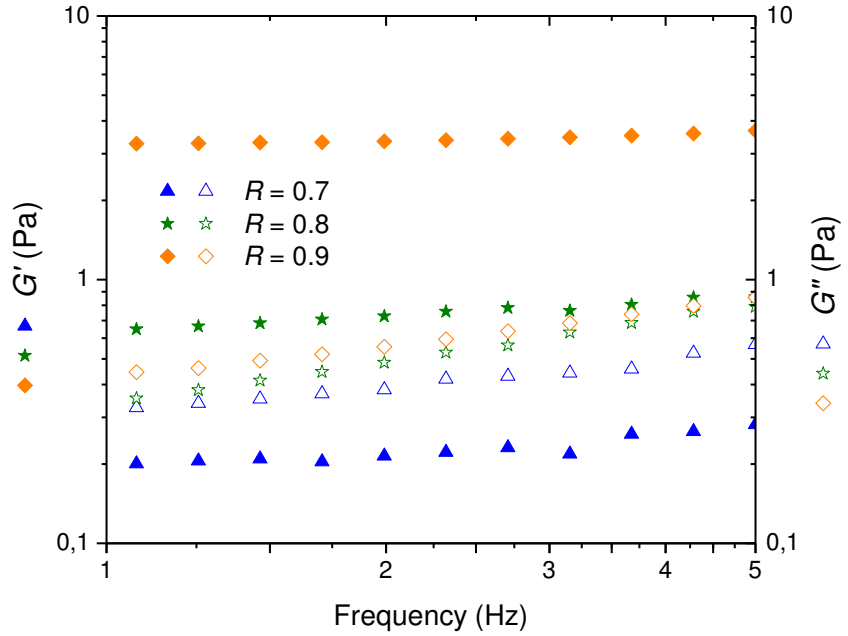

Figure 5.18 *Variation of G' and G'' with frequency for poly(HEMAm-g-GulA$_{10}$) solutions ($c_{polymer} \approx 20.0$ g L^{-1}) in NaCl (0.05 mol L^{-1}) at varying R = 2[Ca^{2+}]/[COO$^-$] at 25°C.*

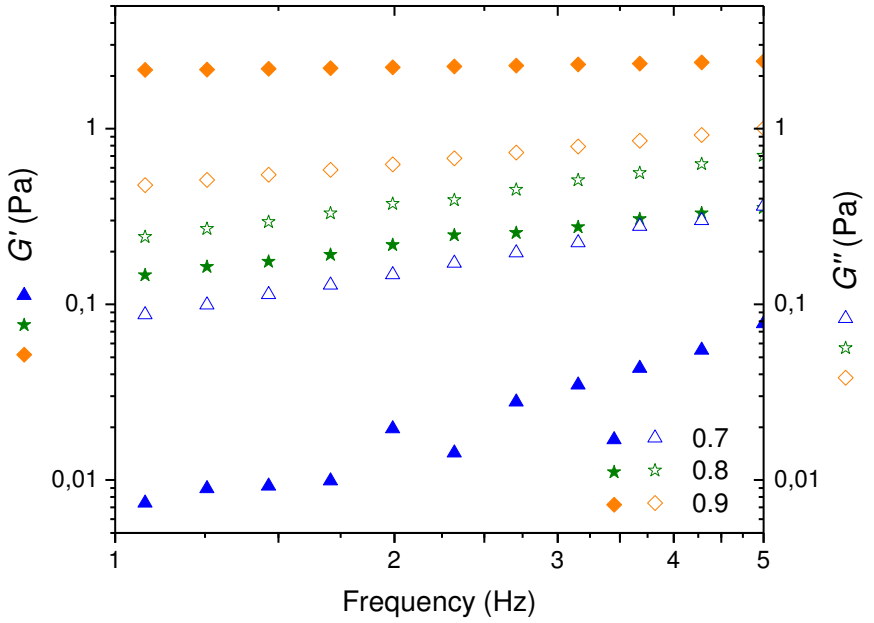

Figure 5.19 *Variation of G' and G'' with frequency for poly(HEMAm-g-GulA$_{10}$) solutions ($c_{polymer} \approx 20.0$ g L^{-1}) in DI water at varying R = 2[Ca^{2+}]/[COO$^-$] at 25°C.*

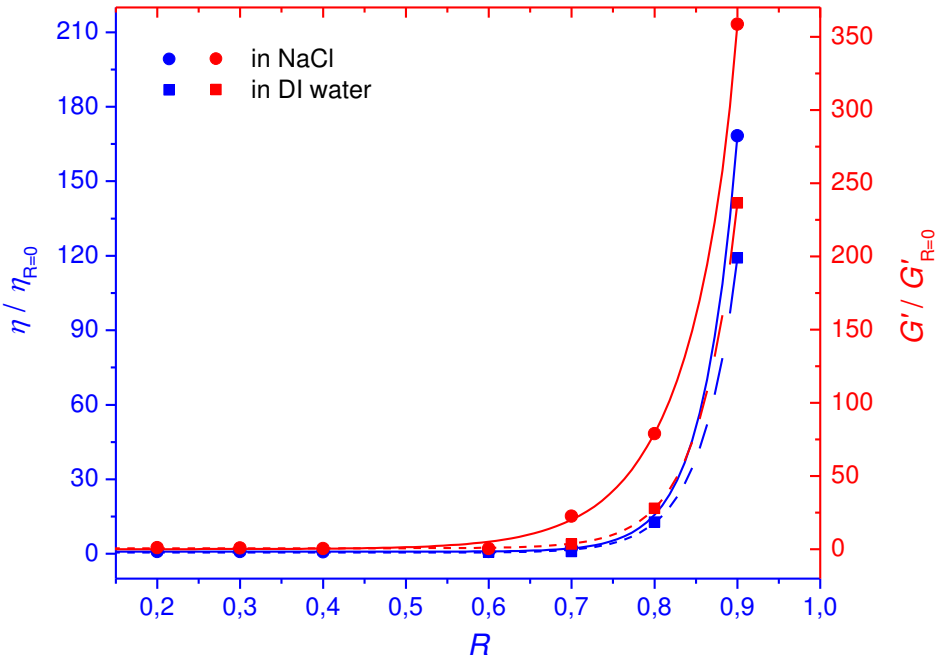

Figure 5.20 *Dependence of normalized viscosity and storage modulus (G') on varying $R = 2[Ca^{2+}]/[COO^-]$ for poly(HEMAm-g-GulA$_{10}$) solutions ($c_{polymer} \approx 20.0$ g L^{-1}) in NaCl (0.05 mol L^{-1}) or DI water at 25°C. Values of G' and η were taken at 3.2 Hz and 5 s^{-1}, respectively.*

In order to compare the degree of crosslinking (reflected by storage modulus - *G'*) for different neo-alginates, experimental results obtained at the same *R* value are given in Table 5.9. It is interesting to point out that at the same polymer concentration in g L^{-1}, neo-alginate with grafted G-blocks having 20 repeating units gives stronger gel than that with 10 repeating units, even if polymer with $X = 10$ contains more guluronic units (ratio 1.4). In addition, in the presence of water the modulus is lower, probably due to interchain electrostatic repulsions.

Table 5.9 *Storage moduli (G') taken at 1 Hz, for neo-alginate gels obtained at R = 0.8.*

	poly(HEMAm-g-GulA$_{20}$)	***poly(HEMAm-g-GulA$_{10}$)***	***poly(HEMAm-g-GulA$_{10}$)***
G' (Pa)	40.4	0.65	0.15
solvent	NaCl	NaCl	DI water
$F_{m,\,GulA}$ (%)	28	42.6	42.6

Note: F_m is the weight fraction of guluronan in polymer.

3.4.4. Gelation by dialysis against an excess of $CaCl_2$

The statement that alginates form hydrogels under addition of calcium ions in aqueous solution has been already mentioned many times. Therefore, the main objective of the study described below was to verify if the designed neo-alginate, *i.e.* poly(HEMAm-g-$GulA_{20}$) containing oligo(1→4)-α-L-guluronan grafted chains with 20 repeating units ($F_{m,\,GulA}$ = 28%, Table 5.8), could mimic the gelation behavior of alginates. On that purpose, the gelation method of dialysis against an excess of $CaCl_2$ was used. However, in order to make a comparison, gels of both poly(HEMAm-*g*-$GulA_{20}$) and alginate were prepared in the same way (for more details see paragraph 3.3.4.4).

As shown in Figure 5.21, alginate as well as poly(HEMAm-*g*-$GulA_{20}$) formed self-standing and transparent hydrogels but a neo-alginate gel looked more homogeneous.

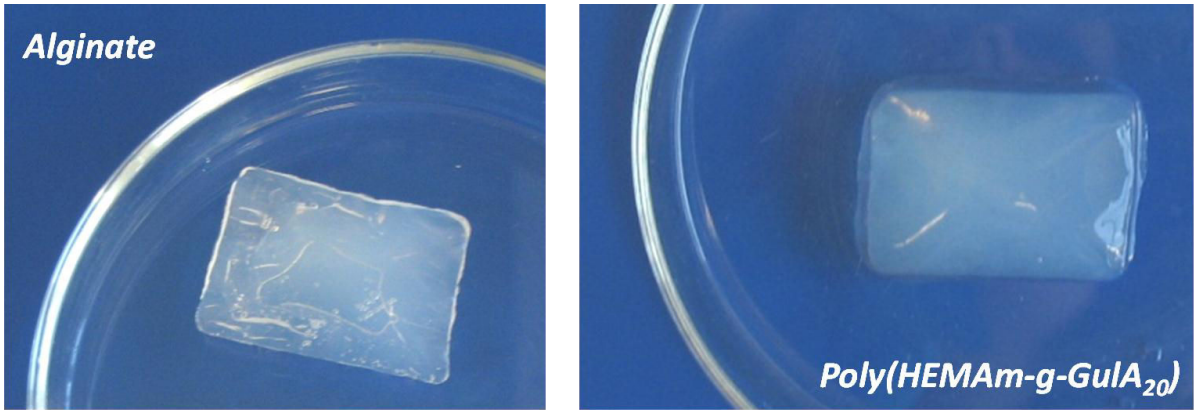

Figure 5.21 *Gels obtained after dialyzing alginate ($c_{alginate}$ = 12.5 g L^{-1}) and neo-alginate ($c_{polymer}$ = 20.0 g L^{-1}) solutions in NaCl (0.05 mol L^{-1}) against $CaCl_2$ at 0.5 mol L^{-1}.*

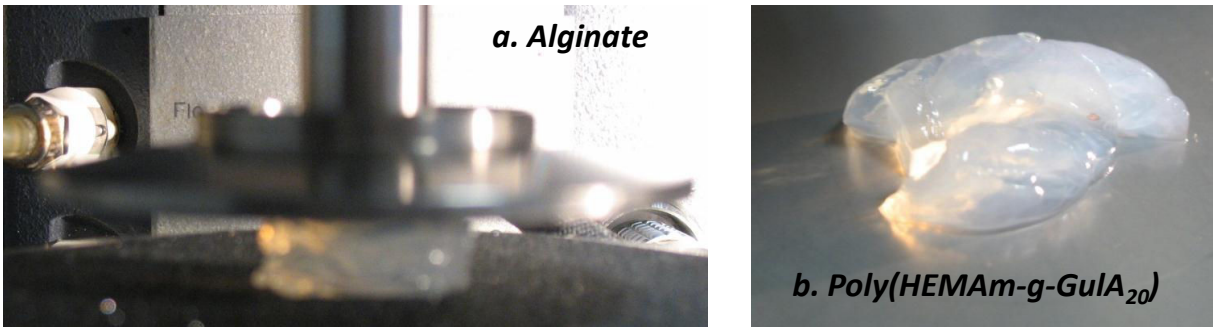

Figure 5.22 *A compression experiment. An alginate gel disk during squeezing by a rheometer (a) and squeezed neo-alginate gel disk after compression experiment (b).*

Furthermore, in order to investigate the stiffness of gels, disks of diameter ≈ 2 cm were punched out from obtained materials and compression experiments were performed. Thus, in separate experiments, a gel disk of known surface area S ($\pi \cdot r^2$) was first placed between two parallel plates of the rheometer (Figure 5.22a). Then, the rheometer started squeezing the gel slowly and exerted backward force was registered (see the Appendix, Figure 5A.7 and Figure 5A.8).

Ali Ghadban in his PhD thesis [28] performed similar experiments for poly(HEMAm-g-GulA$_{20}$) neo-alginate hydrogel with higher weight fraction of guluronan ($F_{m,\ GulA}$ = 44%, Table 5.10) and calculated the elastic modulus *E* from the slope of the tangent at the origin of the curve *F vs.* $|\Delta y|/y_0$ according to the following equation:

$$E = (\tan|\Delta y|/y_0)/S \qquad \text{(Eq. 5.12)}$$

Thus, the same method was applied for the hydrogels obtained in those studies. Some results are reported in Table 5.10, whereas the detailed characteristic is given in the Appendix (Table 5A.4). One of the most significant findings to emerge from this study is that the strength of the gel is related to the content of guluronan blocks, *i.e.* the higher this content is, the stronger gel is obtained.

Table 5.10 *Characteristics of alginate and neo-alginate hydrogels.*

	poly(HEMAm-g-GulA$_{20}$)	***poly(HEMAm-g-GulA$_{20}$) Ghadban et al.*** [13]	***Alginate SG150***
$F_{m,\ GulA}$ (%)	**28**	**44**	**81**
solvent	NaCl	DI water	NaCl
E (Pa)	**1180**	**5410**	**18650**
G' (Pa)	**240**	**1770**	**11250**

Note: F_m is the weight fraction of guluronan in polymer, E is the elastic modulus and G' is the storage modulus (taken at 1 Hz).

In addition, oscillatory experiments were performed and the results are shown in Figure 5.23. In both cases, *G'* and *G"* were independent of frequency, what confirms obtaining hydrogels. The values of *G'* were 47 times higher for alginate-gel (even at lower polymer concentration) than for poly(HEMAm-*g*-GulA$_{20}$)-gel what must be related to higher content of guluronan (81% for alginate and 28% for polymer by mass). However, it is worth noting that this difference is also attributed to the way in which guluronan units are incorporated into the material. In the case of alginate, G-units are in the main chain that leads to larger stiffness

of the chain and finally stronger gel. From Figure 5.21, poly(HEMAm-*g*-GulA$_{20}$)-gel looks more homogeneous, but oscillatory experiment (Figure 5.23) confirmed that it is softer, what is also contributed in part to the fact that G-units are incorporated into pendant chains.

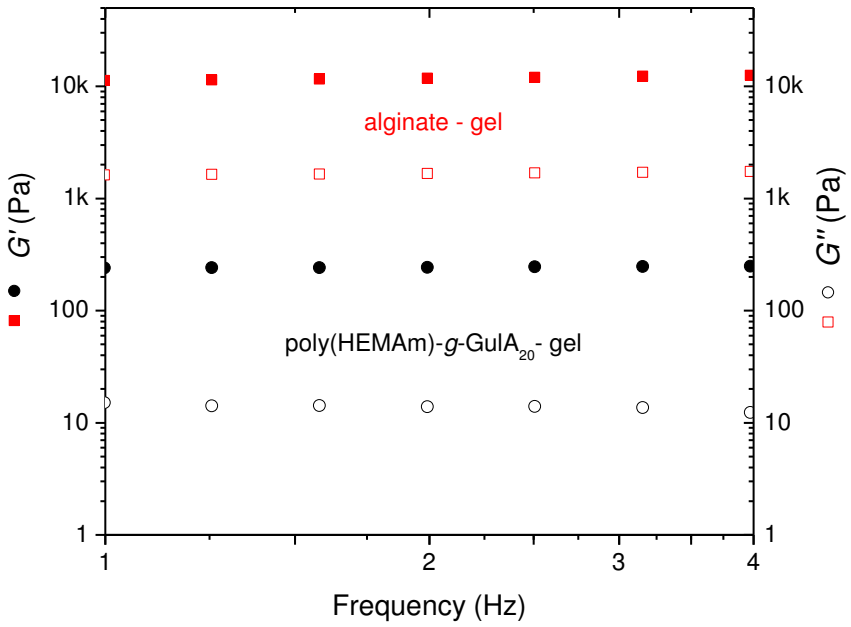

Figure 5.23 *Variation of G' and G'' with frequency at 25°C for the hydrogels obtained from alginate solution at 12.5 g L^{-1} (squares) and neo-alginate solution at 20.0 g L^{-1} (circles) prepared in NaCl (0.05 mol L^{-1}).*

3.5. Conclusion

The transition from a sol-like to a gel-like state was determined on the basis of rapid increase of monitored properties observed via LS and rheology during controlled changes in the charge stoichiometric ratio (R = 2[Ca^{2+}]/[COO^{-}]).

It has been found via LS that the threshold of aggregate formation in alginate, homo-oligoalginate and neo-alginate solutions depends on the concentration of the sample (the higher the concentration is, the faster aggregation occurs), the structure (*i.e.* degree of polymerization (X) and configuration of the uronic acids: Gul or Man) and the composition of the solvent (water or salt screening the electrostatic repulsions). Furthermore, detailed studies of homo-oligoalginates revealed that lower X together with NaCl environment favors aggregation in the presence of calcium ions. Nevertheless, very high affinity of oligomannuronan (ManA$_{10}$ and ManA$_{18}$) to Ca^{2+} observed in dilute solutions is an original result.

In addition, investigations performed in semi-dilute solutions via rheology have also enabled to observe a sol-gel transition, thus a progressive network formation being stabilized by junction zones including calcium ions. However, rheological studies were mainly designed to investigate the gelling ability of two biohybrid polymers featuring (1→4)-α-L-guluronan sequences (X = 10 or 20) as side chains. It was shown that both of them undergo gelation but neo-alginate with $GulA_{20}$ as side chains gives stronger gel (even at lower content of guluronan units). For instance, a self-standing gel of poly(HEMAm-g-$GulA_{20}$) was obtained at R = 0.8 ($c_{polymer}$ = 20.0 g L^{-1}, c_{CaCl_2}= 0.05 mol L^{-1}) but also by dialysis against an excess of $CaCl_2$ ($c_{polymer}$ = 20.0 g L^{-1}, c_{CaCl_2}= 0.5 mol L^{-1}). Further, the gel obtained by dialysis was compared with alginate-Ca^{2+} gel, prepared under the same experimental conditions. Rheological studies have shown that the strength of the gel depends on the content of guluronan blocks (the higher the content is, the stronger gel is formed) but also on the way in which guluronan units are incorporated into the material, *i.e.* in the backbone (as in alginate) or as side chains (as in the neo-alginates). Since alginate sample was richer in guluronan (81%) and guluronan units were including in the main chain, thus the alginate hydrogel was stronger and stiffer. This may be also attributed to larger degree of aggregation of junction zones in this system than in neo-alginate samples, where the probability of association between G-blocks is lower.

However, the most obvious finding to emerge from this study is that the addition of free G- or M-blocks to the preformed gel obtained from alginate or alginate-derived polymer reduces the gel strength, thus also the aggregation in junction zones, which may play a role in modifying the strength of the gel network.

4. Conclusion

Taken together, these results suggest that Atomic Force Spectroscopy (AFS), Light Scattering (LS) and rheology are techniques which may be applied for studying the interactions or association of alginate-derived polymers in the presence of calcium ions.

In addition, LS and rheology are also suitable for studying the transition from a sol-like to a gel-like state of alginate-derived polymers during progressive addition of $CaCl_2$, for which the application of a pseudo-percolation model was proposed. A general remark is that in the sodium chloride environment, the critical charge stoichiometric ratio (R_c) is higher in dilute solutions (for LS) than R_{max} estimated from rheological experiments what is in agreement with data from literature (on alginates by Wang [17,18] and pectins by Thibault [21]).

Complexation occurring between (1→4)-α-L-guluronan sequences and calcium ions was not surprising at all because it has been already examined in depth by many authors. Nevertheless, the large affinity of M-blocks to Ca^{2+} observed several times in present studies provides a new understanding of the role of M-blocks in the formation of the junction zones together with their ability to form aggregates in dilute solutions. The originality of presented results is mainly related to this phenomenon but also the role of M-blocks on the network disruption (having nearly the same efficiency as G-blocks).

5. Appendix

Table 5A.1 *Statistics of the average difference in cantilever deflection* $\langle \Delta z_c \rangle$ *(average values with standard deviation).*

Experiment code	*Solution*	*Sweep duration (s)*	$\langle \Delta z_c \rangle$ *(nm)*	σ *(nm)*
AW-12-01-**$ManA_{18}$**	water (DI)	6	5.2	1.7
	$CaCl_2$ in DI (0.01 M L^{-1})	6	9.8	3.9
AW-12-01-**$GulA_{20}$**	water (DI)	6	1.4	0.9
	$CaCl_2$ in DI (0.01 M L^{-1})	6	5.3	4.5
AW-12-01-**$GulA_{20}$**	water (DI)	100	2.5	1.2
	$CaCl_2$ in DI (0.01 M L^{-1})	100	6.0	1.5

Table 5A.2 *Statistics of the average difference in cantilever deflection* $\langle \Delta z_c \rangle$ *(average values with standard deviation).*

Experiment code	*Solution*	$\langle \Delta z_c \rangle$ *(nm)*	σ *(nm)*
AW-12-06-**$ManA_{18}$**	NaOH at 10^{-6} M L^{-1}	3.1	0.6
	$CaCl_2$ in DI (0.10 M L^{-1})	3.4	1.2
AW-12-06-**$GulA_{20}$**	NaOH at 10^{-6} M L^{-1}	3.5	1.9
	$CaCl_2$ in DI (0.10 M L^{-1})	8.0	2.5

Table 5A.3 *Statistics of the average difference in cantilever deflection* $\langle \Delta z_c \rangle$ *(average values with standard deviation).*

Experiment code	*Solution*	$\langle \Delta z_c \rangle$ *(nm)*	σ *(nm)*
AW-12-09-**$ManA_{18}$(tip)-$ManA_{18}$(wafer)**	DI water	19.5	11.1
	$CaCl_2$ in DI (0.01 M L^{-1})	23.5	11.8
	NaCl in DI (0.02 M L^{-1})	13.0	3.8
AW-12-09-**$ManA_{18}$(tip)-$GulA_{20}$(wafer)**	DI water	17.7	11.0
	$CaCl_2$ in DI (0.01 M L^{-1})	23.5	10.6
	NaCl in DI (0.02 M L^{-1})	27.0	16.0
AW-12-09-**$GulA_{20}$(tip)- $ManA_{18}$(wafer)**	DI water	60.3	18.2
	$CaCl_2$ in DI (0.01 M L^{-1})	65.4	16.3
	NaCl in DI (0.02 M L^{-1})	7.5	5.9
AW-12-09-**$GulA_{20}$(tip)-$GulA_{20}$(wafer)**	DI water	9.9	5.2
	$CaCl_2$ in DI (0.01 M L^{-1})	16.2	5.6
	NaCl in DI (0.02 M L^{-1})	3.7	4.7

Another way of analyzing the data obtained from force measurements is plotting histograms of determined adhesion forces, followed by fitting the results to Gaussian peak. In that case, the average adhesion force is equal to the peak position. An exemplary graph is shown in Figure 5A.1.

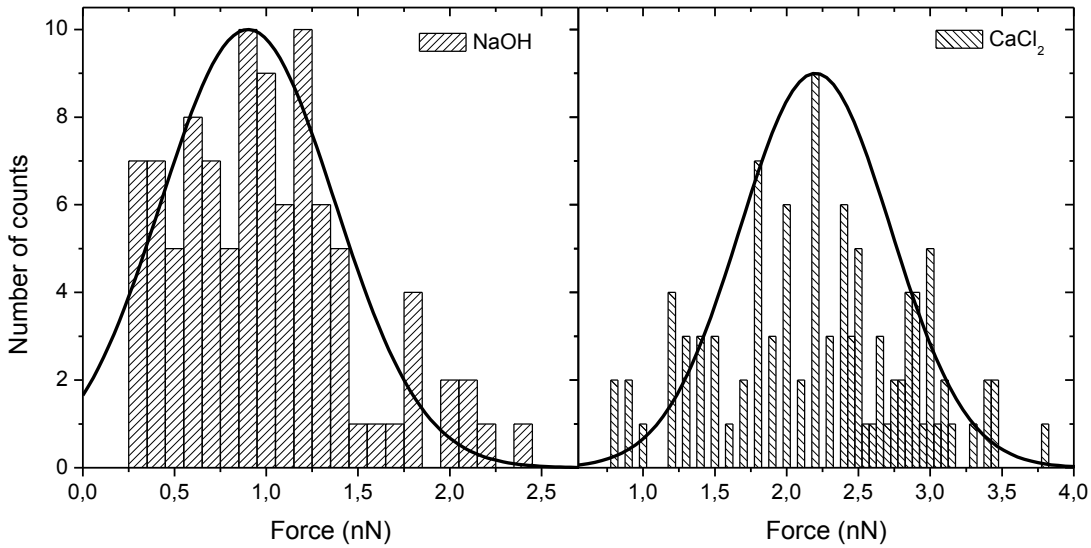

Figure 5A.1 *Histograms of adhesion forces determined for (1→4)-α-L-guluronan (X = 20, $GulA_{20}$) oligomers grafted to gold surfaces (tip and wafer) in the presence of NaOH solution at 10^{-6} M L^{-1} (pH ≅ 8.4) and $CaCl_2$ (pH = 9.0). The solid lines represent Gaussian curves fitted to the histograms.*

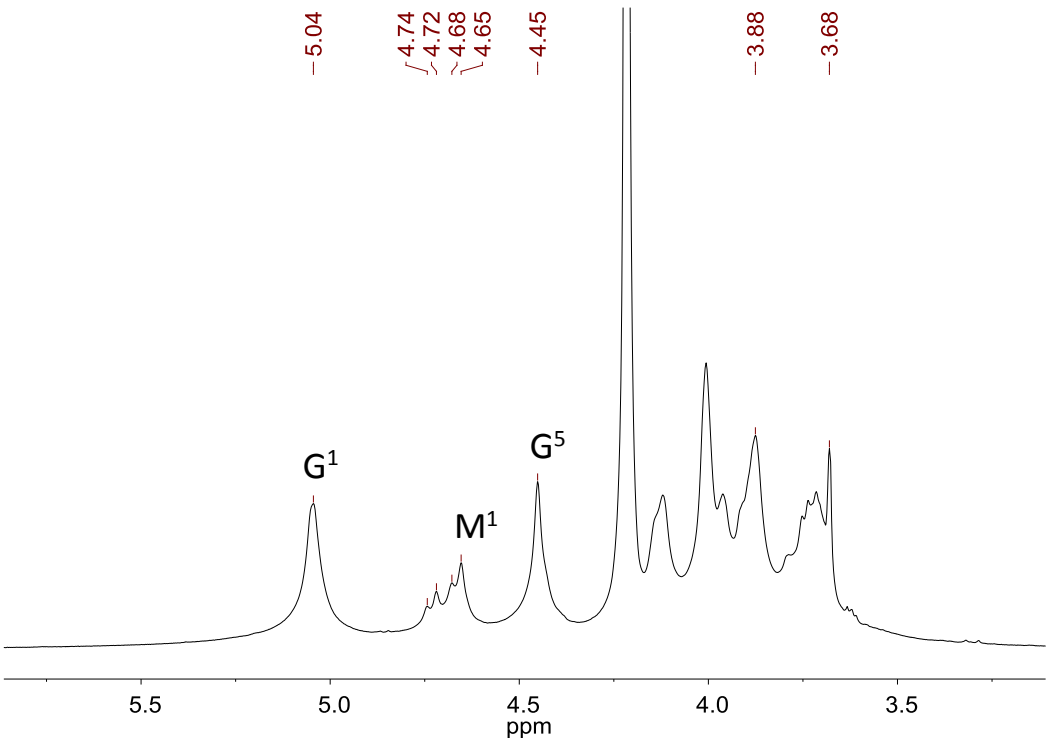

Figure 5A.2 *^1H NMR spectrum of alginate SG150 dialyzed. Conditions: 400 MHz, D_2O, 1.2 % w/w, 353K, number of scans (ns) = 256.*

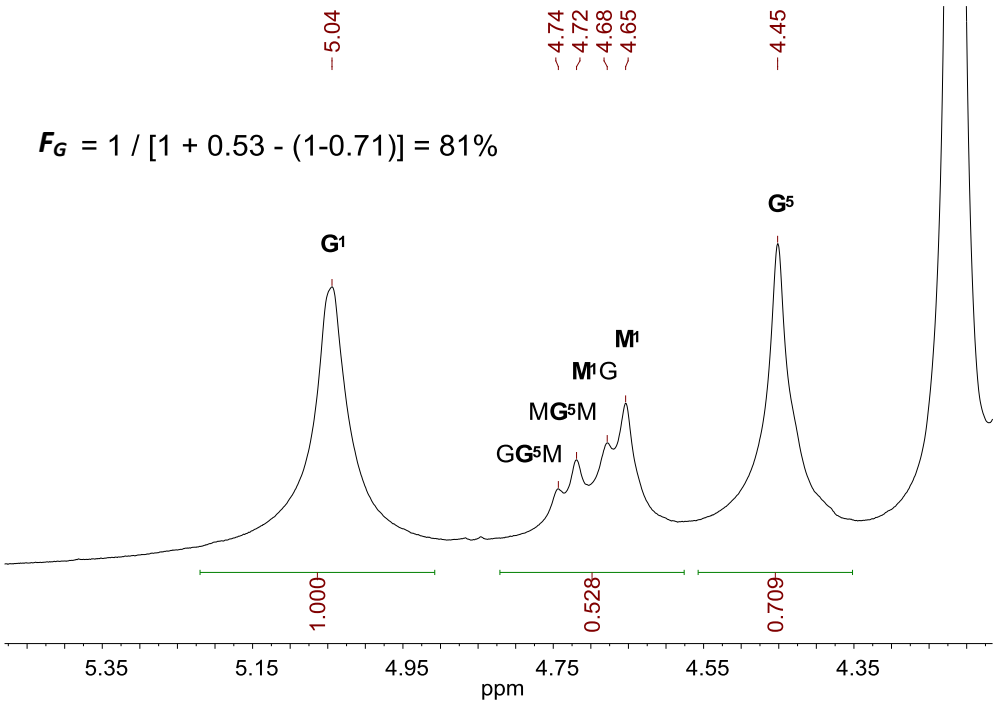

Figure 5A.3 *Low-field region of the ^1H NMR spectrum of alginate SG150 dialyzed. Conditions: 400 MHz, D_2O, 1.2 % w/w, 353K, number of scans (ns) = 256. F_G was determined on the basis of assigned peaks.*

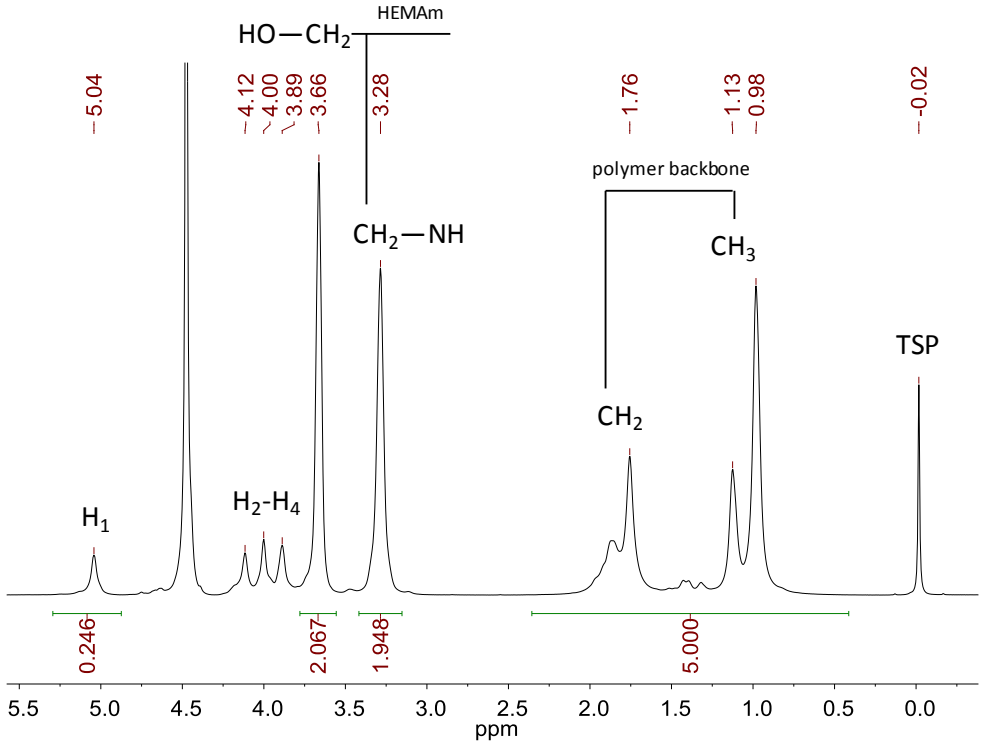

Figure 5A.4 *^1H NMR spectrum of poly(HEMAm-g-GulA_{20}). Conditions: 400 MHz, D_2O, 2 % w/w, 328K, number of scans (ns) = 128.*

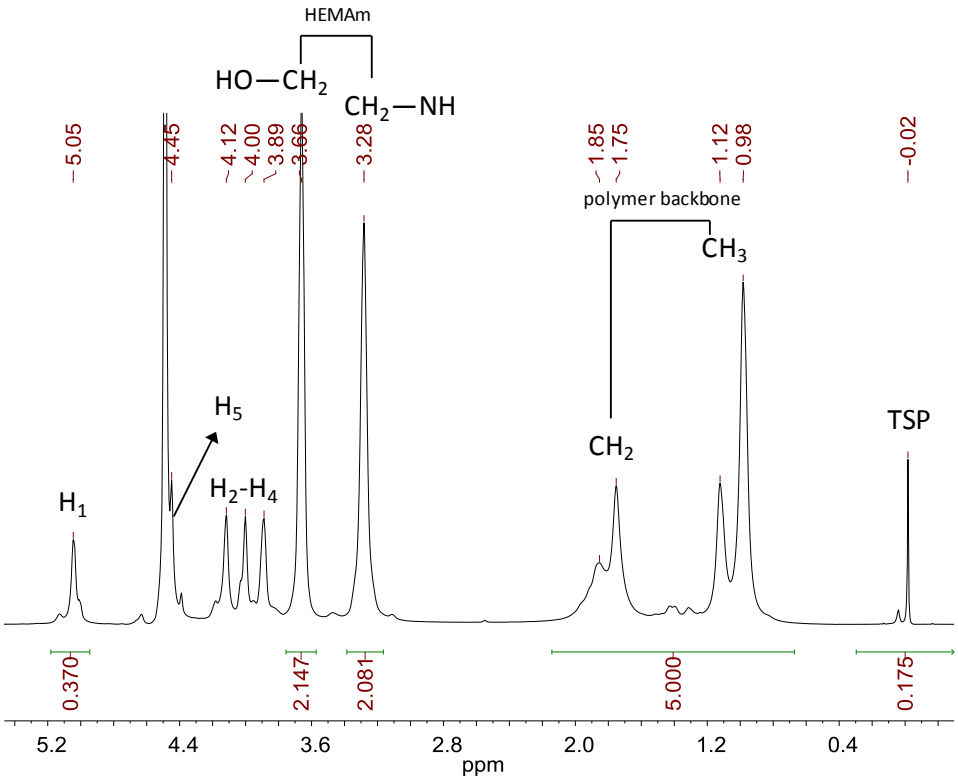

Figure 5A.5 *^{1}H NMR spectrum of poly(HEMAm-g-GulA$_{10}$). Conditions: 400 MHz, D_2O, 2 % w/w, 328K, number of scans (ns) = 128.*

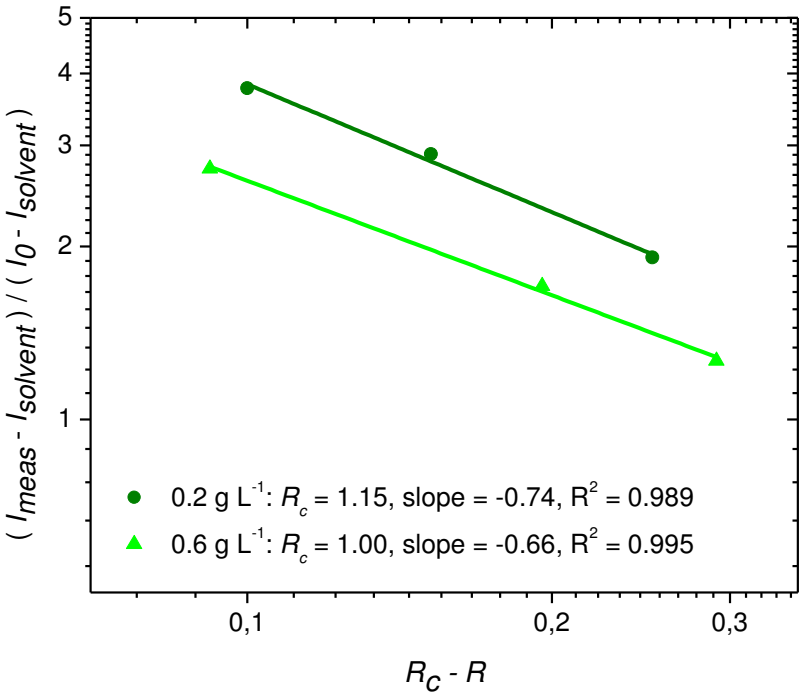

Figure 5A.6 *Determining the critical charge stoichiometric ratio (R_c) for alginate SG150 dialyzed samples from LS measurements on the basis of linear fitting method proposed by Thibault et al.* [21]

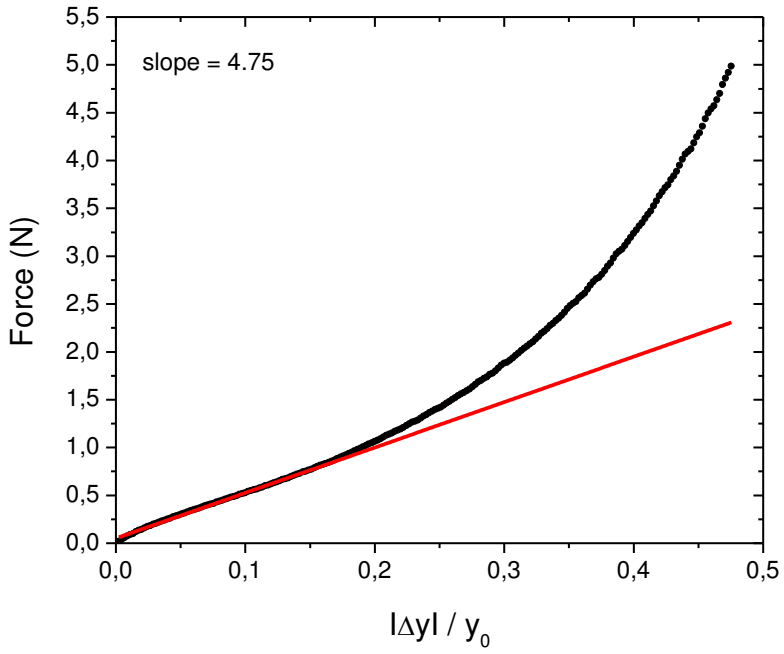

Figure 5A.7 *Variation of the force applied by the gel of alginate ($c_{alginate}$ = 12.5 g L^{-1}) in NaCl (0.05 M L^{-1}) under compression.*

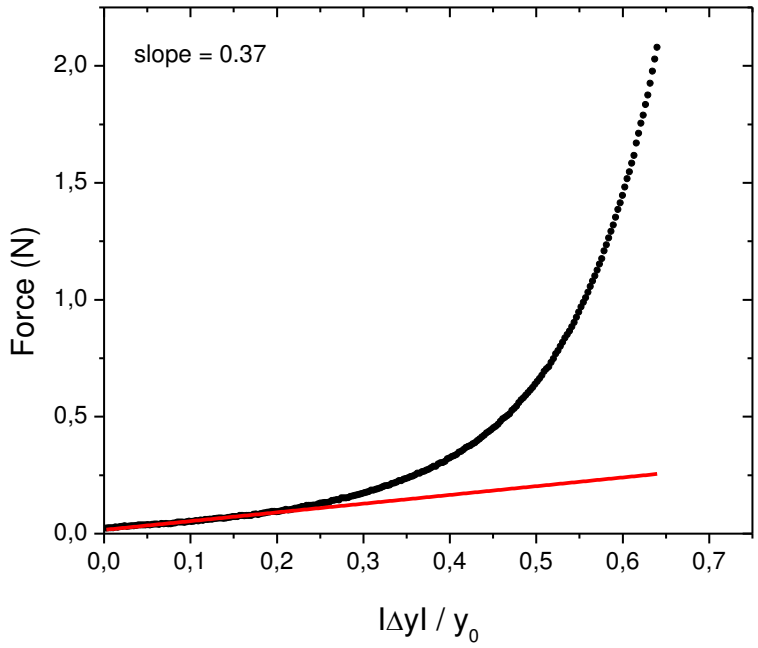

Figure 5A.8 *Variation of the force applied by the gel of poly(HEMAm-g-$GulA_{20}$) ($c_{polymer}$ = 20.0 g L^{-1}) in NaCl (0.05 M L^{-1}) under compression.*

Table 5A.4 *Detailed characteristics of alginate and neo-alginate hydrogels.*

	Alginate SG150	***poly(HEMAm-g-GulA$_{20}$)***	***poly(HEMAm-g-GulA$_{20}$) Ghadban et al.*** [13]
$F_{m,\,GulA}$ (%)	81	28	44
solvent	NaCl	NaCl	DI water
$c_{polymer}$ ($g\ L^{-1}$)	12.5	20	18
c_{CaCl_2} ($M\ L^{-1}$)	0.5	0.5	0.5
r (m)	0.009	0.01	0.01
S	2.54 E-4	3.14 E-4	3.14 E-4
$tan\lvert\Delta y\rvert/y_0$	4.75	0.37	1.7
E (Pa)	18650	1180	5410
G' (Pa)	11250	240	1770

Note: F_m is the weight fraction of guluronan in polymer, r is the radius of a gel disk, S is the surface of a gel disk, $tan\lvert\Delta y\rvert/y_0$ is the tangent at the origin of the curve F vs. $\lvert\Delta y\rvert/y_0$, E is the elastic modulus and G' is the storage modulus (taken at 1 Hz).

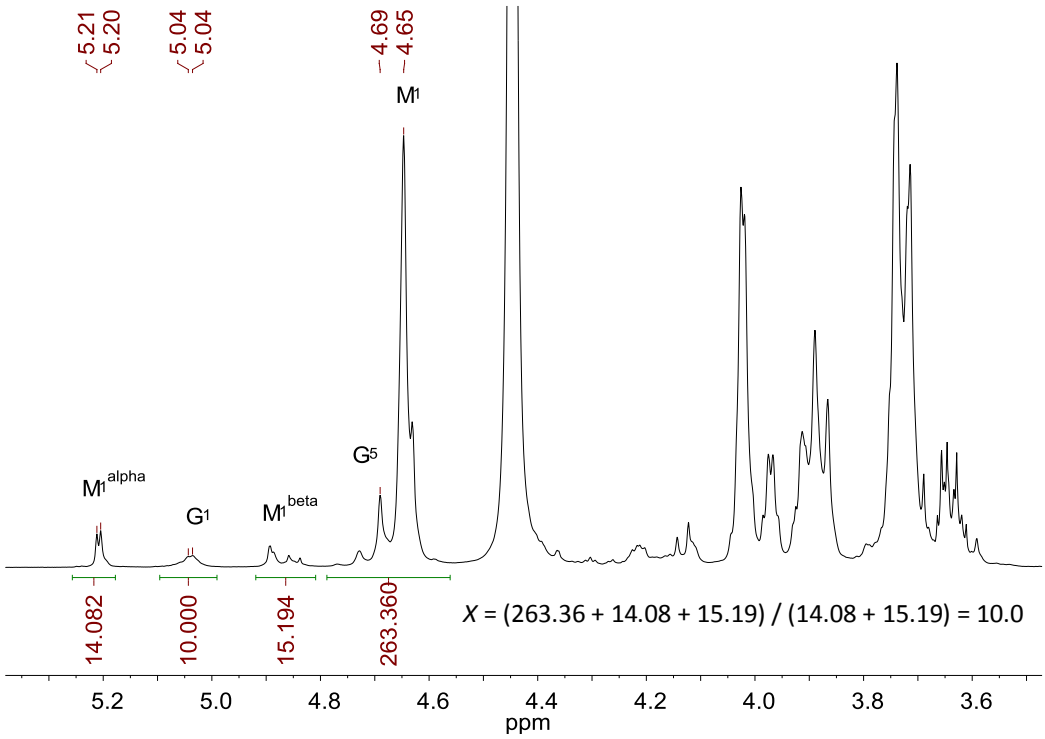

Figure 5A.9 *^{1}H NMR spectrum of (1→4)-β-D-mannuronan (X=10). Conditions: 400 MHz, D_2O, 5 % w/w, 328K, number of scans (ns) = 128.*

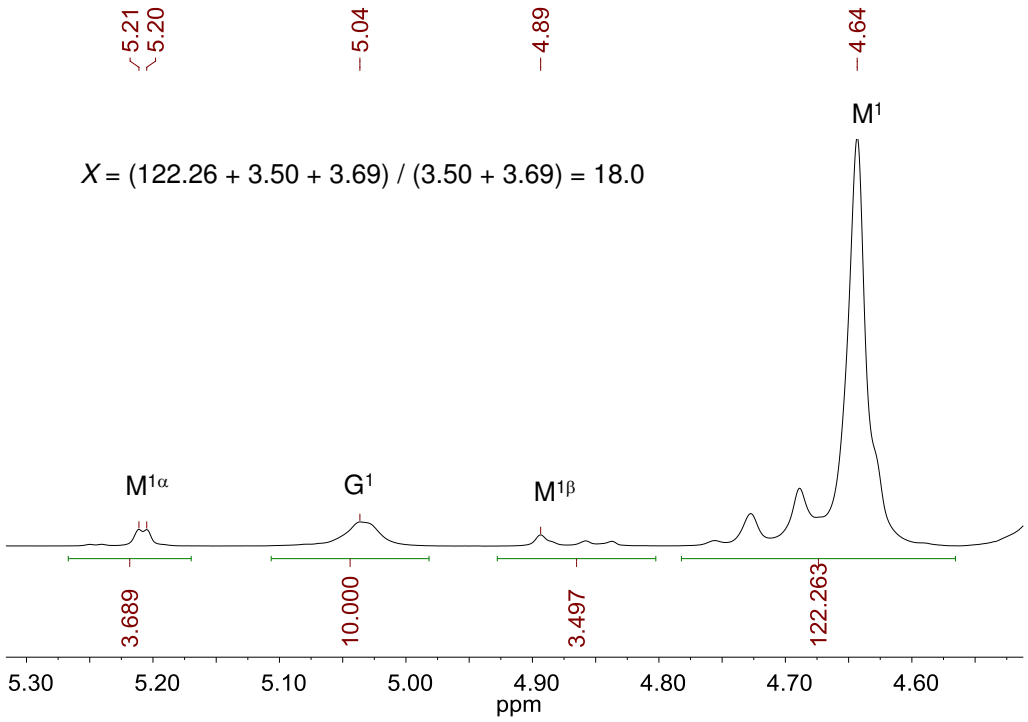

Figure 5A.10 *^{1}H NMR spectrum of (1→4)-β-D-mannuronan (X=18). Conditions: 400 MHz, D_2O, 2 % w/w, 328K, number of scans (ns) = 128.*

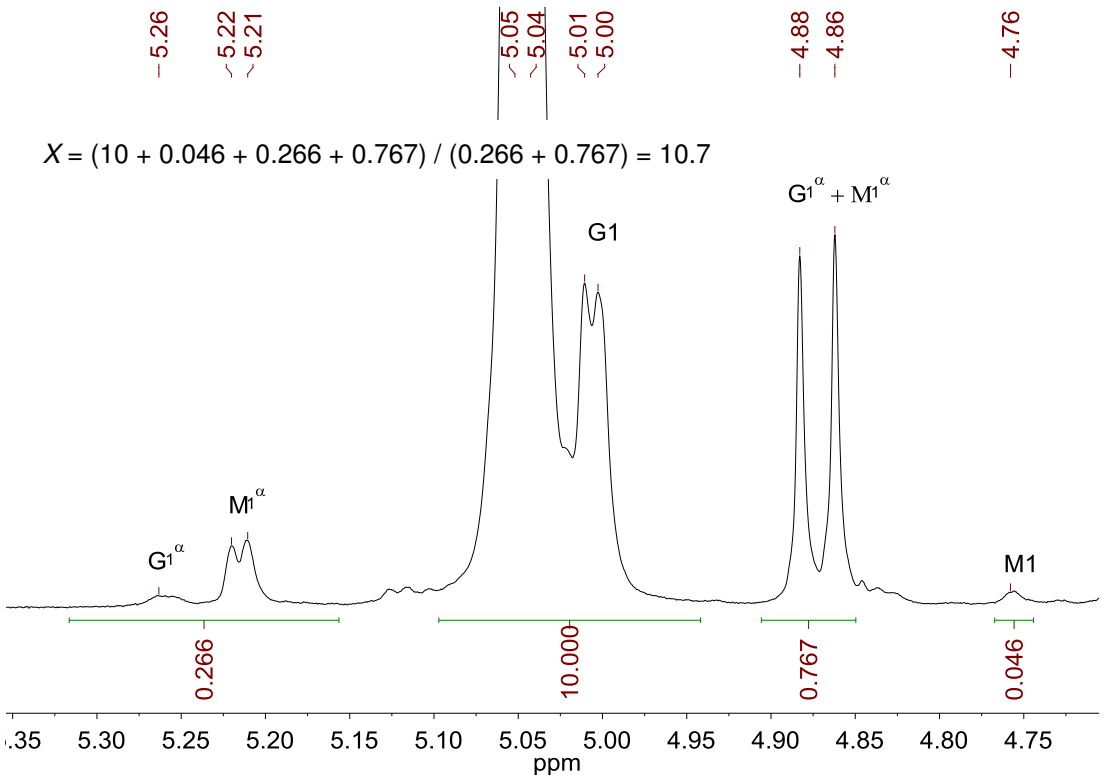

Figure 5A.11 *^{1}H NMR spectrum of (1→4)-α-L-guluronan (X=10). Conditions: 400 MHz, D_2O, 5 % w/w, 328K, number of scans (ns) = 128.*

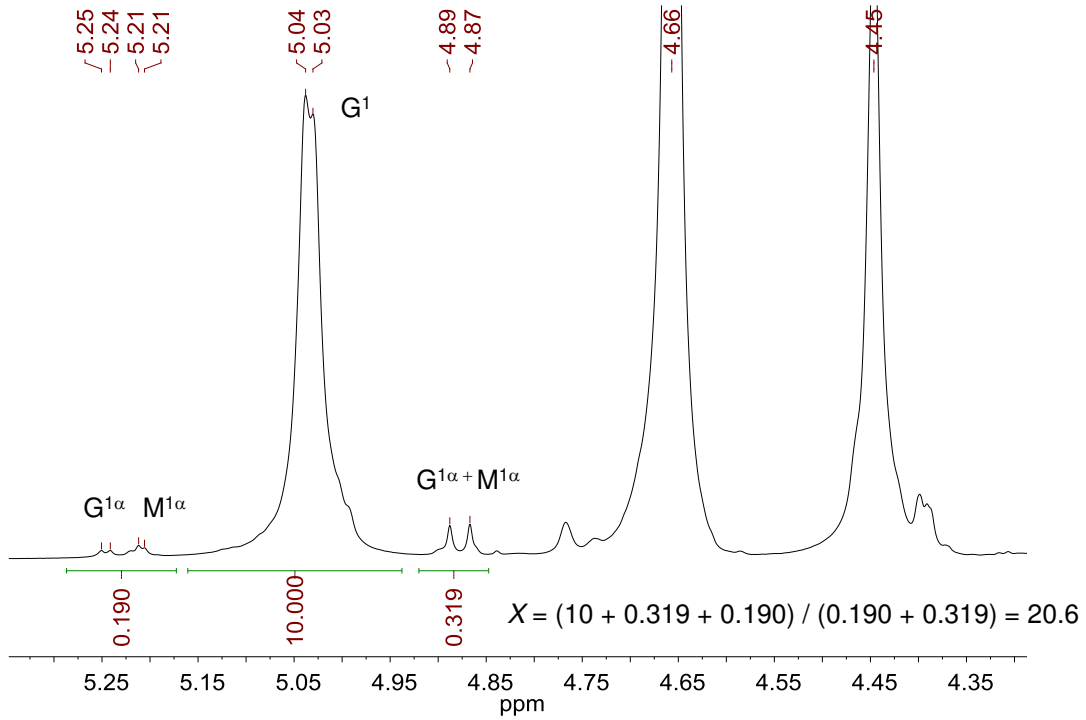

Figure 5A.12 *^{1}H NMR spectrum of (1→4)-α-L-guluronan (X=20). Conditions: 400 MHz, D_2O, 2.5 % w/w, 308K, number of scans (ns) = 128.*

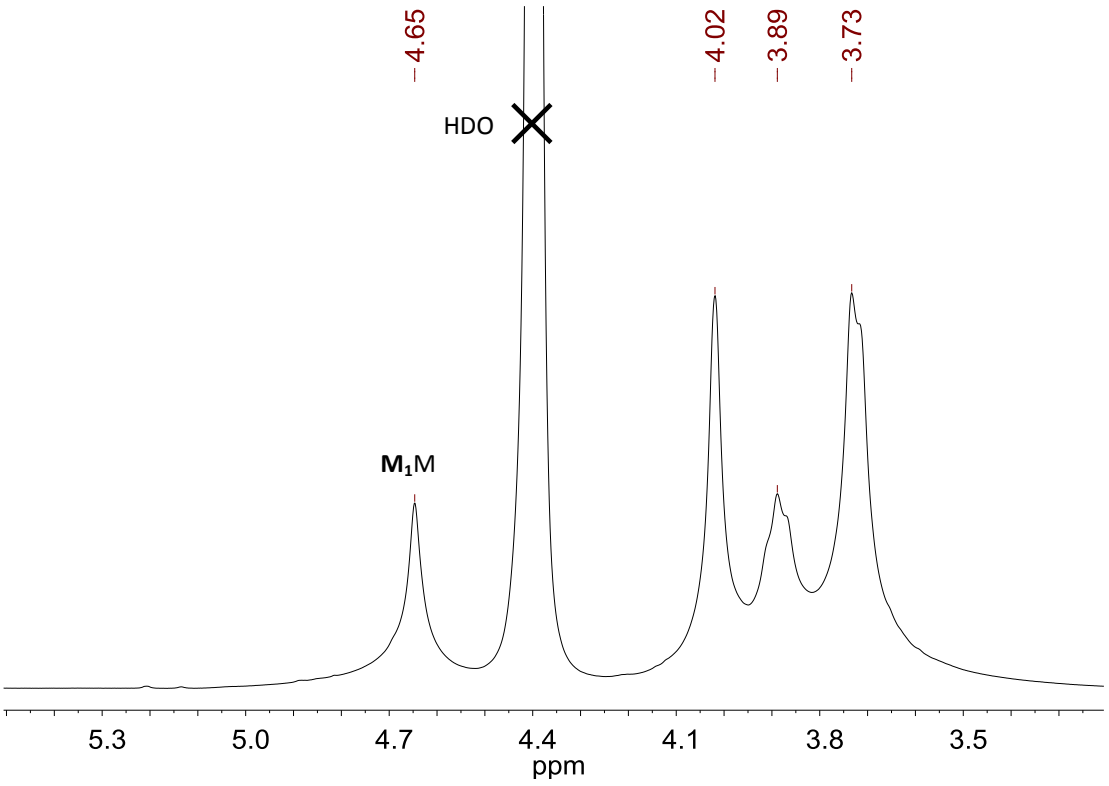

Figure 5A.13 *^{1}H NMR spectrum of (1→4)-β-D-mannuronan (X=300, isolated from C5 epimerase negative mutant of Pseudomonas fluorescens). Conditions: 400 MHz, D_2O, 1.5 % w/w, 338K, number of scans (ns) = 1024.*

6. References

(1) Rief, M.; Oesterhelt, F.; Heymann, B.; Gaub, H. E. Science (Washington, D. C.) 1997, 275, 1295.

(2) Marszalek, P. E.; Oberhauser, A. F.; Pang, Y.-P.; Fernandez, J. M. Nature (London) 1998, 396, 661.

(3) Marszalek, P.; Li, H.; Fernandez, J. M. Nat. Biotechnol. 2001, 19, 258.

(4) Sletmoen, M.; Skjak-Braek, G.; Stokke, B. T. Biomacromolecules 2004, 5, 1288.

(5) Hoidal, H. K.; Ertesvag, H.; Skjak-Braek, G.; Stokke, B. T.; Valla, S. J. Biol. Chem. 1999, 274, 12316.

(6) Gudmundsdottir, A. V.; Paul, C. E.; Nitz, M. Carbohydr. Res. 2009, 344, 278.

(7) Gudmundsdottir, A. V.; Nitz, M. Carbohydr. Res. 2007, 342, 749.

(8) Flinn, N. S.; Quibell, M.; Monk, T. P.; Ramjee, M. K.; Urch, C. J. Bioconjugate Chem. 2005, 16, 722.

(9) Hutter, J. L.; Bechhoefer, J. Rev. Sci. Instrum. 1993, 64, 1868.

(10) Riet, J. t.; Katan, A. J.; Rankl, C.; Stahl, S. W.; Buul, A. M. v.; Phang, I. Y.; Gomez-Casado, A.; Schon, P.; Gerritsen, J. W.; Cambi, A.; Rowan, A. E.; Vancso, G. J.; Jonkheijm, P.; Huskens, J.; Oosterkamp, T. H.; Gaub, H.; Hinterdorfer, P.; Figdor, C. G.; Speller, S. Ultramicroscopy 2011, 111, 1659.

(11) Sader, J. E.; Pacifico, J.; Green, C. P.; Mulvaney, P. J. Appl. Phys. 2005, 97, 124903/1.

(12) Sader, J. E.; Chon, J. W. M.; Mulvaney, P. Rev. Sci. Instrum. 1999, 70, 3967.

(13) Ghadban, A.; Albertin, L.; Rinaudo, M.; Heyraud, A. Biomacromolecules 2012, 13, 3108.

(14) Dentini, M.; Rinaldi, G.; Barbetta, A.; Risica, D.; Anselmi, C.; Skjåk-Bræk, G. Carbohydrate Polymers 2007, 67, 465.

(15) Peric, L.; Pereira, C. S.; Perez, S.; Hunenberger, P. H. Mol. Simul. 2008, 34, 421.

(16) Plazinski, W. Carbohydr. Res. 2012, 357, 111.

(17) Wang, Z.; Zhang, Q.; Konno, M.; Saito, S. Chem. Phys. Lett. 1991, 186, 463.

(18) Wang, Z. Y.; Zhang, Q. Z.; Konno, M.; Saito, S. Biopolymers 1994, 34, 737.

(19) Wang, Z. Y.; Zhang, Q. Z.; Konno, M.; Saito, S. Biopolymers 1993, 33, 703.

(20) Wang, Z.-Y.; White, J. W.; Konno, M.; Saito, S.; Nozawa, T. Biopolymers 1995, 35, 227.

(21) Thibault, J. F.; Rinaudo, M. Br. Polym. J. 1985, 17, 181.

(22) Cardenas, A.; Goycoolea, F. M.; Rinaudo, M. Carbohydr. Polym. 2008, 73, 212.

(23) Draget, K. I.; Taylor, C. Food Hydrocolloids 2011, 25, 251.

(24) Kohn, R.; Larsen, B. Acta Chem Scand 1972, 26, 2455.

(25) Kohn, R. Pure Appl. Chem. 1975, 42, 371.

(26) Grant, G. T.; Morris, E. R.; Rees, D. A.; Smith, P. J. C.; Thom, D. FEBS Letters 1973, 32, 195.

(27) Morris, E. R.; Rees, D. A.; Robinson, G.; Young, G. A. J. Mol. Biol. 1980, 138, 363.

(28) Ghadban, A. PhD thesis, Université de Grenoble, 2012.

Chapter VI:

Conclusions

This PhD study was a part of ALGIMAT (Advanced functional **MAT**erials from algal **ALGI**nates) project which has developed an original approach to the use of alginates as a primary source of molecular bricks for the synthesis of new materials with a well-defined structure. However, beside the synthesis of biohybrid polymers featuring (1→4)-α-L-guluronan sequences as side chains, their characterization in terms of physico-chemical properties was of great importance and had become the main objective of the present study.

Among many significant features of alginate-derived polymers (neo-alginates), their capability of the ionotropic gelation under mild conditions is particularly attractive because it may be applied for many industrial and biomedical applications. For this reason, Ca^{2+}-driven association of neo-alginates in both dilute (via Light Scattering; LS) and semi-dilute (via rheology) solutions, together with detailed examination of their side chain interactions mediated by Ca^{2+} at the molecular level (by molecular modeling and Atomic Force Spectroscopy; AFS) were probed.

Experimentally, the gelation process was investigated at two levels: in dilute solution to indicate a germ of the primary gel network and in semi-dilute domain to obtain a complete picture of the gelation mechanism. Both studies were performed during slow and progressive addition of $CaCl_2$ to neo-alginate (*i.e.* poly(HEMAm-g-$GulA_x$), where X = 10 or 20) solution in NaCl as well as in deionized water. The transition from a solution to a gel-like state was determined on the basis of rapid increase of monitored properties observed during controlled changes in the charge stoichiometric ratio ($R = 2[Ca^{2+}]/[COO^-]$). The results of this study showed that in sodium chloride environment, the critical charge stoichiometric ratio (R_c) is higher in dilute solutions than for rheological experiments which is in agreement with data from the literature (on alginates by Wang [1,2] and pectins by Thibault [3]).

Rheology was the tool of choice to determine not only a sol-gel transition for these two biohybrid polymers featuring (1→4)-α-L-guluronan sequences as side chains, but also to investigate their gelling ability. Comparing the two, both underwent ionotropic gelation but neo-alginate with longer guluronan chains ($GulA_{20}$) gave stronger gel (even at almost the same content of guluronan units). In order to examine the strength of this hydrogel, additional experiment was performed, *i.e.* polymer carrying (1→4)-α-L-guluronan residues ($X = 20$) was dialyzed against $CaCl_2$ and compared with alginate-Ca^{2+} gel (prepared from purified commercial alginate; Satialgine SG150, under the same conditions). This study showed that the strength of a hydrogel depends on the content of guluronan blocks (the higher it is, the stronger gel is formed) and the way in which guluronan units are incorporated into the material, *i.e.* in the backbone (as in alginate) or as side chains (neo-alginates). Since alginate sample was richer in guluronan (81% by mass in comparison with 28% for polymer) and guluronan units were included in the main chain, thus the alginate hydrogel was stronger and stiffer. This examination gave an evidence that biohybrid polymers featuring (1→4)-α-L-guluronan sequences as side chains form soft hydrogels.

Further studies of the gel strength were based on the addition of free oligosaccharide chains (either guluronan or mannuronan) which may disconnect previously formed junction, according to Morris *et al.*[4] suggestions. The findings indeed confirmed not only the hypothesis that the addition of free chains reduces the gel strength but also the role of mannuronan chains in the formation of junction zones (almost the same efficiency of both mannuronan and guluronan chains).

Besides probing the Ca^{2+}-driven association and ionotropic gelation of biohybrid polymers by rheology and Light Scattering, a particular focus of this PhD project was aimed to their side chain interactions mediated by Ca^{2+} at the molecular level.

Several attempts have been made in order to investigate the atomistic structure of the junction zone of Ca^{2+}-alginate by molecular modeling, its description proposed by Plazinski[5] seems to be the most satisfactory. However, his work examined guluronan chains with only 10 repeating units and did not analyze their structural features. In order to fill this gap, guluronan blocks were examined in this study in terms of their length, *i.e.* degree of polymerization ($2 \leq X \leq 20$), and helical conformation. An ionotropic association between (1→4)-α-L-guluronan chains (generated according to Braccini *et al.*[6]) and Ca^{2+} ions (neutralized amount) was probed by using molecular dynamics simulations in explicit water

environment at 300 K using similar parameters to those applied by Plazinski [5]. In addition, all systems were allowed full conformational freedom.

The chain length effect was probed in single chain systems and duplexes (parallel and antiparallel) starting from 2_1 helical conformation. These studies revealed that in duplexes with $X \geq 8$ more than 50% of calcium ions present in examined systems were complexed by two carboxylate groups of guluronan chains. Thus, chains having ~8 (1→4)-α-L-guluronic acid residues units form aggregates. This result is correlated with previous investigations by Stokke *et al.* [7] which showed that ~8 repeating units are required to form stable junction zones. However, the most interesting finding from studying the chain length effect was a helical twist (around 10°) of guluronan chains observed in simulated systems (both single and paired, $4 \leq X \leq 20$), which gave an idea to conduct a molecular dynamics investigation of the helical forms adopted by guluronan blocks. For this reason, single chains and duplexes were modeled starting both from 2_1 or 3_2 helical conformation. It has been noticed that the initial perfect helices with integral screw symmetries were lost at the very beginning of simulations and two distinct behaviors were observed:

- At equilibrium 2_1 models mostly retained 2_1 local helical conformations while exploring 3_2 ones the rest of the time. In duplexes the two chains behaved similarly, were well extended and slightly twisted.

- By contrast, the chains in 3_2 duplex models were dissimilar and explored a much broader conformational space in which 2_1 and 3_2 local helical conformations were dominant and equally represented, but 3_1 and other conformations were also present.

The wide variety of conformations revealed in this study may explain in part the general difficulty in obtaining crystals of Ca^{2+}-guluronate with suitable lateral dimensions for crystallographic studies.[8-10] Thus, it can be postulated that the substantial conformational disorder of the chains in the junction zone precludes their lateral association.

However, a recent molecular dynamics study performed by Plazinski and Rudzinski [11] has shown several stable modes of association of two dimers of guluronan chains. Furthermore, some aggregates of chains were also observed in present studies, *e.g.* in parallel 2_1 duplex model composed of (1→4)-α-L-guluronan chains with 14 repeating units. Thus, studying the association of (1→4)-α-L-guluronan duplexes in the presence of Ca^{2+} ions could be an important issue for future research.

In order to obtain a better atomistic picture of side chain associations via Ca^{2+}, some force measurements (via Atomic Force Microscopy) were performed. The main aim of this study was to investigate interactions between guluronan oligomers with 20 repeating units attached to both a tip and a wafer in the presence of Ca^{2+}. Since a natural alginate is composed of heterogeneous blocks, and oligomers of mannuronan with almost the same chain length (18 repeating units) were also available, thus the same experiments were performed in that case as well. In addition, besides studying only homotypic interactions (*i.e.* between surfaces grafted with the same type of oligomer), this examination was also aimed to heterotypic interactions. The strength of observed interactions was estimated on the basis of observed difference in the average adhesion force ($\Delta\langle F\rangle$), determined from experiments performed in $CaCl_2$ solution and deionized water (or NaOH solution). The results obtained for homotypic oligomers attached to silicon or gold surfaces showed that interactions between guluronan chains are stronger than mannuronan ones. On the other hand, heterotypic interactions between oligomers grafted onto silicon surfaces revealed that their strength increased in the following order:

$$\text{M-M} < \text{M-G or G-M} < \text{G-G}$$

Interestingly, observed difference in the average adhesion force ($\Delta\langle F\rangle$) for M-M interactions has proofed that M-blocks are complexed via Ca^{2+} and can be involved in both homotypic and heterotypic associations. Certainly, their contribution is lower than G-blocks but nevertheless may also impact on the formation of junction zones.

During studying interactions between oligomers (attached to a tip and a surface) in calcium chloride environment the grafting density was not under control. Therefore, it could be interesting to use in future studies some PEG spacers in order to observe single interactions and to be able to compare energy of associations determined by Atomic Force Spectroscopy to molecular dynamics simulations.

Since it was shown that Light Scattering is a method which may detect the threshold of aggregate formation during slow and progressive addition of $CaCl_2$ in the neo-alginates, thus it was also applied for solutions of some oligomers: (1→4)-β-D-mannuronan with 10 or 18 repeating units and (1→4)-α-L-guluronan with 11 or 20 repeating units. This study has found that lower degree of polymerization together with NaCl environment favors aggregation in the presence of calcium ions. Although very high affinity of oligomannuronan chains to Ca^{2+} was an original result. However, it was also observed via rheology that the

addition of free mannuronan block has high influence on the gel strength of neo-alginate (*i.e.* poly(HEMAm-g-GulA_{20}), and its effect is comparable to the addition of free guluronan blocks. This large affinity of M-blocks to Ca^{2+} was noticed several times in present studies which should provide a new understanding of the role of M-blocks in the formation of junction zones together with their ability to form aggregates in dilute solutions.

Finally, it is worth noting that the current study was multidisciplinary. First of all, the association of (1→4)-α-L-guluronan blocks via calcium ions was investigated in depth by molecular modeling. Additionally, Atomic Force Spectroscopy and Light Scattering also allowed probing these interactions either at the molecular level, or in dilute solutions. Rheology was used to study mainly the transition from a solution to a gel-like state of synthesized biohybrid polymers featuring (1→4)-α-L-guluronan sequences as side chains and their gelling ability. Many aims of this PhD project have been achieved but unfortunately mannuronan blocks were not examined by molecular modeling. Therefore, future studies on the current topic are recommended.

References

(1) *Wang, Z.; Zhang, Q.; Konno, M.; Saito, S. Chem. Phys. Lett. 1991, 186, 463.*

(2) *Wang, Z. Y.; Zhang, Q. Z.; Konno, M.; Saito, S. Biopolymers 1994, 34, 737.*

(3) *Thibault, J. F.; Rinaudo, M. Br. Polym. J. 1985, 17, 181.*

(4) *Morris, E. R.; Rees, D. A.; Robinson, G.; Young, G. A. J. Mol. Biol. 1980, 138, 363.*

(5) *Plazinski, W. J. Comput. Chem. 2011, 32, 2988.*

(6) *Braccini, I.; Grasso, R. P.; Perez, S. Carbohydr. Res. 1999, 317, 119.*

(7) *Stokke, B. T.; Smidsroed, O.; Bruheim, P.; Skjaak-Braek, G. Macromolecules 1991, 24, 4637.*

(8) *Li, L.; Fang, Y.; Vreeker, R.; Appelqvist, I.; Mendes, E. Biomacromolecules 2007, 8, 464.*

(9) *Sikorski, P.; Mo, F.; Skjk-Brk, G.; Stokke, B. T. Biomacromolecules 2007, 8, 2098.*

(10) *Mackie, W.; Perez, S.; Rizzo, R.; Taravel, F.; Vignon, M. Int. J. Biol. Macromol. 1983, 5, 329.*

(11) *Plazinski, W.; Rudzinski, W. Struct. Chem. 2012, 23, 1409.*